Studies on HIF hydroxylases

A thesis submitted for the degree of Doctor of Philosophy

Trinity Term 2008

James D Webb

Merton College



Studies on HIF hydroxylases

James D Webb, Merton College
Thesis submitted for the degree of Doctor of Philosophy
Nuffield Department of Clinical Medicine, University of Oxford
Trinity Term 2008

Hypoxia-inducible factor (HIF) is the master regulator of genes involved in adaptation to hypoxia. The stability and transcriptional activity of HIF are regulated by post-translational hydroxylations: prolyl hydroxylation by the prolyl hydroxylase domain-containing enzymes PHD1 – 3 earmarks HIF for proteasomal degradation, whilst asparaginyl hydroxylation by factor inhibiting HIF (FIH) blocks the interaction of HIF with the transcriptional coactivators p300/CBP. The PHDs and FIH hydroxylate HIF directly from molecular oxygen and are therefore oxygen sensors.

Recent literature shows that FIH also hydroxylates a number of proteins containing an ankyrin-repeat domain (ARD). Together with reports suggesting that the PHDs are involved in HIF-independent pathways, this suggests that the HIF hydroxylases may have a wide range of non-HIF targets. This thesis describes my investigations into novel substrates of the HIF hydroxylases.

This work has characterized the FIH-dependent hydroxylation of the ARD-containing protein Notch1, and defined a consensus sequence for hydroxylation that corresponds to the ankyrin-repeat consensus. Using this consensus potential sites of hydroxylation in a novel ARD FIH substrate, myosin phosphatase targeting subunit 1 (MYPT1), were identified then subsequently confirmed and characterized.

Notch1 competes with HIF for FIH hydroxylation. My experiments show that this occurs because Notch1 is a more efficient substrate than HIF, whilst studies on MYPT1 and other proteins indicate that competitive inhibition of FIH may be a general property of ARDs.

There are more than 300 ARD proteins in the human genome, and this thesis demonstrates that FIH may hydroxylate a significant percentage of these. In addition to the analysis of ARD hydroxylation a proteomic investigation into novel PHD3 substrates has identified two candidate proteins, suggesting that the PHDs may also have multiple targets. These results have important implications for oxygen sensing, and indicate that post-translational hydroxylation is likely to be a widespread modification in cell biology.

Declaration

The thesis that I am submitting is wholly my own work, with the exception of the experiments shown in Figures 4.7 and 4.9B, which were carried out by Dr Matthew Cockman. This is acknowledged in the text and figure legends.

Table of contents

Abstract....i
Declaration....ii
Table of contents....iii
List of figures and tables....vii
Abbreviations....x

Chapter 1: Introduction....1
1.1 The importance of post-translational modifications in biology....2
1.2 Protein hydroxylation and the 2OG dioxygenase enzymes....3
1.2.1 *Scope of the 2OG dioxygenase family*....3
1.2.2 *2OG dioxygenase structure and mechanism*....4
1.3 Extracellular protein hydroxylation by the 2OG dioxygenases....6
1.3.1 *Collagen*....6
1.3.2 *Epidermal growth factor (EGF)-like domains*....12
1.4 Intracellular protein hydroxylation by the 2OG dioxygenases....13
1.4.1 *Histone demethylation*....13
1.4.2 *Hypoxia-inducible factor (HIF) signalling*....17
1.4.3 *Asparaginyl hydroxylation of ankyrin-repeat domain-containing proteins by FIH*....36
1.5 Aims and scope of this thesis....39

Chapter 2: Characterization of Notch1 as a substrate for FIH....41
2.1 Introduction....42
2.2 Results....48
2.2.1 *Mutation of the primary sequence of Notch1*....48
2.2.2 *Analysis of the primary sequence determinants of mN1 hydroxylation*....51
2.2.3 *Analysis of the effects of Notch1 mutations on binding to FIH*....59
2.2.4 *Mutations to investigate the structural determinants of Notch1 hydroxylation*....67
2.2.5 *Analysis of the thermal stability of Notch1 structural mutants by circular dichroism*....69
2.2.6 *Analysis of the effect of structural mutants on Notch1 hydroxylation*....74
2.2.7 *Analysis of the effects of structural mutations on Notch binding to FIH*....74
2.2.8 *Analysis of the effect of Notch1 mutations on the competitive inhibition of FIH*....76
2.2.9 *Kinetic analysis of Notch1 hydroxylation*....80
2.3 Discussion....86

Chapter 3: Identification and characterization of MYPT1 as a substrate for FIH....93
3.1 Introduction....94
3.2 Results....100
3.2.1 *MYPT1 is a potential FIH substrate*....100
3.2.2 *Identification of hydroxylation sites in MYPT1 by MS/MS*....100

3.2.3 *FIH and MYPT1 interact in 293T cells*....109
3.2.4 *FIH is necessary and sufficient for hydroxylation of the MYPT1 ARD*....109
3.2.5 *Endogenous MYPT1 is hydroxylated*....112
3.2.6 *Structural consequences of MYPT1 hydroxylation*....115
3.2.7 *FIH does not affect the interaction between MYPT1 and PP1cδ*....120
3.2.8 *FIH overexpression or suppression do not affect MLC phosphorylation status*....120
3.2.9 *MYPT1 ARD can influence the transcriptional activity of HIF1α through competition for FIH*....122
3.3 Discussion

Chapter 4: A proteomic approach for identifying novel PHD3 substrates....**132**
4.1 Introduction....133
4.2 Results....138
4.2.1 *Tandem affinity tagging of PHD3*....138
4.2.2 *Development of a mixing strategy for capturing PHD3 interactors*....143
4.2.3 *An alternative strategy for capturing DMOG-inducible PHD3 interactors*....149
4.2.4 *SKIP interacts specifically with PHD3 in a DMOG-inducible manner*....153
4.2.5 *Mapping the PHD3-interacting domain of SKIP*....157
4.2.6 *Using mass spectrometry to search for prolyl hydroxylation in SKIP*....160
4.2.7 *PHD3 does not affect SKIP levels* in vivo....165
4.2.8 *Attempts to prepare recombinant SKIP in* E. coli....165
4.2.9 *SV40 LTag interacts specifically with PHD3 in a DMOG-inducible manner*....168
4.2.10 *Attempting to map the PHD3-interacting domain of LTag*....171
4.2.11 *PHD3 does not affect the interaction of LTag and p53, nor its stability*....171
4.2.12 *LTag can modestly affect the degradation kinetic of HIF*....173
4.2.13 *LTag does not affect the cellular localization of PHD3*....175
4.2.14 *Attempts to prepare a recombinant LTag fragment*....177
4.2.15 *Mass spectrometric analysis of LTag*....177
4.3 Discussion

Chapter 5: Final discussion....**190**
5.1 Introduction....191
5.2 A consensus sequence for ARD hydroxylation by FIH....191
5.3 The function of ARD hydroxylation: structure or signalling?....192
5.4 Novel substrates of the PHDs....195
5.5 Closing remarks....196

Chapter 6: Materials and methods....**198**
6.1 Reagents....199
6.1.1 *Chemicals*....199

6.1.2 *Buffers*....199
6.1.3 *Cell biology reagents*....201
6.2 Bacterial techniques....202
6.2.1 *Solutions and media*....202
6.2.2 *Bacterial strains*....202
6.2.3 *Preparation of competent* E. coli *for transformation*....203
6.2.4 *Transformation*....203
6.3 DNA techniques....204
6.3.1 *Isolation and purification of plasmid DNA*....204
6.3.2 *DNA quantitation*....204
6.3.3 *Amplification of DNA by polymerase chain reaction (PCR)*....204
6.3.4 *Agarose gel electrophoresis*....205
6.3.5 *Purification of DNA from agarose gels or from solution*....205
6.3.6 *Restriction enzyme digestion*....205
6.3.7 *Alkaline phosphatase treatment*....205
6.3.8 *Ligation*....205
6.3.9 *Site-directed mutagenesis (SDM)*....206
6.3.10 *DNA sequencing*....206
6.4 Protein techniques....207
6.4.1 *Protein quantitation*....207
6.4.2 *Sodium dodecylsulfate polyacrylamide gel electrophoresis (SDS-PAGE)*....207
6.4.3 *Immunoblotting*....208
6.4.4 *Antibodies*....209
6.4.5 *Preparation of agarose-conjugated antibodies for immunoprecipitation*....210
6.5 Mammalian cell culture techniques....212
6.5.1 *Cell culture*....212
6.5.2 *Plasmid transfection*....212
6.5.3 *siRNA transfection*....213
6.5.4 *Mammalian cell lysate preparation*....215
6.5.5 *Immunoprecipitation*....215
6.5.6 *Cycloheximide chase*....216
6.5.7 *Fractionation of cells into nuclear and cytoplasmic components*....216
6.6 Mass spectrometric techniques....217
6.6.1 *Digestion of protein from gel bands*....218
6.6.2 *Digestion of proteins in solution*....219
6.6.3 *LC-MS and LC-MS/MS analysis using Bruker Daltonics HCTplus ion trap instrument*....220
6.6.4 *High-resolution LC-MS analysis using Waters QToF Premier instrument*....220
6.6.5 *Stable isotope labelling of amino acids in cell culture (SILAC)*....221
6.6.6 *Quantitation of peptide hydroxylation from extracted ion chromatograms*....222

6.7 *In vitro* assays and protein synthesis....222
6.7.1 *Preparation of GST-tagged Notch1 ARD proteins for binding assays*....223
6.7.2 *Preparation of cleaved Notch1 ARD proteins for circular dichroism analysis*....223
6.7.3 In vitro *GST pulldown assays*....224
6.7.4 *Far-Western blotting*....225
6.7.5 In vitro *kinetic assays*....225
6.7.6 *Circular dichroism (CD)*....226
6.7.7 *HIF1α CAD reporter gene assays*....227
6.7.8 In vitro *transcription/translation of proteins (IVTT)*....228
6.7.9 *pVHL capture assays*....228
6.8 Plasmids and oligonucleotide primers....229
6.8.1 *Oligonucleotide primers*....229
6.8.2 *Plasmids for protein expression in mammalian cells*....232
6.8.3 *Plasmids for protein expression in bacteria*....236

Chapter 7: Bibliography....238

Acknowledgments....264

List of figures and tables

Figures

Figure 1.1 Reaction scheme for substrate hydroxylation by a 2OG dioxygenase enzyme....5
Figure 1.2 Schematic diagram of nucleosome structure and mechanism of histone demethylation by 2OG-dependent dioxygenases....14
Figure 1.3 Schematic diagram of the HIF signalling pathway....20
Figure 1.4 Domain structures of HIF1α, HIF2α and HIFβ....22
Figure 1.5 Structure of an ankyrin repeat domain (ARD)....37

Figure 2.1 Alignment of FIH substrates....49
Figure 2.2A Analysis of Notch1 hydroxylation by quantitative MS (i)....53
Figure 2.2B Analysis of Notch1 hydroxylation by quantitative MS (i)....54
Figure 2.2C Analysis of Notch1 hydroxylation by quantitative MS (i)....55
Figure 2.3 Analysis of Notch1 hydroxylation by quantitative MS (ii)....58
Figure 2.4 Purification of GST-tagged mN1 ARD primary sequence mutants....60
Figure 2.5 GST-pulldown assays for mN1 mutant binding to FIH....62
Figure 2.6 Far-western blotting assay for mutant mN1 binding to FIH....65
Figure 2.7 Destabilizing mutations in *Drosophila* Notch....68
Figure 2.8 Preparation of untagged Notch1 ARD structural mutants....70
Figure 2.9 Analysis of ARD melting temperatures by CD spectroscopy (i)....72
Figure 2.10 Analysis of ARD melting temperatures by CD spectroscopy (ii)....73
Figure 2.11 Analysis of mN1 structural mutant hydroxylation....75
Figure 2.12 GST-pulldown assays for mN1 structural mutant binding to FIH....75
Figure 2.13 Far-western blotting assay for structural mutant mN1 binding to FIH....77
Figure 2.14 Schematic representation of the Gal4DBD-HIF1α CAD luciferase reporter assay....77
Figure 2.15 Assaying the effect of mN1 mutants on FIH inhibition (i)....79
Figure 2.16 Assaying the effect of mN1 mutants on FIH inhibition (ii)....79
Figure 2.17 Kinetic analyses of mN1 hydroxylation (i)....83
Figure 2.18 Kinetic analysis of mN1 hydroxylation (ii)....84

Figure 3.1 Subunit structure of myosin phosphatase....96
Figure 3.2 MYPT1 is a potential substrate for FIH....101
Figure 3.3 Tandem MS....103
Figure 3.4A Identification of Asn-67 as a hydroxylation site in MYPT1....106
Figure 3.4B Identification of Asn-100 as a hydroxylation site in MYPT1....107
Figure 3.4C Identification of Asn-226 as a hydroxylation site in MYPT1....108
Figure 3.5 FIH and MYPT1 interact in 293T cells....110
Figure 3.6 FIH is necessary and sufficient for MYPT1 hydroxylation (i)....113
Figure 3.7 FIH is necessary and sufficient for MYPT1 hydroxylation (ii)....114
Figure 3.8A & B Endogenous MYPT1 is hydroxylated (i)....116

Figure 3.8C Endogenous MYPT1 is hydroxylated (i)....117
Figure 3.9 Endogenous MYPT1 is hydroxylated (ii)....118
Figure 3.10 Structural consequences of MYPT1 hydroxylation....119
Figure 3.11 FIH does not affect the interaction between MYPT1 and PP1cδ....121
Figure 3.12 FIH overexpression or suppression do not affect MLC phosphorylation status....121
Figure 3.13 MYPT1 can influence the transcriptional activity of HIF1α through competition for FIH....123

Figure 4.1 Schematic diagram of the basic AP-MS experiment....135
Figure 4.2 SPA-tagging of PHD3....140
Figure 4.3 The SPA tag does not adversely affect the activity of PHD3....142
Figure 4.4 Substrate trapping using DMOG....145
Figure 4.5 Optimization of conditions for 293T/PC12 mixing experiment....147
Figure 4.6 Proteomic-scale mixing experiment and SPA purification....150
Figure 4.7 SPA purification of the HIF hydroxylases....152
Figure 4.8 Validation of the PHD3/SKIP interaction....154
Figure 4.9 Attempting to demonstrate an endogenous PHD3/SKIP interaction....156
Figure 4.10 Mapping the PHD3/SKIP interaction....158
Figure 4.11 Co-precipitation of endogenous PHD3 by FLAG-SKIP....162
Figure 4.12 Schema of SILAC approach....162
Figure 4.13 Evidence for hydroxylation of Pro-173 in SKIP....164
Figure 4.14 SKIP levels are not affected by PHD3 knock-down....164
Figure 4.15 Attempts to prepare recombinant SKIP in *E. coli*....167
Figure 4.16 Validation of the PHD3/LTag interaction....170
Figure 4.17 Attempts to show an endogenous PHD3/LTag interaction....170
Figure 4.18 PHD3 overexpression or knock-down do not affect the LTag/p53 interaction....172
Figure 4.19 LTag modestly affects HIF degradation on reoxygenation....174
Figure 4.20 LTag does not affect the cellular localization of PHD3....176
Figure 4.21 Attempts to prepare recombinant LTag in *E. coli*....176
Figure 4.22 Immunoprecipitation of LTag for MS analysis....178

Tables

Table 2.1 Primary sequence mutations made in mN1....53

Table 4.1 MS/MS assignment of rat HIF2α as a DMOG-inducible protein co-precipitating with PHD3....150
Table 4.2 MS/MS identification of SKIP and SV40 large T antigen as DMOG-inducible proteins co-precipitating with PHD3....152
Table 4.3 SV40 LTag expression constructs....172
Table 4.4 Results of LC-MS/MS analysis of LTag from DMOG- or PHD3-treated cells....178

Table 6.1 Antibodies....211
Table 6.2 siRNA duplexes....214
Table 6.3 Oligonucleotide primers for SDM....230
Table 6.4 Oligonucleotide primers for cloning and sequencing....231

Abbreviations

2OG	2-oxoglutarate
4Hyp	4-hydroxyproline
ADP	adenosine diphosphate
AP	affinity purification
AR	ankyrin repeat
ARD	ankyrin-repeat domain
ARD1	arrest defective protein 1
ARNT	aryl hydrocarbon nuclear translocator
ASB4	ankyrin repeat and SOCS box protein 4
ASBH	aspartyl (asparaginyl) β-hydroxylase
ATF4	activating transcription factor 4
bHLH	basic helix-loop-helix
BSA	bovine serum albumen
CAD	C-terminal transactivation domain
CB	Coomassie blue
CD	circular dichroism
CHX	cycloheximide
CODD	C-terminal oxygen-dependent degradation domain
Da	Dalton
DFO	desferrioxamine
DMEM	Dulbecco's modified Eagle's medium
DMOG	dimethyloxalylglycine
DNA	deoxyribonucleic acid
dNTP	2'-deoxynucleotide 5'-triphosphate
DTT	DL-dithiothreitol
ECD	extracellular domain
ECM	extracellular matrix
EDTA	ethylenediaminetetraacetic acid
EGF	epidermal growth factor
EGFP	enhanced green fluorescent protein
EIC	extracted ion chromatogram
Epo	erythropoietin
EYFP	enhanced yellow fluorescent protein
FCS	foetal calf serum
FIH	factor inhibiting HIF
g	acceleration due to gravity
Gal4-DBD	Gal4-DNA binding domain
GFP	green fluorescent protein
GST	glutathione *S*-transferase
HA	haemagglutinin
HEK293	human embryonic kidney 293 cells
HEPES	4-(2-hydroxyethyl)piperazine-1-ethanesulfonic acid
HIF	hypoxia-inducible factor
HRE	hypoxia-responsive enhancer
HRP	horseradish peroxidase
Hx	hypoxia
Hyp	hydroxyproline

IκBα	inhibitor of NF-κB α
ICD	intracellular domain
IP	immunoprecipitation
IPAS	inhibitory PAS domain protein
IPTG	isopropyl-β-D-thiogalactopyranoside
IVTT	*in vitro* transcription/translation
JmjC	jumonji C domain-containing
K_m	Michaelis constant
LB	Luria Bertani medium
LC	liquid chromatography
LTag	*SV40* large T antigen
mAb	monoclonal antibody
MAPK	mitogen-activated protein kinase
mdeg	millidegree
MLC	myosin light chain
MLCK	myosin light chain kinase
mN1	mouse Notch1
MP	myosin phosphatase
mRNA	messenger RNA
MS	mass spectrometry
MS/MS	tandem mass spectrometry
MYPT1	myosin phosphatase targeting subunit 1
NAD	N-terminal transactivation domain
NF-κB	nuclear factor κB
NGF	nerve growth factor
NODD	N-terminal oxygen-dependent degradation domain
NOG	*N*-oxalylglycine
NP40	Nonidet P-40
Nx	normoxia
OD_x	optical density at *x* nm
OI	osteogenesis imperfecta
pAb	polyclonal antibody
PAGE	polyacrylamide gel electrophoresis
PAS	Per-ARNT-Sim
PBS	phosphate-buffered saline
PCR	polymerase chain reaction
PDI	protein disulfide isomerase
PHD	prolyl hydroxylase domain-containing protein
PP1cδ	protein phosphatase type 1cδ
PTM	post-translational modification
PVDF	polyvinylidene fluoride
pVHL	von Hippel-Lindau tumour suppressor protein
QToF	quadrupole time-of-flight
RCC	renal clear cell carcinoma
RNA	ribonucleic acid
ROCK	Rho-associated kinase
Rx	reoxygenation
SDM	site-directed mutagenesis

SDS	sodium dodecylsulfate
SEM	standard error of the mean
shRNA	short hairpin RNA
SILAC	stable isotope labelling of amino acids in cell culture
siRNA	small interfering RNA
SKIP	Ski-interacting protein
SPA	sequential peptide affinity
SUMO	small ubiquitin-like modifier
SV40	*Simian Virus 40*
TAP	tandem affinity purification
TEV	tobacco etch virus
T_m	melting temperature
Tris	*tris*-(hydroxymethyl)aminomethane
UAS	upstream activation site
UV	ultraviolet
v/v	volume for volume
V_{max}	maximum rate of an enzymatic reaction
w/v	weight for volume
WT	wild-type

Chapter 1
Introduction

1.1 The importance of post-translational modifications in biology

Post-translational modification of proteins enables nature to expand the number of available functional protein side chains beyond those provided by the twenty proteinogenic amino acids alone, and a huge range of post-translational modifications (PTMs) has been identified. These may consist of the addition of small functional groups such as phosphorylation, methylation, acetylation, carboxylation, amidation, oxidation or hydroxylation. Alternatively whole molecules may be appended to protein side chains: glycosylation and lipidation are examples. In the case of ubiquitination and SUMOylation (for small ubiquitin-like modifier) entire proteins are conjugated to amino acid side chains (Walsh, 2006).

PTMs can have a huge range of functional effects: phosphorylation of proteins in particular is of vast and wide-ranging importance in cell signalling. Other examples of the effects of PTMs include switching "on" or "off" enzyme activity, altering the cellular localization of a protein, affecting the lifetime of a protein within a cell by tagging it for destruction or preservation, or influencing the structure of protein molecules (Walsh, 2006).

This thesis is concerned with the post-translational hydroxylation of proteins. Protein hydroxylation is perceived as a relatively uncommon PTM (Walsh, 2006). However, because of the crucial importance of post-translational hydroxylation in proteins of the collagen family, which constitute around 30% of the total protein mass of the human body (Myllyharju and Kivirikko, 2004), collagen hydroxylation has been the subject of decades of research and is discussed in more detail below. Despite the perception of protein hydroxylation as rare, recent advances in our knowledge of mammalian oxygen

sensing enzymes (discussed below) and the work presented in this thesis suggest that it may be a much more widespread modification than has previously been appreciated.

1.2 Protein hydroxylation and the 2OG dioxygenase enzymes

1.2.1 *Scope of the 2OG dioxygenase family*

The protein hydroxylations described below are all catalysed by enzymes of the family of 2-oxoglutarate- and iron(II)-dependent dioxygenases ("2OG dioxygenases"). These enzymes have the remarkable ability to oxidize a substrate directly from molecular oxygen, and require 2OG and iron(II) as co-factors (Ozer and Bruick, 2007). The first dioxygenase enzyme reported was a collagen prolyl hydroxylase identified in 1967 (Hutton et al., 1967a). Based on sequence analyses and structural predictions there are currently thought to be more than sixty 2OG dioxygenases in the human genome, although for many no function has been defined (Loenarz and Schofield, 2008). Many more 2OG dioxygenases are known in other animals, bacteria and plants (Clifton et al., 2006).

Before discussing post-translational protein hydroxylation in detail it should be emphasized that 2OG dioxygenases catalyse a wide range of other oxidation processes on small molecules and DNA. For example, trimethyllysine hydroxylase (TMLH) and γ-butyrobetaine hydroxylase (GBBH) catalyse the first and last steps respectively in the biosynthesis of carnitine (which is essential for fatty acid metabolism) from N^{ε}-trimethyllysine (Hulse et al., 1978; Lindblad et al., 1969; Lindstedt and Lindstedt, 1970; Vaz and Wanders, 2002). Phytanoyl-coenzyme A 2-hydroxylase (PAHX) is essential for metabolism of the dietary-derived fatty acid phytanic acid, and mutations in the gene encoding PAHX can cause Refsum's disease, a progressive neurological syndrome

(Mukherji et al., 2001; Wierzbicki et al., 2000). AlkB, ABH2, ABH3 and FTO are examples of DNA-modifying enzymes. The *Escherichia coli* enzyme AlkB repairs single-stranded DNA and RNA by hydroxylating and subsequently removing 1-methyladenine and 3-methylcytosine lesions, as do two of its human homologues ABH2 and ABH3 (Duncan et al., 2002; Falnes et al., 2002; Welford et al., 2003), whilst FTO is a DNA demethylase associated with obesity, by a mechanism as-yet unknown (Gerken et al., 2007).

1.2.2 *2OG dioxygenase structure and mechanism*

Members of the 2OG dioxygenase family share a conserved fold structure known as the double-stranded β-helix or "jelly-roll" motif (Clifton et al., 2006). In contrast to haem-containing proteins where an iron atom is tightly bound within a prosthetic group, the iron centre in 2OG dioxygenase enzymes is much more loosely coordinated. In the vast majority of family members iron(II) binding involves a motif consisting of one carboxylate and two histidine residues (Clifton et al., 2006; Costas et al., 2004). Conservation of this HXD/E…H motif is not absolute however (Loenarz and Schofield, 2008), as discussed further below.

The mechanism of protein hydroxylation by a 2OG dioxygenase is shown in Figure 1.1. The first step of a catalytic cycle involves binding of 2-oxoglutarate (2OG) to the iron(II) centre (Figure 1.1A) (Costas et al., 2004). Following the binding of 2OG, the substrate and molecular oxygen bind (Figure 1.1B and C), although the order in which this occurs is controversial: steady-state kinetic studies on a collagen prolyl hydroxylase suggest that oxygen binds before the substrate (Myllylä et al., 1977; Tuderman et al., 1977). However, more recent spectroscopic studies on *Escherichia coli*

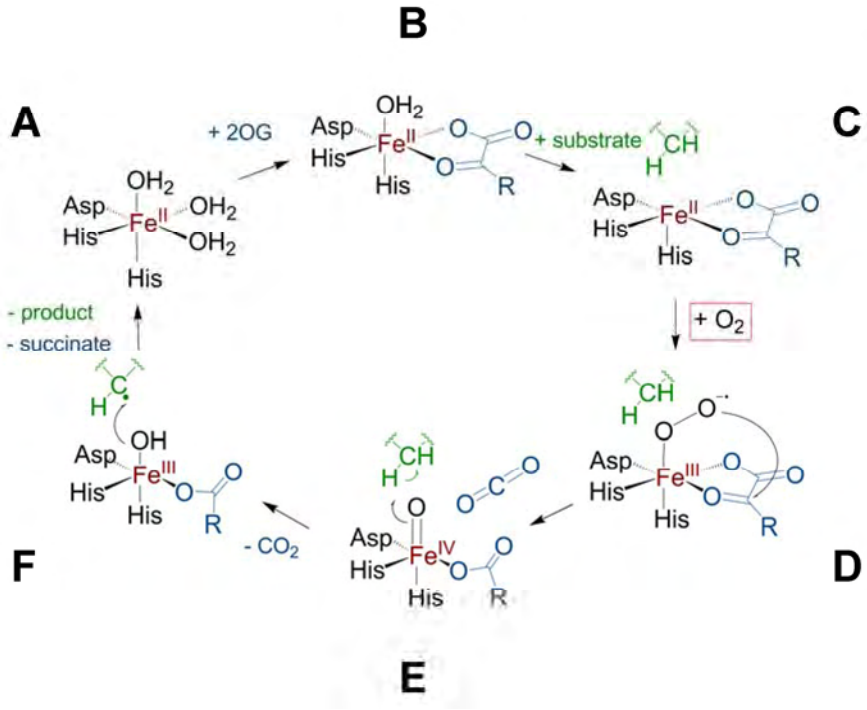


Figure 1.1
General reaction scheme for substrate hydroxylation by a 2OG dioxygenase enzyme.

TauD (which catalyses conversion of the non-essential amino acid taurine to sulfite and aminoacetaldehyde) and clavaminic acid synthase have suggested the reverse (Ryle et al., 1999; Zhou et al., 2001). Regardless of the order in which these events occur, once oxygen and substrate have bound to the iron(II) centre, oxygen attacks 2OG (Figure 1.1D) resulting in oxidative decarboxylation and the formation of an iron(IV)-containing intermediate (Figure 1.1E), the existence of which has been confirmed by Mössbauer spectroscopy (Price et al., 2003). Protein hydroxylation occurs next through radicalar abstraction of a hydrogen atom by the oxo-iron(IV) centre followed by "oxygen rebound" onto the substrate (Figure 1.1F). Finally, after release of the hydroxylated substrate and succinate, the reaction cycle repeats (Costas et al., 2004).

1.3 Extracellular protein hydroxylation by the 2OG dioxygenases

1.3.1 *Collagen*

Undoubtedly the best-known examples of proteins that undergo post-translational hydroxylation are the members of the collagen family, where the presence of hydroxylated amino acids has been studied for decades (Van Slyke and Hiller, 1921). Collagens are structural proteins of the extracellular matrix (ECM): there are at least 28 known forms, referred to as types I – XXVIII in the order of their discovery (Myllyharju and Kivirikko, 2004; van der Rest and Garrone, 1991; Veit et al., 2006). All collagen molecules consist of three polypeptide α-chains (which may or may not be of the same type) that wrap around each other in a triple helical structure forming a rope-like molecule. All collagen α-chains contain at least one domain of repeating Gly-Xxx-Yyy sequence: the presence of repeating, small glycine residues in the sequence is essential for adoption of the triple helical structure. Any amino acid may occur at the Xxx and Yyy positions, but proline is frequently found at the Xxx position and 4-

hydroxyproline at the Yyy position, where it plays an essential part in stabilizing the triple helix (Myllyharju and Kivirikko, 2004).

Collagens can form a wide range of supramolecular structures, and are often classified on the basis of these assemblies (Myllyharju and Kivirikko, 2004; Prockop and Kivirikko, 1995). Collagen types I, II, III, V, XI, XXIV and XXVII are structural proteins containing large triple-helical domains and assemble into fibrils, with parallel cross-linked collagen molecules offset from their nearest neighbours by around a quarter of their length. Fibrils (which may contain more than one type of collagen) are the principal type of collagen found in bone, skin, tendon and other connective tissues. Fibril-associated collagens with interrupted triple helices (FACIT collagens), including types IX, XII, XIV, XVI, XIX, XX, XXI, XXII and XXVI, do not themselves form fibrils but associate with the surface of existing fibrils. Other classes of collagen form sheet-like structures, and are important in the formation of sheets or protein membranes that surround tissues and organisms. Collagens VIII and X form hexagonal networks in Descemet's membrane, which separates the stroma of the eye from the endothelial layer of the cornea (van der Rest and Garrone, 1991). Basement membranes, structures supporting layers of epithelial or endothelial cells, are composed of two types of collagen IV. Type VI collagen forms beaded filaments, whilst type VII forms anchoring fibrils for basement membranes. The supramolecular structures of other collagens are unknown, although types XIII, XVII, XXIII and XXV contain transmembrane domains (Myllyharju and Kivirikko, 2004).

Post-translational hydroxylation during the intracellular processing of collagens occurs in the lumen of the endoplasmic reticulum, following translation but before assembly of

the triple helix and secretion of the protein (Myllyharju and Kivirikko, 2004; Prockop and Kivirikko, 1995). Three types of post-translational hydroxylation are known to occur in collagen proteins: prolyl 4-hydroxylation, prolyl 3-hydroxylation and lysyl hydroxylation. Each has a distinct function and is catalysed by a different family of enzyme (Myllyharju and Kivirikko, 2004).

Collagen prolyl 4-hydroxylation

The importance of 4-hydroxylproline (4Hyp) residues in stabilizing the triple helical structure of collagen chains has already been stated: the structural importance of prolyl 4-hydroxylation is emphasized by the observation that the triple helices do not form during the intracellular processing of collagen until the individual chains have acquired around 100 4Hyp residues (Prockop and Kivirikko, 1995). Early experiments on collagen established that isotopically-labelled dietary hydroxyproline (Hyp) was not absorbed to any significant extent, suggesting that instead Hyp was formed by the oxidation of prolyl residues (Stetten, 1949). Subsequent reports identified prolyl hydroxylase activity in chick embryo extract (Ebert and Prockop, 1962; Peterkofsky and Udenfriend, 1963; Prockop and Juva, 1965), with further work demonstrating that the collagen prolyl 4-hydroxylase (CP4H) required 2OG, iron(II) and ascorbate as cofactors, thus identifying it as the first known 2OG dioxygenase (Hutton et al., 1967a; Hutton et al., 1967b). The first human CP4H (now termed type I) was cloned in 1989 (Helaakoski et al., 1989). Although it had long been assumed that there was only one isoform of CP4H (Myllyharju, 2003), two further isoforms have since been identified, named types II and III respectively (Annunen et al., 1997; Kukkola et al., 2003). Type I CP4H appears to be the predominant isoform in most cells, with type II the major form expressed in chondrocytes, osteoblasts and endothelial cells (Annunen et al.,

1998; Nissi et al., 2001). Type III CP4H mRNA is expressed in a wide range of tissues but at a much lower level than type I and II mRNAs (Kukkola et al., 2003).

All known CP4H enzymes form $\alpha_2\beta_2$ tetramers, in which the β-subunit is invariably protein disulfide isomerase (PDI) (Myllyharju, 2003). In a given CP4H tetramer the α-subunits are both of type I, II or III (Myllyharju, 2003): the formation of tetramers containing different α-subunits appears unlikely based on co-expression data in insect cells (Annunen et al., 1997). The crucial role for CP4Hs in collagen synthesis and development is underscored by the embryonic-lethal phenotype of CP4H type I null mice, although interestingly CP4H type II mice are viable, suggesting that whilst CP4H type I may be able to compensate for loss of type II, the converse does not apply (Holster et al., 2007; Myllyharju and Kivirikko, 2004).

Collagen prolyl 3-hydroxylation

Although the function of collagen prolyl 4-hydroxylation is firmly established, the role of collagen prolyl 3-hydroxylation is less well understood. The presence of 3-hydroxyproline residues at the Xxx position of Xxx-4Hyp-Gly repeats has been shown to have a destabilizing effect on the triple helix (Jenkins et al., 2003; Mizuno et al., 2004), and it is proposed that this local destabilization of the helix may be important for the assembly of supramolecular collagen structures (Mizuno et al., 2004). The first collagen prolyl 3-hydroxylase (CP3H) was identified in chick embryo extract almost 30 years ago (Tryggvason et al., 1979), but the enzyme was not cloned from tissues until much more recently (Vranka et al., 2004). A family of three CP3H enzymes has been indentified, of which two (CP3H1 and CP3H2 respectively) have been expressed and characterized (Tiainen et al., 2008; Vranka et al., 2004). In contrast with the CP4H

enzymes, the CP3Hs do not adopt a multimeric structure or require PDI as a subunit. However, CP3H1 co-purifies with a cartilage-associated protein (CRTAP): although CP3H1 is active *in vitro* in the absence of CRTAP, the latter is required for its full activity *in vivo* (Vranka et al., 2004). Mice lacking CRTAP suffer from a severe phenotype similar to osteogenesis imperfecta (OI, a hereditable disorder characterized by bone fragility and a low bone mass (Glorieux, 2008)). The synergistic relationship between C3PH1 and CRTAP is reinforced by studies showing that a deficiency of either protein in humans has similar effects. Under-production of CRTAP in humans leads to varying degrees of severity of OI (from neonatal lethality to a milder phenotype depending on the nature of the mutation) (Barnes et al., 2006; Morello et al., 2006), whilst recent data indicate that mutations in the gene encoding CP3H1 in humans can also cause lethal-to-severe OI (Cabral et al., 2007). Taking these data together it is clear that, although the mechanism by which it operates is not fully understood, prolyl 3-hydroxylation of collagen proteins is essential for normal bone development.

Collagen lysyl hydroxylation

Hydroxylysine residues in fibrillar collagens are important for the formation of cross-links between triple helices. Although unmodified lysine residues can also form cross-links *via* a similar pathway, hydroxylysyl cross-links predominate in bone, cartilage, ligament and most connective tissues as they are significantly more stable than their lysine-derived counterparts (Myllylä et al., 2007). A second role of hydroxylysine residues is as sites for glycosylation with the monosaccharide galactose or a glucose-galactose disaccharide: these modifications are unique to collagen proteins (Myllylä et al., 2007). Three lysyl hydroxylase enzymes have been identified in humans, LH1, LH2

and LH3 (Hautala et al., 1992; Valtavaara et al., 1997; Valtavaara et al., 1998). Whilst LH1 and LH2 appear solely to have lysyl hydroxylase activity, LH3 has been demonstrated to exhibit additional collagen glucosyltransferase and galactosyltransferase activities *in vitro* (Heikkinen et al., 2000; Wang et al., 2002). Studies in mouse models have confirmed the multifunctionality of LH3, and its importance in embryonic development (Rautavuoma et al., 2004; Ruotsalainen et al., 2006). The LH3 knockout caused embryonic lethality due to defective basement membrane formation, whilst a lack of glucosyltransferase activity in fibroblasts derived from knockout embryos suggests that LH3 may be the only such enzyme in these tissues. It thus appears that glycosylation of collagen chains catalysed by the glucosyltransferase activity of LH3 is essential for basement membrane formation and embryonic viability (Ruotsalainen et al., 2006).

Argonaute2: an example of intracellular protein hydroxylation by CP4H1

In addition to the collagens, a disparate range of extracellular proteins containing a triple-helical collagenous domain are known to be substrates for the CP4Hs, including the C1q component of complement, adiponectin and macrophage receptors (Myllyharju and Kivirikko, 2004). A very recent report also indicates that the intracellular protein Argonaute2 (Ago2), an essential component of the RNA-induced silencing complexes, is post-translationally hydroxylated by CP4H1 (Qi et al., 2008). Although Ago2 does not contain a triple-helical domain, it does contain three highly conserved Xxx-Pro-Gly triplets, and mass spectrometric analysis of endogenous Ago2 showed that the prolyl residue in one of these triplets, Pro-700, was hydroxylated in 293ET cells. The hydroxylation of Pro-700 regulates the stability of Ago2: Ago2 containing a P700A mutation has a significantly shorter half-life than wild-type protein,

and the protein half-life is similarly reduced when CP4H1 is suppressed (Qi et al., 2008). Impaired CP4H activity also leads to a reduction in the function of the RNA-induced silencing complex. This study has therefore defined a novel role for the CP4Hs and protein hydroxylation in the regulation of RNA interference.

1.3.2 *Epidermal growth factor (EGF)-like domains*

Epidermal growth factor (EGF) is a 53-residue polypeptide formed by the release of EGF domains in the C-terminal part of the large EGF precursor protein (Stenflo et al., 1987). A range of extracellular proteins contain repeating domains with homology to EGF known as EGF-like domains, including vitamin K-dependent plasma proteins, some coagulation factors, and transmembrane receptors and ligands such as Notch, Delta and Serrate (Bray, 2006; Stenflo, 1991; Stenflo et al., 1987). Certain proteins with EGF-like domains, including factors VII, IX and X, have long been known to contain post-translational hydroxylations on aspartate and asparagine residues (McMullen et al., 1983; Stenflo et al., 1987). A 2OG dioxygenase with both aspartyl and asparaginyl hydroxylase activities, termed aspartyl (asparaginyl) beta-hydroxylase (ASBH or BAH), was subsequently identified and characterized as the enzyme responsible for these hydroxylations (Gronke et al., 1989; Gronke et al., 1990; Stenflo et al., 1989). ASBH (also termed EGF hydroxylase, EGFH) is an unusual 2OG dioxygenase since although it contains a double-stranded β-helix, there is no HXD iron binding sequence. Although lacking this "classical" 2OG dioxygenase motif, sequence alignments and mutational studies suggest that there are likely to be two histidine residue in ASBH involved in iron(II) coordination, with the possibility that a third iron-binding residue may come from a different part of the structure from those in structurally characterized 2OG dioxygenases (Lancaster et al., 2004a; McGinnis et al., 1996). The exact physiological

role of ASBH is not yet defined. However, residues critical for catalytic activity are significantly conserved from humans to *Drosophila melanogaster*, and loss of ASBH catalytic activity in mice promotes the formation of tumours (Dinchuk et al., 2002). In humans ASBH may have a role in determining the "receptivity" of the uterine endometrium, as reduced expression in placental cells, decidua and endometrial glands has been associated with spontaneous abortion and small-for-gestational-age deliveries (Gundogan et al., 2007). Further, ASBH is overexpressed in various malignant tumours including hepatocellular carcinomas where it has been proposed to contribute to the malignant phenotype by activating Notch and insulin-like growth factor signalling (Cantarini et al., 2006). A high level of ASBH overexpression in hepatocellular carcinoma is associated with intrahepatic metastasis and tumour progression, leading to the suggestion that ASBH be used as a prognostic marker in this disease (Xian et al., 2006). Whilst it seems clear that ASBH can affect Notch signalling, the mechanism by which this occurs is not established. Notch has EGF-like repeats in its extracellular domain that contain consensus motifs for ASBH-mediated hydroxylation and ASBH knock-out mice show abnormalities reminiscent of mice with Notch ligand mutations. However, direct hydroxylation of the Notch EGF repeats by ASBH has not been reported (Dinchuk et al., 2002). Notch signalling is discussed in more detail in Chapter 2.

1.4 Intracellular protein hydroxylation by the 2OG dioxygenases

1.4.1 *Histone demethylation*

Cellular DNA is packaged into chromatin, the fundamental unit of which is the nucleosome. Each nucleosome consists of an octamer of four core histone proteins

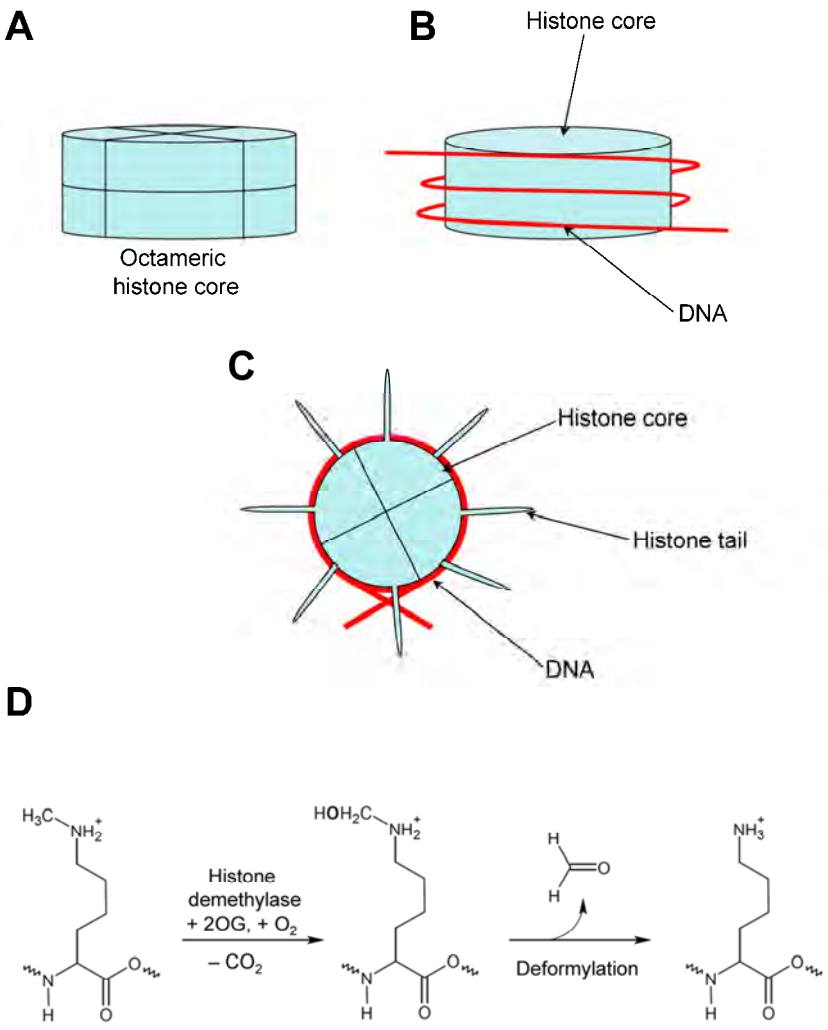


Figure 1.2
Schematic diagram of nucleosome structure. Each nucleosome consists of a core of eight histone proteins (**A**)*, which is wrapped in 147 base pairs of DNA* (**B**)*. Eight histone tails, one from each histone molecule, project out from the nucleosome* (**C**)*.* (**D**) *shows the mechanism of lysine demethylation by a JmjC demethylase: the methyl group is enzymatically hydroxylated to form an unstable hydroxymethyl intermediate which undergoes a spontaneous deformylation reaction to restore the unmodified lysine residue.*

(two each of H3, H4, H2A and H2B, Figure 1.2A) wrapped in 147 base pairs of DNA (Figure 1.2B). Whilst the core of a histone protein is globular, each has an extended, unstructured N-terminal "tail" which projects out from the nucleosome (Figure 1.2C). These histone tails are heavily punctuated with post-translational modifications, including acetylation of lysine, methylation of lysine or arginine, phosphorylation of serine or threonine, ubiquitination and sumoylation of lysine, ADP ribosylation of glutamate, deimination of arginine or isomerisation of proline (Kouzarides, 2007).

Methylation of lysine and arginine residues can have a range of effects on chromatin structure, transcription and DNA repair (Klose and Zhang, 2007; Kouzarides, 2007). In fission yeast, the borders between transcriptionally silent heterochromatin (where DNA is "inaccessible" for transcription) and transcriptionally active euchromatin (where DNA is available for transcription) are demarcated by methylation of residues Lys-4 and Lys-9 in H3 (denoted H3K4 and H3K9). H3K4, H3K36 and H3K79 methylations are implicated in transcriptional activation whilst methylation of H3K9, H3K27 and H4K20 is (consistent with its abundance in heterochromatin) associated with transcriptional repression. Further, in fission yeast nuclear foci at sites of DNA repair contain methylated H4K20. Arginine methylation may also have activating or repressive effects on transcription depending on the site at which it occurs (Kouzarides, 2007; Zhang and Reinberg, 2001). Both arginine and lysine can exist in three different methylated states (monomethyl, symmetrical dimethyl and asymmetrical dimethyl for arginine; monomethyl, dimethyl and trimethyl for lysine), and these differing methylation states can lead to differing functional outcomes (Klose and Zhang, 2007).

Although historically histone methylation was assumed to be a static modification, recent data have shown that, in common with other histone modifications, it is highly dynamic (Klose and Zhang, 2007; Kouzarides, 2007). A range of arginine and lysine methyltransferase enzymes can methylate histone proteins including members of the protein arginine methyl transferase (PRMT) and su(var)3–9, enhancer of zeste, trithorax (SET) families (Kouzarides, 2007; Zhang and Reinberg, 2001). The first histone lysine demethylase (LSD1, which is not a member of the 2OG dioxygenase family) was not discovered until 2004 (Shi et al., 2004). Since this report, a number of 2OG dioxygenases of the JmjC (Jumonji-C domain-containing) family have also been shown to have histone lysine demethylase activity: this family of proteins is named for the mouse jumonji protein (Jmj), which contains a double-stranded β-helix and is involved in the regulation of gene expression (Takeuchi et al., 2006). Many enzymes containing a JmjC domain have established roles in transcriptional regulation and sequence similarities to the 2OG dioxygenase and DNA demethylase AlkB, making them good candidates as histone demethylases (Klose and Zhang, 2007). Since the initial identification of the JmjC protein JHDM1 as a histone demethylase (Tsukada et al., 2006), at least fifteen more such proteins have been identified as histone lysine demethylases in humans (Lan et al., 2008). A further JmjC protein, JMJD6, has recently been assigned as an arginyl demethylase (Chang et al., 2007).

The JmjC histone demethylases share a common demethylation mechanism with the DNA repair enzyme AlkB (Welford et al., 2003). The methyl group is initially hydroxylated, following which spontaneous deformylation occurs to restore the unmodified histone residue (Figure 1.2D) (Klose and Zhang, 2007). Thus in addition to its vital structural role in proteins of the collagen family, post-translational protein

hydroxylation by 2OG dioxygenases also plays an essential role in chromatin modification and epigenetic regulation of gene expression, potentially providing a direct link between oxygen availability and gene expression through the histone demethylase enzymes. Another family of 2OG dioxygenases is also vital for the oxygen-dependent regulation of gene expression through post-translational hydroxylation of the hypoxia-inducible transcription factor, and these enzymes are discussed in detail in the following section.

1.4.2 *Hypoxia-inducible factor (HIF) signalling*

Protein hydroxylation has other cell-signalling roles in addition to histone demethylation. In recent years it has been shown that animals, from nematodes to man, detect their cellular oxygen levels by an unprecedented mechanism involving the post-translational hydroxylation of the transcription factor hypoxia-inducible factor (HIF) by a family of 2OG dioxygenases that function as cellular oxygen sensors. These HIF hydroxylases are the subject of the work carried out in this thesis, and this section introduces our current understanding of the HIF signalling pathway.

Discovery of the HIF system

The HIF system was discovered as a result of studies to determine the mechanism by which the glycoprotein hormone erythropoietin (Epo), which stimulates erythrocyte production and is produced in response to falls in oxygen levels, was regulated. Epo levels have long been known to be elevated in patients suffering from anaemia (iron deficiency) or hypoxaemia (a low concentration of oxygen in arterial blood) (Erslev, 1953). It was determined that whilst reduced oxygen delivery to the tissues did stimulate Epo production, metabolic poisons such as cyanide, which uncouples

mitochondrial respiration, did not have any effect, thus suggesting an oxygen-sensing mechanism that detected oxygen concentrations directly rather than *via* a failure of mitochondrial function (Nečas and Thorling, 1972). The later discovery that both oxygen sensing and Epo production could occur in the same cell type was a major breakthrough, as it paved the way for work that followed to dissect the mechanism of oxygen sensing using cultured human cells as a model system (Goldberg et al., 1988; Goldberg et al., 1987).

In 1991 a hypoxia-responsive enhancer (HRE) was identified lying 3' to the mouse and human *Epo* genes (Pugh et al., 1991; Semenza et al., 1991). Subsequent analyses of species that bind to the HRE identified a protein, termed hypoxia-inducible factor 1 (HIF1) (Semenza and Wang, 1992; Wang and Semenza, 1993a, b). HIF1 was cloned and characterized in 1995 (Wang et al., 1995a; Wang and Semenza, 1995): it is an $\alpha\beta$-heterodimer consisting of an oxygen-sensitive α-subunit and an oxygen-insensitive β-subunit. Two further forms of HIFα have been identified, HIF2α (Ema et al., 1997; Tian et al., 1997) and HIF3α (Gu et al., 1998).

In the presence of oxygen HIFα subunits are extremely labile, being bound by the von Hippel-Lindau tumour suppressor protein E3 ligase (pVHL), ubiquitinated and proteasomally degraded (Cockman et al., 2000; Maxwell et al., 1999; Ohh et al., 2000). Following the identification of prolyl hydroxylation as the marker for pVHL recognition of HIFα proteins (Ivan et al., 2001; Jaakkola et al., 2001), three 2OG dioxygenase enzymes were identified as HIF prolyl hydroxylases in humans, termed prolyl hydroxylase domain-containing 1, 2 and 3 (PHD1 – 3) (Bruick and McKnight, 2001; Epstein et al., 2001). A fourth 2OG dioxygenase, factor inhibiting HIF (FIH), which

hydroxylates an asparagine residue towards the C-terminus of HIF, thereby blocking co-activator recruitment and limiting HIF transcriptional activity, was identified in separate studies (Hewitson et al., 2002; Lando et al., 2002a; Lando et al., 2002b; Mahon et al., 2001). The HIFs, PHDs and FIH are all discussed in more detail below.

Our current understanding of the basic HIF signalling pathway is shown in Figure 1.3. Under conditions of normoxia, HIFα subunits are hydroxylated by the PHDs and FIH: prolyl hydroxylation by the PHDs leads to recognition of HIFα by pVHL, followed by its ubiquitination and proteasomal destruction. HIF asparaginyl hydroxylation by FIH renders the HIFα subunit transcriptionally inactive by blocking recruitment of the transcriptional co-activators p300 and CBP (Lando et al., 2002b), both of which regulate transcription through their histone acetyltransferase activity (Bannister and Kouzarides, 1996; Ogryzko et al., 1998; Simone et al., 2004). Under hypoxia, reduced availability of molecular oxygen inhibits the HIF hydroxylase enzymes: HIFα proteins accumulate and are translocated to the nucleus where they form a transcriptionally active complex with HIFβ and p300/CBP, "switching on" the expression of HIF target genes (Figure 1.3).

HIFs

HIFs are αβ-heterodimers, containing an oxygen-sensitive α-subunit and an oxygen-insensitive β-subunit. There are currently three known HIFα subunits, HIF1α, HIF2α and HIF3α (Schofield and Ratcliffe, 2004). Three HIFβ chains, ARNT1, 2 and 3, are constitutively expressed but are not subject to oxygen-dependent regulation (Hirose et al., 1996; Hoffman et al., 1991; Hogenesch et al., 1998; Hogenesch et al., 2000; Ikeda and Nomura, 1997).

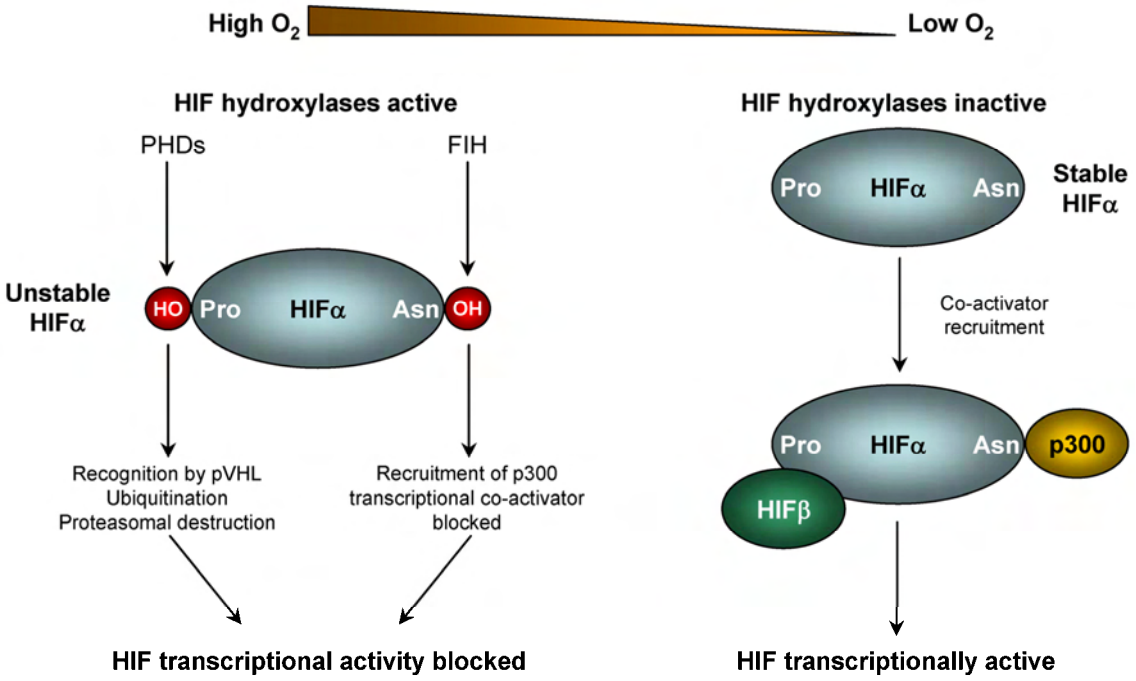


Figure 1.3
Schematic diagram of the HIF signalling pathway. Adapted from (Schofield and Ratcliffe, 2004).

HIF3α has no known role as an active transcription factor, and has been postulated to act as a negative regulator of HIF-mediated transcription (Gu et al., 1998): in support of this hypothesis, an alternative transcript of HIF3α, termed inhibitory PAS domain protein (IPAS), has been shown to dimerize with and sequester HIFβ, inhibiting HIF-mediated transcription (Makino et al., 2001). The alternative splicing that forms IPAS appears to be hypoxia-inducible, suggesting that IPAS may provide a negative feedback loop for HIF signalling (Heidbreder et al., 2003; Makino et al., 2002).

In contrast with HIF3α, HIF1α and HIF2α are known to control the transcription of a wide range of genes as a response to low oxygen levels, including genes involved in angiogenesis, glycolytic energy metabolism, erythrocyte production, vasomotor regulation, cell migration and growth (reviewed in (Schofield and Ratcliffe, 2004)). Between them, HIF1α and HIF2α directly control the transcription of more than seventy target genes (and therefore may vicariously control the transcription of many more), and are considered to be the key regulators of oxygen homeostasis in organisms from nematodes to man (Coleman and Ratcliffe, 2007; Lisy and Peet, 2008; Schofield and Ratcliffe, 2004).

HIF1α and HIF2α are proteins of 826 and 870 amino acids respectively: their domain structures are shown in Figure 1.4. Both contain basic helix-loop-helix (bHLH) and Per-ARNT-Sim (PAS) domains, through which dimerization with the HIFβ subunit occurs (Schofield and Ratcliffe, 2004). N-terminal and C-terminal oxygen-dependent degradation domains (NODD and CODD respectively) are present, within which lie the prolyl residues that are hydroxylated and recognized by pVHL (Pro-402 and Pro-

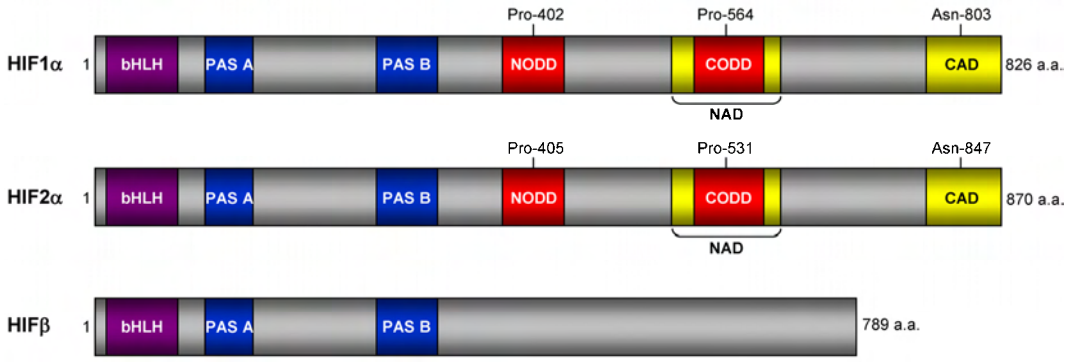


Figure 1.4
Domain structures of HIF1 α, HIF2 α and HIF β.

564 in HIF1α, Pro-405 and Pro-531 in HIF2α). Both proteins also contain N-terminal and C-terminal transactivation domains (NAD and CAD respectively): the asparaginyl residue that undergoes FIH-dependent hydroxylation (Asn-803 in HIF1α, Asn-847 in HIF2α) is located in the CAD. Conservation between HIF1α and HIF2α is 48% overall, but significantly higher within the shared functional domains: the bHLH and PAS domains are over 90% conserved, whilst conservation in the NAD and CAD domains is over 80% (Bracken et al., 2003; O'Rourke et al., 1999).

Although HIF1α and HIF2α are regulated by a similar mechanism, evidence is mounting that they do not have equivalent effects. Genetic studies have shown that knocking out either HIF1α or HIF2α in mice leads to lethality, demonstrating that the two proteins are non-redundant: this non-redundancy is emphasized by the significant difference in the phenotypes of HIF-null animals. HIF1α-null mice die around day 10.5 of embryogenesis from defects in heart development, vascularization and neural tube closure (Iyer et al., 1998; Ryan et al., 1998). HIF2α-null animals have been reported to have diverse phenotypes depending on the genetic background used: mice may die *in utero* from defective catecholamine production or defective vascularization, or shortly after birth due to respiratory distress or mitochondrial dysfunction (Compernolle et al., 2002; Peng et al., 2000; Scortegagna et al., 2003; Tian et al., 1998).

Despite the non-redundancy of HIF1α and HIF2α, analyses of the responses of hypoxia-inducible genes to manipulations in the levels of HIF1α and HIF2α have produced mixed results. In HEK293 cells it has been reported that HIF1α, but not HIF2α, controls the transcription of glycolytic genes (Hu et al., 2003). Although HIF1α

appears to be the principal regulator of gene expression, a separate study has suggested that several unique target genes were preferentially activated by transfection of HIF2α. However, most of these "HIF2α" genes were not themselves hypoxia-responsive (Wang et al., 2005). The dominance of HIF1α in the regulation of hypoxic genes appears to be confirmed by a later report, which identified a relatively small number of hypoxia-induced genes dependent on HIF2α expression (Elvidge et al., 2006). The origins of any target gene selectivity between HIF1α and HIF2α are not entirely clear, and continue to be debated. A domain-swapping study has suggested that switching the NAD between HIF proteins is sufficient to make HIF1α behave like HIF2α and *vice versa* (Hu et al., 2007). However, a separate experiment analysing the binding of HIFs to HREs *in vivo* by chromatin immunoprecipitation suggests that target gene selectivity is conferred by post-DNA binding mechanisms that are different for HIF1α and HIF2α and depend on the non-equivalent C-terminal regions of the two proteins (Lau et al., 2007).

Whilst it is uncertain whether differences in HIF1α and HIF2α target gene selectivity alone can fully account for the non-redundant effects of the two proteins, significant differences certainly exist between them. HIF1α has a natural antisense transcript, aHIF, that is overexpressed in hypoxia (Thrash-Bingham and Tartof, 1999). It has been proposed that during prolonged hypoxia aHIF is induced and negatively regulates HIF1α expression whilst HIF2α expression remains unaffected, providing a potential mechanism through which the HIF transcriptional readout could be modulated (Uchida et al., 2004). Further, in certain systems the two proteins can have opposite effects. In renal clear cell carcinoma (RCC) cells, HIF1α and HIF2α appear to act in a mutually

suppressive fashion. Overexpression of HIF2α is associated with pro-tumorigenic gene induction whilst overexpression of HIF1α promotes apoptotic gene expression, indicating that, at least in RCCs, the two HIFα forms regulate different target genes and have opposite effects on the biology of the cells (Raval et al., 2005). A later study may further elucidate the mechanism underlying the differential effects of the two HIFα subunits on the growth of tumours: HIF1α and HIF2α have been shown to have opposite effects on cell proliferation in RCC through a mechanism involving direct protein-protein interactions rather than HIF target gene transcription (Gordan et al., 2007a; Gordan et al., 2007b). HIF1α and HIF2α have opposite effects on c-Myc, a transcription factor that activates growth-promoting genes, with HIF1α proposed to sequester c-Myc binding partners and inhibit transcriptional activity whilst HIF2α binds to and stabilizes the c-Myc transcriptional complex.

Whilst it is clear that HIF1α and HIF2α can operate independently of (and even antagonistically to) each other, further work will be required in order to understand the origins and consequences of the differences between the two proteins more fully.

PHDs

Following the identification of EGL9 in the nematode worm *Caenorhabditis elegans* as a prolyl hydroxylase enzyme targeting HIF, three 2OG dioxygenases termed PHD1, PHD2 and PHD3 were identified as the HIF prolyl hydroxylases in humans (Epstein et al., 2001). These enzymes all target specific prolyl residues within the NODD and CODD of HIF1α and HIF2α for hydroxylation (Figure 1.4). In common with all other 2OG dioxygenase enzymes, the PHDs have an absolute requirement for molecular oxygen as a cosubstrate, thus making them ideal candidates for oxygen sensing.

Reported K_m values of the PHDs for O_2 have ranged from around 250 μM in a study using short peptide substrates to around 70 μM with a longer protein substrate (Ehrismann et al., 2007; Hirsilä et al., 2003). Tissue oxygen concentrations are thought to vary between around 4 and 40 μM, so although the reported K_m values vary significantly both are well above physiological O_2 levels. This implies that under physiological conditions O_2 availability is the factor limiting the prolyl hydroxylation of HIF by the PHDs, suggesting that they may indeed be cellular oxygen sensors.

PHD1, PHD2 and PHD3 are proteins of 44 kDa, 46 kDa and 27 kDa respectively. Structural data are available only for a truncation mutant of PHD2: although this enzyme crystallizes as a homotrimer, data in solution suggest that the protein is monomeric (McDonough et al., 2006), in contrast to the heteromultimeric structure of the CP4H enzymes. This finding should however be interpreted with caution given that no structural studies on the intact protein have yet been published. The three proteins show differences in their cellular localization: an immmunofluorescence study using overexpressed, GFP-tagged PHD enzymes in U2OS cells suggests that PHD1 is localized predominantly to the nucleus and PHD2 predominantly to the cytoplasm with PHD3 distributed relatively evenly throughout the cell (Metzen et al., 2003). Although reports on the tissue distribution of the PHD proteins are limited, a study has investigated the tissue specificity of PHD mRNAs (Dupuy et al., 2000). PHD1 mRNA was highly expressed in the testis (where other PHDs were essentially absent), heart, brain, liver and kidney. Expression of PHD2 was more widely and evenly distributed, being detected in the heart, brain, liver, skeletal muscle and kidney, with lower levels detected in the lung and spleen. PHD3 was highly expressed in the heart, brain,

skeletal muscle and kidney. The functional relevance of these differing PHD enzyme tissue distributions is not yet understood.

There is evidence to suggest that of the three PHD enzymes, PHD2 is the most important for controlling HIF levels under normoxia. Studies using small interfering RNA (siRNA) to knock down each PHD individually have shown that suppression of PHD2 alone (but not PHD1 or PHD3) is sufficient to increase HIF levels in normoxic cells (Appelhoff et al., 2004; Berra et al., 2003). Further, PHD2 is the most abundant of the three enzymes in most cell types in normoxia and suppression of PHD1 and PHD3 alone under these conditions do not affect the expression of HIF target genes (Appelhoff et al., 2004). Consistent with the importance of PHD2 in normoxia PHD2-null mice die *in utero*, whilst PHD1- and PHD3-null mice are viable (Takeda et al., 2006). Interestingly, and consistent with the high expression of PHD3 mRNA in the brain reported by Dupuy *et al.*, PHD3-null mice show neuronal abnormalities (Bishop et al., 2008). The critical role of PHD2 in HIF regulation is also emphasized by a study showing that a hereditary mutation in PHD2 is sufficient to cause HIF dysregulation resulting in excessive Epo production and erythrocytosis (an overproduction of erythrocytes). This mutation (P317R) affects the crucial HXD…H iron-binding motif in PHD2, thus impairing the enzyme's catalytic activity (Percy et al., 2006).

Whilst PHD2 may be the principal regulator of HIF in normoxic conditions, in other circumstances PHD1 and PHD3 play a significant role. PHD1 can be induced by oestrogen stimulation (Seth et al., 2002) and PHD3 by hypoxia (Appelhoff et al., 2004) to levels comparable with PHD2 and under these conditions make a detectable contribution to HIF regulation. PHD3 shows the greatest hypoxic inducibility of the

three enzymes (PHD2 is more modestly induced by hypoxia whilst PHD1 remains unaffected) and appears to retain significant activity in oxygen-deficient conditions. It has thus been proposed that PHD3 plays an important role in limiting the physiological activation of HIF in hypoxia (Appelhoff et al., 2004).

The three PHDs show a degree of selectivity, both between HIFα subunits and between CODD and NODD regions within HIFα subunits. Experiments in normoxic MCF7 cells showed that suppression of PHD2 elicited a larger induction of HIF1α than HIF2α, whilst suppression of PHD1 and PHD3 together had the reverse effect. In MCF7 cells, knock-down of PHD3 had substantial effects on HIF2α levels both in hypoxia and under reoxygenation that were not observed with suppression of PHD1 or PHD2. Thus it appears that PHD3 may preferentially target HIF2α, and PHD2 may preferentially target HIF1α (Appelhoff et al., 2004). There are also differences in selectivity between the PHDs for NODD and CODD prolyl hydroxylation sites: PHD3 was the most active enzyme at suppressing the activity of CODD domains in a reporter gene assay, but was essentially inactive towards HIF1α or HIF2α NODD fusions, consistent with *in vitro* studies suggesting that PHD3 does not hydroxylate NODD sequences (Appelhoff et al., 2004; Epstein et al., 2001; Hirsilä et al., 2003).

FIH

HIF asparaginyl hydroxylation (at Asn-803 in HIF1α and Asn-847 in HIF2α, Figure 1.4) by FIH is a complementary process to prolyl hydroxylation as the modification is not degradative: instead hydroxylation blocks the recruitment of the transcriptional co-activators p300 and CBP, so rendering the HIF CAD transcriptionally inactive (Lando et al., 2002a; Lando et al., 2002b).

FIH is a 40 kDa protein that forms a homodimer (Elkins et al., 2003). Dimer formation is necessary for the catalytic activity of the enzyme, and it has been demonstrated that a L340R mutant of FIH which cannot dimerize shows defective hydroxylase activity *in vitro* (Lancaster et al., 2004b). Reported O_2 K_m values for FIH vary significantly: a study using peptide substrates reports a K_m of around 90 μM, somewhat lower than those determined for the PHDs by the same group (Hirsilä et al., 2003; Koivunen et al., 2004). However, a more recent study using longer protein substrates for FIH reports values of around 240 μM for FIH and 80 μM for PHD2 (Ehrismann et al., 2007). Although *in vitro* data in the literature are contradictory, FIH and the PHDs certainly appear to make non-redundant contributions to oxygen sensing *in vivo*. FIH suppression using siRNA can upregulate HIF target gene expression in normoxia in a range of cell lines, indicating that levels of HIF1α in these cells are very low but potentially active, with FIH suppressing this transcriptional activity (Stolze et al., 2004). FIH was also shown to modulate HIF activity in U2OS cells over a range of oxygen concentrations: GLUT1 mRNA was downregulated by FIH overexpression even at 0.2% atmospheric oxygen, in contrast with PHD2 which had no detectable effect at these low oxygen levels (Stolze et al., 2004). A further report extends these findings and suggests that they may be cell type-specific, as the authors identify two classes of cell, one (including 293T, HeLa and COS1 cells) in which FIH is less sensitive than PHDs to falling oxygen levels and another (including PC12, CACO2 and HepG2) in which it is more sensitive (Bracken et al., 2006). The origins and consequences of this effect are currently unknown.

It appears that FIH may play a role in regulating HIF target gene selectivity: HIFα subunits contain two transactivation domains (the NAD and the CAD), of which only

the CAD is subject to oxygen-dependent regulation (Jiang et al., 1997). A recent report has suggested that there are two groups of HIF1α target genes: the majority appear to be activated by the CAD, as their expression is suppressed by FIH. However, a subset of HIFα target genes appears to be induced *via* the NAD and so shows no response to manipulation of FIH levels (Dayan et al., 2006).

Other PTMs affecting HIF

After hydroxylation, ubiquitination is perhaps the most important PTM involved in HIF regulation, since this is the modification that marks prolyl-hydroxylated HIF for proteasomal degradation (Cockman et al., 2000; Ohh et al., 2000). Ubiquitin is an 8 kDa protein that can be covalently attached to a lysine residue through a series of enzymatic processes. Following the attachment of the first ubiquitin moiety, a poly-ubiquitin chain is formed by the successive addition of ubiquitin molecules to Lys-48 of the previous unit (Hershko and Ciechanover, 1998).

Ubiquitination requires the concerted activity of three enzymes: firstly the ubiquitin-activating enzyme E1 binds ubiquitin, following which the ubiquitin is transferred to a ubiquitin-conjugating enzyme E2. In the third step a ubiquitin ligase enzyme E3, containing the substrate recognition component, binds the target protein and recruits the E2 enzyme which then carries out several iterations of ubiquitination on the target protein (Hershko and Ciechanover, 1998; Kaluz et al., 2008). The genome of a typical organism contains one E1 enzyme, more then 25 E2 enzymes and hundreds of E3 enzymes (Kaluz et al., 2008). In the case of HIF the E2 component is UbcH5 (Iwai et al., 1999), and the E3 enzyme a complex containing pVHL (the substrate recognition component), elongin B, elongin C, Cul2 and Rbx1 (Kondo and Kaelin, 2001).

The lysine residues in HIF1α that appear to be critical for ubiquitination are Lys-532, Lys-538 and Lys-547 (Paltoglou and Roberts, 2007; Tanimoto et al., 2000); these residues are highly conserved, both between HIF1α and HIF2α and also between species (Paltoglou and Roberts, 2007). Mutation of all three lysine residues to arginine prevented HIF1α ubiquitination and destruction, but the presence of any one of the three lysines restored full ubiquitination suggesting that they are redundant. Further, the critical lysine residues could be moved around the primary sequence of HIF1α with only minor losses in the efficiency of ubiquitination, suggesting that the critical determinant of ubiquitination in HIF is the binding of pVHL to hydroxyproline residues rather than specific flanking sequences adjacent to the target lysine residues (Paltoglou and Roberts, 2007).

Phosphorylation of HIF is a long-established phenomenon (Wang et al., 1995b), but the function of these modifications is frequently unclear. However, phosphorylation of HIF1α at Thr-796 by casein kinase II has been postulated to enhance HIF transcriptional activity (Gradin et al., 2002), and consistent with this observation a synthetic CAD peptide phosphorylated at this position is poorly hydroxylated by FIH *in vitro* (Lancaster et al., 2004b). Mitogen-activated protein kinase (MAPK) also appears to affect CAD activity, as enhanced MAPK activation correlated with increased HIF1α transactivation; conversely MAPK inhibition disrupts the HIF/p300 interaction and reduces transactivation (Sang et al., 2003). MAPK has also been reported to phosphorylate Ser-641 and Ser-632 of HIF1α, promoting transcriptional activity by suppressing CRM1-mediated nuclear export of HIF (Mylonis et al., 2006).

SUMOylation of HIF1α, postulated to increase HIF stability and transcriptional activity, was originally reported in 2004 (Bae et al., 2004), with a further report suggesting a role for SUMOylation in stabilizing HIF1α during hypoxia (Carbia-Nagashima et al., 2007). However, two later studies suggest that in fact SUMOylation reduces transcriptional activity, with Cheng *et al.* reporting that a SUMO-specific protease is necessary to prevent SUMOylation and proteasomal degradation of HIF1α during hypoxia (Berta et al., 2007; Cheng et al., 2007).

Acetylation of residue Lys-532 (one of the residues now thought to be targeted for ubiquitination) in HIF1α by arrest-defective-protein 1 (ARD1) was reported to be critical for the interaction of hydroxylated HIF1α with pVHL and subsequent proteasomal degradation (Jeong et al., 2002). However, at least three independent studies since have contradicted this result, indicating that HIF1α stability is not affected by ARD1, that purified ARD1 did not catalyse acetylation of HIF1α *in vitro*, and that although ARD1 and HIF1α do appear to bind specifically, this interaction does not result in acetylation (Arnesen et al., 2005; Bilton et al., 2005; Murray-Rust et al., 2006).

An endoplasmic reticulum transmembrane prolyl 4-hydroxylase (P4H-TM) has recently been shown to be induced by hypoxia and act on HIFα (Koivunen et al., 2007): this enzyme had previously been postulated as "PHD4" but had not been robustly assigned as a HIF prolyl hydroxylase enzyme (Oehme et al., 2002). P4H-TM bears more sequence similarity to the CP4H enzymes than the PHDs, and is an *N*-glycosylated homodimer located in the endoplasmic reticulum membrane. P4H-TM knock-down and overexpression stimulated and reduced HIFα transcriptional activity respectively, as measured by a reporter assay. The authors suggest that P4H-TM may have specific

functions reflecting its specific cellular localization, and could work in a complementary fashion to the PHDs (Koivunen et al., 2007).

Factors affecting HIF hydroxylase activity

In addition to direct effects, HIF signalling may also be modulated indirectly *via* the activity of the PHDs or FIH, and a range of proteins that interact with and affect the HIF hydroxylases has been reported.

The E3 ligases Siah1a and Siah2 have been shown to earmark PHD1 and PHD3 for proteasomal degradation by ubiquitination, with PHD3 being stabilized in *Siah2*$^{-/-}$ embryonic fibroblasts and an impaired induction of HIF1α in these cells (Nakayama et al., 2004). Siah1 has also been reported to be involved in the ubiquitination and degradation of FIH (Fukuba et al., 2008; Fukuba et al., 2007). The authors suggest that this is a feedback mechanism resulting in hypoxia-dependent FIH degradation and hence enhancing HIF transcriptional activity under oxygen stress. However, this is difficult to reconcile with previous observations that levels of FIH are unaffected by hypoxia (Stolze et al., 2004). PHD2 is also regulated through a proteolytic mechanism through an interaction with the peptidyl prolyl *cis/trans* isomerase enzyme FKBP38 (Barth et al., 2007). FKBP38 suppression with siRNA results in enhanced hydroxylation activity in cell extracts and increased PHD2 half-life. This regulation of PHD2 stability does not appear to form any part of a feedback loop, since FKBP38 is regulated neither by HIF nor by hypoxia.

The protein OS9 interacts with HIF1α, PHD2 and PHD3 and is reported to potentiate the activity of the prolyl hydroxylases, perhaps through the formation of a ternary

complex (Baek et al., 2005). In support of this hypothesis, knock-down of OS9 by RNA interference in 293 cells elicited a modest induction in levels of HIF1α protein. However, the precise physiological relevance of this interaction is unclear.

In addition to proteins, certain small molecules also affect HIF signalling including tricarboxylic acid (TCA) cycle intermediates and reactive oxygen species (ROS). TCA cycle intermediates such as succinate and fumarate appear to inhibit the HIF hydroxylases, as tumours and cell lines from individuals with germline mutations in fumarate hydratase and succinate dehydrogenase show reduced hydroxylase activity and enhanced HIF activity. This effect has been proposed to operate through a direct competitive inhibition of the hydroxylase enzymes as fumarate and succinate are closely structurally related to 2OG (Isaacs et al., 2005; Pollard et al., 2005). Whilst it seems clear that ROS can indeed affect HIF signalling, a definitive role for them in oxygen sensing has yet to be established, and their importance remains a controversial subject (Cash et al., 2007).

The possibility of other substrates for the HIF hydroxylases

Since the discovery of the HIF hydroxylases a great deal of work has gone into efforts to determine whether they have any novel, "non-HIF" substrates, and there is a growing body of evidence to suggest that this may be the case. Studies in *Drosophila melanogaster* show that the single HIF prolyl hydroxylase in that organism is a downstream target of the Cyclin D/Cdk4 complex which induces cell growth and cell proliferation (Frei and Edgar, 2004). In this system it thus appears that the HIF prolyl hydroxylase is a regulator of growth in addition to its role in hypoxia signalling, and may therefore have downstream targets other than HIF. A study of genes regulated by

the pVHL tumour suppressor in *Caenorhabditis elegans* demonstrated that some genes are regulated by EGL9 (the single HIF prolyl hydroxylase in this organism) in a HIF-independent manner, suggesting that EGL9 also has targets other than HIF (Bishop et al., 2004).

Enzymes such as kinases and phosphatases may have a wide range of substrates, for example protein phosphatase 1 type c (discussed in more detail in Chapter 3) whose substrate specificity is determined by binding to regulatory subunits (Alessi et al., 1992). CP4H1 is an example of a 2OG dioxygenase with multiple substrates, given its dual roles in collagen biosynthesis and the regulation of Ago2 stability (Myllyharju, 2003; Qi et al., 2008), and several recent reports suggest that the PHD enzymes may also hydroxylate multiple targets. The rat homologue of PHD3, SM20, was originally identified as a protein with importance in developmental neuronal apoptosis before its assignment as a HIF hydroxylase (Lipscomb et al., 1999; Lipscomb et al., 2001; Straub et al., 2003). A later study in the rat neuronal cell line PC12 indicated that PHD3 was necessary and sufficient for apoptosis, and that this effect required the enzymatic activity of PHD3 but appeared to operate independently of HIF (Lee et al., 2005). Although these results strongly suggest that PHD3 may have an alternative substrate in a pathway related to neuronal apoptosis, none has yet been reported. The possibility of a HIF-independent role for PHD3 is discussed in more detail in Chapter 4.

Several recent studies have claimed direct effects of the PHD enzymes on proteins other than HIF. PHD1 has been proposed to upregulate the activity of the NF-κB signalling pathway in hypoxia by hydroxylation of IKKβ (Cummins et al., 2006), PHD3 has been proposed to regulate the stability of the transcription factor ATF4 (Köditz et

al., 2007) and PHD1 and 2 together have been proposed to regulate the large subunit of RNA polymerase II (Kuznetsova et al., 2003; Mikhaylova et al., 2008). Although these studies all point to the existence of novel PHD substrates, none has demonstrated conclusively through the use of mass spectrometry that prolyl hydroxylation occurs.

The search for non-HIF targets of the asparaginyl hydroxylase FIH has been more fruitful with a family of proteins discovered, many members of which have potential as substrates. This discovery may represent a significant increase in the number of proteins that are known to be post-translationally hydroxylated, and is discussed in the following section.

1.4.3 *Asparaginyl hydroxylation of ankyrin-repeat domain-containing proteins by FIH*

Recent studies have shown that, in addition to its role as a HIF asparaginyl hydroxylase, FIH will also hydroxylate asparaginyl residues in a range of other proteins including p105, IκBα (both of which are proteins of the NF-κB signalling pathway), Notch family members and ASB4, all of which contain an ankyrin repeat domain (ARD) (Cockman et al., 2006; Coleman et al., 2007; Ferguson et al., 2007; Zheng et al., 2008). These post-translational protein hydroxylations have all been demonstrated in the endogenous proteins purified from tissue culture cells, and shown to be FIH-dependent.

ARDs contain varying numbers of 33-residue ankyrin repeats (ARs), consisting of pairs of antiparallel α-helices connected by a β-hairpin loop (Figure 1.5). The ARs stack together to form a protein-protein interaction surface. The ARD is one of the most common motifs in nature, and conserved in all kingdoms of life (Li et al., 2006; Mosavi

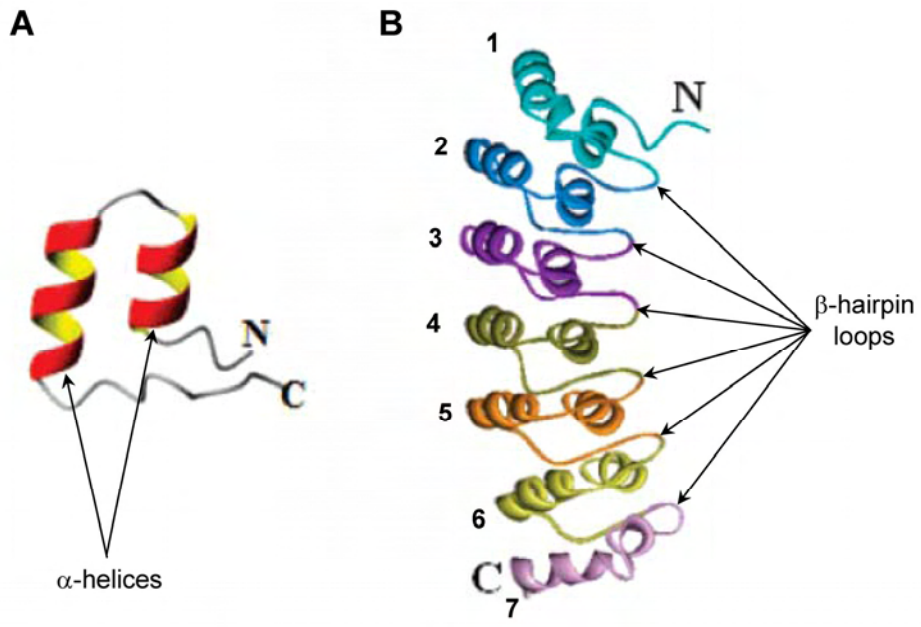


Figure 1.5
Structure of an ankyrin repeat domain (ARD). (**A**) *shows a single ankyrin repeat from gankyrin (which contains a seven-repeat ARD) consisting of two α-helices connected by a short loop.* (**B**) *shows the complete ARD of gankyrin. Individual ankyrin repeats are numbered and coloured differently; the β-hairpin loops that connect individual ankyrin repeats are indicated. Adapted from (Li et al., 2006).*

et al., 2004), with the human genome predicted to contain around 300 such proteins (SMART database, (Schultz et al., 1998)).

Although hypoxia has been shown to influence signalling in both the NF-κB and Notch pathways (Gustafsson et al., 2005; Påhlman et al., 2004; Zampetaki et al., 2004), functional insights into the role of FIH-mediated ARD hydroxylation are limited to date. Zheng *et al.* and Ferguson *et al.* have reported that FIH-dependent hydroxylation is necessary for Notch signalling and ASB4 function respectively. However, it is not clear that these effects depend on the enzymatic activity of FIH as the experiments used proteins with mutated asparaginyl residues that could cause loss-of-function by another mechanism (Ferguson et al., 2007; Zheng et al., 2008). In addition, whilst Zheng *et al.* showed an increase in myogenic differentiation in C2C12 cells when FIH was overexpressed, the same effect was observed with two hydroxylase-defective FIH mutants (H199A and D201A), indicating that this phenomenon does not require the enzymatic activity of FIH (Zheng et al., 2008). Two other studies have used FIH overexpression and suppression to alter the extent of ARD hydroxylation directly and not observed any hydroxylation-dependent effect on either NF-κB or Notch signalling (Cockman et al., 2006; Coleman et al., 2007). The clearest reported function of ARD hydroxylation to date is in the modulation of HIFα CAD signalling: overexpression of the intracellular domain of Notch1 has been shown to enhance the activity of a HIFα CAD reporter gene significantly through competitive inhibition of FIH (Coleman et al., 2007; Zheng et al., 2008).

It is possible that ARD hydroxylation may play a structural rather than a signalling role: comparison of the crystal structures of hydroxylated and unhydroxylated Notch1 ARD

suggests that hydroxylation forms an additional hydrogen bond within the β-hairpin loop, thus potentially enhancing the conformational stability of the targeted ankyrin repeat or the whole ARD (Coleman et al., 2007).

Given that there are over 300 ARD-containing proteins in the human genome, the recent discovery of ARD hydroxylation by FIH may represent a vast increase in the number of known targets of post-translational protein hydroxylation. It also raises a number of questions: how many of these ARD proteins are indeed substrates for FIH, and is it possible to define a consensus motif for hydroxylation and establish how general ARD hydroxylation might be? Is the biological role of ARD hydroxylation structural (as for collagens) or in signalling (as for HIF)? All ARD hydroxylations of endogenous proteins to date have been incomplete, which may imply the latter, although it is unclear if this incomplete hydroxylation is an artefact of the tissue culture conditions used in these studies. Do all ARDs compete with HIF for FIH, and if so what are the implications for modulation of the HIF signalling pathway and cellular oxygen sensing? Much further work will be required to understand the biological role of ARD hydroxylation fully, and studies to investigate some of the questions above form part of this thesis.

1.5 Aims and scope of this thesis

Although until very recently the post-translational hydroxylation of proteins was considered to be uncommon (Walsh, 2006), recent advances in knowledge, especially those regarding the roles of protein hydroxylation in histone demethylation and oxygen sensing, suggest that it is a widespread and important modification with roles both in maintaining protein structure and in cell signalling. The aim of this thesis is to

expand current knowledge of protein hydroxylation by investigating non-HIF substrates of the HIF hydroxylase enzymes.

Chapter 2 describes work undertaken to investigate the sequence and structural determinants of hydroxylation in an established FIH substrate, Notch1. A bioinformatic alignment of known FIH substrates was used to inform the preparation of a series of Notch1 proteins mutated at conserved positions, whilst a set of mutations predicted to have structural effects was also made. These mutant proteins were analysed using quantitative mass spectrometry and binding assays to determine their effects on Notch1 hydroxylation and FIH binding. The effect of the mutations on the ability of Notch1 to compete with HIF in a reporter gene assay was also determined. The identification and characterization of a novel ARD-containing substrate of FIH, myosin phosphatase targeting subunit 1 (MYPT1) is described in Chapter 3, together with studies to investigate whether ARD hydroxylation is a true, *in vivo* phenomenon and whether competitive inhibition of FIH might be a general property of these proteins. Chapter 4 describes work undertaken using a proteomic strategy to investigate the existence of alternative substrates for PHD3, and the characterization of two promising PHD3 candidate substrates.

The techniques used and topics covered are introduced in more detail at the beginning of the respective experimental chapters. The results of each chapter are discussed individually, whilst Chapter 5 discusses common themes and possible future directions for this work.

Chapter 2

Characterization of Notch1 as a substrate for FIH

2.1 Introduction

Notch is a transmembrane receptor protein, the gene for which was discovered in *Drosophila melanogaster* in 1919 by virtue of the "notched" wing margins displayed by flies with a partial loss of function due to haploinsufficiency (Artavanis-Tsakonas et al., 1999; Mohr, 1919). Notch signalling is crucial for a wide range of developmental processes, affecting differentiation, proliferation and apoptosis, and the dysfunction of this pathway has been implicated in a range of cancerous conditions (Artavanis-Tsakonas et al., 1999; Bray, 2006). The number of Notch receptor paralogues varies between species: *Drosophila* has one, *Caenorhabditis elegans* has two and mammals have four (Bray, 2006).

The Notch receptor protein itself is large, at around 300 kDa, and consists of an extracellular domain (ECD) containing 36 tandem EGF-like repeats (see Section 1.3.2) and an intracellular domain (ICD) containing a seven-repeat ARD (Artavanis-Tsakonas et al., 1999). Binding of extracellular Notch ligands (such as Delta and Jagged) to the EGF repeats of the ECD activates the ICD by two sequential proteolytic cleavages: an initial cleavage at the S2 site by an ADAM-family metalloprotease sets the scene for a second cleavage by the γ-secretase complex, which releases the ICD from the cell membrane (Brou et al., 2000; Mumm et al., 2000; Okochi et al., 2002; Schweisguth, 2004). The ICD subsequently enters the nucleus and activates the transcription of Notch target genes including *HES* and *HESR*/*HEY*, which allow cells to respond to environmental stimuli and may maintain a progenitor state or induce differentiation, depending on the cell type and the stimulus (Sainson and Harris, 2006).

Notch proteins have recently been shown to be substrates for the HIF asparaginyl hydroxylase, FIH (Coleman et al., 2007). Three of the four human Notch paralogues, Notch1 – 3, were shown to coimmunoprecipitate with FIH from U2OS cells. Whilst purified glutathione-*S*-transferase (GST)-tagged Notch1 and Notch3 ARD proteins were substrates for FIH *in vitro*, promoting the decarboxylation of 2OG and undergoing hydroxylation, Notch4 was not (Coleman et al., 2007).

The hydroxylation of mouse Notch1 (mN1) has been characterized in detail: the ARD of this protein contains two asparaginyl residues that are targets for FIH, Asn-1945 and Asn-2012 (Coleman et al., 2007). When a construct encoding the ICD of mN1 was overexpressed in 293T cells, immunopurified and analysed by mass spectrometry (MS), levels of hydroxylation were around 35% at Asn-1945 and 3% at Asn-2012; co-expression of FIH (but not a hydroxylase-defective mutant, D201A) with the mN1 ICD protein enhanced levels of hydroxylation at the two sites to 96% and 81% respectively, whilst treatment of 293T cells with FIH siRNA prior to transfecting the mN1 ICD resulted in significantly reduced levels of hydroxylation (7% at Asn-1945, 1.5% at Asn-2012). Further, endogenous human Notch1 was immunopurified from 293T cells and shown to be hydroxylated to almost 100% at Asn-1956 (equivalent to Asn-1945 in the mouse protein); the levels of hydroxylation in Notch1 recovered from cells treated with hypoxia or FIH siRNA were 40% and 25% respectively, clearly demonstrating that this endogenous hydroxylation is FIH-dependent. The crystal structure of FIH complexed with a Notch1 peptide was solved, and showed that Notch1 binds in a similar manner to the HIF1α CAD, with the target asparagine residue at the apex of a sharp turn, surrounded by regions of substrate that adopt a relatively extended

conformation, thus requiring a significant conformational rearrangement of the ARD (Coleman et al., 2007).

Although the FIH-dependent asparaginyl hydroxylation of the Notch1 ARD has been clearly demonstrated, the functional significance of this modification is not fully understood. Recent reports suggest that there is "cross talk" between hypoxia and Notch signalling: in certain stem and precursor cell populations hypoxia causes the undifferentiated state to be maintained and this process appears to be mediated through the activation of Notch signalling (Diez et al., 2007; Gustafsson et al., 2005). Gustafsson *et al.* have further reported that HIF1α and Notch1 interact directly, with HIF being recruited to Notch-responsive promoters under hypoxia, and suggested that FIH can inhibit Notch signalling in certain settings (Gustafsson et al., 2005). However this effect, although reproducible, is non-enzymatic as subsequent studies have shown that hydroxylase-defective mutants of FIH (D201A and H199A) will elicit comparable reductions in Notch activity to wild-type enzyme, and that suppression of FIH by siRNA has no effect on Notch transcriptional activity (Coleman et al., 2007; Zheng et al., 2008). Activation of Notch signalling by the extracellular ligand Delta is not affected by FIH overexpression or suppression, and hydroxylated Notch1 ARD purified *in vitro* shows no differences in binding to Notch partner proteins from unhydroxylated Notch1 ARD (Coleman et al., 2007). It therefore seems highly unlikely on balance that FIH modulates Notch transcriptional activity through direct hydroxylation of the ARD.

Although FIH-dependent hydroxylation does not appear to affect canonical Notch signalling, it has been clearly demonstrated that Notch can act as a competitive FIH inhibitor, thus influencing HIF CAD activity (Coleman et al., 2007). Incubation of a

purified mN1 ARD protein with HIF1α CAD protein and FIH *in vitro* results in a striking inhibition of HIF hydroxylation compared to the incubation of HIF1α CAD and FIH alone, whilst in the converse experiment the addition of HIF1α has little effect on the kinetics of mN1 ARD hydroxylation. Competitive inhibition is also observed *in vivo*: a mN1 ICD protein is a potent inhibitor of HIF1α CAD hydroxylation (as determined by immunopurification and mass spectrometry) when co-transfected with HIF1α CAD into 293T cells, and transfection of Notch1 or Notch3 fragments into HeLa cells leads to an increase in HIF1α CAD transcriptional activity as measured by a reporter gene assay (Coleman et al., 2007).

This chapter describes my investigations to (i) characterize the determinants of Notch1 hydroxylation, with the aim of understanding more about how and when FIH hydroxylates ARD-containing proteins, and (ii) define a consensus for hydroxylation to help in the identification of other candidate hydroxylation sites. *In vitro* kinetic studies on 20-residue peptides containing Asn-1945 and Asn-2012 of mN1 have shown that the Asn-1945 peptide is hydroxylated approximately twice as fast as the Asn-2012 peptide[1], providing evidence that the primary sequence in the vicinity of the target asparagine regulates hydroxylation. In order to begin defining these primary sequence elements necessary for hydroxylation I prepared a series of point mutants based on previous structural analyses (Coleman et al., 2007) and residues that were conserved in a range of aligned FIH substrates. The preparation of these primary sequence mutants is described in more detail in Section 2.2.1 below.

[1] Charlotte Coles and Christopher Schofield, personal communication

It also appears that there may be structural factors that influence Notch hydroxylation. Time-course analyses carried out *in vitro* on a complete Notch1 ARD protein containing both sites of hydroxylation indicate that the kinetics of hydroxylation at Asn-2012 are markedly slower than at Asn-1945. This difference in the rate of hydroxylation is not attributable entirely to the primary amino acid sequence surrounding the two sites of hydroxylation, as isolated 20-residue peptides containing Asn-1945 and Asn-2012 show much less pronounced differences in hydroxylation kinetics[2]. Structural data indicate that target ankyrin repeats must partially unfold and adopt an extended conformation in order to bind FIH and undergo hydroxylation (Coleman et al., 2007). I therefore hypothesized that differences in local stability of ankyrin repeats could explain differences in the level of hydroxylation between target asparagine residues, such as the difference observed between Asn-1945 and Asn-2012.

A range of mutations in *Drosophila* Notch that destabilize the ARD has been reported (Bradley and Barrick, 2002). In order to determine whether these mutations could facilitate unfolding of the individual ankyrin repeats in Notch and consequently enhance hydroxylation at Asn-2012, I tested a series of destabilizing mutant proteins as described in more detail in Section 2.2.4.

The mutant proteins have all been analysed for hydroxylation by quantitative MS, and have been tested in both native and denaturing binding assays to investigate their effects on the interaction between FIH and Notch. All of the mutant proteins have additionally been tested in a reporter gene assay to explore their effects on the efficacy of Notch as a competitive inhibitor of FIH. Finally, in an attempt to discover why

[2] Charlotte Coles and Christopher Schofield, personal communication

Notch is so effective at "out competing" HIF, an investigation has been undertaken to determine the *in vitro* kinetics of Notch1 hydroxylation.

2.2 Results

2.2.1 *Mutation of the primary sequence of Notch1*

In order to identify which residues in the amino acid sequence of Notch1 may be required for hydroxylation by FIH, I aligned the hydroxylation site of HIF1α CAD with sites in a range of ARD-containing proteins which are known to be FIH substrates (Figure 2.1A and B); these were ASB4, Rabankyrin (Ankfy1), IκBα, RNaseL, Tankyrase2, Notch1, Notch2, Notch3 and p105 (Cockman et al., 2006; Cockman et al., 2008; Coleman et al., 2007; Ferguson et al., 2007). This alignment was used to inform the preparation of point mutants of mN1: conserved residues included leucine at the –8 position relative to the target asparagine, alanine at the –3 position, an acidic residue (aspartate or glutamate) at the –2 position, leucine at the +10 position and alanine at the +13 position, suggesting a consensus sequence for hydroxylation of $L_{-8}A_{-3}(D/E)_{-2}NL_{+10}A_{+13}$ (Figure 2.1B). As Asn-1945 is the predominant site of hydroxylation under physiological conditions (Coleman et al., 2007), I focused the mutational analysis on this site. The conserved leucine and aspartate residues were mutated to alanine with the conserved alanine residues being mutated to the much bulkier amino acid phenylalanine.

The crystal structure of FIH interacting with a Notch peptide containing Asn-1945 shows that the side-chain of leucine –8 is buried in a hydrophobic binding pocket on the surface of FIH (Coleman et al., 2007), which taken together with the sequence alignment data further suggests that this residue may be an important determinant of hydroxylation. Additional mutations were made at Leu-1937 in order to investigate the importance of the hydrophobic pocket on the surface of FIH for Notch binding and

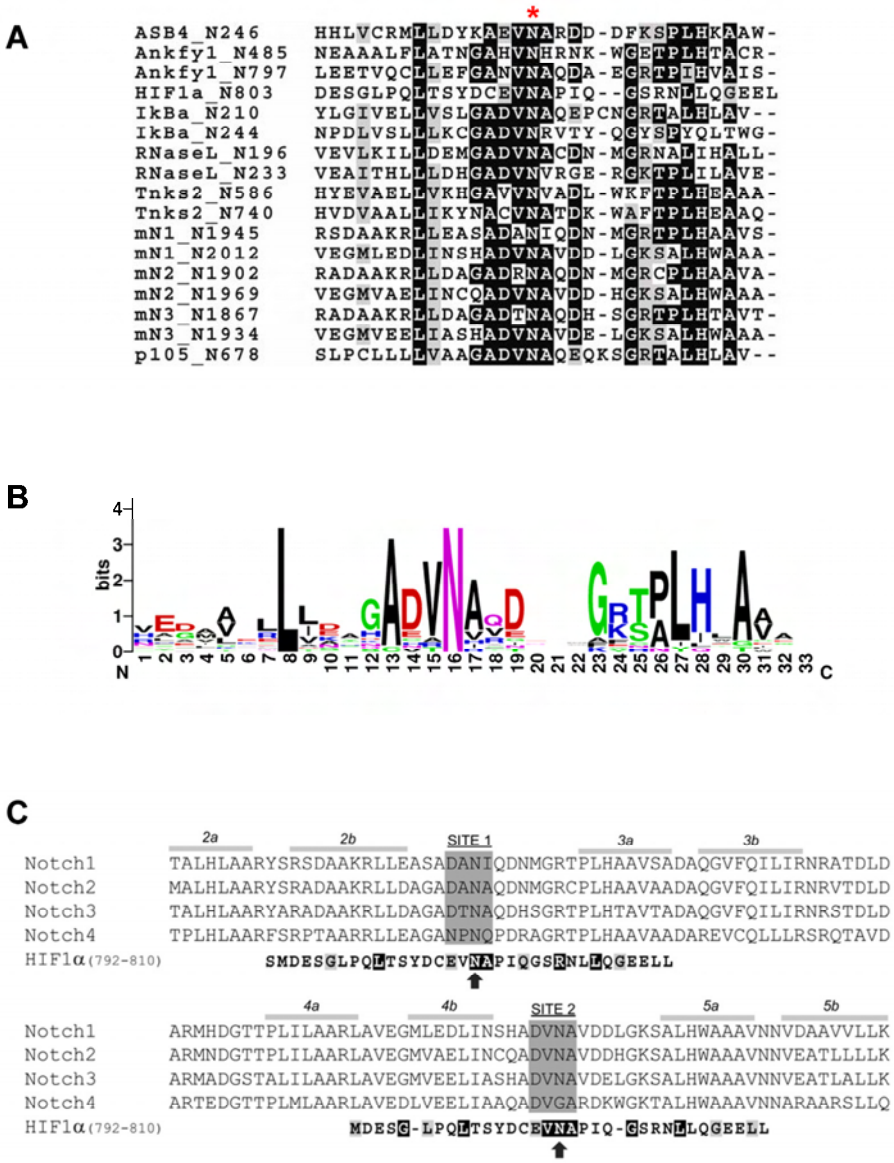


Figure 2.1 ***Alignment of FIH substrates***

(**A**) *Sites of FIH-dependent hydroxylation in ASB4, Rabankyrin (Ankfy1), HIF1α, IκBα, RNaseL, Tankyrase2, Notch1 – 3 (mN1 – 3) and p105 were aligned using the ClustalW2 algorithm. The figure was prepared using BoxShade version 3.21.*

(**B**) *Consensus sequence for the alignment shown in* (**A**)*. Prepared using WebLogo version 2.8.2.*

(**C**) *Alignment of Notch1 – 4, showing sites of hydroxylation relative to the locations of the α-helices of the ankyrin repeats. Ankyrin repeats 2 – 5 are shown, each consisting of two helices, a and b. The sequence surrounding Asn-803 of HIF1α is also shown for comparison.*

catalysis: conservative substitutions to isoleucine and valine (which has a slightly smaller hydrophobic side-chain than leucine and so would be predicted also to fit the binding pocket) were prepared, together with a non-conservative substitution to the larger, positively-charged residue lysine.

The FIH/Notch1 structural studies further show that Notch1 binds to FIH in a largely elongated conformation with Asn-1945 at the apex of a tight turn, requiring the β-hairpin loop in which Asn-1945 is located to extend, and also requiring a significant rotation about the peptide bond connecting Asn-1945 with Ala-1944 (Coleman et al., 2007). This largely extended conformation of the bound Notch1 peptide is interesting in view of the observation that Notch4 does not appear to be a substrate for FIH. In Notch4 the analogous asparagine residue to Asn-1945 of mN1 lies in a "NPNQ" motif (Figure 2.1C). Thus the potential site of hydroxylation in Notch4 is conformationally restricted by a proline residue which would be expected both to prevent the formation of the tight turn at the asparagine residue and to prevent the elongation of the structure either side of the asparagine residue: both these processes appear to be required in order for a Notch substrate to bind FIH and undergo hydroxylation (Coleman et al., 2007). It is also noticeable that Notch4 lacks the acidic residue at the –2 position: this lack of an acidic residue, and the presence of a proline residue at the –1 position, have both been postulated as reasons why Notch4 does not appear to be an FIH substrate (Coleman et al., 2007). I therefore also mutated Ala-1944 in Notch1 to proline, which together with the alanine mutation at Asp-1943 (prepared based on the sequence alignment) would enable me to determine whether either of these factors explains why Notch4 is not an FIH substrate.

Structural evidence on the binding of a HIF1α peptide to FIH indicates that there are two distinct binding sites, termed site 1 and site 2 (Elkins et al., 2003). Site 1 involves the hydroxylation site itself, whilst site 2 is a secondary interaction involving a region of the HIF1α CAD around 10 residues C-terminal to the substrate asparagine, Asn-803, that adopts an α-helical structure upon binding to FIH. Although HIF peptides containing only site 1 are substrates for FIH, the presence of site 2 enhances the efficiency of asparaginyl hydroxylation (Elkins et al., 2003). Both Asn-1945 and Asn-2012 of Notch1 have α-helical ankyrin-repeat regions approximately the same distance from the site of hydroxylation (Figure 2.1C). In order to determine whether these "site 2" α-helices are required for Notch hydroxylation by FIH I mutated Pro-1954 to alanine and leucine: both of these mutations are predicted to destabilize the α-helix, with the P1954L mutant having a stronger effect than the P1954A mutant due to the steric bulk of the larger leucine side-chain. A full list of the mutations made is shown in Table 2.1: all were prepared in a construct encoding residues 1751 – 2191 of mN1 with a C-terminal V5 epitope tag (ΔmN1^{ICD}, (Coleman et al., 2007)).

2.2.2 *Analysis of the primary sequence determinants of mN1 hydroxylation*

Having made the mutant mN1 proteins, I next analysed the effects that these mutations had on the hydroxylation of Notch *in vivo*. Wild-type and mutant ΔmN1^{ICD} plasmids were co-transfected into 293T cells along with FIH or empty vector (EV) as a control; the mN1:FIH/EV ratio was 4:1. After 48 h cells were lysed and the epitope-tagged mN1 proteins immunoprecipitated using anti-V5 resin. The immunopurified proteins were resolved by SDS-PAGE, stained with Coomassie blue and the Notch-containing bands excised. Proteins were digested with trypsin, and the resulting

peptides eluted and analysed by quantitative liquid chromatography-mass spectrometry (LC-MS), as described below.

Figure 2.2A shows a typical liquid chromatogram for a tryptic digest of the ΔmN1^{ICD} protein. Extracted ion chromatograms (EICs), showing only species of a specific mass-to-charge ratio (m/z) were prepared to investigate the extent of hydroxylation at either Asn-1945 ("DANI") or Asn-2012 ("DVNA") as appropriate. Previous work in this laboratory using a combination of LC-MS and tandem MS had established the mass spectrometric characteristics of the tryptic peptides containing both Asn-1945 and Asn-2012 (Coleman et al., 2007); for a detailed discussion of the experiments necessary to characterize peptides containing target asparagine residues in a newly-defined substrate, see Chapter 3 on MYPT1. As both the DANI and DVNA tryptic peptides contained a methionine residue, which is often subject to artefactual oxidation during sample preparation (Kinter and Sherman, 2000), each peptide was observed in three mass states: unoxidized, singly-oxidized (either at methionine or at asparagine) or doubly-oxidized (both methionine and asparagine). Peptide sequencing using tandem MS had shown that methionine oxidation had a significant effect on the time at which a peptide eluted from the LC column, whereas asparaginyl hydroxylation did not: methionine-oxidized peptides eluted several minutes earlier than their unoxidized counterparts, whilst asparaginyl hydroxylation caused a shift in elution time of less than one minute (Figure 2.2B(i) and 2.2C(i)). The raw mass spectra for each peptide observed in the EICs were also interrogated to confirm that the peptides had the expected mass and charge: because of the number of atoms a peptide contains and the natural isotopic distributions of elements such as carbon (98.89% ^{12}C, 1.10% ^{13}C

Feature	Mutation
Leucine –8	L1937A
	L1937I
	L1937K
	L1937V
Alanine –3	A1942F
Aspartate/Glutamate –2	D1943A
Leucine +10	L1955A
Alanine +13	A1958F
"Notch4-like" proline	A1944P
"Site 2" α-helix	P1954A
	P1954L

Table 2.1 ***Primary sequence mutations made in mN1***

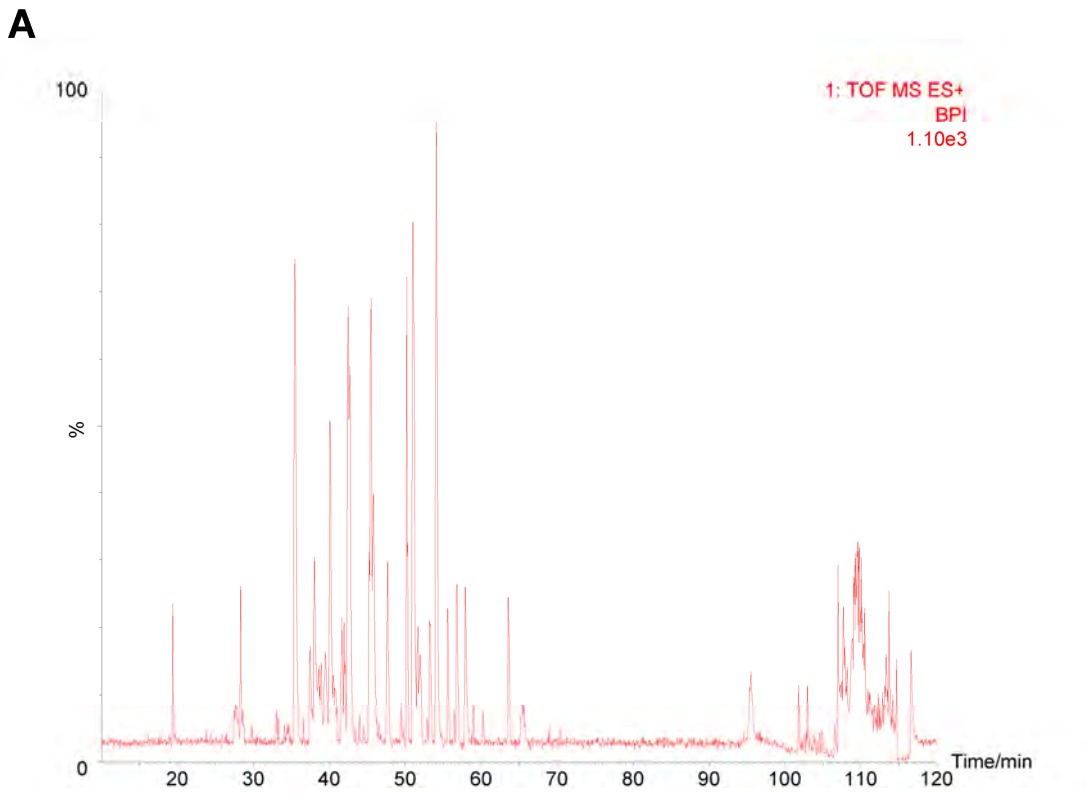


Figure 2.2 ***Analysis of Notch1 hydroxylation by quantitative MS (i)***
(**A**) *Representative total LC-MS chromatogram for a tryptic digest of the* $\Delta mN1^{ICD}$ *protein from an SDS-PAGE gel band.*

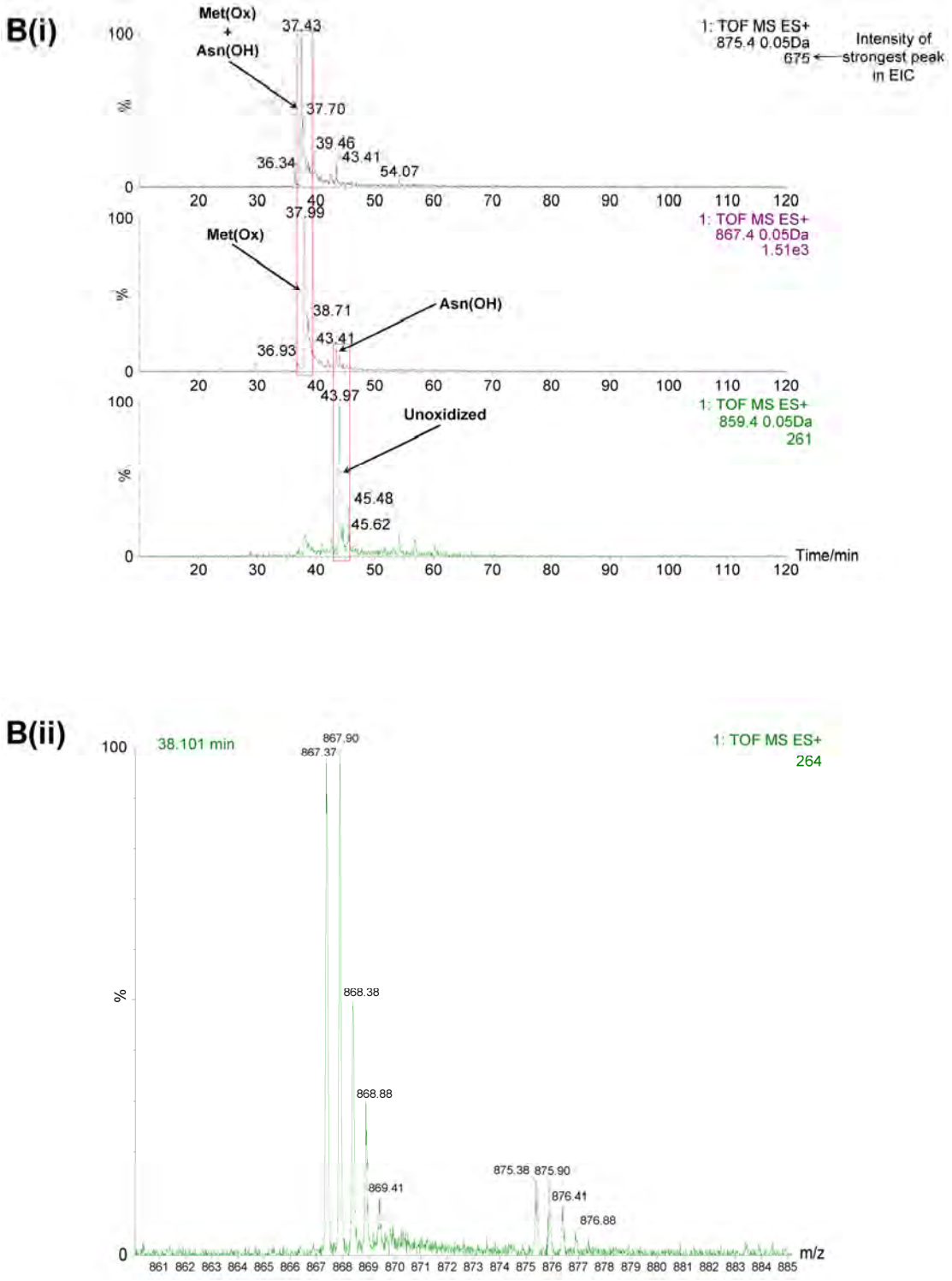


Figure 2.2 ***Analysis of Notch1 hydroxylation by quantitative MS (i)***
(**B**(**i**)) *Representative EIC traces for the three mass states observed for the tryptic peptide containing Asn-1945 (see text for a detailed explanation). Peptide pairs used for quantitation are shown boxed.*
(**B**(**ii**)) *Representative raw MS data for the doubly-charged, singly-oxidized Asn-1945-containing tryptic peptide.*

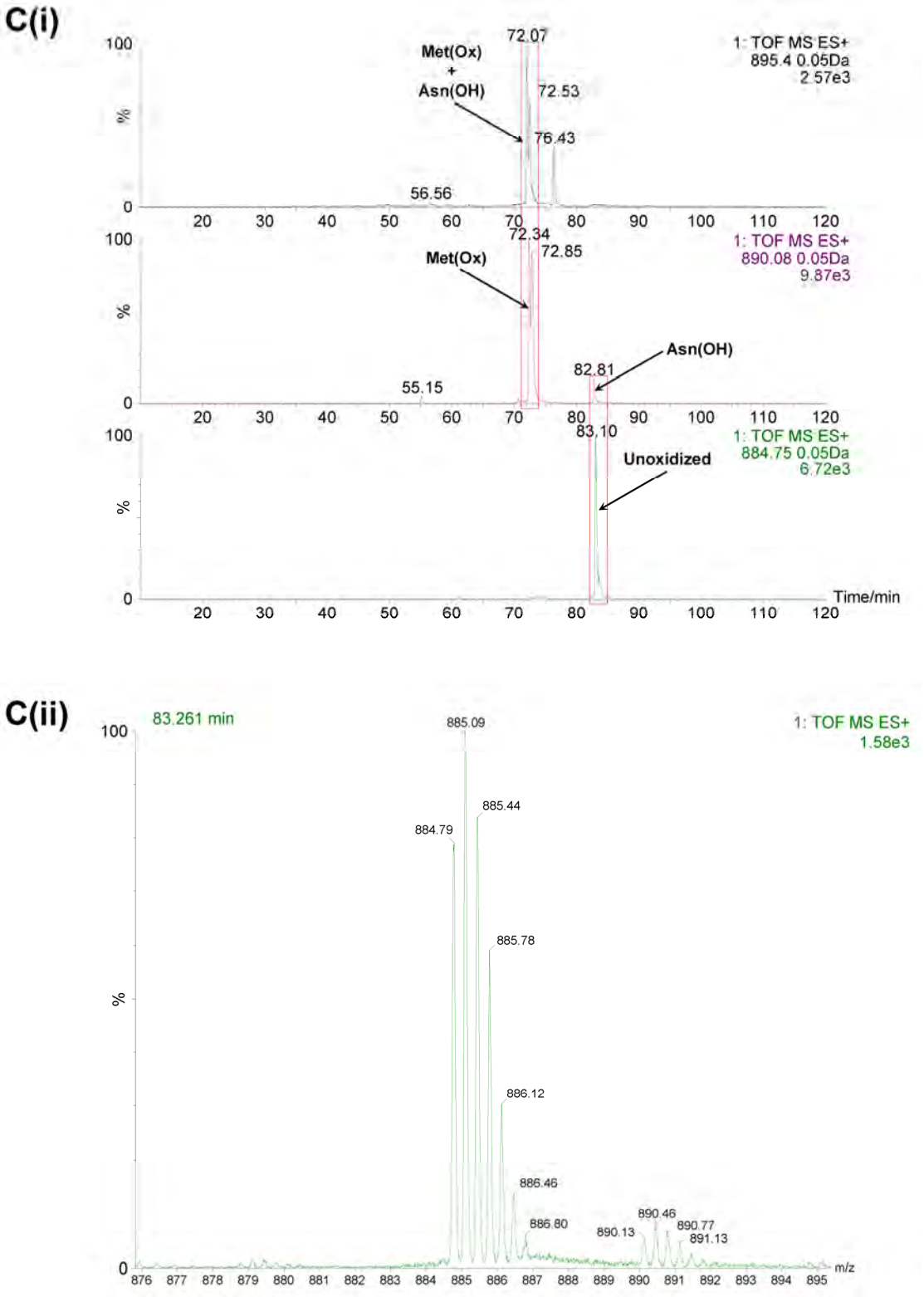


Figure 2.2 ***Analysis of Notch1 hydroxylation by quantitative MS (i)***
(**C**(**i**)) *Representative EIC traces for the three mass states observed for the tryptic peptide containing Asn-2012 (see text for a detailed explanation). Peptide pairs used for quantitation are shown boxed.*
(**C**(**ii**)) *Representative raw MS data for the triply-charged, singly-oxidized Asn-2012-containing tryptic peptide.*

plus traces of other isotopes) and nitrogen (99.63% ^{14}N, 0.37% ^{15}N (Kaye and Laby, 1973)) a given peptide actually exists as a range of different species which differ from each other in mass by 1 Da. This is reflected in the mass spectra of peptides, which also consist of a series of isotopic peaks. However, because a mass spectrometer measures m/z and not simply mass, the separation between these isotopic peaks in the mass spectrum is dependent on the charge borne by the peptide ion: thus a 1+ peptide ion will appear as a series of peaks separated by 1 Da, a 2+ peptide ion as a series of peaks separated by 0.5 Da, a 3+ peptide ion as a series of peaks separated by 0.33 Da, and so on.

For the wild-type DANI tryptic species, m/z values observed for the unoxidized, singly-oxidized and doubly-oxidized peptides were 859.4 Da, 867.4 Da and 875.4 Da respectively (Figure 2.2B(i)). As expected, two peaks were observed in the EIC of 867.4 Da m/z (Figure 2.2B(i), centre panel); the asparaginyl-hydroxylated peptide eluted at around 43 minutes, whilst the methionine-oxidized peptide eluted earlier at around 38 minutes. This peptide was seen with a +2 charge, so the raw MS data were checked to ensure that the species seen in the EIC had the expected mass and charge: Figure 2.2B(ii) shows the raw MS data at 38.101 minutes from the EIC traces in Figure 2.2B(i). As expected, two species are seen, one with m/z 867.37 Da and a charge of +2 and another with m/z 875.38 Da, also with a +2 charge.

The corresponding m/z values for the unoxidized, singly-oxidized and doubly-oxidized DVNA peptide were 884.75 Da, 890.08 Da and 895.4 Da respectively (Figure 2.2C(i)). Again, two peaks were observed in the EIC of 890.08 Da m/z, with the methionine-oxidized species eluting at around 72 minutes and the asparagine-hydroxylated species

eluting at around 82 minutes (Figure 2.2C(i), centre panel). The DVNA peptide was seen with a +3 charge, which was confirmed by analysis of the raw MS data: Figure 2.2C(ii) shows the data at 83.261 minutes from the EIC traces in Figure 2.2B(i). As expected, in this spectrum peptides with m/z values of 884.79 Da and 890.13 Da are observed, both with a charge of +3.

Once the peptides in the EICs had been identified and assigned, the percentage hydroxylation at the DANI and DVNA sites was estimated using the relative intensities of the asparagine-hydroxylated and asparagine-unoxidized peaks (either one of the two pairs shown in red boxes in Figure 2.2B(i) and 2.2C(i)).

The primary sequence mutants were analysed in two sets: in both cases the level of hydroxylation at Asn-1945 was quantitated with endogenous levels of FIH and also with FIH overexpression (Figure 2.3). With endogenous levels of FIH, the wild-type protein was hydroxylated to around 50% (Figure 2.3A). Of the mutations made to Leu-1937 (the leucine –8 residue relative to Asn-1945), L1937A reduced hydroxylation, with a much more pronounced reduction for L1937K where hydroxylation at Asn-1945 was only 5%. The conservative substitutions L1937I and L1937V, and the D1943A mutation were all well tolerated, whilst mutation of the leucine +10 residue, L1955A, also resulted in a reduction in hydroxylation (Figure 2.3A). Overexpression of FIH rescued all of these effects, resulting in >95% hydroxylation in all cases except for L1937K, where hydroxylation was 86% (Figure 2.3A).

In the second experiment, the wild-type protein was hydroxylated to approximately

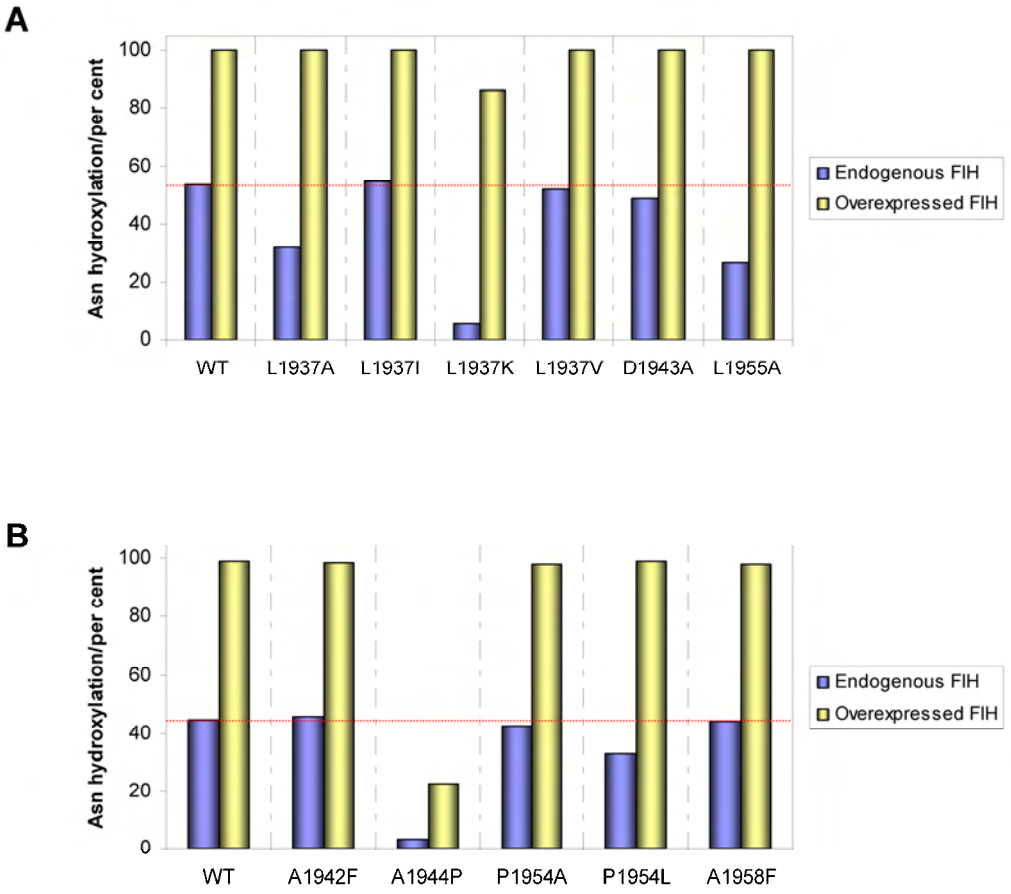


Figure 2.3 ***Analysis of mN1 mutant hydroxylation by quantitative MS (ii)***
293T cells were co-transfected with the indicated ΔmN1^{ICD} mutant construct plus FIH or empty vector control in a 4:1 ratio. After 48 h cells were lysed and the mN1 proteins immunopurified, resolved by SDS-PAGE, stained with Coomassie blue and digested using trypsin. Digests were analysed by LC-MS and levels of hydroxylation quantitated as shown in Figure 2.2. (**A**) *shows the first set of mutations analysed, whilst* (**B**) *shows the second set.*

45% with endogenous levels of FIH (Figure 2.3B). The A1942F, P1954A, P1954L and A1958F mutants all showed no large differences in hydroxylation from the wild-type protein either with endogenous or overexpressed FIH. However, in the A1944P mutant hydroxylation was strikingly compromised: Asn-1945 was hydroxylated only to 3% with endogenous FIH, and even with FIH overexpression the level of hydroxylation was only 22%, compared to nearer 100% with every other mutant protein tested (Figure 2.3B).

In summary, these results demonstrated that a hydrophobic residue is required at the –8 position, and that the presence of a leucine residue at the +10 position also appears to be of some importance for hydroxylation. The introduction of a proline residue at the –1 position inhibited hydroxylation, explaining why Notch4 is not an FIH substrate. The loss of an alanine at the –3 position, an acidic residue at the –2 position and alanine at the +13 position had no effect in this assay, suggesting that these are not important determinants of FIH-dependent hydroxylation in an intact ARD.

2.2.3 *Analysis of the effects of Notch1 mutations on binding to FIH*

In order to investigate how the differences in asparaginyl hydroxylation between the mutant proteins were related to their ability to bind FIH, I analysed the binding of mN1 ARD mutants to FIH *in vitro*. Mutant mN1 ARD proteins, containing residues 1898 – 2105 of mN1 with an N-terminal glutathione *S*-transferase (GST) tag were prepared and purified from *Escherichia coli*: these were analysed by SDS-PAGE and purity estimated at >95% (Figure 2.4).

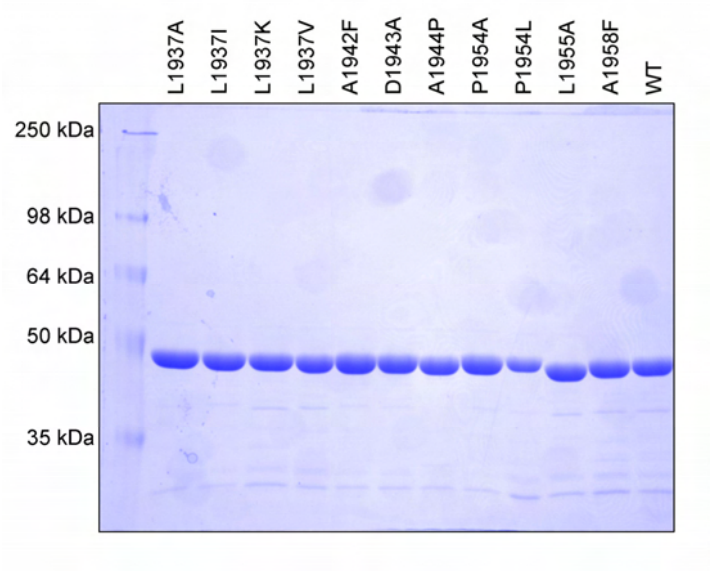


Figure 2.4 ***Purification of GST-tagged mN1 ARD primary sequence mutants***
GST-tagged mN1 ARD mutants were expressed in E. coli *and purified using GST resin. Proteins were eluted using a buffer containing 10 mM glutathione and dialysed overnight against a large volume of PBS. After dialysis mutants were recovered and analysed by SDS-PAGE and Coomassie blue staining: all proteins were estimated to be >95% pure.*

I used two different assays to analyse the binding of the GST-mN1 ARD mutants to FIH: the first was a GST-pulldown assay under native conditions, in which the purified GST-mN1 ARD proteins were bound to Glutathione Sepharose 4 Fast Flow ("GST resin") and the coated GST resin subsequently incubated with purified FIH with an N-terminal His_6-tag (His_6-FIH).

As a first step towards optimizing the conditions to use for the GST pulldown assay, 5 µg wild-type mN1 ARD was bound to 50 µl GST resin in Jie's buffer containing 100 mM NaCl. After washing, the protein-coated resin was divided between five fresh tubes and each aliquot of resin incubated with 1 µg His_6-FIH in Jie's buffer containing NaCl concentrations between 100 and 500 mM. After washing with Jie's buffer containing the indicated NaCl concentration, proteins binding to the GST resin were eluted using 2× SDS-PAGE sample buffer; 10% of the eluate was analysed for bound His_6-FIH by immunoblotting using an antibody against the His_6-tag, whilst 50% of the eluate was resolved by SDS-PAGE and stained using Coomassie blue as a loading control (Figure 2.5A). This experiment demonstrated that at a salt concentration of 500 mM a readily-detectable (but non-saturating) percentage of the His_6-FIH was bound to the GST-mN1 ARD. This salt concentration was therefore selected for all further GST pulldown assays.

In order to determine how robust the GST pulldown assay was over a range of His_6-FIH concentrations, three separate experiments were carried out. In each case, 1 µg of the indicated GST-mN1 ARD mutant (or GST alone as a control) was bound to 10 µl GST resin, washed and then incubated with 100 ng, 1 µg or 10 µg His_6-FIH (Figures

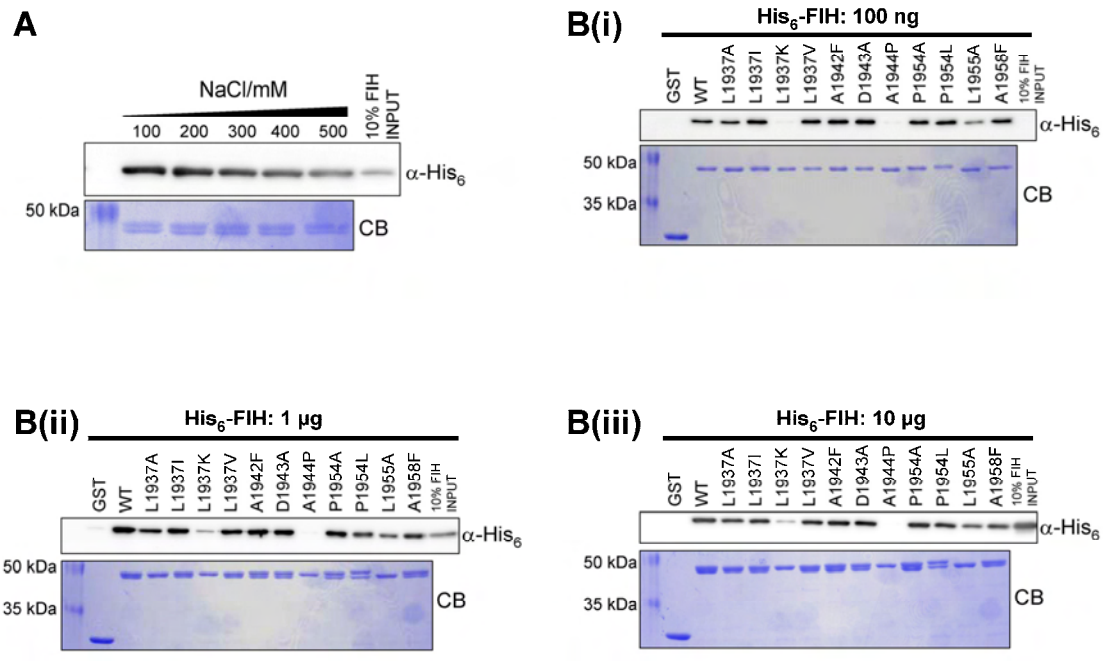


Figure 2.5 *GST-pulldown assays for mN1 mutant binding to FIH*
(**A**) *1 µg GST-mN1 ARD protein was bound to GST resin, which was washed and incubated with 1 µg His_6-FIH in Jie's buffer containing the indicated NaCl concentration. After washing using Jie's buffer containing the same salt concentration, proteins were eluted in 2× SDS-PAGE sample buffer. Bound His_6-FIH was determined by immunoblotting using an anti-His_6 antibody. Eluates were also analysed by SDS-PAGE and Coomassie blue staining (CB) as a loading control.*
(**B**) *1 µg of the indicated GST-mN1 ARD protein was bound to GST resin, which was washed and incubated with the indicated amount (100 ng, 1 µg or 10 µg) of His_6-FIH in Jie's buffer containing 500 mM NaCl. After washing in the same buffer, bound proteins were eluted in 2× SDS-PAGE sample buffer. Bound His_6-FIH was determined by immunoblotting using an anti-His_6 antibody. Eluates were also analysed by SDS-PAGE and Coomassie blue staining (CB) as a loading control.*

Note that in some lanes of the loading controls doublets appear due to the co-precipitation of Coomassie blue-stainable amounts of FIH with the GST-mN1 ARD protein.

2.5B(i), (ii) and (iii) respectively). After washing, bound proteins were eluted in 2× SDS-PAGE sample buffer and analysed by immunoblotting and SDS-PAGE as before.

The effects on binding seen in this assay were essentially constant across a hundred-fold range of His_6-FIH concentrations (Figure 2.5B). Variable effects were seen for mutation at the leucine –8 position, showing that although some mutations here are tolerated, others are not: L1937A had little effect (Figure 2.5B(i)) or caused a very modest reduction in binding (Figures 2.5B(ii) and (iii)) compared to the wild-type GST-mN1 ARD, whilst L1937I and L1937V mutations were completely tolerated. However, mutation to the positively-charged residue lysine (L1937K) virtually abolished binding of the GST-mN1 ARD to FIH, consistent with the dramatic reduction in hydroxylation at Asn-1945 observed with this mutant (Figure 2.3A). This result suggests that, although a leucine may not be essential, a hydrophobic residue is required at this position for binding to FIH. Consistent with the hydroxylation data, the A1942F and D1943A mutants had no effect on binding relative to the wild-type protein, indicating that neither an alanine residue at the –3 position nor an acidic residue at the –2 position are required in order for an ARD protein to bind FIH. Also in accordance with the hydroxylation data (Figure 2.3B), the A1944P mutation showed no detectable binding to FIH, indicating that the ability of the primary sequence immediately adjacent to Asn-1945 to adopt the correct conformation in the active site may be essential for binding to FIH and subsequent hydroxylation. The P1954A and P1954L mutations, predicted to disrupt the α-helix immediately C-terminal to the target asparagine, did not have striking effects on FIH binding. Consistent with a slight reduction in hydroxylation (Figure 2.3), the P1954L mutation may have caused a small reduction in binding (Figure 2.5B(ii)), although this effect was not robust. Mutation of the leucine

residue at the +10 position, L1955A, consistently showed a modest reduction in binding, whilst mutation of the alanine residue at +13 (A1958F) had no appreciable effect. The data from this binding experiment were therefore completely consistent with the hydroxylation data.

In order to confirm the binding of the Notch1 mutant proteins to FIH in a different setting, I developed a far-western assay to determine the binding of FIH to denatured ARD mutants. This assay is similar in principle to an immunoblot, but with a recombinant protein used for the initial incubation instead of a primary antibody, and has been used successfully to investigate the binding of pVHL to HIFα subunits (Ohh et al., 2000). The GST-mN1 ARD proteins were resolved by SDS-PAGE in duplicate and electroblotted onto polyvinylidene fluoride membranes. One membrane was then incubated with blocking solution (see Chapter 6) containing 1 μg ml^{-1} His_6-FIH and the second membrane incubated with blocking solution alone as a control for non-specific antibody binding. After washing, the bound FIH on the membrane was visualized using an anti-His_6 HRP-conjugated antibody and the membrane stained using Coomassie blue as a loading control (Figure 2.6A). The control membrane was also probed, and showed that there was no non-specific binding of the anti-His_6 antibody to the membrane in this experiment (Figure 2.6B).

The far-western assay showed some interesting differences from the GST pulldown assay (Figure 2.6A). Although the L1937A and V mutations were both well tolerated in the GST pulldown assay, L1937A showed a striking reduction in FIH binding in the far-western assay and L1937V showed a modest, but noticeable, reduction in binding

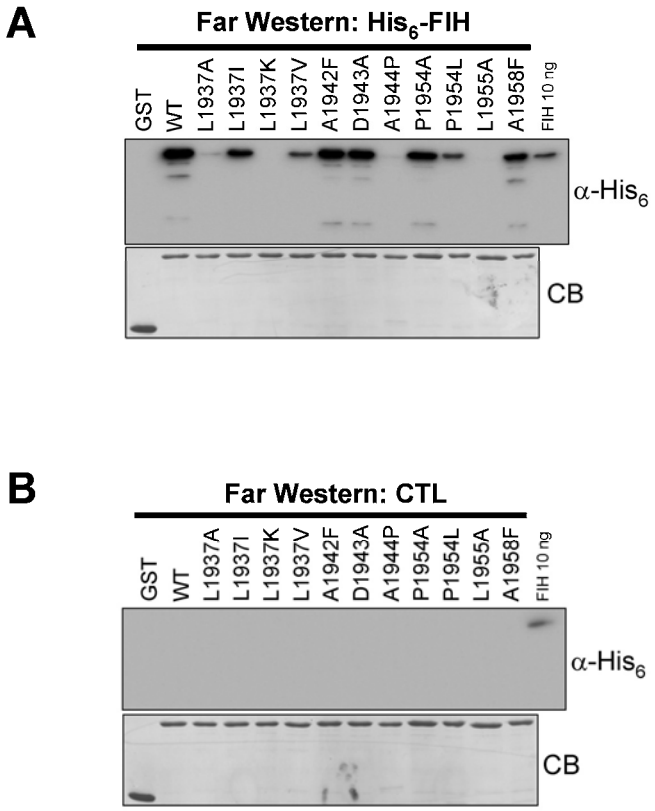


Figure 2.6 ***Far-western blotting assay for mutant mN1 binding to FIH***
200 ng of the indicated GST-mN1 ARD protein was resolved by SDS-PAGE and electroblotted onto PVDF membranes in duplicate. One membrane was incubated with His_6-FIH at 1 μg ml^{-1} in blocking solution (**A**)*, the other membrane was incubated with blocking solution alone as a control* (**B**)*. Bound FIH was visualized by immunoblotting using an anti-His_6 antibody. Membranes were Coomassie blue-stained (CB) as a loading control.*

compared to the wild-type protein. The effect of the L1937K mutation in the far-western assay was even more pronounced than in the GST pulldown experiment, with no detectable binding of this protein to FIH. In agreement with the GST pulldown data, the A1942F and D1943A mutations had no appreciable effect on FIH binding in the far-western, whilst the A1944P mutation again resulted in a near-complete loss of binding, demonstrating that even when this mN1 ARD protein was fully denatured the presence of the proline residue at the –1 position still prevented it from adopting the conformation necessary for FIH binding. Consistent with the modest effects on hydroxylation and variable effects in the GST pulldown assay, the P1954L mutant showed a reduction in binding compared to the wild-type protein. Since the mN1 ARD protein on the membrane was denatured, this is likely to reflect a specific primary-sequence effect on binding rather than an effect of destabilizing the α-helix adjacent to Asn-1945. This result implies that, at least in the far-western assay, there may be a specific requirement for a relatively small residue at this position, and that the larger side-chain of the leucine residue sterically hinders binding of Notch1 to FIH in the absence of the structured ARD. In support of this argument, the P1954A mutation did not influence binding in this assay. Strikingly, in this setting the L1955A mutant almost completely ablated binding of the mN1 ARD to FIH, compared to the GST pulldown assay in which binding was only slightly reduced. The A1958F mutant also showed a modest effect on binding in the far-western assay, which was not observed in the GST pulldown experiment.

The more profound effect of mutation in the far-western assay relative to the native GST pulldown assay is consistent with the existence of positive factors that promote binding of the native ARD to FIH, which are lost in the context of a denatured ARD.

The identity of these "positive factors" is unclear, but could include specific residues distal to the hydroxylation site, or structured regions within the ARD. The assays also showed that Asn-1945 was the preferred site of binding for FIH under these sets of conditions, as point mutations proximal to Asn-1945 (for example A1944P and L1937K) were sufficient to ablate binding completely.

2.2.4 *Mutations to investigate the structural determinants of Notch1 hydroxylation*

Mutation of certain alanine residues to glycine in ankyrin repeats 2 – 7 of *Drosophila* Notch has been shown to have a highly destabilizing effect on the protein: although the mutants retain their secondary and tertiary structures, they are more susceptible to unfolding in response to rises in temperature or the presence of chemical denaturants such as urea (Bradley and Barrick, 2002). Unfolding of the *Drosophila* Notch ARD is highly cooperative, enabling a mutation in a single ankyrin repeat to affect the conformational stability of the entire ARD (Bradley and Barrick, 2002). These alanine residues (indicated with red asterisks in Figure 2.7) are well conserved between species, from *Drosophila* to human.

Given that the binding of the Notch1 ARD to FIH appears to involve a significant conformational rearrangement in Notch (Coleman et al., 2007), and that Asn-2012 hydroxylation appears structurally repressed, I hypothesized that a destabilization of the ARD structure might facilitate this rearrangement and enhance the extent of Asn-2012 hydroxylation. In order to test this theory, I mutated the equivalent six alanine residues (Ala-1926, Ala-1958, Ala-1992, Ala-2025, Ala-2058 and Ala-2091) in the ΔmN1^{ICD} construct to glycine. GST-mN1 ARD vectors containing all six mutations were also prepared.

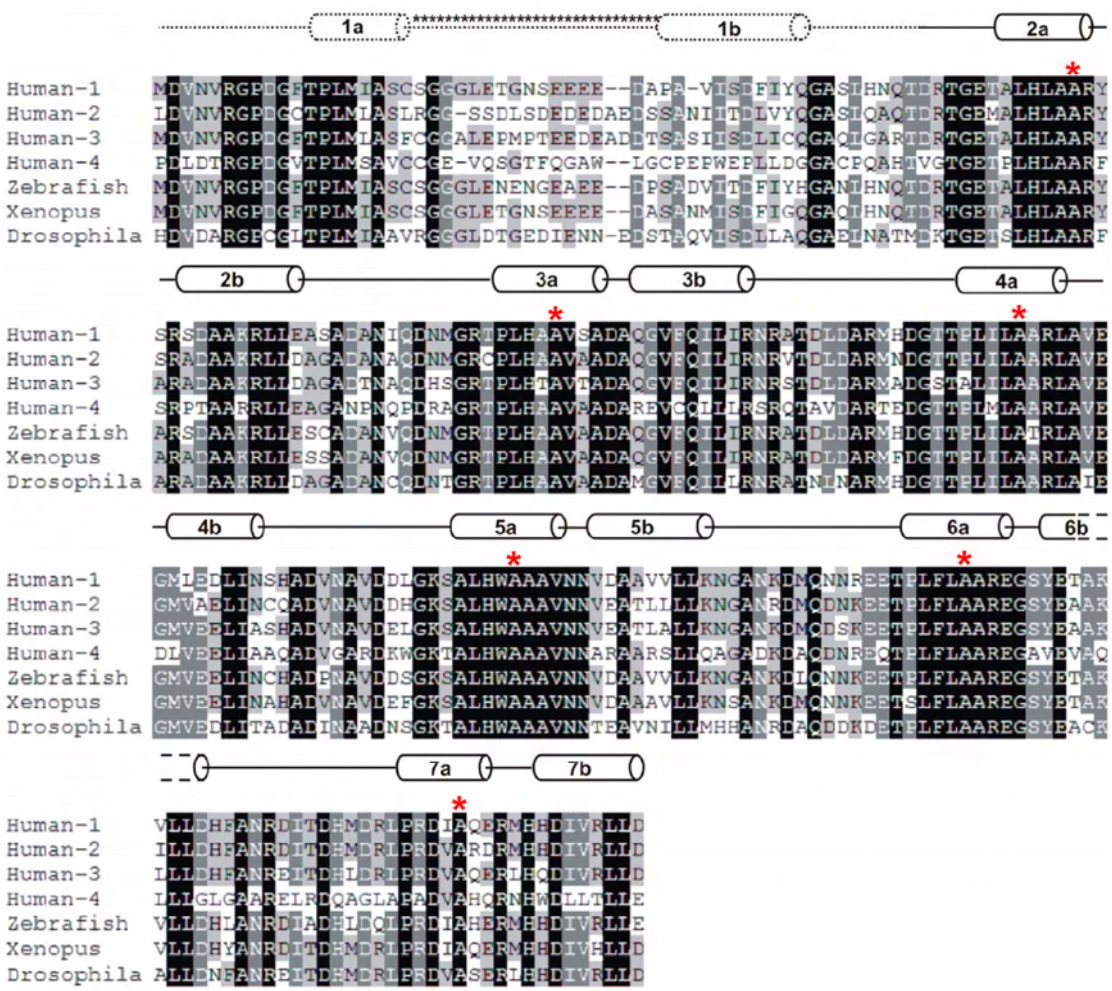


Figure 2.7 *Destabilizing mutations in* Drosophila *Notch*
Alignment showing the amino acid sequences of human Notch paralogues along with zebrafish, Xenopus *and* Drosophila *Notch proteins. The conserved alanine residues mutated to glycine by Bradley and Barrick are indicated with red asterisks (Bradley and Barrick, 2002). Adapted from (Lubman et al., 2004).*

2.2.5 *Analysis of the thermal stability of Notch1 structural mutants by circular dichroism*

In order to determine whether the alanine-to-glycine substitutions had the same effect in mN1 as had been reported for *Drosophila* Notch 1 expressed GST-mN1 ARD proteins containing these mutations in *E. coli*. After the GST-mN1 proteins were purified, the GST-tags were cleaved using thrombin and the purified proteins analysed by SDS-PAGE: all were estimated to be >95% pure (Figure 2.8). The cleaved mN1 ARD proteins were then analysed by circular dichroism (CD) spectroscopy.

Plane-polarized light can be considered to consist of two circularly-polarized components of equal and opposite magnitude which "corkscrew" their way through space: one of these components can be envisaged as a left-handed helix, the other as a right-handed helix. The CD effect is observed if a sample through which the light passes differentially absorbs one of these circularly-polarized components. This may occur if a chromophore is itself chiral, if a chromophore is covalently linked to a chiral centre, or if a chromophore is itself symmetric but placed in an asymmetric environment by virtue of the three-dimensional structure of the molecule surrounding it (Kelly et al., 2005). A CD spectrometer measures the difference in absorbance between the left- and right-handed circularly-polarized components and reports this difference in terms of the ellipticity, θ, in degrees (or, commonly, millidegrees, m deg). In proteins, chromophores of interest include the peptide bonds between amino acid residues (which absorb below 240 nm), aromatic side-chains such as phenylalanine and tyrosine (which absorb in the range 260 – 320 nm) and disulfide bonds (which absorb weakly at around 260 nm) (Kelly et al., 2005).

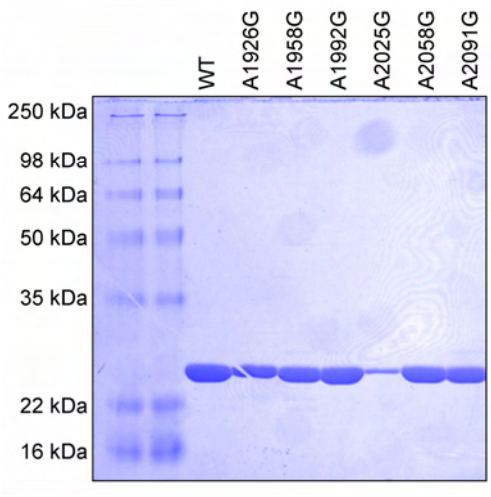


Figure 2.8 ***Preparation of untagged Notch1 ARD structural mutants***
The indicated GST-mN1 ARD proteins were purified using GST resin, and cleaved from the resin using thrombin. Following cleavage, further incubations were performed with p-*aminobenzamidine resin to remove thrombin, and GST resin to remove GST and uncleaved protein contaminants. Protein samples were dialysed overnight against a large volume of PBS, recovered and analysed by SDS-PAGE and Coomassie blue staining; they were estimated to be >95% pure.*

Different protein secondary structures have distinctive CD spectra: Figure 2.9A shows a schematic diagram of typical CD spectra for an α-helical structure and an unfolded, random coil between approximately 200 and 250 nm (Kelly et al., 2005). The spectrum for an α-helical protein has a double-minimum, at 207 and 222 nm. The secondary structure of ARD proteins is principally α-helix, whilst a denatured, unfolded ARD adopts a random coil structure. This means that the temperature- or denaturant-induced unfolding (or "melting") of an ARD can be monitored by following the ellipticity at 222 nm: as the protein unfolds, the magnitude of the ellipticity at 222 nm decreases, reflecting the transition from α-helix to random coil (Figure 2.9A, blue arrow). Measuring the ellipticity at 222 nm as a function of temperature gives a sigmoid melt curve with a point of inflexion: by definition the temperature at this point of inflexion is the melting temperature, T_m (Figure 2.9B). The melt curve is commonly represented as a curve showing the percentage of folded protein, where the ellipticity at the start of the melt is taken as corresponding to 100% folding (Figure 2.9C).

The melting temperatures of the cleaved mN1 ARD proteins were determined by CD spectroscopy as described above: three melts were carried out for each mutant, following which melting curves were fitted to the data using a two-state model for unfolding (Greenfield, 2004) and used to derive the T_m values. Representative melting curves for each mutant protein are shown in Figure 2.10A, whilst the mean melting temperatures (determined from three independent repeat melting experiments) are shown in Figure 2.10B. These experiments showed that three of the structurally destabilizing mutations, A2025G, A2058G and A2091G reduced the melting temperature of the ARDs by 10 – 13 °C when compared to the wild-type protein (Figure 2.10B).

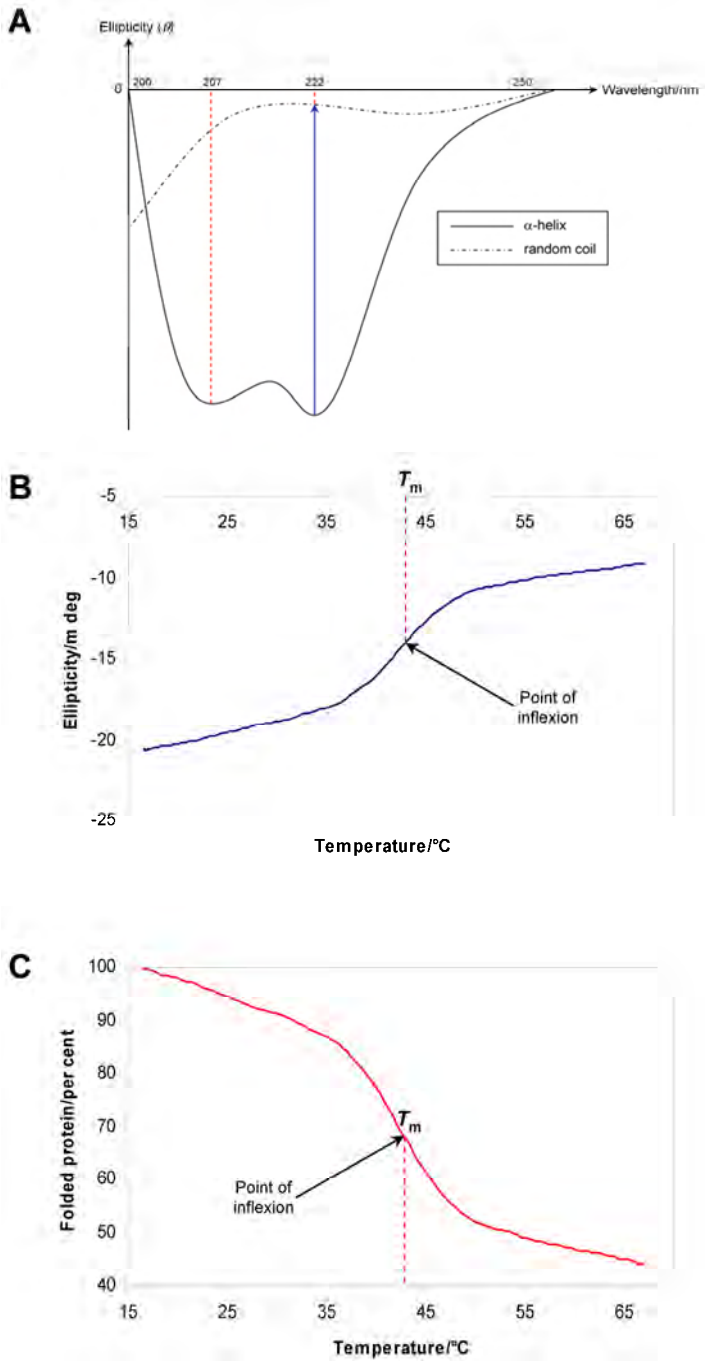


Figure 2.9 ***Analysis of ARD melting temperatures by CD spectroscopy (i)***
(**A**) *Schematic CD spectra between 200 and 250 nm for α-helical and unfolded, random coil protein secondary structures. The α-helical structure has distinctive double minima at 207 and 222 nm. Adapted from (Kelly et al., 2005).*
(**B**) *Representative melting curve for a single mN1 ARD mutant protein, showing the sigmoid decrease in the magnitude of the ellipticity as a function of temperature. The point of inflexion defined as the* T_m *is indicated.*
(**C**) *Representative unfolding curve for a single mN1 ARD mutant protein, calculated from the melting curve in* (**B**).

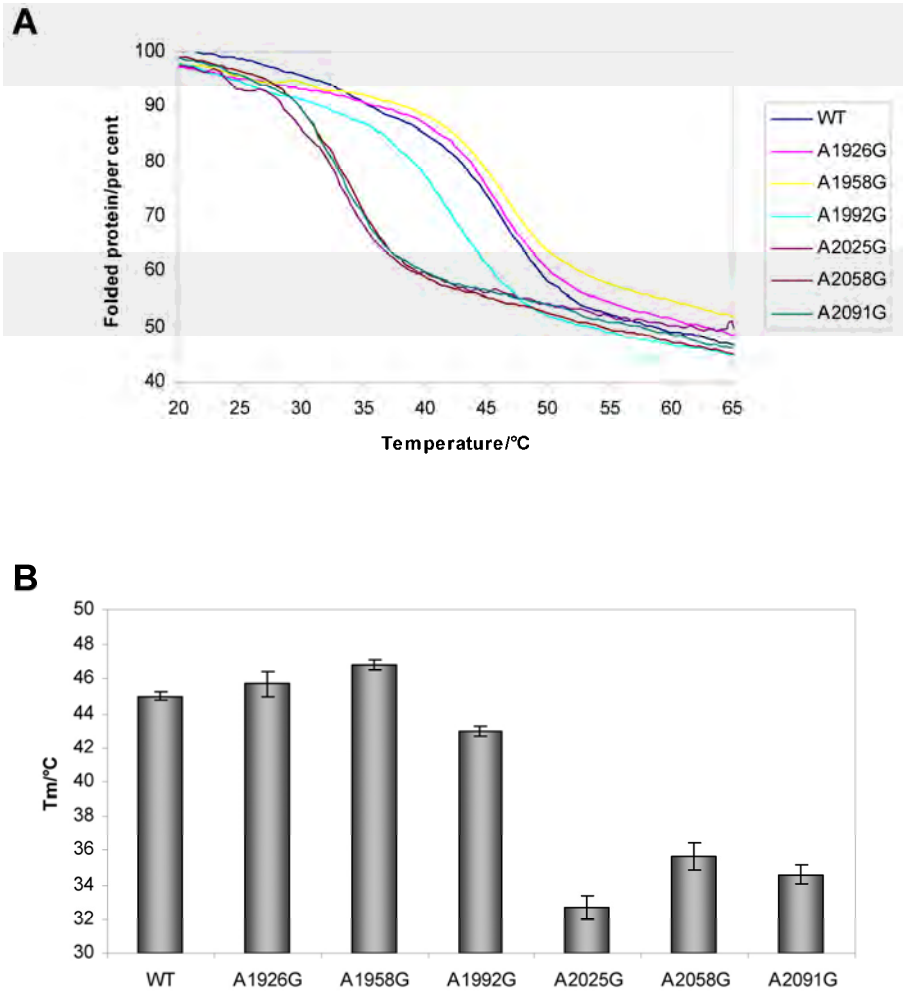


Figure 2.10 ***Analysis of ARD melting temperatures by CD spectroscopy (ii)***
Untagged mN1 ARD proteins at a concentration of 10 μM were heated in a cuvette with a path-length of 1 mm at a rate of 2 °C min^{-1} whilst the ellipticity at 222 nm was monitored. Melt curves were collected in triplicate for each mutant protein. A representative unfolding curve for each mutant is shown in (**A**). *Melting temperatures for each protein were determined in triplicate by curve fitting using a two-state model for unfolding (see for example (Greenfield, 2004)); mean melting temperatures for each mutant are shown in* (**B**). *Error bars represent standard deviation.*

2.2.6 *Analysis of the effect of structural mutants on Notch1 hydroxylation*

I next analysed the effect of these structural mutations on the hydroxylation of Notch1 by expressing the mutant $\Delta mN1^{ICD}$ proteins in 293T cells and determining the extent of hydroxylation at Asn-1945 and Asn-2012 using quantitative mass spectrometry as described in Section 2.2.2: because co-transfection of FIH with the $\Delta mN1^{ICD}$ plasmids in the previous experiment had led to near-saturating levels of hydroxylation at Asn-1945, for this experiment the Notch constructs were transfected alone. Consistent with previous data (Figure 2.3 and (Coleman et al., 2007)) basal levels of hydroxylation were around 50% at Asn-1945 and 3% at Asn-2012 in the wild-type protein (Figure 2.11). The structural mutations did not have any significant effects on hydroxylation at Asn-1945, which remained between 45% and 60% in all cases, suggesting that the ankyrin repeat in which this site is located may already be maximally unstable with respect to the unfolding transition necessary to bind FIH. All of the alanine-to-glycine mutants that destabilized the mN1 ARD also dramatically enhanced hydroxylation at Asn-2012, consistent with a role for tertiary structure in the regulation of hydroxylation at Asn-2012. However one mutant that did not have an appreciable destabilizing effect (A1958G) also enhanced Asn-2012 hydroxylation (see discussion, Section 2.3).

2.2.7 *Analysis of the effects of structural mutations on Notch binding to FIH*

To investigate whether the structural mutants were having significant effects on the binding of Notch1 to FIH, I expressed all six, along with a wild-type control, as GST-mN1 ARD proteins in *E. coli*. The purified proteins were analysed by SDS-PAGE and estimated to be >95% pure (Figure 2.12A). Proteins were then analysed for binding to

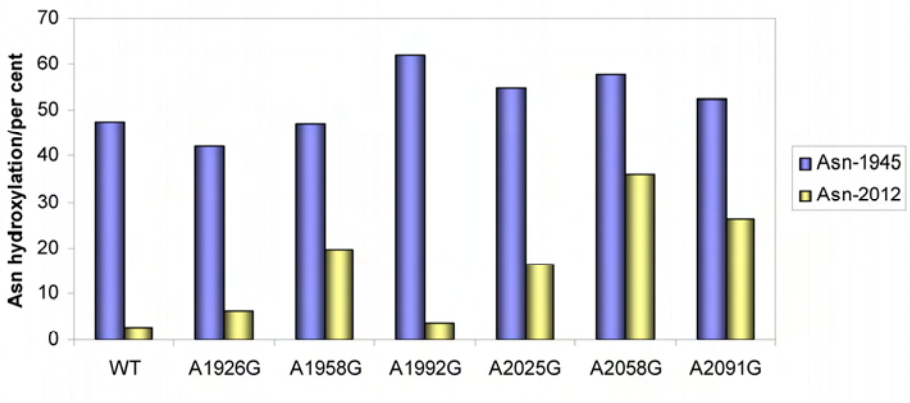


Figure 2.11 ***Analysis of mN1 structural mutant hydroxylation***
293T cells were transfected with the indicated ΔmN1^{ICD} mutant construct and harvested after 48 h. mN1 proteins were immunopurified, digested and analysed by MS exactly as described in Figure 2.3.

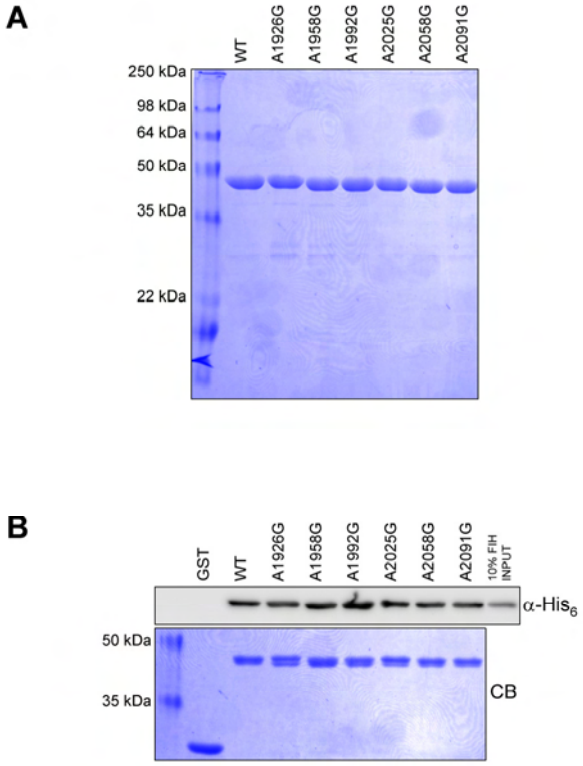


Figure 2.12 ***GST-pulldown assays for mN1 structural mutant binding to FIH***
(**A**) *GST-tagged mN1 ARD proteins containing the indicated mutations were expressed, purified and analysed exactly as described in Figure 2.4. Proteins were estimated to be >95% pure by SDS-PAGE.*
(**B**) *1 μg of the indicated GST-mN1 ARD construct was bound to GST resin which was washed and then incubated with 1 μg His_6-FIH in Jie's buffer containing 500 mM NaCl. After a second washing step, bound proteins were eluted in 2× SDS-PAGE sample buffer. Bound His_6-FIH was determined by immunoblotting using an anti-His_6 antibody. Eluates were also analysed by SDS-PAGE and Coomassie blue staining (CB) as a loading control.*

Note that in some lanes of the loading controls doublets appear due to the co-precipitation of Coomassie blue-stainable amounts of FIH with the GST-mN1 ARD protein.

His_6-FIH using GST pulldown and far-western assays as described in Section 2.2.3. No significant differences were observed between the wild-type protein and any of the mutants in the GST pulldown assay (Figure 2.12B). The result of the far-western assay was similar, with the exception that the A1958G mutation modestly reduced the binding of the mN1 ARD to FIH (Figure 2.13A), consistent with observations made for A1958F (see discussion, Section 2.3). As in the previous far-western assay, the control experiment showed no non-specific binding of the antibody to any species on the membrane (Figure 2.13B).

2.2.8 *Analysis of the effect of Notch1 mutations on the competitive inhibition of FIH*

The only known function of Notch1 hydroxylation to date is modulation of HIF signalling through competitive inhibition of FIH (Coleman et al., 2007; Zheng et al., 2008). In order to determine what effects the primary sequence and structural mutations in Notch1 had on its ability to inhibit FIH competitively, I used a reporter gene assay as described by Coleman *et al.* (Coleman et al., 2007). In this assay, HeLa cells are co-transfected with a luciferase reporter construct containing an upstream activation site (pUAS.tk.luciferase), a HIF1α CAD fusion construct encoding residues 652 – 826 of HIF1α with an N-terminal Gal4 DNA-binding domain (Gal4-DBD) tag, and the indicated $\Delta mN1^{ICD}$ construct. Under basal conditions the Gal4-DBD moiety binds to the upstream activation site (UAS) in the luciferase construct, but endogenous levels of FIH in the HeLa cells are sufficient to hydroxylate Asn-803 in the HIF1α CAD portion of the fusion protein and prevent recruitment of the p300/CBP transcriptional co-activators (Figure 2.14). Inhibition of FIH by Notch1 leads to a reduction in asparaginyl hydroxylation and recruitment of p300/CBP, which drive the transcription

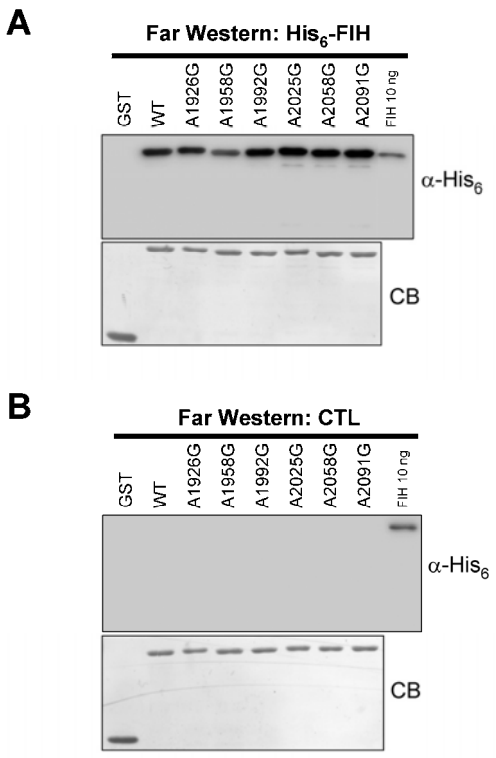


Figure 2.13 ***Far-western blotting assay for structural mutant mN1 binding to FIH***
200 ng of the indicated GST-mN1 ARD protein was resolved by SDS-PAGE and electroblotted onto PVDF membranes in duplicate. One membrane was incubated with His_6-FIH at 1 μg ml^{-1} in blocking solution (**A**)*, the other membrane was incubated with blocking solution alone as a control* (**B**)*. Bound FIH was visualized by immunoblotting using an anti-His_6 antibody. Membranes were-stained with Coomassie blue (CB) as a loading control.*

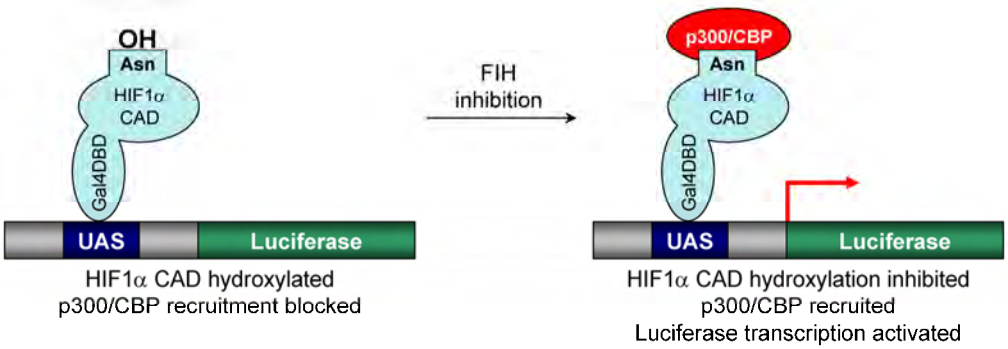


Figure 2.14
Schematic representation of the Gal4DBD-HIF1α CAD luciferase reporter assay.

of the luciferase reporter gene (Figure 2.14). Cells were harvested 48 h after transfection and extracts analysed for luciferase activity as a readout of HIF1α transcriptional activity. A plasmid encoding full-length β-galactosidase was co-transfected along with the HIF, luciferase and ankyrin plasmids as a transfection control: a colorimetric assay for β-galactosidase activity was carried out at the same time as the luciferase assay.

As expected, co-transfection of wild-type Notch1 increased the transcriptional activity of the HIF1α CAD construct significantly compared to empty pcDNA3 vector (Figure 2.15A). The N1945A and NANG mutant (in which both Asn-1945 and Asn-2012 are mutated, to alanine and glycine respectively) showed the expected loss of efficacy as competitive inhibitors, consistent with a previous report (Coleman et al., 2007). The N2012G result was unexpected since previous data (Coleman et al., 2007), and the reporter gene assay in Figure 2.15A, do not show any effect of this mutation. Therefore it seems likely that this result is anomalous.

In good agreement with the hydroxylation and interaction assays, the ability of Notch1 to enhance HIF1α CAD activity was strikingly reduced in the L1937A, L1937K, A1944P and L1955A mutants, and was not affected by the L1937I, A1942F, D1943A and A1958F mutants. Interestingly, modest reductions were seen for L1937V, P1954A and P1954L.

In parallel with the reporter gene assay, cell extracts were analysed by immunoblotting using an anti-V5 antibody to determine the expression of the Notch1 mutant proteins

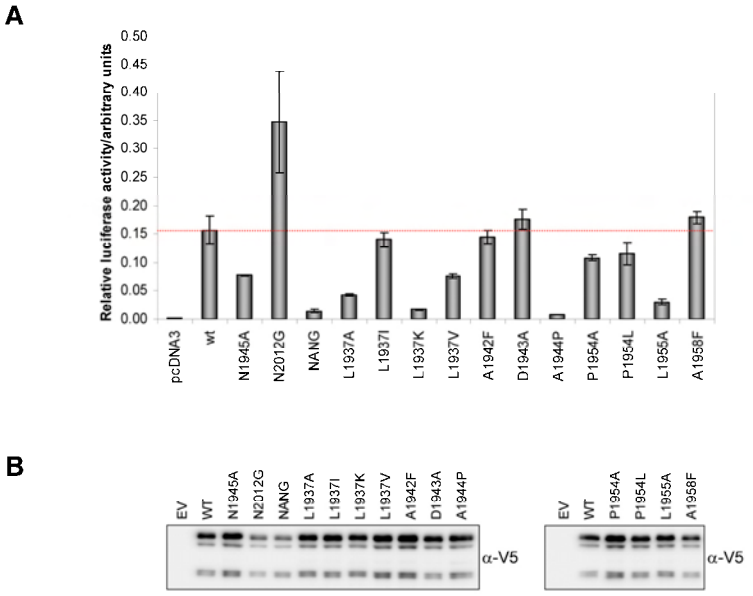


Figure 2.15 ***Assaying the effect of mN1 mutants on FIH inhibition (i)***
(**A**) *HeLa cells were co-transfected in triplicate with the indicated* $\Delta mN1^{ICD}$ *construct (or empty pcDNA3 vector control), pUAS.tk.luciferase, a Gal4DBD-HIF1*α *fusion protein encoding residues 652 – 826 of human HIF1*α *with an N-terminal Gal4DBD tag, and a vector encoding* β*-galactosidase as a transfection control. 48 h post-transfection cells were harvested, and luciferase and* β*-galactosidase activities analysed in parallel. Error bars represent standard deviation.*
(**B**) *Cell extracts were immunoblotted using an anti-V5 antibody in order to determine the relative expression levels of the* $\Delta mN1^{ICD}$ *proteins.*

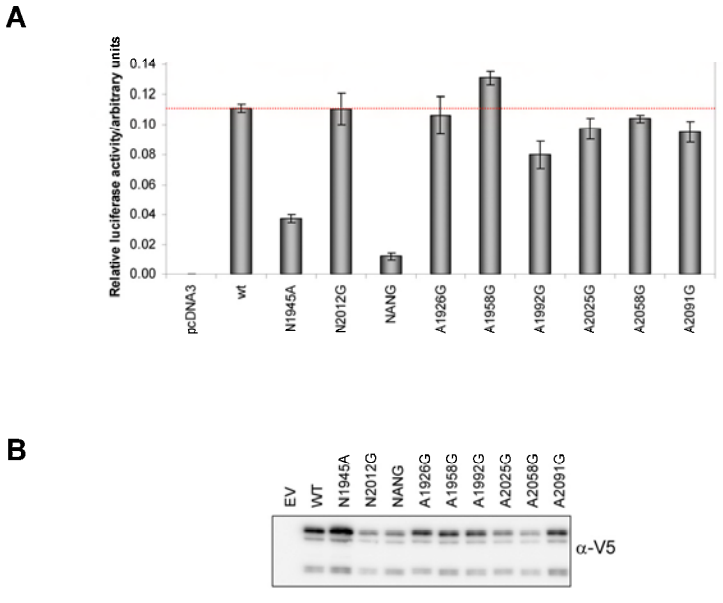


Figure 2.16 ***Assaying the effect of mN1 mutants on FIH inhibition (ii)***
(**A**) *The indicated* $\Delta mN1^{ICD}$ *constructs were assayed exactly as described for Figure 2.15. Error bars represent standard deviation.*
(**B**) *Cell extracts were immunoblotted using an anti-V5 antibody in order to determine the relative expression levels of the* $\Delta mN1^{ICD}$ *proteins.*

(Figure 2.15B). These immunoblots showed that all of the mutant proteins were expressed at a similar level except N2012G and NANG, where expression levels were much lower.

The Notch1 structural mutants were also analysed in the reporter gene assay (Figure 2.16A): in this assay the asparagine point mutants behaved as expected from the report of Coleman *et al.* (Coleman et al., 2007), with N1945A producing a large decrease in the competitive effect and N2012G no significant effect, consistent with Asn-1945 being the predominant site of hydroxylation and binding under physiological conditions. The data on the structural mutants in this assay were more difficult to interpret than in the previous assay because expression levels of the respective proteins, as determined by immunoblotting, were variable (Figure 2.16B). However, no gross differences in FIH inhibition were observed between any of the alanine-to-glycine mutants and the wild-type protein.

In summary the results of the reporter gene assay generally reflected the hydroxylation and native binding data well. However, some mutations such as L1937A and L1937V did have modest effects in this setting, perhaps suggesting that the reporter gene system gives a more sensitive readout of effects on binding and catalysis than the MS and GST pulldown assays.

2.2.9 *Kinetic analysis of Notch1 hydroxylation*

The experiments above showed that there was a good correlation between the efficiency of an ARD protein as an FIH substrate and its ability to enhance the transcriptional activity of the HIF1α CAD in a reporter gene assay, providing further

support for the notion that the Notch1 ARD acts as a competitive FIH inhibitor. In order to understand why this is the case, I carried out an *in vitro* kinetic analysis of the hydroxylation of a Notch1 ARD protein with the aim of determining a Michaelis constant (K_m) for the reaction of FIH with Notch. The K_m represents the substrate concentration that is required in order for an enzymatic reaction to proceed at half its maximum rate: a lower K_m indicates a more "efficient" substrate (Alberts et al., 2002).

In order to measure the kinetics of the hydroxylation of Notch1 by FIH, I used an MS-based assay to measure ARD hydroxylation directly. Recombinant wild-type mN1 ARD protein was incubated in a buffered reaction mix containing FIH and co-factors at 37 °C (see Section 6.7.5); at the desired time points aliquots of reaction mix were removed and stopped by the addition of SDS-PAGE sample buffer to denature the enzyme and substrate. Proteins were resolved by SDS-PAGE and stained with Coomassie blue, following which Notch-containing bands were excised and digested with trypsin before quantitative MS analysis as described in Section 2.2.2.

The Michaelis-Menten equation was used in order to determine the K_m and the maximum velocity (V_{max}, the maximum rate of reaction when all enzyme in the system is bound to substrate) for the hydroxylation of Notch (Alberts et al., 2002; Price and Dwek, 1979). Michaelis-Menten kinetics assume a constant amount of enzyme-substrate complex, so that the rate of enzyme binding to substrate equals the rate of release of product: in this regime the rate of reaction is constant and the reaction proceeds linearly with time. I therefore carried out a time-course experiment using purified GST-tagged mN1 ARD protein and analysed the percentage hydroxylation at Asn-1945 as a function of time (Figure 2.17A). This experiment indicated that the

progress of the reaction under these conditions was linear for around the first 2 minutes. The time point chosen for all further kinetic analyses was therefore 1 minute.

An initial assay to determine the approximate K_m of FIH for the mN1 ARD protein was conducted using GST-mN1 ARD, with a range of concentrations from 0 to 10 μM. The percentage hydroxylation at each substrate concentration was determined by quantitative MS: this value was used to derive the initial rate of reaction in terms of the number of micromoles of substrate hydroxylated per minute. A Michaelis-Menten curve was fitted to these data and used to derive the K_m and V_{max} (Figure 2.17B). This experiment indicated that, for the GST-mN1 ARD protein, the K_m of FIH was approximately 0.9 μM, with a V_{max} value of approximately 0.7 μmol min^{-1} mg^{-1}.

After establishing the approximate kinetic parameters for the hydroxylation of the mN1 ARD protein by FIH, three independent experiments were carried out using untagged mN1 ARD protein in order to derive more robust values for the K_m and V_{max} (Figure 2.18A, B and C). These experiments gave K_m values of 0.63 μM, 0.91 μM and 0.82 μM, with V_{max} values of 1.23 μmol min^{-1} mg^{-1}, 0.97 μmol min^{-1} mg^{-1} and 0.98 μmol min^{-1} mg^{-1} respectively. Thus the K_m of FIH for the mN1 ARD protein was determined to be 0.79 ± 0.14 μM, with a V_{max} of 1.06 ± 0.15 μmol min^{-1} mg^{-1}. An incidental observation was that the similarity in these values between the GST-tagged and untagged proteins suggests that the GST moiety had little effect on the hydroxylation of the mN1 ARD in the optimization experiments.

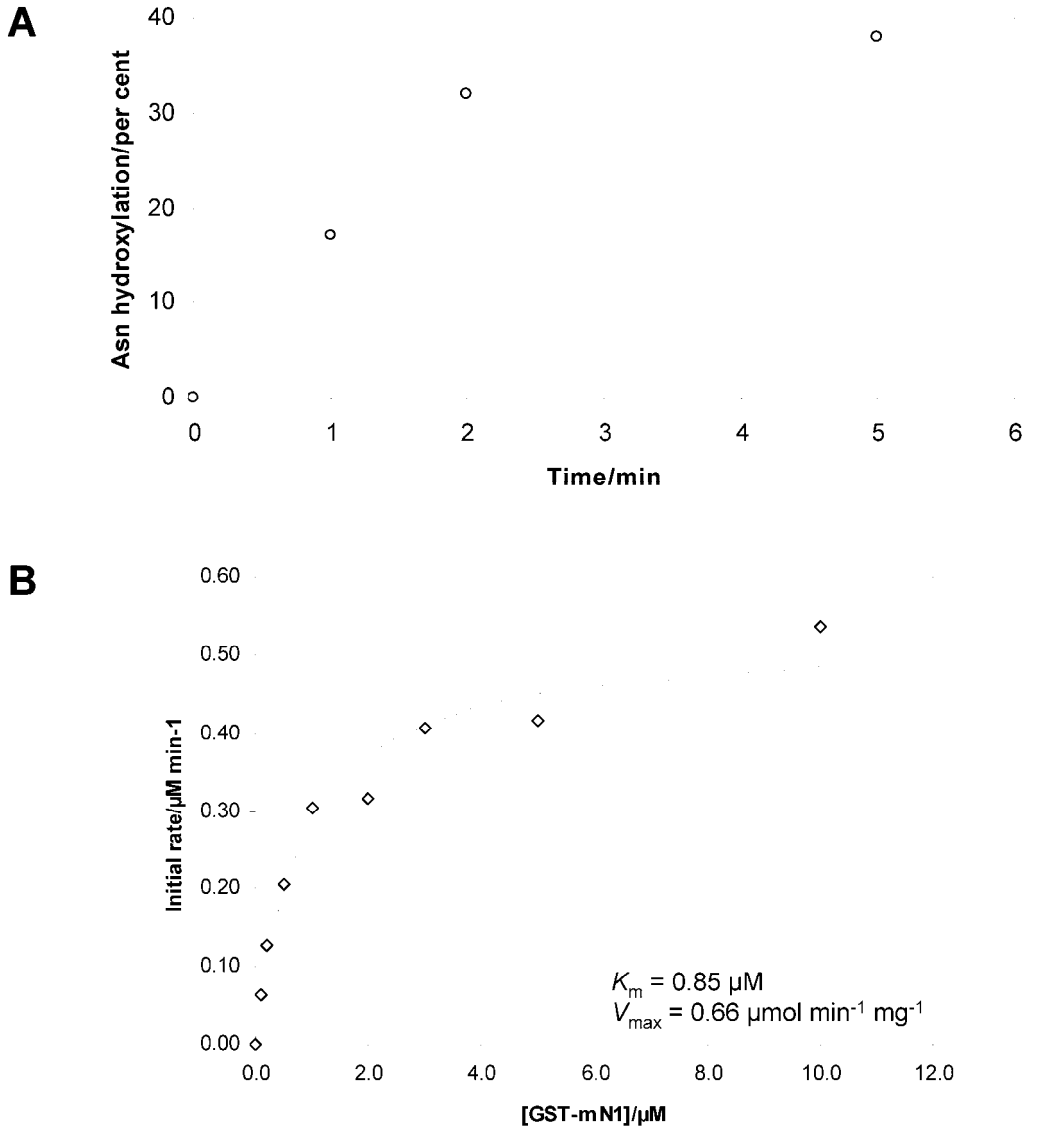


Figure 2.17 ***Kinetic analyses of mN1 hydroxylation (i)***

*His_6-FIH (20 nM) was incubated with the indicated concentrations of wild-type mN1 ARD substrate at 37 °C in a reaction mix containing TrisHCl pH 7.5 50 mM, L-ascorbate 4 mM, 2OG 160 μM, iron(II) sulfate 80 μM and DTT 1 mM. Reactions were started by the addition of enzyme, incubated for the indicated length of time and stopped by the addition of 4 μl 6× SDS-PAGE sample buffer to a 20 μl aliquot of reaction mix. Samples were resolved by SDS-PAGE following which mN1-ARD containing bands were excised, digested using trypsin and hydroxylation quantitated as described for Figure 2.3. Panel (***A***) shows a time-course reaction containing 4 μM GST-mN1 ARD over 5 minutes. Panel (***B***) shows a substrate titration using the indicated concentrations of GST-mN1 ARD with each reaction incubated for 1 minute.*

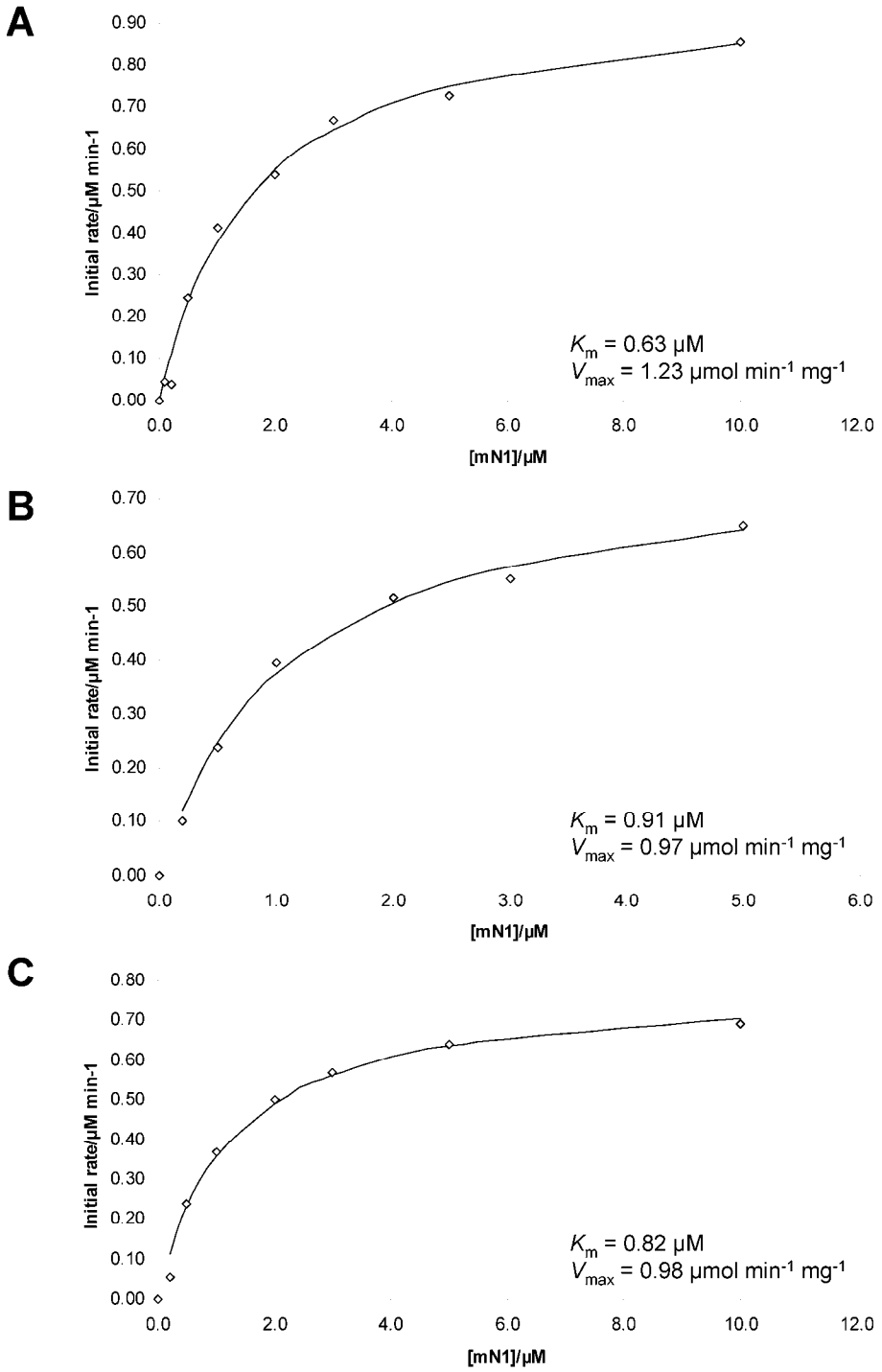


Figure 2.18 ***Kinetic analyses of mN1 hydroxylation (ii)***

His_6-FIH (20 nM) was incubated with the indicated concentrations of wild-type mN1 ARD substrate at 37 °C in a reaction mix containing TrisHCl pH 7.5 50 mM, L-ascorbate 4 mM, 2OG 160 μM, iron(II) sulfate 80 μM and DTT 1 mM. Reactions were started by the addition of enzyme, incubated for the indicated length of time and stopped by the addition of 4 μl 6× SDS-PAGE sample buffer to a 20 μl aliquot of reaction mix. Samples were resolved by SDS-PAGE following which mN1-ARD-containing bands were excised, digested using trypsin and hydroxylation quantitated as described for Figure 2.3. Panel (**A - C**) *show three independent substrate titrations using the indicated concentrations of untagged mN1 ARD with each reaction incubated for 1 minute.*

This result therefore showed that the K_m of FIH for a Notch1 ARD protein was significantly lower than for HIF1α CAD (published values for which range between 10 μM and 285 μM: see discussion, Section 2.3), which therefore explains the efficacy of the Notch1 ARD as a competitive inhibitor of FIH-dependent HIF hydroxylation.

2.3 Discussion

This chapter describes experiments aimed at elucidating the sequence and structural determinants of asparaginyl hydroxylation in the ARD of Notch1, and this discussion section focuses on the results of these; a more detailed discussion of the possible functions of ARD hydroxylation, whether related to structure or signalling, forms part of Chapter 5.

The alignments presented in Figure 2.1 suggested a consensus sequence in previously-determined ARD FIH substrates of $L_{-8}A_{-3}(D/E)_{-2}NL_{+10}A_{+13}$. By mutating these residues in Notch1 and directly analysing the effects on hydroxylation by quantitative mass spectrometry, I have shown that the consensus is less specific than this, as mutation of the alanine –3, aspartate/glutamate –2 and alanine +13 residues had no deleterious effect on hydroxylation at Asn-1945. Consistent with structural data showing that the leucine –8 residue forms a potentially important interaction with a hydrophobic binding pocket on the surface of FIH (Coleman et al., 2007), only certain mutations at this position are tolerated: mutation of the leucine –8 residue to alanine produced a moderate reduction in the extent of hydroxylation, whilst mutation to lysine, which has a much larger, positively-charged side-chain, almost completely ablated hydroxylation at Asn-1945 with endogenous levels of FIH. However even this gross reduction in hydroxylation could be rescued by FIH overexpression. Perhaps not surprisingly, valine and isoleucine residues, both of which are hydrophobic and similar in size to leucine, were well tolerated. It appears that the leucine +10 residue is also of some importance for hydroxylation, as an alanine mutation here led to a 50% reduction in the level of hydroxylation at Asn-1945. Structural data suggest that the adoption of an extended conformation with Asn-1945 at the apex of a tight turn is

critical for Notch1 to bind to and be hydroxylated by FIH (Coleman et al., 2007). This hypothesis is supported by the A1944P mutation, which showed a near-ablation of hydroxylation at Asn-1945, and provides an explanation for why Notch4 is not apparently an FIH substrate: Notch4 does not contain an asparagine residue at the analogous site to Asn-2012 in mN1, and the analogous residue to Asn-1945 is hindered by the presence of a proline at the –1 position. It is notable however that even this mutant, which showed dramatic reductions both in hydroxylation and binding to FIH (see below) was hydroxylated to around 20% when FIH was overexpressed, highlighting the ability of FIH to hydroxylate non-physiological substrates under such conditions.

Analysis of the binding of FIH to the Notch1 ARD mutants in their native state showed that, as might be expected, the variations in the binding of FIH to Notch1 reflected the variations in hydroxylation well. The observation that certain point mutations adjacent to Asn-1945 (L1937K and A1944P) virtually ablate binding of Notch1 to FIH suggests that interaction occurs mainly at the Asn-1945 site, with only a very minor contribution from Asn-2012, consistent with the much lower levels of hydroxylation observed at Asn-2012 under basal conditions. The binding of HIF1α to FIH occurs through two sites, a main site ("site 1") immediately adjacent to Asn-803 with a second site of interaction ("site 2") involving an α-helical sequence C-terminal to Asn-803 making a secondary contribution: HIF1α fragments containing only site 1 are hydroxylated, but less efficiently than those containing sites 1 and 2 (Elkins et al., 2003). It is not clear whether a similar mechanism operates in Notch however: although the P1954A and P1954L mutations were predicted to destabilize the α-helix C-terminal to Asn-1945, there is no direct structural evidence that they did so and no

large effect of either mutant was observed on the binding of Notch1 to FIH under native conditions.

Interestingly, more striking effects of Notch1 point mutations on binding to FIH were apparent in the far-western assay than in the GST pulldown assay. The L1937A and L1955A mutations, despite being reasonably well tolerated in the GST pulldown and hydroxylation assays, also resulted in a near-total loss of binding in the far-western assay. Further, the L1937V mutant, despite causing no reduction of hydroxylation or native ARD binding, also resulted in a noticeable decrease in binding in the far-western.

The observation that certain critical requirements for the binding of an unstructured substrate to FIH can be relaxed in the context of a structured ARD protein raises some interesting comparisons between ARDs and HIF as FIH substrates. The leucine +10 residue in Notch1 appears to potentiate asparaginyl hydroxylation, and whilst mutation of this residue showed a reduction in native binding to FIH, a more striking effect was seen in the far-western assay. This residue is conserved in HIF1α (as Leu-813), the CAD of which is reported to be unstructured in solution (Dames et al., 2002). Given the particular importance of Leu-1955 of Notch1 for binding to FIH in an unstructured setting, this work therefore suggests that Leu-813 in HIF may be important for hydroxylation, and indeed structural data show that this residue makes contact with the surface of FIH (Elkins et al., 2003). Although a mutational study investigating the substrate requirements of FIH with respect to HIF has been published (Linke et al., 2004), Leu-813 was not included and so determination of the effect of this residue on HIF hydroxylation will be of interest.

The mutational study of Linke *et al.* provides further evidence that positive effects in a structured ARD may override specific primary sequence requirements for hydroxylation in an unstructured protein: a V802A HIF1α mutant was reported to show a gross reduction in hydroxylation (although not FIH binding) when compared to wild-type HIF (Linke et al., 2004). This is an interesting finding in the context of Asn-1945 in Notch1, which has an alanine residue at the –1 position and yet appears to be hydroxylated far more efficiently than Asn-803 of HIF1α.

Analysis of the mutations predicted to affect the conformational stability of the Notch1 ARD yielded two principal results: firstly, that although Asn-2012 is not a site of significant *in vivo* hydroxylation in wild-type Notch1, under the right conditions it can be derepressed. It is not yet fully clear if this effect operates directly through a structural derepression of the target AR. However, the second clear result from this experiment is that mutations distal to a target asparagine residue can exert strong influences on hydroxylation. Three of the alanine-to-glycine mutants, A2025G, A2058G and A2091G, had a pronounced effect on the melting temperature of the Notch1 ARD, reducing it by 10 – 13 °C relative to the wild-type protein, and these mutants also enhanced hydroxylation at Asn-2012. Taking these results in isolation, it could be argued that these mutations decrease the conformational stability of the ARD, facilitating the partial unfolding of individual ankyrin repeats and thus enhancing FIH binding and hydroxylation at target asparagine residues. However, an increase in hydroxylation at Asn-2012 was also observed for the A1958G protein even though this mutation had no effect on the melting temperature of the intact ARD. Whilst it does not appear that this enhancement operated through a structural effect in the intact ARD, a specific primary sequence effect of the mutation is conceivable. Although

the A1958G mutant did not show a detectable effect on hydroxylation at Asn-1945 (Figure 2.11) or on binding in the GST pulldown assay (Figure 2.12B), in common with the A1958F mutation it did have a modest effect on binding in the far-western assay (Figure 2.13A), suggesting that this mutation could play a weak role in reducing FIH binding at Asn-1945 that releases more FIH for hydroxylation at Asn-2012. The lack of an apparent effect of the structurally destabilizing mutants (A2025G, A2058G and A2091G) on FIH binding in the GST pulldown assay likely reflects the fact that binding at the higher-affinity site, Asn-1945, masks weaker effects on binding at Asn-2012. Clearly mutations which influence the stability of the secondary and tertiary structure of a protein would not be expected to influence binding in a far-western experiment, where the protein of interest is denatured and bound to a membrane.

The differences in the abilities of the Notch mutants to enhance HIF1α CAD reporter gene activity reflected the variations in their hydroxylation and binding to FIH well, providing good evidence to support published data demonstrating that the ICD of Notch1 is a competitive FIH inhibitor. Further support for the role of Notch1 in competitive FIH inhibition came from a kinetic analysis of the hydroxylation of a wild-type Notch1 ARD protein, which gave a K_m value of less than 1 μM. Reported K_m values of FIH for HIF1α vary widely: an early study used a radioactive 2OG decarboxylation assay and reported a 'preliminary' value of 10 μM (Hewitson et al., 2002). Later reports suggest that this value may be too low: K_ms of 40 μM and 100 μM have been derived for HIF1α polypeptides (residues 737 – 826 and 775 – 826 respectively) using a 2OG decarboxylation assay (Koivunen et al., 2004; Linke et al., 2004). Alternative approaches using a fluorescence-based assay and an oxygen consumption assay have reported values of 285 μM and 154 μM respectively

(Ehrismann et al., 2007; McNeill et al., 2005). Although these studies disagree with respect to the absolute K_m value of FIH for HIF1α, the K_m for Notch1 derived in this chapter is an order of magnitude lower than even the lowest estimate for HIF1α. This supports published dissociation constant data indicating that a Notch1 ARD binds FIH more tightly than a HIF1α CAD protein (Coleman et al., 2007) and provides a kinetic rationale for the competitive inhibition of FIH that is observed.

In summary, the work described in this chapter has shed further light on the Notch1-dependent competitive inhibition of HIF asparaginyl hydroxylation, indicating that this phenomenon occurs because Notch1 is a much more efficient substrate for FIH than HIF1α. It appears that the determinants of Notch1 hydroxylation by FIH can be divided into two groups: structural determinants and primary sequence determinants. Further work will be required to determine the exact mechanism through which the structural determinants of hydroxylation operate robustly, but it would appear that the structural cooperativity of ankyrin-repeat proteins allows hydroxylation at asparaginyl residues to be modulated by mutations distal to the substrate residue.

One of the aims of the work in this chapter was to test conserved amino acids in ankyrin-repeat substrates of FIH and determine which of these conserved residues are required for hydroxylation. These experiments have shown that the consensus may be relatively broad, as a range of amino acid substitutions are tolerated in the primary sequence adjacent to the substrate residues. However, certain requirements have been defined: Primary sequence factors such as prolyl residues preventing the adoption of the necessary conformation for FIH binding cannot be tolerated, a hydrophobic residue at the –8 position is a requirement for asparaginyl hydroxylation, and it

appears that hydroxylation may be potentiated by the presence of a leucinyl residue at the +10 position. The requirements for hydroxylation in non-conserved regions of the ARD substrates of FIH, which did not form part of the scope of this study, have not yet been investigated. However, in the light of the characterization of the A1944P Notch1 mutant it is interesting to note for example that there are no prolyl residues between the leucine –8 residue and the target asparagine residue in any of the ARD substrates of FIH characterized to date (Figures 2.1A and 2.1B).

All of the FIH-dependent hydroxylations of ARD proteins reported to date have been located in a β-hairpin loop connecting ARs (Cockman et al., 2006; Coleman et al., 2007; Ferguson et al., 2007): it therefore appears that this may be an important structural determinant of hydroxylation. Around 6% of eukaryotic proteins contain an ARD (Barrick et al., 2008), and the consensus sequence of ARs has been extensively studied and robustly determined (reviewed by (Barrick et al., 2008; Li et al., 2006; Mosavi et al., 2004)). Strikingly, an asparagine residue is present in the β-hairpin loop of published consensus ankyrin-repeat sequences, together with the leucine –8 and leucine +10 residues. Taken together these observations suggest that hydroxylation of ARD-containing proteins may be a widespread phenomenon. In order to investigate how widespread AR hydroxylation might be, and whether it was possible to predict substrates of FIH *in silico*, I next undertook a range of experiments on MYPT1, an ARD-containing protein that had not previously been assigned as an FIH substrate. These experiments form the subject of the next chapter.

Chapter 3

Identification and characterization of MYPT1 as a substrate for FIH

3.1 Introduction

The work carried out to determine the requirements for FIH-dependent ARD hydroxylation in Chapter 2 indicated that the consensus sequence was relatively broad and corresponded well with published consensus sequences for the ankyrin repeat itself (Barrick et al., 2008; Li et al., 2006; Mosavi et al., 2004). Given that there are over 300 ankyrin-repeat domain-containing proteins encoded in the human genome (SMART database, (Schultz et al., 1998)), it therefore appeared that the FIH-dependent hydroxylation of ankyrin repeats might be a widespread PTM.

In order to investigate how widespread ARD hydroxylation might be, and also to determine whether it would be possible to predict sites of hydroxylation *in silico*, I next carried out a study on myosin phosphatase targeting subunit 1 (MYPT1) which contains an eight-repeat ARD, had not been assigned previously as an FIH substrate and for which a cDNA was readily available. A bioinformatic analysis of the MYPT1 ARD based on the findings in Chapter 2, as described in more detail in Section 3.2.1, identified four potential sites of FIH-dependent asparaginyl hydroxylation in this molecule.

MYPT1 is the targeting subunit of smooth muscle myosin phosphatase (MP), which together with a range of serine/threonine kinases determines the extent of phosphorylation of the regulatory myosin light chain (MLC) in smooth muscle and non-muscle myosin II. The degree of MLC phosphorylation in turn regulates smooth muscle tone *via* actin/myosin-based cell contraction: a decrease in MLC phosphorylation (which may result from an increase in MP activity or a decrease in kinase activity) results in smooth muscle relaxation. An increase in MLC phosphorylation (arising from MP activation of kinase inhibition) leads to smooth muscle contraction. Myosin

phosphatase is therefore implicated in a wide range of cellular processes including cytokinesis, migration and invasion – for reviews see (Ito et al., 2004) and (Matsumura and Hartshorne, 2008). Although MLC can be phosphorylated by several kinases, including myosin light chain kinase (MLCK) and Rho-associated kinase (ROCK), myosin phosphatase is the only enzyme known to dephosphorylate myosin light chains.

Smooth muscle myosin phosphatase was originally isolated from chicken gizzard, and consists of three subunits (Alessi et al., 1992; Mitsui et al., 1992). These are a 37 kDa catalytic subunit of protein phosphatase type 1c (PP1cδ, also known as PP1cβ), a 20 kDa subunit of unknown function (M20) and a large, targeting subunit of approximately 110 kDa (MYPT1) – see Figure 3.1. Most of the properties of MP are attributable to MYPT1, which in addition to binding of the catalytic PP1cδ subunit targets the holoenzyme to myosin (Ito et al., 2004); there is no evidence to date suggesting that M20 is a functional subunit of MP (Matsumura and Hartshorne, 2008).

MYPT1 is widely expressed although its concentration is higher in smooth muscle than in other tissues: one study reported detection of MYPT1 in every tissue tested except liver and skeletal muscle (Okubo et al., 1994). Since the discovery of MYPT1 four other proteins have been identified as members of an MYPT family: MYPT2 (Fujioka et al., 1998), MBS85 (Tan et al., 2001), MYPT3 (Skinner and Saltiel, 2001) and TGF-β-inhibited membrane associated protein (TIMAP) (Cao et al., 2002). MYPT2 is expressed in brain, heart and skeletal muscle (Arimura et al., 2001; Fujioka et al., 1998) and is the only other member of the MYPT family to have a proposed function: in skeletal muscle it has been shown to form a specific complex with PP1cδ, and hence is



Figure 3.1 ***Subunit structure of myosin phosphatase***
Schematic representation of the subunit structure of myosin phosphatase, showing the large targeting subunit (MYPT1), the catalytic subunit (PP1cδ) and M20, of unknown function. The ARD of MYPT1 (containing two groups of four ankyrin repeats) is also indicated. PP1cδ interacts with the N-terminal region of MYPT1, including the ARD, whereas M20 binds to the C-terminus. Adapted from (Ito et al., 2004).

thought to be the targeting subunit of myosin phosphatase in this setting (Moorhead et al., 1998). Although in many cases the members of the MYPT family are substantially different from each other, both in terms of size and amino acid conservation, all contain ankyrin repeats: MYPT2 (in common with MYPT1) contains eight, MSB85 contains seven, whilst MYPT3 and TIMAP both contain five repeats (Ito et al., 2004).

MYPT1 contains an ARD with eight repeats (in two groups of four) towards its N-terminus, from residues 39 – 296. This region of the molecule is highly conserved between species, with over 96% conservation between chicken and human proteins. This compares to 78% conservation between human and chicken for the amino acid sequence from residues 297 – 1030, suggesting particular functional importance of the ARD. A four-residue binding motif for PP1cδ (KVKF) lies immediately N-terminal to the ARD, from residues 35 – 38.

The binding of PP1cδ to MYPT1 is essential for the correct catalytic activity of the MP holoenzyme (Alessi et al., 1992). Although isolated PP1cδ will dephosphorylate MLC *in vitro*, binding to MYPT1 both activates PP1cδ and also enhances its specificity for MLC (Hirano et al., 1997; Tanaka et al., 1998). *In vitro* studies using surface plasmon resonance have suggested that the critical residues for binding are located in the KVKF motif just outside the ARD (Tóth et al., 2000b). However biochemical studies have demonstrated that, whilst the KVKF motif is required for binding, the complete ARD is necessary for the correct activation and enhancement of selectivity of the holoenzyme (Tanaka et al., 1998). It appears therefore that binding occurs in stages: initially PP1cδ interacts with the KVKF binding motif, and subsequently establishes interactions at sites within the ARD.

The crystal structure of PP1cδ complexed to the ARD of MYPT1 has been solved. This shows that the catalytic cleft of PP1cδ combines with an acidic groove created by the ankyrin repeat α-helices towards the N-terminus of MYPT1, resulting in an extended binding site for phosphorylated MLC and explaining the enhanced selectivity of the MP holoenzyme compared to isolated PP1cδ (Terrak et al., 2004). A further role of the ARD involves the formation of secondary interactions with PP1cδ: the β-hairpins of the two groups of four ankyrin repeats form a "clamp" around the C-terminal tail of the molecule.

Several examples of MYPT1 regulation by post-translational modifications have been reported. After an initial study indicating that ROCK inhibited MP (Kimura et al., 1996), two sites of phosphorylation by ROCK were subsequently identified: these are Thr-696 and Thr-853 in the human protein, with Thr-696 being the inhibitory site (Feng et al., 1999). Other kinases including the ZIP-like MYPT1 kinase and integrin-linked kinase (ILK) have also been shown to phosphorylate the inhibitory site (MacDonald et al., 2001; Murányi et al., 2002). The mechanism of inhibition is presumed to involve the phosphorylated C-terminus of MYPT1 folding into the MLC binding groove of myosin phosphatase and blocking substrate binding (Terrak et al., 2004). Two protein kinase C-dependent inhibitory phosphorylations, one at Thr-34 and another apparently within the ARD, have also been reported (Tóth et al., 2000a).

This chapter describes my investigations resulting in the identification of MYPT1 as a substrate for FIH. MYPT1 was initially identified as a candidate substrate by a bioinformatic approach informed by the results described in Chapter 2. An overexpressed MYPT1 ARD truncation was shown to be hydroxylated in 293T cells,

with the FIH dependence of this effect established by using a combination of gene knockdown and overexpression. Analysis of a sample of purified endogenous avian MYPT1 showed that the hydroxylations observed are physiologically relevant. Experiments to investigate possible effects of ARD hydroxylation on the activity of MP are presented, along with data showing that overexpression of the MYPT1 ARD (and a range of other ARD-containing proteins) can modulate HIF signalling, apparently through competitive inhibition of FIH-dependent HIF CAD hydroxylation.

3.2 Results

3.2.1 *MYPT1 is a potential FIH substrate*

In order to look for potential sites of FIH-dependent hydroxylation in the ARD of MYPT1 I used the criteria defined in Chapter 2, namely the presence of an asparagine residue in a β-hairpin loop with leucine residues at the –8 and +10 positions. This analysis identified Asn-67, Asn-100 and Asn-226 of MYPT1 as potential hydroxylation targets. A fourth potential site, Asn-288 which conformed to the first two requirements but lacked the leucine +10 residue, was also identified. These candidate sites were aligned along with the CAD of HIF1α and the same published ARD sites of hydroxylation used in Chapter 2 (Figure 3.2); this alignment identified several of the same conserved residues in the amino acid sequence surrounding MYPT1 Asn-67, Asn-100 and Asn-226, whilst the primary sequence around Asn-288 showed less conservation.

3.2.2 *Identification of hydroxylation sites in MYPT1 by MS/MS*

Post-translation modifications can be detected by mass spectrometry (MS) as a mass gain or a mass loss relative to the parent protein. However, these mass shifts only indicate that a modification has occurred somewhere in the peptide or protein being analysed: more detailed information is required in order to assign the modification unambiguously to a particular residue. This is particularly important in the case of hydroxylations: hydroxylation corresponds to the formal insertion of an oxygen atom into a C–H bond, leading to a mass shift of +16 Da. Several amino acids other than asparagine may also be oxidized, including proline, methionine and tryptophan (Kinter and Sherman, 2000; Larsen et al., 2006): methionine oxidation in particular occurs as a common artefact during the preparation of protein digests from gel bands.

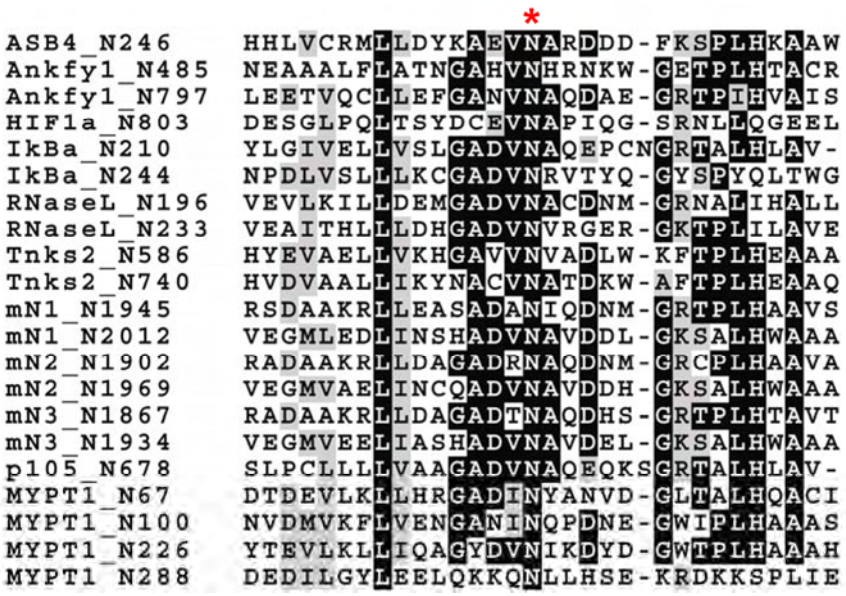


Figure 3.2 *MYPT1 is a potential substrate for FIH*

Alignment of HIF1α CAD and published ankyrin repeat-containing substrates of FIH with four putative sites of hydroxylation in MYPT1: Asn-67, Asn-100, Asn-226 and Asn-288. The substrate asparagine residues are indicated with a red asterisk.

Tandem mass spectrometry (MS/MS) can be used to determine the amino acid sequence of peptides and also to assign post-translational modifications with certainty. In this technique, the masses of the peptide ions in a protein digest are initially determined by simple MS. In the second step, ions of interest are isolated or "trapped" in a collision cell based on their mass-to-charge ratio (m/z). Once a peptide ion has been trapped it is then further fragmented, generally by collision with an inert gas that imparts energy to the peptide and induces fragmentation. Finally the m/z values of these fragment ions are analysed in a second MS step. Fragmentation tends to occur principally at the amide bonds between amino acid residues, which results in an MS/MS spectrum consisting of a series of peaks that reveal the amino acid sequence (Larsen et al., 2006). The MS/MS data can then be searched against a database of protein sequences in order both to identify the protein of interest and also to assign any observed post-translational modifications. As a further refinement to this technique, peptides are often resolved by capillary liquid chromatography before MS/MS analysis (LC-MS/MS), which allows analysis of a complex mixture of peptides in a single experiment.

A schematic MS/MS spectrum for modified and unmodified peptides is shown in Figure 3.3A: the post-translational modification imparts an additional mass to all of the fragment ions containing the modified residue. By convention the series of fragment ions that builds up from the N-terminus of a peptide is referred to as the b-ion series; the fragment ions that build up from the C-terminus of a peptide are referred to as the y-ion series (Figure 3.3B). Thus the MS/MS spectra in Figure 3.3A both represent a complete b-ion series for the unmodified and modified peptides. MS/MS analysis allows

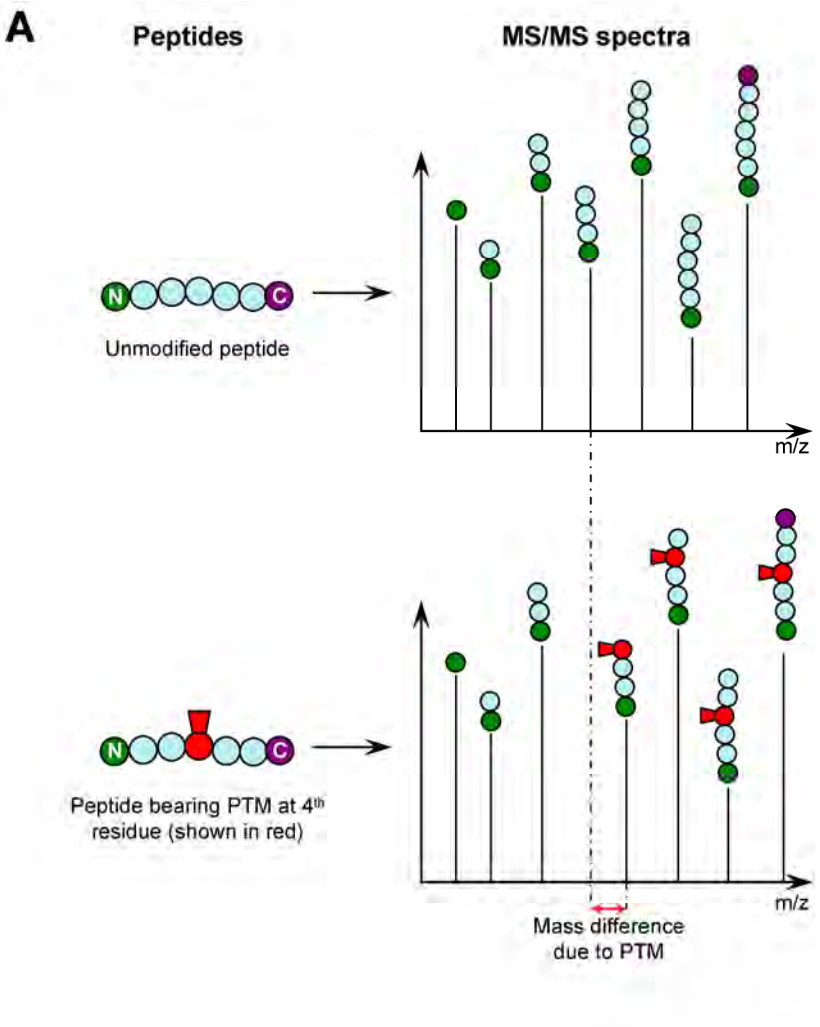


Figure 3.3 *Tandem MS*
(**A**) *Schematic MS/MS fragmentation spectra for a seven-residue peptide in modified and unmodified states. All fragment ions containing the modification bear an additional mass. Adapted from (Larsen et al., 2006).*
(**B**) *Conventional nomenclature for MS/MS fragment ions – the b-ion series builds up from the N-terminus, the y-ion series builds up from the C-terminus.*

asparaginyl hydroxylations to be unambiguously assigned, removing the issue of confounding and potentially artefactual oxidations elsewhere on a peptide.

In order to determine whether MYPT1 could be a substrate for FIH, I transfected 293T cells with a V5-MYPT1 ARD expression vector (containing residues 1 – 296 of human MYPT1, in pEF1/V5-His A with a C-terminal V5 tag) or with full-length, myc-tagged MYPT1 (pCMV6-MYPT1). In addition, cells were co-transfected either with wild-type FIH (pEF-FIH) or an empty vector control (pcDNA3); MYPT1 and FIH/pcDNA3 were transfected in a 4:1 ratio. Cells were lysed 48 hours after transfection, and the respective MYPT1 proteins immunopurified using either anti-V5 or anti-myc affinity resin as appropriate. After immunopurification samples were resolved by SDS-PAGE, MYPT1-containing bands excised and digested with trypsin (which cleaves proteins C-terminal to lysine or arginine residues) or endoproteinase GluC in bicarbonate buffer (which under these conditions cleaves peptides C-terminal to glutamate residues). Following digestion peptide samples were analysed by LC-MS/MS using a Bruker ion-trap mass spectrometer, with MS/MS data analysed initially using Mascot database searching software (Perkins et al., 1999).

Expression of the pCMV6-MYPT1 construct was poor (data not shown), and analysis of the digests derived from the recovered full-length protein gave incomplete peptide coverage of the ARD. Expression of the MYPT1 ARD construct was much better (data not shown), and asparaginyl hydroxylation was assigned at three of the putative substrate residues, Asn-67, Asn-100 and Asn-226. However this was only observed under conditions of FIH overexpression, raising the possibility that forced expression of FIH was leading to artefactual hydroxylation of the ARD protein.

To test for MYPT1 hydroxylation in a less artefactual setting I overexpressed the MYPT1 ARD plasmid in 293T cells in the absence of overexpressed FIH. However, I reasoned that overexpression of the MYPT1 ARD could saturate the endogenous levels of FIH, leading to a low relative abundance of hydroxylated peptides in the samples and consequently failure to detect hydroxylation. To increase the sensitivity of LC-MS/MS analysis of these samples I used an inclusion list in the data acquisition software: this biases MS/MS fragmentation towards ions of a specified m/z, thus increasing the chances of detecting peptides of interest that are present at a low abundance. The expected m/z ratios for the hydroxylated and unhydroxylated peptides, derived from the previous MS/MS experiment, were used to form the inclusion list. Use of the inclusion list improved detection of hydroxylated peptides significantly, and by combining the results from the trypsin and GluC digests all four candidate asparagine residues were covered by MS/MS sequencing. The trypsin digest gave coverage of Asn-67, Asn-226 and Asn-288; GluC digestion gave MS/MS sequence data for Asn-100. Peptides containing hydroxyasparagine at positions 67 and 226 were detected in the samples derived from cells expressing endogenous levels of FIH (Figure 3.4A and C respectively). A +16 Da mass shift was also observed in the GluC-derived peptide containing Asn-100: this is likely to indicate hydroxylation of Asn-100 but the MS/MS fragmentation data were insufficient to assign the modification absolutely to Asn-100 and leave open the formal possibility of an oxidation on Gln-101 (Figure 3.4B). Although a peptide containing Asn-288 was observed and sequenced by MS/MS, hydroxylation was not detected even with forced expression of FIH, suggesting that this residue is not a *bona fide* FIH substrate. Thus three residues in the ARD of MYPT1 are hydroxylated in 293T cells.

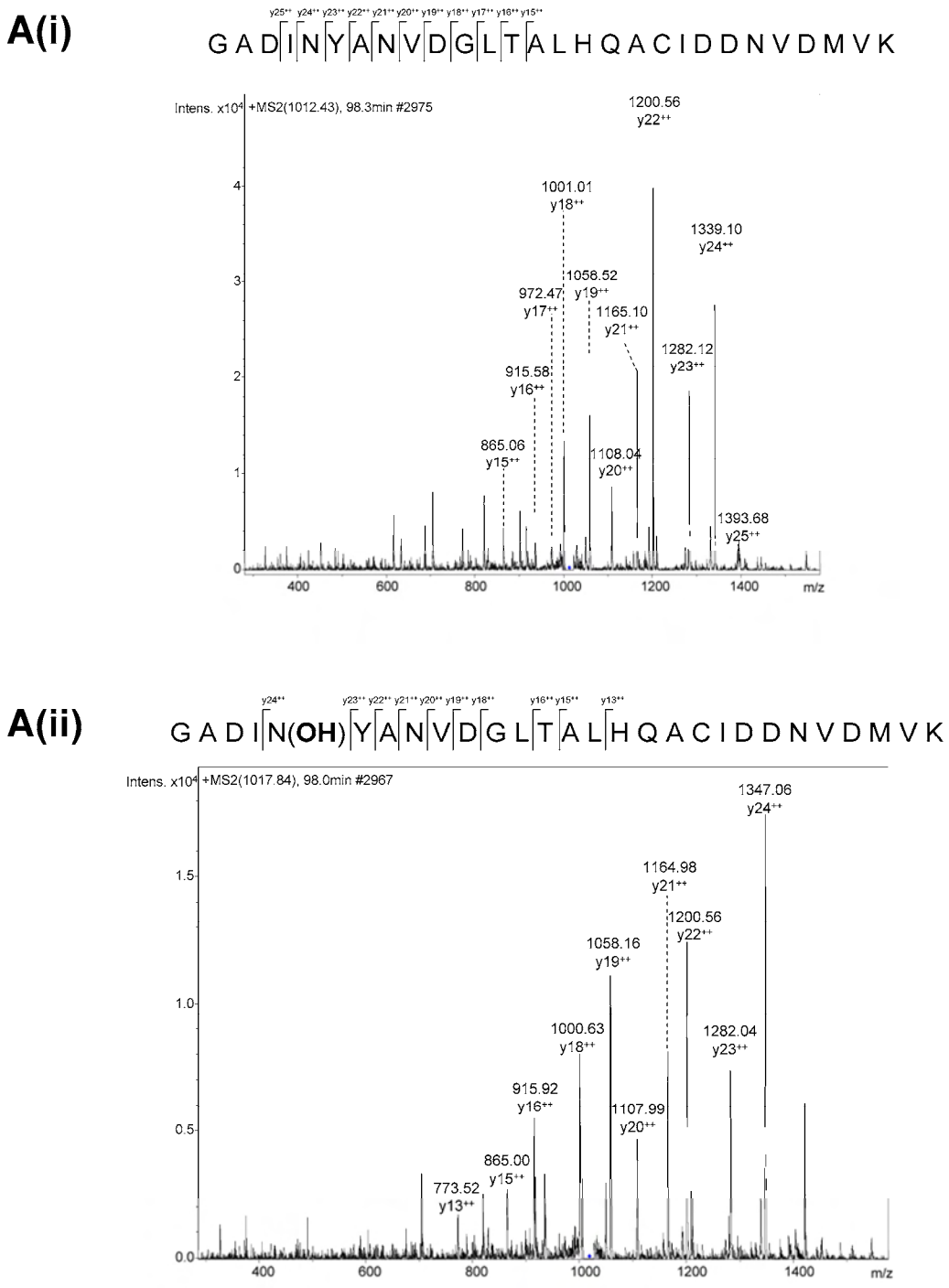


Figure 3.4A *Identification of Asn-67 as a hydroxylation site in MYPT1*
MS/MS spectra showing the tryptic fragment of human MYPT1 containing Asn-67 in unoxidized and hydroxylated states. Spectrum (**i**) *shows the unoxidized peptide. In spectrum* (**ii**)*, an additional mass of 8 Da is observed in the doubly-charged $y24^{++}$ ion, indicating hydroxylation at Asn-67. The m/z difference of 5.41 between the two triply charged precursor peptide ions corresponds to a mass difference between the uncharged peptides of 16 Da within the mass resolution of the instrument.*

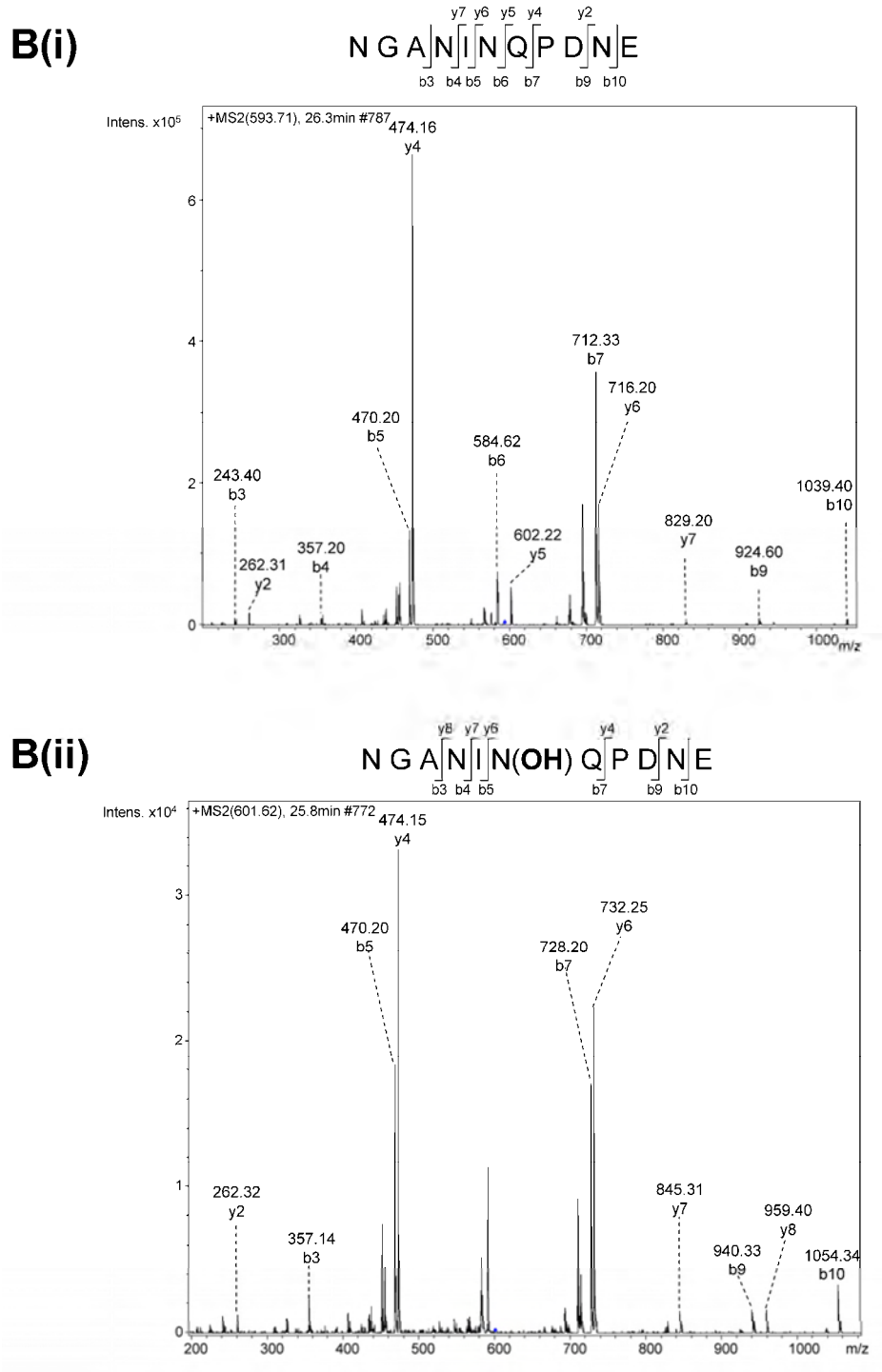


Figure 3.4B ***Identification of Asn-100 as a hydroxylation site in MYPT1***
MS/MS spectra showing the GluC fragment of human MYPT1 containing Asn-100 in unoxidized and hydroxylated states. Spectrum (**i**) *shows the unoxidized peptide. In spectrum* (**ii**)*, an additional mass of 16 Da is observed in the b-ion series from b7 and in the y-ion series from y6, indicating hydroxylation at Asn-100 (or oxidation at Gln-101). The m/z difference of 7.91 between the two doubly charged precursor peptide ions corresponds to a mass difference between the uncharged peptides of 16 Da within the mass resolution of the instrument.*

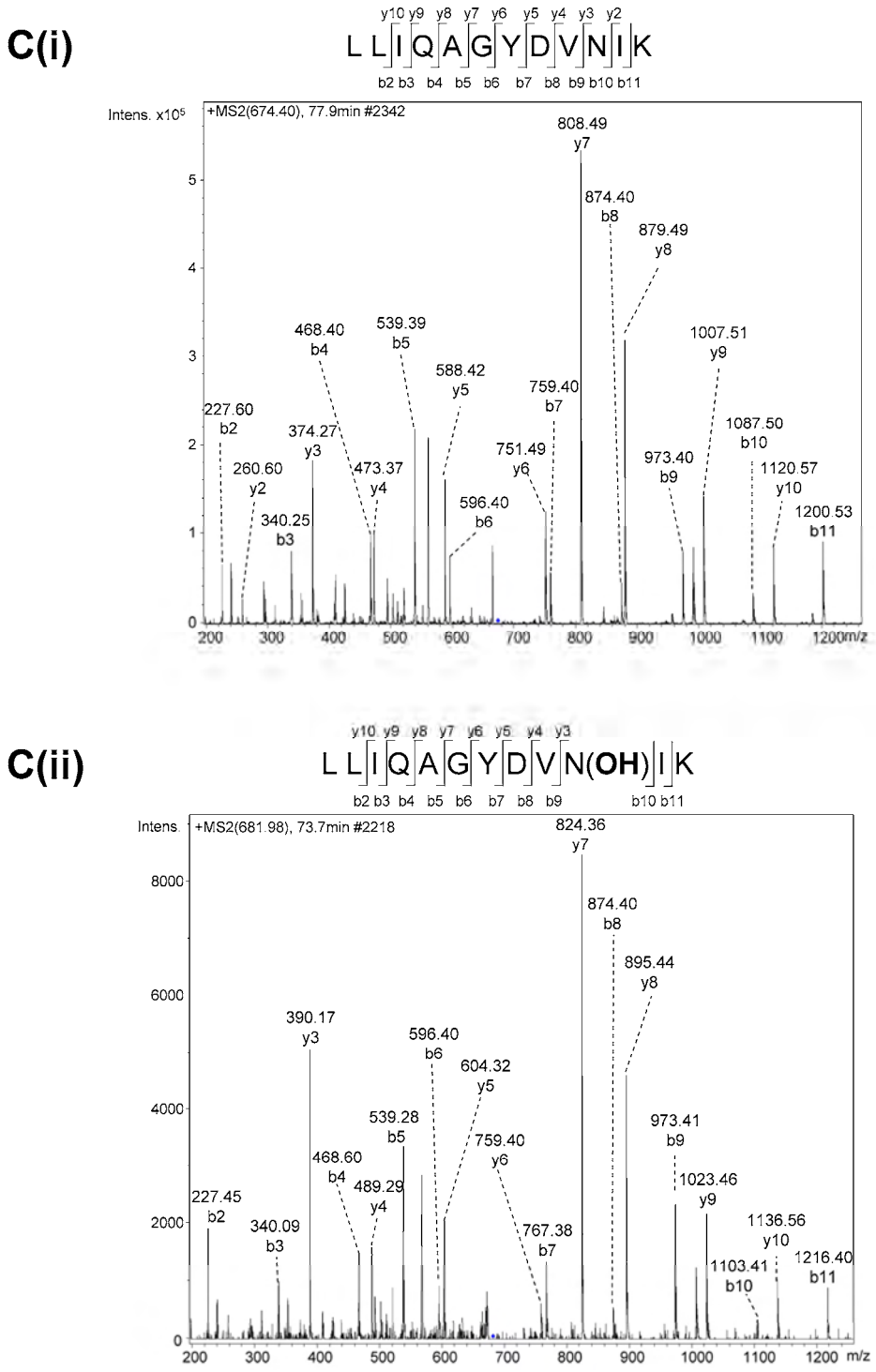


Figure 3.4C *Identification of Asn-226 as a hydroxylation site in MYPT1*
MS/MS spectra showing the tryptic fragment of human MYPT1 containing Asn-226 in unoxidized and hydroxylated states. Spectrum (**i**) *shows the unoxidized peptide. In spectrum* (**ii**)*, an additional mass of 16 Da is observed in the b-ion series from b10 and the y-ion series from y3, indicating hydroxylation at Asn-226. The m/z difference of 7.58 between the two doubly charged peptide precursor ions corresponds to a mass difference between the uncharged peptides of 16 Da within the mass resolution of the instrument.*

3.2.3 *FIH and MYPT1 interact in 293T cells*

In order to determine if mutation of any of the substrate asparagine residues observed in Figure 3.3 affected binding of the MYPT1 ARD to FIH, I carried out an immunoprecipitation experiment. MYPT1 ARD point mutants were prepared in pEF1/V5-His with the substrate asparagine residues mutated to alanine (N67A, N100A and N226A), along with a triple asparagine mutant. These plasmids were overexpressed in 293T cells (along with an empty vector control), followed by anti-V5 immunoprecipitation. Immunoprecipitates and input samples were analysed by immunoblotting for FIH and V5 (Figure 3.5). This experiment showed that the MYPT1 ARD could co-immunoprecipitate endogenous FIH. Mutation of all three asparagine residues ablated binding completely: although this result may suggest that there are no additional sites of hydroxylation in MYPT1, it should be interpreted with caution as it is also possible that these mutations affect binding by altering the structure of the ARD fold.

3.2.4 *FIH is necessary and sufficient for hydroxylation of the MYPT1 ARD*

Having shown that three residues in the ARD of MYPT1 were hydroxylated *in vivo*, I next sought to determine unequivocally that this effect was dependent on FIH. In order to achieve this I quantitated the level of hydroxylation at the three sites of interest by liquid chromatography-mass spectrometry (LC-MS) under four conditions: endogenous levels of FIH, overexpression of hydroxylase-deficient mutant FIH, overexpression of wild-type FIH or knockdown of FIH using small interfering RNA (siRNA).

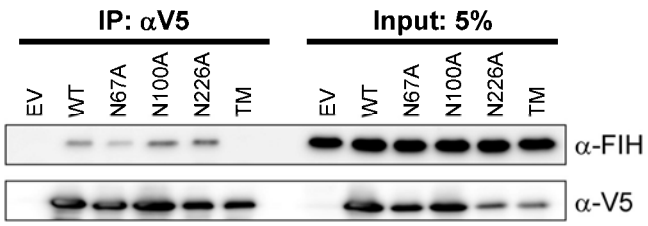


Figure 3.5 ***FIH and MYPT1 interact in 293T cells***
293T cells were transfected with V5-tagged plasmids encoding wild-type MYPT1 ARD (WT), the indicated point mutants, a triple asparagine mutant (TM) or an empty vector control (EV). Cells were harvested 48 h post-transfection, and the respective MYPT1 proteins immunoprecipitated using V5 resin. Immunoprecipitates were analysed by immunoblotting for capture of MYPT1 and co-precipitation of endogenous FIH.

A similar methodology was employed to that used for quantitation of Notch1 hydroxylation in Chapter 2, using extracted ion chromatograms and comparing the intensities of the peaks of interest. As the peptides of interest had not been previously characterized in this case, it was necessary to run samples twice. Firstly the samples were analysed by LC-MS/MS in order to determine both the exact masses of the peptides of interest and also their elution characteristics: the time during the chromatography gradient at which a peptide elutes is linked to its MS/MS spectrum by the data analysis software. Secondly, the samples were run in LC-MS mode: from the LC-MS data, extracted ion chromatograms were generated as before and the identity of the peaks of interest confirmed using the recorded elution times. After identification of the relevant peaks in the extracted ion chromatogram, hydroxylation was quantitated using the relative peak intensities of the hydroxylated and unhydroxylated peaks.

293T cells were transfected twice with siRNA duplexes targeting either FIH or an irrelevant control sequence (*Drosophila melanogaster* HIF, dHIF). Following the second transfection cells were re-seeded and transfected with MYPT1 ARD together with either empty pcDNA3 vector, pEF-FIH or a hydroxylase-deficient FIH mutant (pEF-FIH D201A) in which Asp-201, one of the critical catalytic triad of residues, has been mutated to an alanine residue (Stolze et al., 2004): MYPT1 ARD and pcDNA3 or FIH plasmids were transfected in a 4:1 ratio. Following the plasmid transfection, cells were lysed and MYPT1 ARD immunopurified, digested and analysed as before: the same inclusion list as previously was used for MS/MS analysis.

Representative extracted ion chromatograms for one of the sites of hydroxylation under the four conditions are shown in Figure 3.6. Quantitative data for all three sites of hydroxylation under all four conditions tested (except Asn-226 with FIH D201A overexpression, where levels of hydroxylation were low but poor chromatography precluded precise quantitation) are shown in Figure 3.7A and Figure 3.7B. Cell extracts were immunoblotted to confirm the efficacy of the FIH interventions (Figure 3.7C). These data show that levels of hydroxylation at the three sites with endogenous FIH were around 5%, with FIH overexpression boosting hydroxylation almost to completion. FIH D201A overexpression had no effect. Further, knockdown of FIH protein levels by siRNA reduced hydroxylation almost below the limit of detection in all three cases. Thus FIH is necessary and sufficient for hydroxylation at all three asparagine residues, and the effect is enzymatic. These data also suggest that the +16 Da mass shift on the peptide containing Asn-100 in Figure 3.3B does indeed represent asparaginyl hydroxylation, as the modification is FIH dependent.

3.2.5 *Endogenous MYPT1 is hydroxylated*

The data shown so far have established that MYPT1 can be post-translationally hydroxylated *in vivo*, and that these hydroxylations are FIH-dependent. However, all of these experiments had used overexpressed MYPT1 ARD in tissue culture cells. In order to determine whether the hydroxylations were physiologically relevant, I decided to analyse an animal sample of endogenous MYPT1. A sample of MP holoenzyme prepared from turkey gizzard was purified as described (Shimizu et al., 1994) and kindly provided by Andrea Murányi and David J Hartshorne (University of Arizona, Tucson, AZ): this was resolved by SDS-PAGE and stained using Coomassie

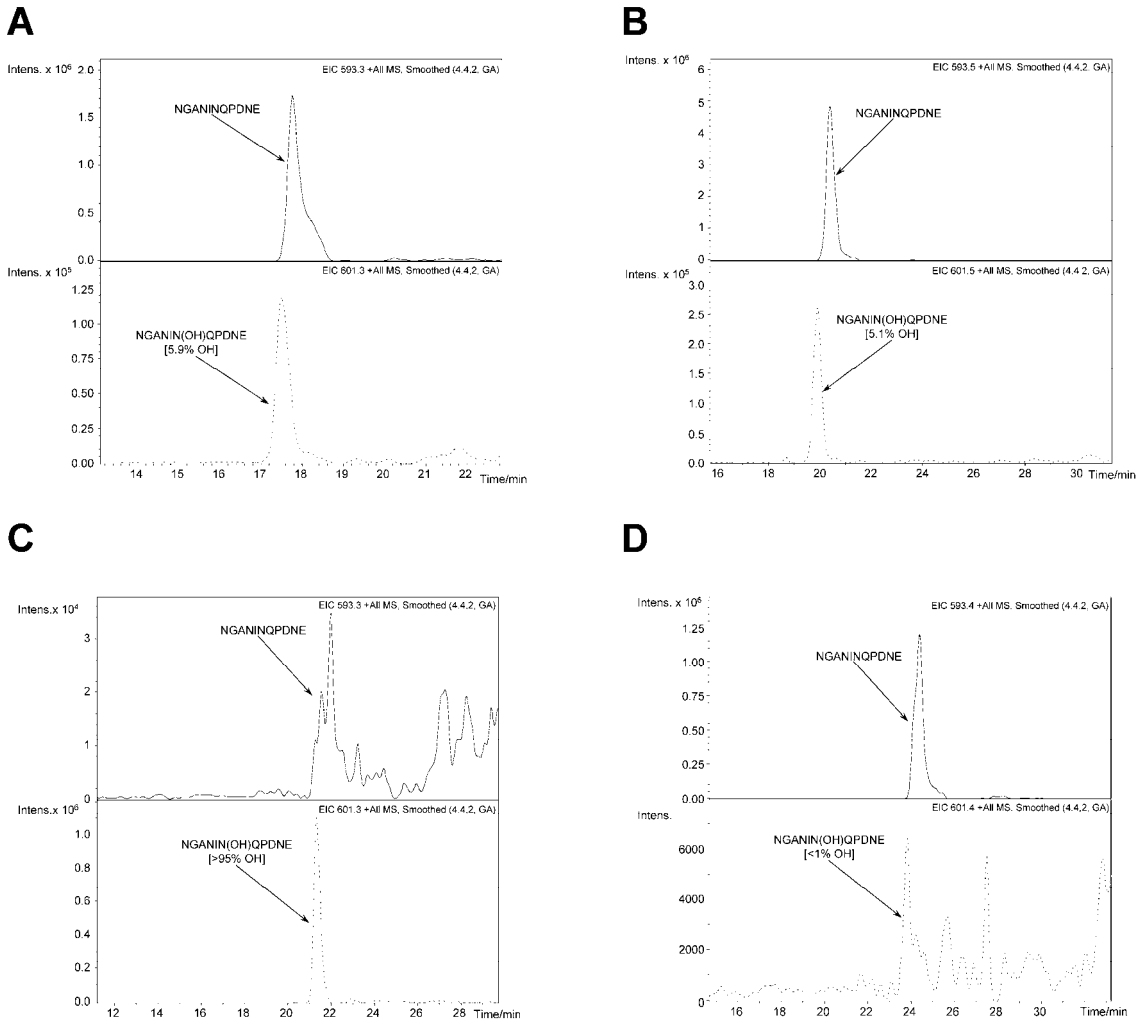
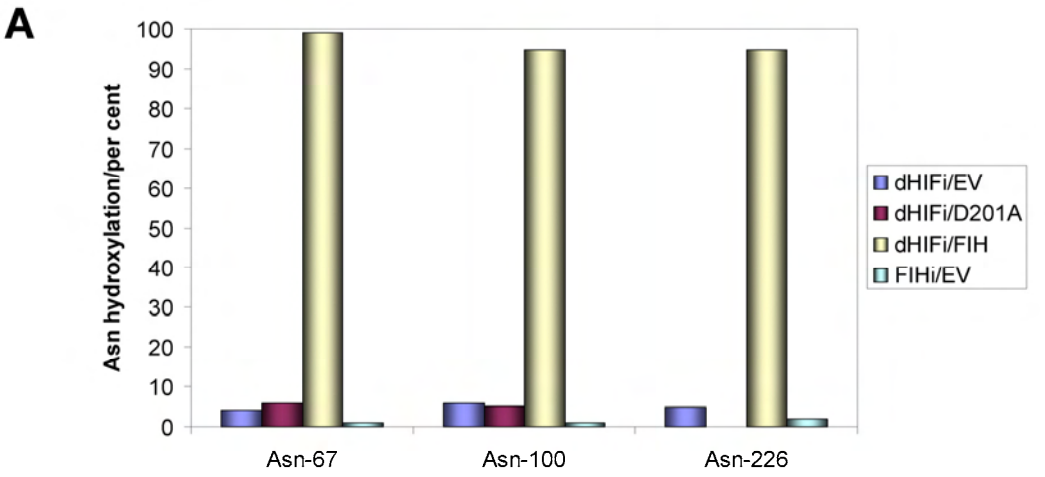


Figure 3.6 ***FIH is necessary and sufficient for MYPT1 hydroxylation (i)***
Extracted ion chromatograms showing GluC peptides containing one of the hydroxylation sites (Asn-100) in unoxidized state (solid line) and hydroxylated state (broken line) under the following conditions: (**A**) *control siRNA, empty vector transfection,* (**B**) *control siRNA, FIH D201A transfection,* (**C**) *control siRNA, FIH wild type transfection,* (**D**) *FIH siRNA, empty vector transfection. The percentage hydroxylation in each sample was determined by comparing the relative intensities of the hydroxylated and unoxidized peaks. Note the differing y-axis scales between panels: in* (**C**) *and* (**D**) *the intensities of the unoxidized and hydroxylated peaks respectively are approaching the limit of detection as shown by the increased "noise" in these traces. The elution times of the peptides vary slightly between samples due to instrumental limitations, however the hydroxylated peptide reproducibly elutes slightly earlier than the unoxidized peptide, consistent with its increased hydrophilicity.*



B

	dHIFi/EV	dHIFi/ D201A	dHIFi/ FIH	FIHi/EV
Asn-67	4.1%	5.9%	>99%	0.9%
Asn-100	5.9%	5.1%	>95%	<1%
Asn-226	<5%	ND	>95%	<2%

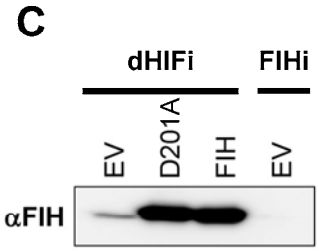


Figure 3.7 ***FIH is necessary and sufficient for MYPT1 hydroxylation (ii)***
(**A**) *and* (**B**) *Quantitation of hydroxylation at the three sites in MYPT1 under the indicated conditions of control siRNA (dHIFi) or FIH siRNA (FIHi) together with pcDNA3 (EV), pEF-FIH D201A (D201A), or pEF-FIH (FIH) transfection. ND indicates that the extent of hydroxylation was not determined.*
(**C**) *Anti-FIH immunoblot of cell extracts to confirm the efficiency of the FIH interventions.*

blue. As expected the holoenzyme contained subunits of around 110 kDa and 37 kDa corresponding to MYPT1 and PP1cδ respectively (Figure 3.8A). At 20 kDa, the M20 subunit was too small to be resolved under the electrophoresis conditions used. The MYPT1 bands were excised and digested using both trypsin and GluC. LC-MS/MS analysis assigned hydroxylation at two sites, Asn-67 and Asn-100 (Figure 3.8B and Figure 3.8C, respectively). No peptide containing Asn-226 was observed in this experiment: see discussion, Section 3.3. Following assignment of the hydroxylation sites, the digests were analysed by LC-MS to determine the extent of hydroxylation: this experiment revealed that hydroxylation at Asn-67 was approximately 48%, with Asn-100 hydroxylated to around 43% (Figure 3.9). Hydroxylation of MYPT1 is therefore an endogenous and physiologically relevant phenomenon.

3.2.6 *Structural consequences of MYPT1 hydroxylation*

The structure of the MYPT1 ARD complexed to PP1cδ has been published previously (Terrak et al., 2004). Given that the ARD has been shown to be important in conferring both correct substrate selectivity and enzymatic activity on the MP holoenzyme (Hirano et al., 1997; Tanaka et al., 1998), I mapped the three sites of hydroxylation onto the structure to determine whether any of them might be expected to affect the MYPT1/PP1cδ interaction (Figure 3.10A). In common with the ARD of Notch1 (Coleman et al., 2007), the substrate residues in MYPT1 are oriented such that hydroxylation can lead to the formation of an additional hydrogen bond between the target asparagine residue and the residue at the –2 position. Figure 3.10B shows the potential hydrogen bonding between Asn-67/Asp-65 and Asn-100/Asn-98; Figure 3.10C shows the bond that could form between Asn-226 and Asp-224. It is

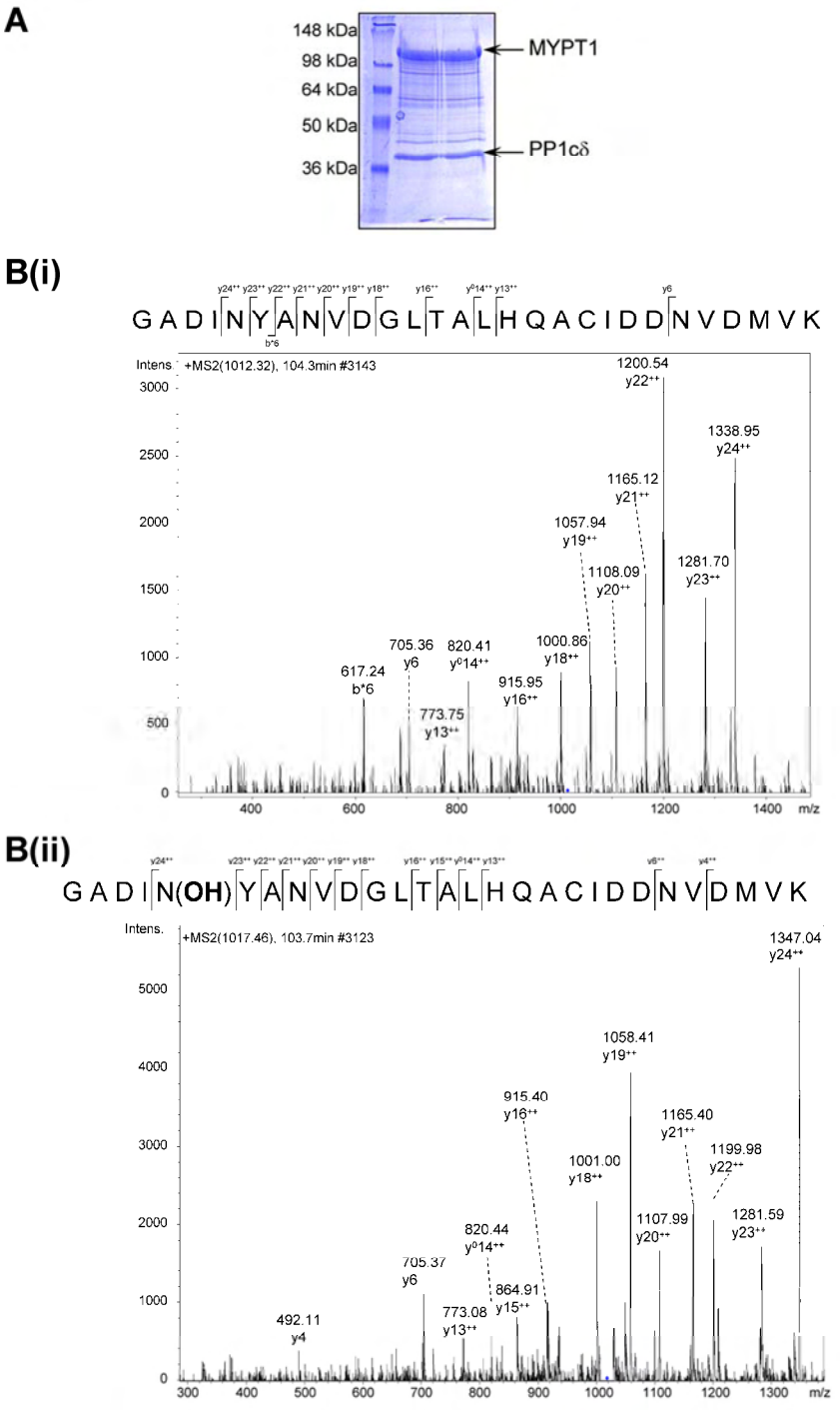


Figure 3.8A and B *Endogenous MYPT1 is hydroxylated (i)*

(**A**) *SDS-PAGE gel showing the avian myosin phosphatase sample resolved into MYPT1 and PP1cδ subunits.*

(**B**) *MS/MS spectra showing the tryptic fragment of turkey MYPT1 containing Asn-67 in unoxidized and hydroxylated states. Spectrum* (**i**) *shows the unoxidized peptide. In spectrum* (**ii**)*, an additional mass of 8 Da is observed in the doubly-charged $y24^{++}$ ion, indicating hydroxylation at Asn-67. The m/z difference of 5.14 between the two triply charged precursor peptide ions corresponds to a mass difference between the uncharged peptides of 16 Da within the mass resolution of the instrument.*

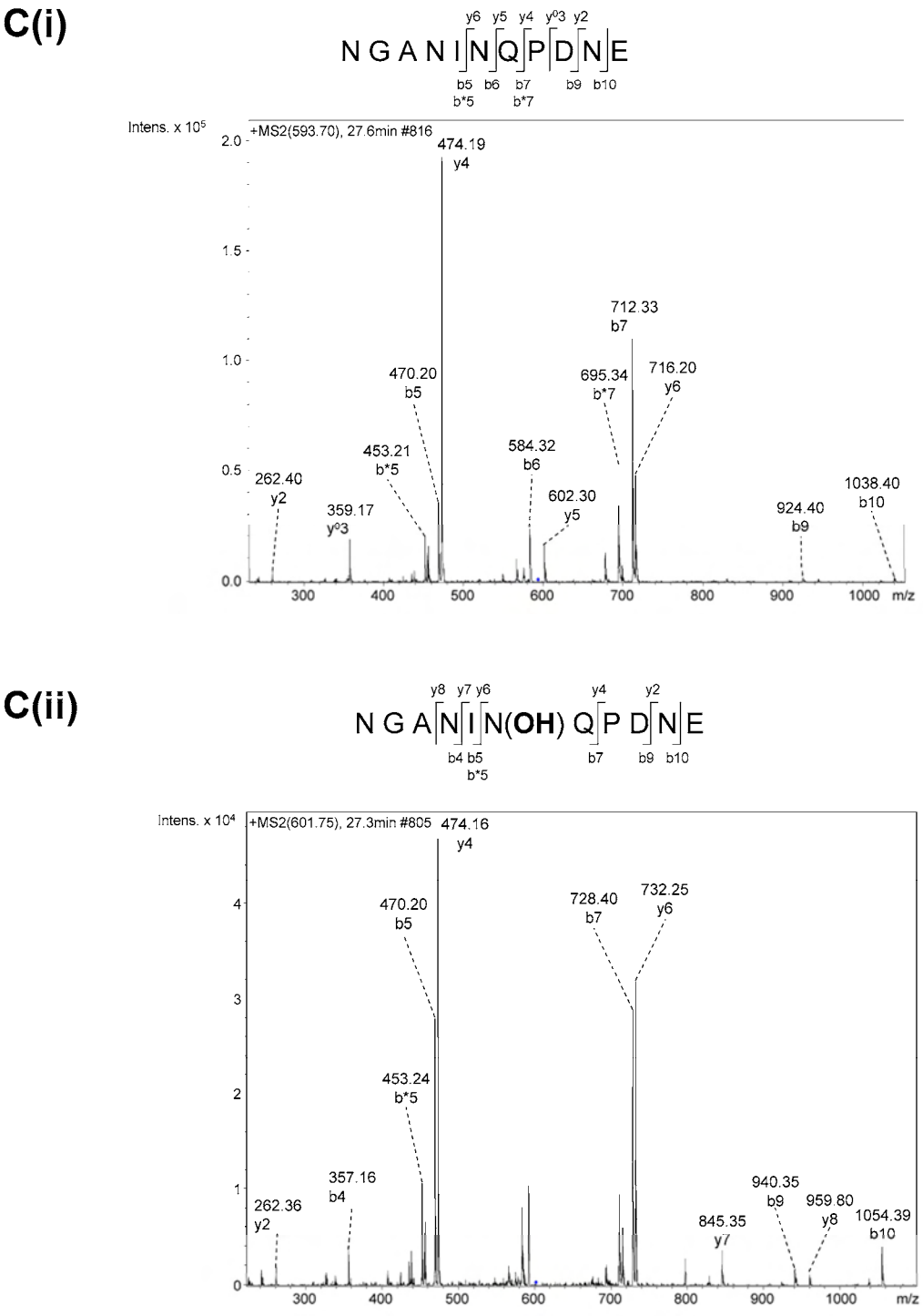


Figure 3.8C *Endogenous MYPT1 is hydroxylated (i)*

MS/MS spectra showing the GluC fragment of turkey MYPT1 containing Asn-100 in unoxidized and hydroxylated states. Spectrum (**i**) *shows the unoxidized peptide. In spectrum* (**ii**)*, an additional mass of 16 Da is observed in the b-ion series from b7 and in the y-ion series from y6, indicating hydroxylation at Asn-100 (or oxidation at Gln-101). The m/z difference of 8.05 between the two doubly charged ions corresponds to a mass difference between the uncharged peptides of 16 Da within the mass resolution of the instrument.*

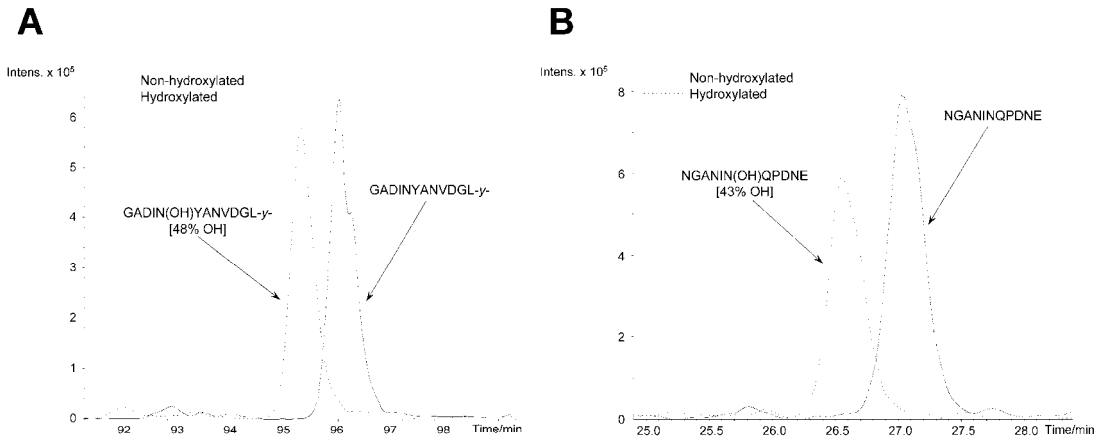


Figure 3.9 *Endogenous MYPT1 is hydroxylated (ii)*
Extracted ion chromatograms of peptides derived from turkey MYPT1 containing (**A**) *Asn-67 and* (**B**) *Asn-100 in unoxidized state (solid line) and hydroxylated state (broken line). Percentage hydroxylation was calculated by comparing the intensities of the hydroxylated and non-hydroxylated peaks.*

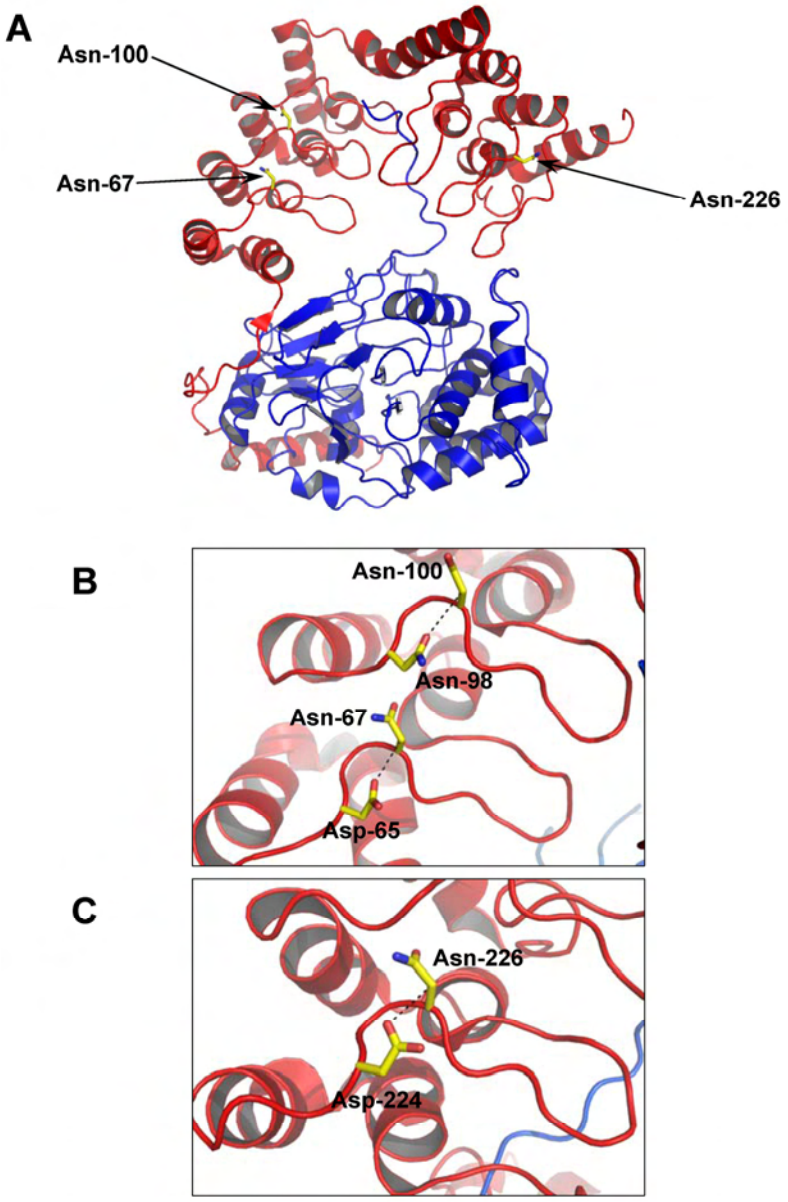


Figure 3.10 ***Structural consequences of MYPT1 hydroxylation***
(**A**) *Ribbon representation of the structure of MYPT1 ARD (in red) complexed to PP1cδ (in blue) showing the location of Asn-67, Asn-100 and Asn-226 (Protein Data Bank accession number 1S70, (Terrak et al., 2004)).*
(**B**) *Close-up of Asn-67 and Asn-100, showing the additional hydrogen bonds potentially formed to Asp-65 and Asn-98 respectively upon hydroxylation of the substrate residues.*
(**C**) *Close-up of Asn-226, showing the additional hydrogen bond potentially formed to Asp-224 upon hydroxylation of the substrate residue.*

therefore possible that post-translational hydroxylation at these sites could conformationally stabilize the ARD of MYPT1 (see discussion, Section 3.3).

3.2.7 *FIH does not affect the interaction between MYPT1 and PP1cδ*

The crystal structure of the MYPT1 ARD/PP1cδ complex shows that the ARD mediates interactions additional to the principal interaction at the well-characterized KVKF binding motif (Terrak et al., 2004). There are several residues in the ARD which interact with PP1cδ in forming the β-hairpin "clamp", including Val-71 (adjacent to Asn-67), Asp-229 and Trp-231 (both C-terminal to Asn-226). To determine whether FIH-dependent hydroxylation might affect MYPT1/PP1cδ binding, I immunoprecipitated endogenous MYPT1 from 293T cells that had been treated with the same FIH interventions as previously (Figure 3.11). This experiment clearly demonstrated that FIH overexpression or knockdown did not affect the interaction between MYPT1 and PP1cδ *in vivo*.

3.2.8 *FIH overexpression or suppression do not affect MLC phosphorylation status*

Structural data indicate that the phosphorylated MLC binding site of the MP holoenzyme is made up of the catalytic groove of PP1cδ together with an acidic cleft on MYPT1 formed by the α-helices of the ARD (Terrak et al., 2004). Although FIH did not affect the MYPT1/PP1cδ interaction, it remained possible that FIH could modulate the binding of substrate to MP (and hence MLC phosphorylation) *via* ARD hydroxylation. This hypothesis was tested by immunoblotting, using antibodies specific to phosphorylated MLC (either Ser-19 or Thr-18/Ser-19). 293T cells were transfected with pcDNA3 empty vector, pEF-FIH D201A, pEF-FIH, control siRNA duplex or

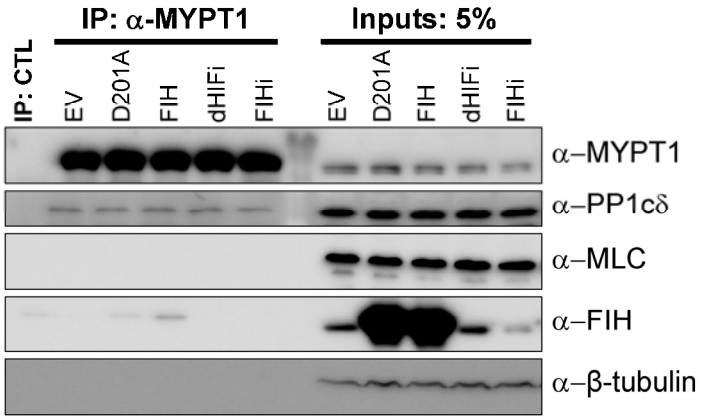


Figure 3.11 ***FIH does not affect the interaction between MYPT1 and PP1cδ***
293T cells were transfected with pcDNA3 (EV), pEF FIH D201A (D201A), pEF FIH (FIH), control siRNA (dHIFi) or siRNA targeting FIH (FIHi). Cells were harvested and the endogenous MYPT1 immunoprecipitated. Immunoprecipitates and cell extracts (inputs) were probed for MYPT1, PP1cδ, MLC, FIH and β-tubulin as a loading control.

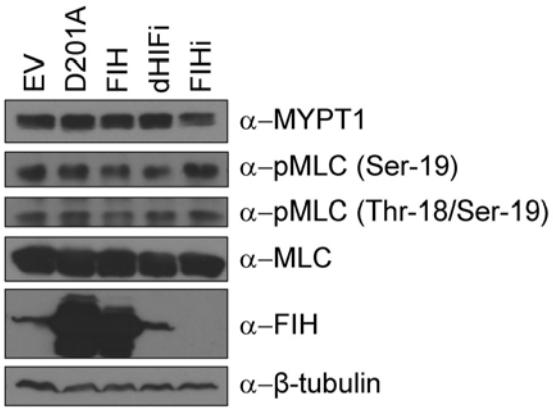


Figure 3.12 ***FIH overexpression or suppression do not affect MLC phosphorylation status***
293T cells were transfected with pcDNA3 (EV), pEF FIH D201A (D201A), pEF FIH (FIH), control siRNA (dHIFi) or siRNA targeting FIH (FIHi). 48 h post-transfection cells were harvested and extracts immunoblotted for phospho-MLC (Ser-19 and Thr-18/Ser-19), MLC, FIH and β-tubulin as a loading control.

siRNA duplex targeting FIH, following which extracts were analysed by immunoblotting (Figure 3.12). This experiment showed that, despite the FIH interventions working very efficiently, the level of MLC phosphorylation was unaffected even when FIH was grossly overexpressed or completely suppressed.

3.2.9 *MYPT1 ARD can influence the transcriptional activity of HIF1α through competition for FIH.*

A previous study has shown that the intracellular domain (ICD) of Notch can modulate HIF1α CAD activity through competitive inhibition of FIH hydroxylation (Coleman et al., 2007), consistent with the much lower K_m of FIH for Notch1 than HIF1α CAD (see Chapter 2). This competition results in enhanced HIF1α CAD activity that can be detected using the luciferase reporter assay in HeLa cells based on UAS luciferase and a HIF1α CAD-Gal4-DNA binding domain (Gal4-DBD) fusion protein, as used in Chapter 2. I used this assay to determine whether MYPT1 can also modulate HIF1α CAD activity, and whether this effect may be general to ARD-containing proteins.

As expected, the Notch1 ICD significantly enhanced reporter gene activity (30-fold) compared to HeLa extracts transfected with HIF1α CAD-Gal4-DBD and UAS luciferase alone (Figure 3.13A). Transfection of the MYPT1 ARD construct enhanced activity to almost the same extent, consistent with MYPT1 acting as a competitive FIH inhibitor. The full length MYPT1 construct enhanced HIF1α CAD activity only slightly (two-fold): this is likely due to the much lower expression level of this construct compared to the ARD as determined by immunoblotting the HeLa extracts (Figure 3.13B, left-hand panel).

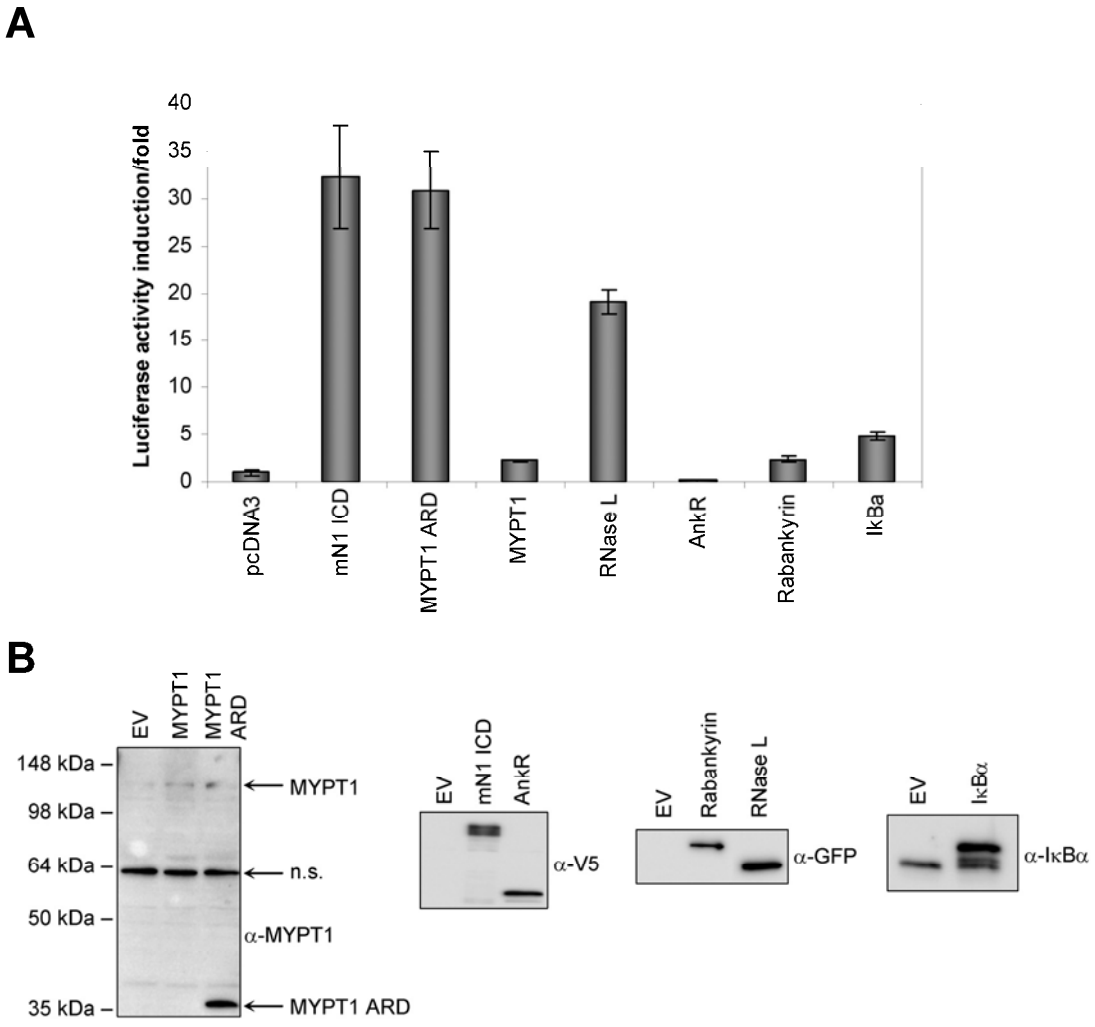


Figure 3.13 ***MYPT1 can influence the transcriptional activity of HIF1α through competition for FIH***

(**A**) *HeLa cells were transfected with UAS luciferase, HIF1α CAD-Gal4-DBD, the indicated ARD protein and β-galactosidase as a transfection control. 48 h post transfection, cells were harvested and analysed in parallel for luciferase and β-galactosidase activity. Relative luciferase activity (corrected for β-galactosidase activity) is shown; error bars represent SEM.*
(**B**) *Cell extracts were analysed by immunoblotting using the indicated antibodies to confirm expression of the ARD proteins. In the left-hand panel, MYPT1, MYPT1 ARD and non-specific (n.s.) bands are indicated.*

In order to investigate whether the modulation of HIF1α CAD activity is a general property of ARD-containing proteins, I tested a range of other molecules for which cDNA was available. These were IκBα (see Chapter 1), RNaseL (a protein containing nine ankyrin repeats involved in the antiviral response (Tanaka et al., 2004)), Rabankyrin (a 21-repeat protein implicated in endocytosis and macropinocytosis (Schnatwinkel et al., 2004)) and AnkyrinR (a structural component of erythrocyte membranes (Kolondra et al., 2008) containing a 24-repeat ARD (Michaely et al., 2002)). RNaseL increased HIF1α CAD activity approximately 20-fold whilst Rabankyrin, although expressed to a comparable level (Figure 3.13B, centre-right panel) produced a more modest enhancement (two-fold). IκBα produced a five-fold induction in reporter activity. RNaseL, Rabankyrin and IκBα have all been identified as FIH substrates (Cockman et al., 2006; Cockman et al., 2008). Interestingly, cotransfection of ARs 13 – 24 of AnkyrinR (containing at least three hydroxylation sites)[1] had no competitive effect at all in this assay, even though the protein was expressed at a comparable level to Notch1 ICD (Figure 3.13B, centre-left panel). This assay shows that MYPT1 can inhibit FIH-mediated suppression of HIF1α CAD transcriptional activity and that this effect is general to most (but not all) ARD-containing proteins (see discussion, Section 3.3).

[1] Ming Yang and Christopher Schofield, personal communication

3.3 Discussion

Recent publications have shown that FIH can hydroxylate several ankyrin repeat-containing proteins (Cockman et al., 2006; Coleman et al., 2007; Ferguson et al., 2007). Taking these reports together with the results of the experiments reported in Chapter 2, where the consensus sequence for FIH-dependent hydroxylation appeared to mirror the consensus sequence for ankyrin repeats closely, it therefore appeared that the post-translational hydroxylation of ARDs by FIH might be a widespread modification. I rationalized that if this were the case then it should be possible to identify novel candidate substrates *in silico*: the work in this chapter has shown that three of four candidate hydroxylation sites identified bioinformatically in MYPT1, are indeed genuine FIH targets, providing further evidence for the generality of FIH-mediated ARD hydroxylation.

Four candidate sites for hydroxylation were identified, based on the results of Chapter 2. These were Asn-67 (in ankyrin repeat 1), Asn-100 (in ankyrin repeat 2), Asn-226 (in ankyrin repeat 6) and Asn-288 (in ankyrin repeat 8). Asn-67, Asn-100 and Asn-226 were all hydroxylated, whereas Asn-288 was not. This is consistent with the observation that the primary sequence surrounding Asn-288 showed the least similarity of all the target residues to established substrates, including the lack of Leu +10 and also perhaps with structural data showing that ankyrin repeat 8 of MYPT1 does not adopt a canonical fold structure (Terrak et al., 2004). Hydroxylation of Asn-100 is of interest as all previous substrate asparagine residues have conformed to a $L_{(-8)}D/E_{(-2)}XN$ motif, and supports the results of Chapter 2 showing that an acidic residue at the –2 position is not a requirement for hydroxylation. No unanticipated sites of hydroxylation were observed in the ARD of MYPT1, even with forced

expression of FIH: it remains a formal possibility though that there may be additional sites of asparaginyl hydroxylation that were not detected in these experiments.

Analysis of the endogenous sample of avian myosin phosphatase was significant for two reasons. This is the first demonstration of ankyrin-repeat hydroxylation in an animal sample (as opposed to cell culture), showing that ARD hydroxylation does occur *in vivo* and is a true, physiologically relevant, non-artefactual post-translational modification. Further, this result is the first demonstration of ARD hydroxylation in a non-mammalian system, showing that this modification is conserved from mammals to birds: it will be of interest to determine how well conserved this system is throughout the animal kingdom and beyond.

Although the gene encoding turkey MYPT1 has not been sequenced, the amino acid sequence of the chicken protein is available (NCBInr database, gi number 633038). It has previously been stated that conservation of the MYPT1 ARD between chicken and human is over 96%, and thus it seems reasonable to assume good conservation between the chicken and turkey proteins. Interrogating the MS/MS fragmentation data against the chicken protein sequence gave good coverage of the relevant peptides, validating this assumption. The failure to detect a tryptic peptide containing Asn-226 in the avian myosin phosphatase sample is likely due to a glycine to arginine substitution four residues N-terminal to Asn-226 in the chicken protein compared to the human protein. This introduces an additional cleavage site for trypsin, resulting in a very short tryptic fragment (six residues) that is not amenable either to MS detection or to MS/MS sequencing.

In contrast to IκBα and Notch1, both of which contain two substrate asparaginyl residues that are differentially hydroxylated (Cockman et al., 2006; Coleman et al., 2007), the three sites in MYPT1 appear to be hydroxylated to approximately the same extent. Although when the MYPT1 ARD was overexpressed in 293T cells the levels of hydroxylation observed were relatively modest at around 5%, co-transfection of MYPT1 ARD with FIH forced hydroxylation of the ARD protein virtually to completion at all three sites, suggesting that endogenous FIH was saturated. Although levels of hydroxylation in the sample of purified avian MP holoenzyme at the two substrate asparaginyl residues observed were significantly higher at 40 – 50%, it is not possible to make a comparison between these two systems without any knowledge of their relative FIH levels. However, incomplete hydroxylation is consistent with previous observations in tissue culture cells, and suggests that rather than being an artefact of cell culture conditions incomplete asparaginyl hydroxylation of ARDs is physiologically relevant, perhaps reflecting saturation of endogenous FIH *in vivo* due to the ubiquity and abundance of its substrates. Incomplete hydroxylation could also reflect a signalling role for FIH in this system: this possibility is discussed further in Chapter 5.

Only one other post-translational modification of the MYPT1 ARD has been reported previously, a phosphorylation by protein kinase C which inhibits binding of MYPT1 both to PP1cδ and also the phosphorylated MLC substrate *in vitro* (Tóth et al., 2000a). Whilst a biophysical study using surface plasmon resonance has suggested that only the KVKF motif in MYPT1 is necessary for binding of PP1cδ (Tóth et al., 2000b), biochemical studies have demonstrated that the intact ARD is important for imparting the correct catalytic properties to the holoenzyme (Hirano et al., 1997; Tanaka et al.,

1998). Further, structural data indicate that two of the three hydroxylation sites lie proximal to sites of interaction between MYPT1 and PP1cδ. Taking these results together, it seemed reasonable to hypothesize that hydroxylation of the ARD could potentially modulate the MYPT1/PP1cδ interaction and influence the activity of myosin phosphatase. However, FIH intervention did not significantly affect the interaction between MYPT1 and PP1cδ, nor the activity of myosin phosphatase towards MLC. With respect to the MYPT1/PP1cδ interaction, this may not be surprising: the KVKF motif is necessary and sufficient for the two proteins to interact (Tóth et al., 2000b), and close analysis of structural data shows that Asn-67 and Asn-226 project away from the interaction surface (Terrak et al., 2004). Additionally, although the α-helices of the ankyrin repeats are important for the formation of an extended acidic groove constituting the MLC binding site in the myosin phosphatase holoenzyme, the hydroxylated residues are located in the β-hairpin loops on the opposite face of the ARD (Terrak et al., 2004), which may explain why no effect of FIH intervention was noted on the activity of myosin phosphatase towards MLC.

A physical consequence of ARD hydroxylation is the formation of a hydrogen bond between the hydroxyasparagine residue and an acceptor residue at the –2 position, in all characterized cases an aspartate (Coleman et al., 2007). Asn-67 and Asn-226 both have aspartate residues at the –2 position, whilst for Asn-100 there is an asparagine residue, also capable of accepting a hydrogen bond. Structural analysis of the MYPT1 ARD suggests that all three substrate asparagine residues are potentially capable of forming an additional hydrogen bond once hydroxylated: in several ankyrin-repeat proteins this phenomenon has been shown to enhance the stability of the ARD

towards thermally- or chemically-induced denaturation[2]. Studies on the ARD of the Notch receptor protein in *Drosophila melanogaster* have shown that structural effects in ankyrin repeat domains can be highly co-operative, with a single amino acid substitution in one repeat affecting stability throughout the ARD (Bradley and Barrick, 2002). Taking these observations together, the existence of at least three sites of hydroxylation in MYPT1 suggests that FIH-dependent hydroxylation could cooperatively enhance the conformational stability of the ARD. Although this did not have any effect on the activity of myosin phosphatase under the conditions studied, it is interesting to note that in some circumstances alterations in local ankyrin-repeat stability can influence biological activity (Truhlar et al., 2008). The possibilities of a structural or signalling role for FIH-mediated ankyrin-repeat protein hydroxylation are discussed further in Chapter 5.

It remains possible that hydroxylation could modulate other functions of MYPT1. The number of known MYPT1 interacting partners has increased significantly in recent years, suggesting that myosin phosphatase may be involved in a diverse range of cellular processes in addition to actin/myosin-based cell contractility. In support of this hypothesis, some of these interacting partners also appear to be substrates (Matsumura and Hartshorne, 2008). One example is the dephosphorylation of histone deacetylase 7, which implies a role for myosin phosphatase in transcriptional regulation (Parra et al., 2007). A second example is a report implicating MP as a phosphatase for the retinoblastoma protein, potentially influencing cell cycle progression; this interaction appears to involve the ARD (Wu et al., 2005). It is therefore possible that

[2] Leanne Kelly and Christopher Schofield, personal communication

hydroxylation of MYPT1 could have effects under other conditions or in different systems from those tested so far.

The data presented in this chapter also demonstrate that the ARD of MYPT1 can influence HIF1α CAD activity. It was not possible to demonstrate unequivocally that this effect was dependent on the target asparagine residues as the asparagine mutant ARD constructs only expressed to a detectable level in 293T cells. These cells replicate plasmids episomally, and are therefore not an appropriate system to use for a reporter assay in which artefactual differential plasmid amplification could distort results significantly. The effect of an ARD-containing protein was reported previously for Notch1 (Coleman et al., 2007), but the data here provide the first evidence that modulation of HIF signalling by competitive inhibition of FIH is a more general characteristic of ankyrin repeat-containing proteins. Interestingly however, the differences observed in competition did not appear entirely to reflect differences in expression: RNaseL and Rabankyrin were expressed to a similar extent but differed significantly in their efficacy as a competitive inhibitor. Likewise, whilst expression levels of Notch1 ICD and AnkyrinR were comparable, the latter had no detectable effect on HIF1α CAD activity at all. It therefore seems plausible that the ability of an ARD protein to out-compete HIF may be related to its efficiency as an FIH substrate, but further work to determine K_m values for the reaction of FIH with these ankyrin-repeat proteins will be required to confirm this.

The human genome encodes over 300 proteins predicted to contain an ARD motif (SMART database, (Schultz et al., 1998)). The evidence presented here and elsewhere suggests that many of these proteins could be substrates for FIH, raising the possibility

that a cellular pool of ARD proteins acts as a "sink" for FIH. One possibility is that, given the non-degradative nature of ARD hydroxylation, hydroxylation of a pool of ARD-containing proteins may provide a record of recent cellular oxygen levels, enabling a cell to "tune" its oxygen-sensing mechanisms. Another hypothesis is that ARD proteins in the cell act as a brake on FIH activity. It has been shown previously that even under normoxic conditions siRNA-mediated FIH suppression increases HIF target gene expression whilst modest FIH overexpression has the opposite effect, suggesting that the activity of FIH towards HIF is suboptimal in normoxic cells (Stolze et al., 2004). The existence of a cellular ARD sink would explain not only the limiting activity of FIH towards HIF in tissue culture cells but also incomplete hydroxylation of the ARDs themselves arising from "cross competition". In either case, it is possible that post-translational hydroxylation of ARDs forms part of a novel mechanism regulating the transcriptional activity of HIF.

In summary, the experiments presented in this chapter have demonstrated three sites of FIH-dependent hydroxylation in the MYPT1 ARD, of which two have been verified in an endogenous protein sample. Although under the conditions tested manipulation of FIH levels did not appear to affect the activity of the myosin phosphatase holoenzyme, the hydroxylations observed are predicted to have a stabilizing effect on the ARD as a whole. Further, the data demonstrate that, in common with other ARD-containing proteins, MYPT1 may form part of a novel regulatory mechanism for HIF signalling.

Chapter 4

A proteomic approach for identifying novel PHD3 substrates

4.1 Introduction

The work discussed in the previous two chapters has focused on the identification and characterization of "non-HIF" substrates for the asparaginyl hydroxylase FIH. This chapter extends the scope of these findings by presenting experiments carried out with the aim of identifying novel substrates of the prolyl hydroxylase enzyme, PHD3.

Evidence from model organisms and cell culture studies suggesting that there may be alternative, non-HIF substrates of the PHDs is discussed in Chapter 1. In deciding on a candidate PHD to investigate, various factors can be taken into consideration: are any of the enzymes associated with a clear function that is not directly related to hypoxia or HIF? Is the enzyme level regulated by a non-hypoxic stimulus? Is niche expression of an enzyme observed in an environment that is not apparently hypoxic? Based on these criteria I selected PHD3 for investigation: whilst PHD1 has been shown to be induced in response to oestrogen (Appelhoff et al., 2004; Seth et al., 2002), no function has yet been attributed to this effect. In contrast, a growing body of literature suggests that PHD3 (but not PHD1 or PHD2) is involved in neuronal apoptosis during development, and that this effect may be HIF-independent, as discussed in Chapter 1 (Lee et al., 2005; Lipscomb et al., 1999; Lipscomb et al., 2001; Straub et al., 2003). With this in mind, I decided to undertake a series of experiments with the aim of identifying novel PHD3 substrates. In contrast to the bioinformatic approach taken for the identification of MYPT1 as an FIH substrate in Chapter 3, the experiments described here are based on a proteomic strategy.

The bioinformatic approach used in chapter 3 was successful in identifying new FIH substrates only because it was possible to derive a consensus (in terms of both the

protein sequence and structure) based on a range of previously published substrates. Currently the only known substrates for the PHDs are the HIFs: in these all of the proline residues targeted for hydroxylation lie in a Leu-X-X-Leu-Ala-Pro (LxxLAP) motif (Ivan et al., 2001; Jaakkola et al., 2001; Masson et al., 2001). However, more recent studies have shown that these leucine residues are not essential and can be substituted with various other amino acids (Huang et al., 2002; Li et al., 2004), suggesting that the only essential residue for hydroxylation may be proline itself. Whilst it has been clearly shown that longer HIF peptides make better substrates than short peptides (Hirsilä et al., 2003; Koivunen et al., 2006), no consensus sequence for prolyl hydroxylation has yet been defined. In the absence of a consensus for prolyl hydroxylation, the bioinformatic approach was clearly inappropriate for seeking novel PHD3 substrates and a proteomic strategy, which can detect *in vivo* protein/protein interactions directly and without bias was adopted.

The development of mass spectrometry and especially tandem mass spectrometry (described in Chapter 3) as tools for peptide identification and sequencing has led to the advent of affinity purification and mass spectrometry (AP-MS) as a method for identifying protein/protein interactions (Gingras et al., 2007). AP-MS has greatly enhanced the understanding of protein/protein interaction networks and also the composition of protein complexes. The basic AP-MS experiment is shown schematically in Figure 4.1: firstly the gene of interest (in this case PHD3) is expressed in tissue culture cells. Following cell lysis the bait protein is affinity purified and washed to remove non-specific interacting proteins. The bait and its binding partners are then eluted from the affinity medium and resolved by SDS-PAGE, where they are seen as

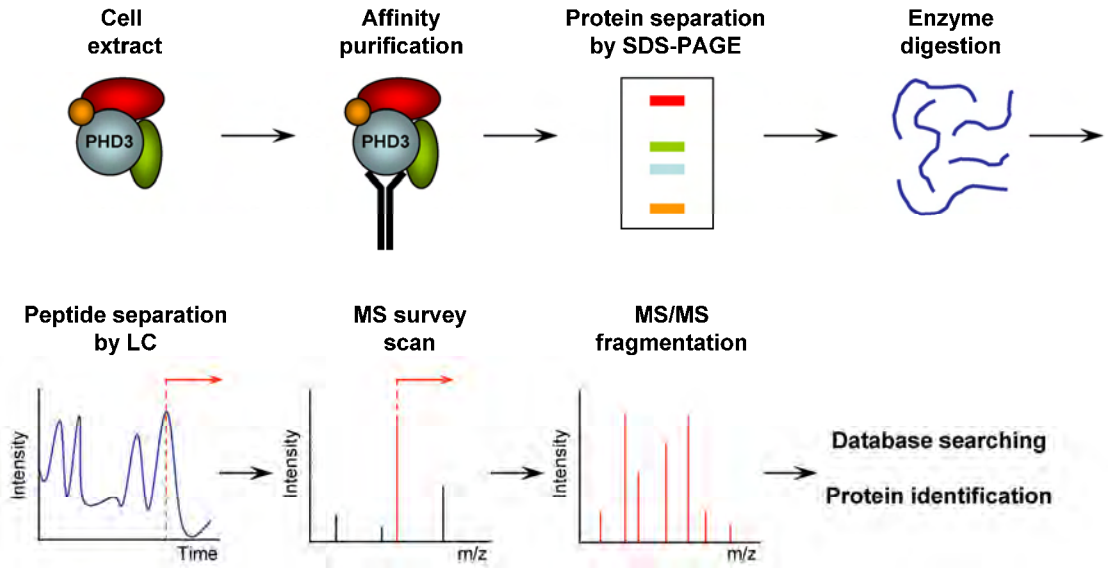


Figure 4.1 *Schematic diagram of the basic AP-MS experiment. Adapted from (Gingras et al., 2005).*

discrete bands. After staining, protein-containing bands are excised from the polyacrylamide gel and digested using a protease enzyme. Trypsin is used most commonly: it cleaves very reliably and specifically after lysine and arginine residues, producing peptides bearing a positively-charged residue at the C-terminus which are particularly amenable to MS detection. Other proteases may also be used if a particular peptide or residues are of interest. Following protein digestion, the peptide mixture is analysed by liquid chromatography-tandem mass spectrometry (LC-MS/MS) and the resulting MS/MS data searched against a database containing *in silico* digests of the relevant genome. Recent advances in liquid chromatography technology can enable the SDS-PAGE step to be omitted for simple mixtures, with the proteins instead being digested in solution and this mixture analysed directly. Adoption of a gel-free strategy is becoming increasingly popular (Gingras et al., 2007): gel-free approaches eliminate the significant sample losses that occur with in-gel digestion and are also more amenable to automation.

MS/MS is an extremely powerful tool, allowing the amino acid sequences of peptides to be assigned (and hence their parent proteins to be identified) and also potentially permitting the identification of post-translational modifications. However, the exquisite sensitivity of MS as a technique means that it can be a major challenge to distinguish *bona fide* interacting partners from non-specific contaminants (Gingras et al., 2005). Increasing the stringency of washing steps provides a partial solution but may also disrupt the binding of weaker, physiologically relevant interactors. The use of epitope-tagged proteins in cell culture is another method that has been widely adopted, as a separate purification from untransfected cells can be used as a control for some of the non-specific, contaminating proteins that may be detected. A more sophisticated

approach is the use of a dual affinity tag (known as tandem affinity purification or TAP) where the gene of interest is fused to two separate moieties separated by a protease cleavage site. TAP confers a high degree of specificity, reducing the need for stringent wash steps (Rigaut et al., 1999), and is discussed in more detail below.

The first experiments presented in this chapter describe the development of a tandem affinity purification strategy for identifying novel PHD3 substrates. Because of their transient nature, protein/protein interactions between enzyme and substrate can be particularly difficult to capture, and the use of a pharmacological PHD inhibitor as a "substrate trapping" agent (and the use of HIF as a positive control) is discussed. These experiments identified two PHD3 interacting proteins that were potential substrates, SKIP and *Simian virus 40* (SV40) large T antigen. Experiments undertaken to characterize these interactions by a range of strategies are presented, as well as attempts to demonstrate by mass spectrometry (including the use of a stable isotope labelling approach) that the proteins involved are true PHD3 substrates. Finally the results of this work are discussed, along with possible alternative strategies for assigning novel substrates for the HIF prolyl hydroxylases.

4.2 Results

4.2.1 *Tandem affinity tagging of PHD3*

The use of TAP as a strategy for enhancing the specificity of proteomic pull-down experiments has already been mentioned: employing two sequential purification steps in theory allows the number of non-specific interacting proteins identified to be significantly reduced without the need for stringent wash steps which might disrupt associations with weak, but true, interactors. The first tandem affinity purification tag to be developed (referred to hereafter as a TAP tag) consists of two IgG binding domains from *Staphylococcus aureus* protein A plus a calmodulin binding peptide (Rigaut et al., 1999). The protein A and calmodulin-binding moieties are separated by a cleavage site for tobacco etch virus (TEV) protease, allowing for an initial IgG affinity purification followed by TEV cleavage and a subsequent calmodulin purification. TAP tagging was originally developed for use in *Saccharomyces cerevisiae*, and has been used in large-scale experiments in this system – one study introduced a TAP tag at the C-terminus of more than 1700 open reading frames in the yeast genome. Of the tagged proteins, 589 were successfully purified (Gavin et al., 2002). The original TAP tag does have disadvantages though: it is large, at around 20 kDa, and may potentially interfere with protein function. In support of this suggestion, when essential proteins in yeast were C-terminally TAP tagged, around 18% of the resulting strains were not viable (Gavin et al., 2002).

A more recent development of the tandem affinity purification methodology involves an alternative tag, termed the sequential peptide affinity (SPA) tag. In the SPA tag the 137-amino acid protein A domain is replaced by a 22-residue 3×FLAG epitope: the TEV cleavage site and calmodulin binding peptide remain (Zeghouf et al., 2004). This

confers two advantages: firstly the SPA tag is significantly smaller than the TAP tag, and secondly the 3×FLAG epitope is recognized with very high specificity by monoclonal antibody M2 which can be used both for immunoprecipitation and immunoblotting (Hernan et al., 2000). Vectors containing PHD3 tagged C-terminally with both SPA and TAP tags were available, and for the reasons above I opted to use the SPA tag for proteomic experiments. A schematic representation of the PHD3-SPA construct is shown in Figure 4.2A. Figure 4.2B shows the main steps of the SPA purification procedure: initially cell extracts are prepared and incubated with anti-FLAG resin. After a series of washes bound PHD3 is eluted from the FLAG resin by overnight TEV cleavage: TEV protease is used as it reliably cleaves at a very specific recognition site, Glu–Asn–Leu–Tyr–Phe–Gln–Gly (Leahy et al., 2000). In the second purification step, the cleaved PHD3 is incubated with calmodulin sepharose in the presence of calcium to bind the calmodulin binding peptide domain. After additional washes, the PHD3 is eluted by calcium chelation.

Although the SPA tag is much smaller than the TAP tag, it is still relatively large at around 8 kDa. In order to ensure that the C-terminal SPA tag did not inhibit PHD3 function I decided to analyse the activity of untagged PHD3 along with three C-terminally tagged constructs: PHD3-V5 (a much smaller tag at only fourteen residues), PHD3-TAP and PHD3-SPA. These four plasmids (all in pcDNA3) were transfected into 293T cells and cell extracts analysed for their ability to hydroxylate HIF by an assay for pVHL capture. In this assay a biotinylated HIF1α peptide is incubated *in vitro* with a source of PHD enzyme (in this case the 293T cell extract) plus co-factors. The reaction is stopped at the desired time point using desferrioxamine (an iron chelator)

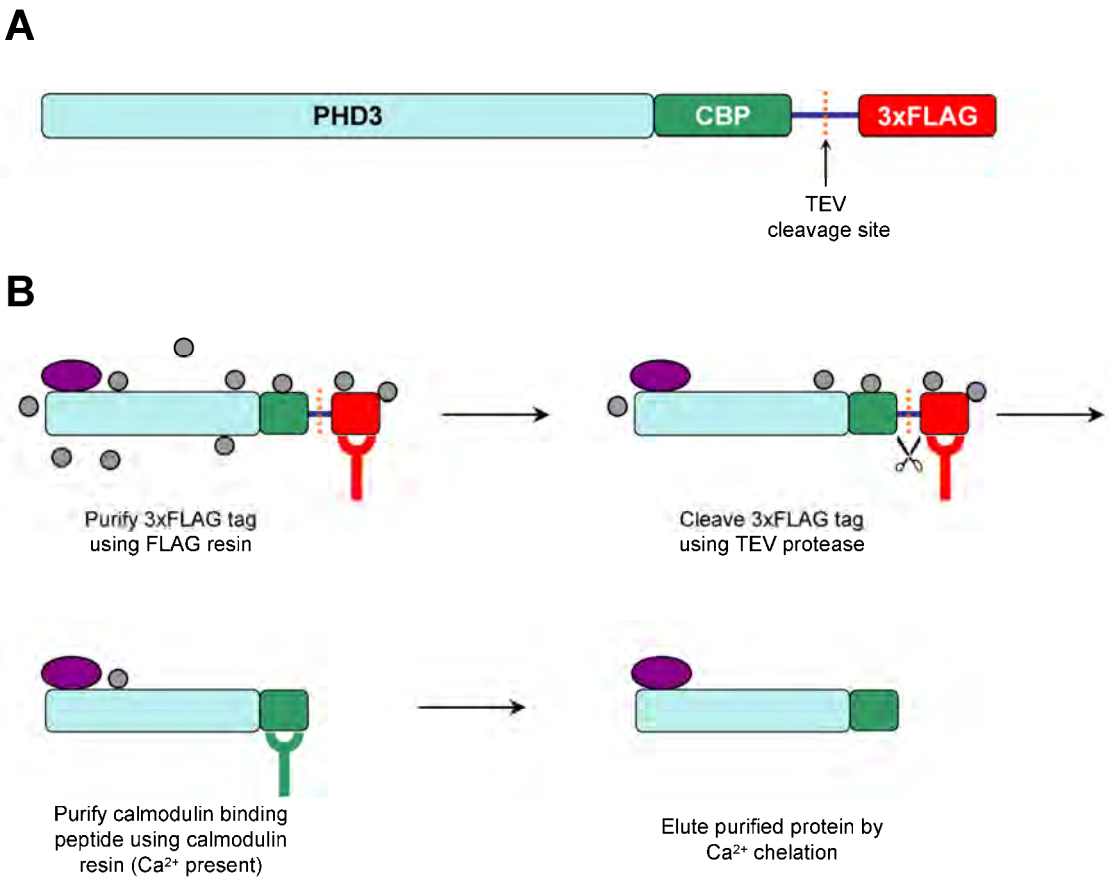


Figure 4.2 *SPA-tagging of PHD3*
(**A**) *Schematic representation of SPA-tagged PHD3.*
(**B**) *Schema showing the principle of SPA purification: the purple ellipse represents a specific interacting protein, with non-specific contaminants shown in grey. CBP denotes calmodulin binding peptide domain. Both panels adapted from (Gingras et al., 2005).*

and the biotinylated peptide immunoprecipitated onto streptavidin-coated beads. The beads are then incubated with [^{35}S]-radiolabelled pVHL. After a series of washing steps, the bound pVHL is eluted using sample buffer, resolved by SDS-PAGE and quantitated using a phosphorimager (Tuckerman et al., 2004). A ten-minute time course was used for each reaction, with samples taken at five and ten minutes. Because mammalian cells contain endogenous PHD1, 2 and 3 in varying quantities, an untransfected cell extract will have a basal level of PHD activity in this assay. In order to control for the endogenous PHD activity of 293T cells a cell extract transfected with empty pcDNA3 vector (EV) was analysed in parallel with the PHD3-transfected extracts.

The results of the pVHL capture assay are shown in Figure 4.3. Figure 4.3A(i) shows the raw phosphorimager data, which were quantitated and are shown graphically in Figure 4.3A(ii). All four of the PHD3-transfected cell extracts showed significantly higher prolyl hydroxylase activity than the extract containing endogenous PHD levels. In order to verify that expression levels of the PHD3 constructs were not grossly different, cell extracts were immunoblotted in triplicate using an anti-PHD3 monoclonal antibody (Figure 4.3B(i)) and quantitated by optical densitometry (Figure 4.3B(ii)). Note that endogenous PHD3 in the 293T cells was below the limit of detection in this experiment: it is likely that the endogenous PHD activity in the control-transfected cells is due largely to PHD2 as this tends to be the most abundant of the PHD enzymes in tissue culture cells under basal conditions (Appelhoff et al., 2004). Since all of the PHD3 constructs were expressed at a similar level, and all showed similar activity in the pVHL capture assay, I concluded that neither the SPA tag nor indeed the TAP tag have a deleterious effect on the prolyl hydroxylase activity of

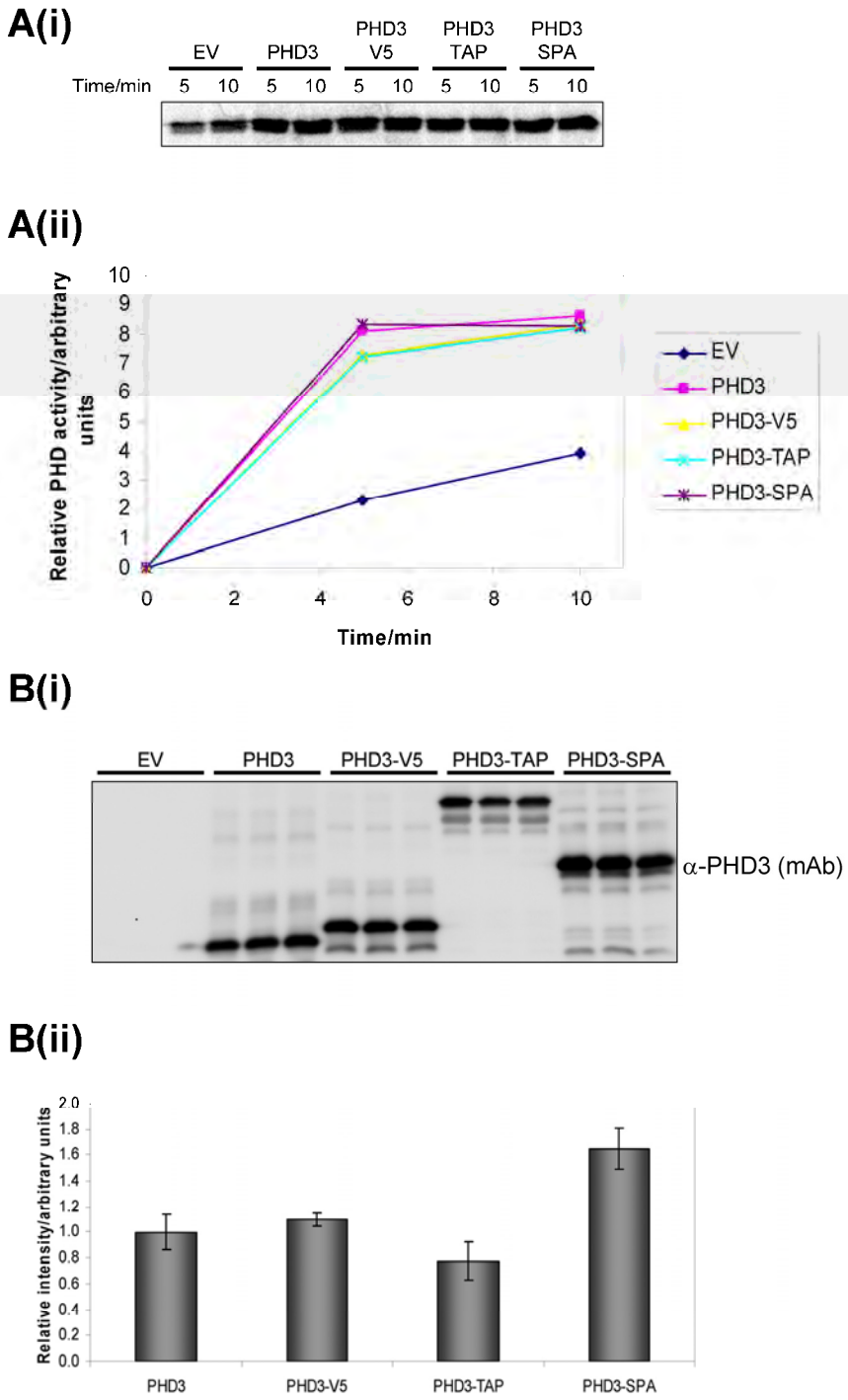


Figure 4.3 ***The SPA tag does not adversely affect the activity of PHD3***
(**A**) *Assay showing capture of radiolabelled pVHL by a hydroxylated HIF1α peptide incubated* in vitro *with 293T cell extract and co-factors. 293T cells were transfected with empty vector (EV) or the indicated PHD3 construct. Autoradiogram is shown in* (**i**)*, quantitative data over reaction time course are shown in* (**ii**).
(**B**) *Immunoblot* (**i**) *showing relative expression of the different PHD3 fusion proteins, quantitated by optical densitometry in* (**ii**). *Error bars represent standard deviation.*

PHD3. However, although the reaction time courses for all four PHD3-transfected cell extracts were very similar, the assay shows a degree of non-linearity suggesting that a near-maximal effect was reached by the five minute time point in all cases. It thus remains a formal possibility that this assay did not detect kinetic differences at very early time points.

4.2.2 *Development of a mixing strategy for capturing PHD3 interactors*

Previous reports on PHD3-dependent neuronal apoptosis have used the rat PC12 cell line as a model for sympathetic neurons (Lipscomb et al., 1999; Lipscomb et al., 2001; Straub et al., 2003 Lee et al., 2005). This cell line is derived from a phaeochromocytoma (a tumour of the adrenal gland, which forms part of the sympatho-adrenal lineage), and is of particular interest given the apparent role of PHD3 in mediating developmental neuronal apoptosis in the sympatho-adrenal system. My initial experiments with the PHD3-SPA construct were therefore aimed at producing a PC12 cell line stably expressing PHD3-SPA under the control of a tetracycline-responsive promoter (Urlinger et al., 2000), with the intention of inducing PHD3-SPA expression and carrying out a proteomic experiment in the time interval between PHD3 induction and the onset of apoptosis. However, it did not prove possible to generate such a cell line.

In the absence of an inducible PC12-based cell line, I decided to adopt an alternative strategy, by using PHD3-SPA expressed in 293T cells as "bait" in a mixing experiment. The principle behind this experiment was to take cell extract from 293T cells expressing PHD3-SPA (or an empty vector control-treated extract) and mix it with extract from PC12 cells, followed by purification of the PHD3 and analysis by MS/MS

for interacting partners using taxonomic-specific database searches to distinguish human proteins (from the 293T extract) versus rat proteins (from the PC12 extract).

Enzyme/substrate interactions are, by their very nature, transient, which can make them difficult to capture using standard proteomic techniques. Because my proteomic experiments were particularly directed towards finding novel PHD3 substrates, I adopted a "substrate trapping" methodology involving the pharmacological 2OG-dependent dioxygenase inhibitor dimethyloxalylglycine (DMOG) that has previously been used successfully to stabilize interactions between FIH and its substrates *in vivo* (Cockman et al., 2006; Cockman et al., 2008).

The reaction cycle of the 2OG-dependent dioxygenase enzymes is proposed to involve binding of 2OG to the active site before binding of the "prime" substrate (Loenarz and Schofield, 2008). Thus, without 2OG bound, PHD3 would not be predicted to bind to substrate. However *N*-oxalylglycine (NOG), a close structural analogue of 2OG in which a methylene group is substituted for a secondary amine, will also bind to the active site of PHD3. DMOG is a cell-permeable diester which is metabolized to NOG *in vivo* (for structures of 2OG, NOG and DMOG see Figure 4.4A). A proposed mechanism for the trapping of substrates by DMOG is shown in Figure 4.4B: the presence of either 2OG or NOG in the active site of PHD3 is thought to permit binding of the prime substrate. However, whilst 2OG can be decarboxylated, allowing the catalytic cycle to proceed and resulting in the eventual release of hydroxylated substrate, succinate and CO_2, NOG blocks the reaction, thus preserving the enzyme-substrate complex. For this reason my proteomic experiments were aimed in

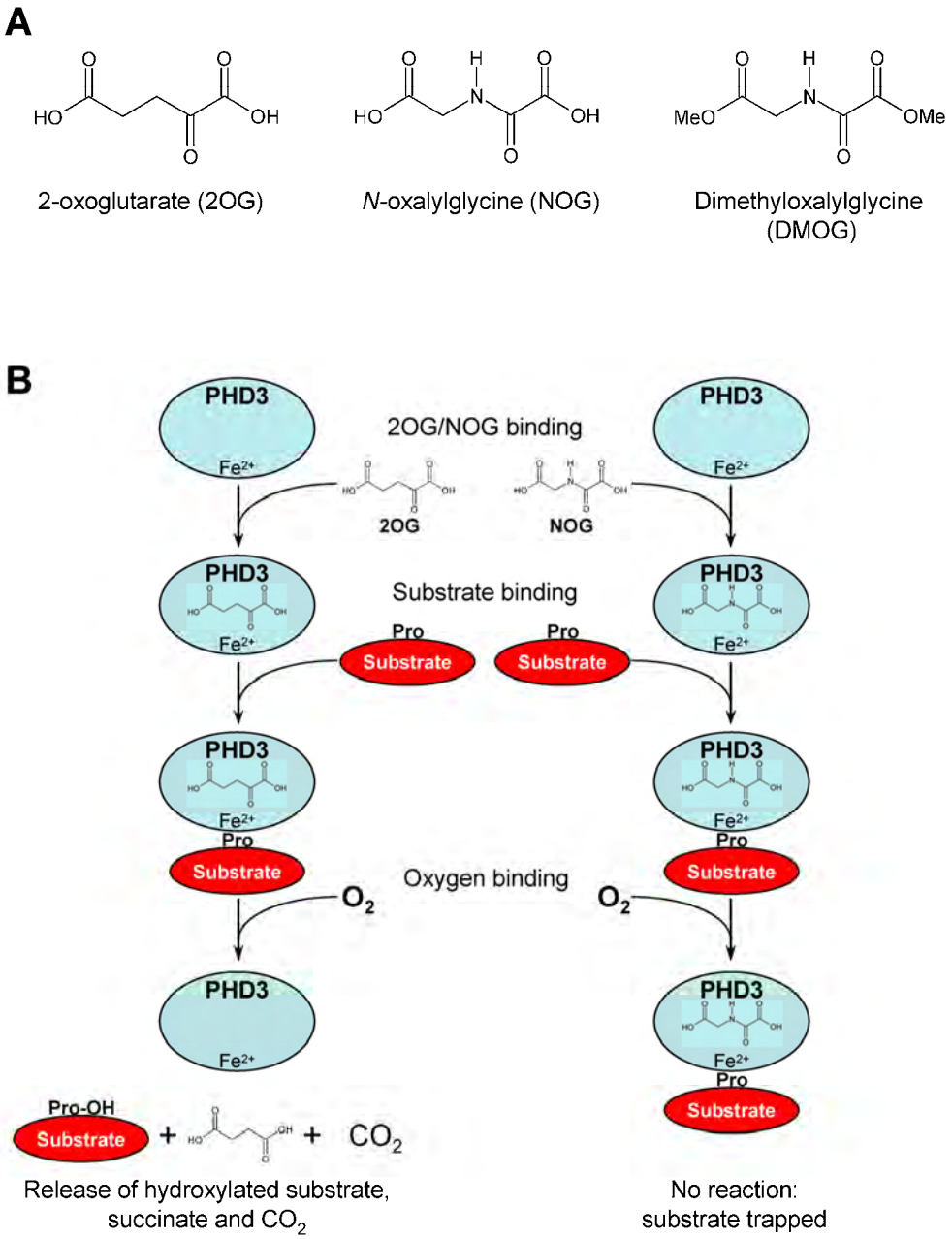


Figure 4.4 *Substrate trapping using DMOG*
(**A**) *Structures of 2OG, NOG and DMOG.*
(**B**) *Reaction scheme for PHD3 showing turnover with 2OG bound (left-hand scheme) but substrate trapping when NOG binds (right-hand scheme).*

particular at identifying interactions that could be enhanced by treating cells with DMOG.

Before attempting a large experiment I optimized the mixing conditions on a small scale using anti-FLAG immunoprecipitation and immunoblotting: the co-precipitation of HIF1α and HIF2α with PHD3 was used as a readout for success at capturing substrates. The first experiment involved mixing varying amounts (100 – 750 µg total protein) of PHD3-SPA-transfected 293T extract with a standard amount (5 mg total protein) of PC12 extract. The PC12 extract was from cells treated either with DMOG (which is expected to be metabolized and carried through to the mixing conditions in the cell lysate) with vehicle alone as a control. Control samples using untransfected 293T extract were also prepared. An additional sample had the co-factors iron(II) and ascorbate added. After mixing, the combined extracts were immunoprecipitated using FLAG resin and analysed by immunoblotting (Figure 4.5A). This experiment showed that human PHD3-SPA could co-precipitate rat HIF1α and HIF2α from PC12 extract, and that these interactions were DMOG-inducible. Increasing the amount of 293T extract used increased the pulldown of HIF. Use of additional iron(II) and ascorbate during the mixing had no effect.

As increasing the amount of 293T extract appeared to enhance the capture of HIF significantly, I carried out an additional experiment using doses of 293T extract ranging from 100 µg to 2000 µg. Figure 4.5B(i) shows that, regardless of the amount of PHD3 used in the mixing experiment, capture of HIF from control-treated PC12 extract was minimal. However Figure 4.5B(ii) shows that HIF capture was greatly enhanced when

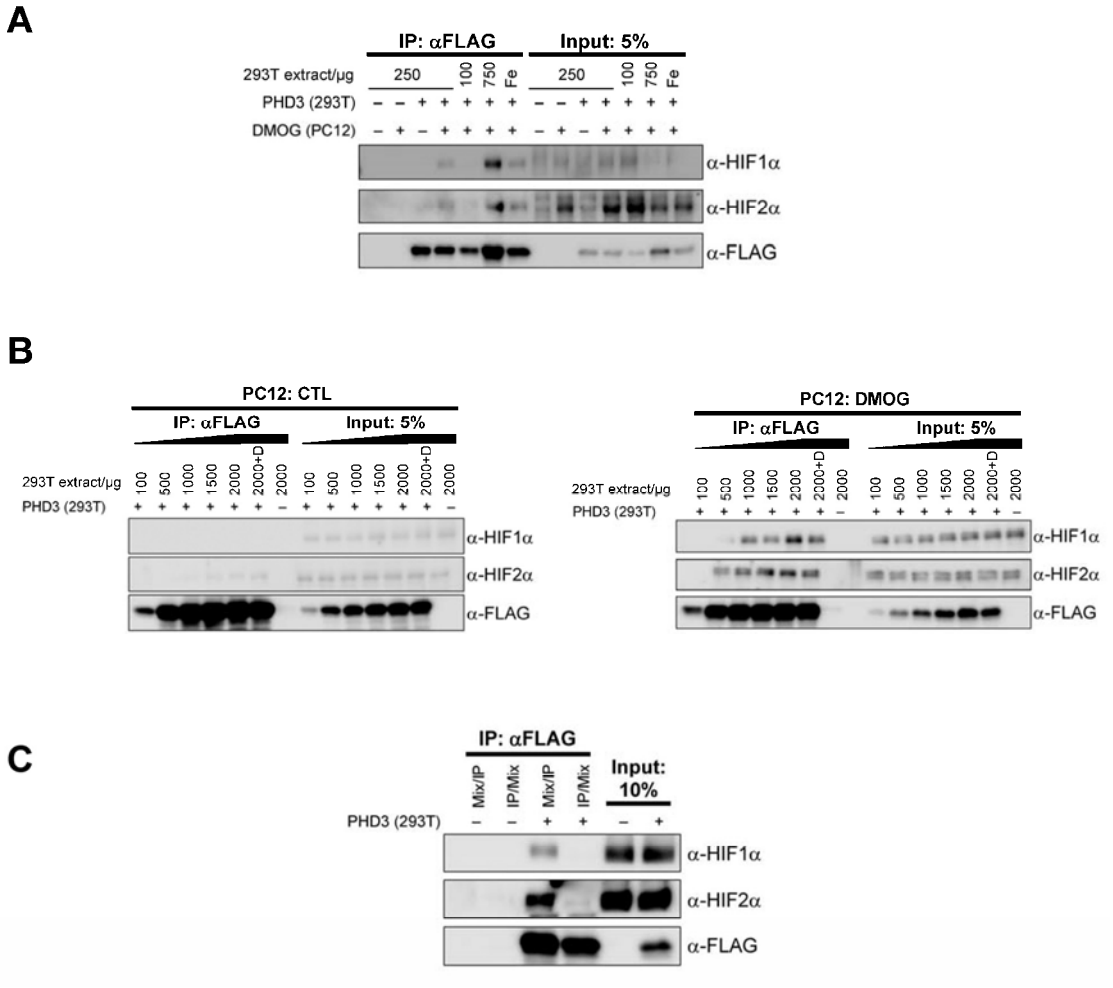


Figure 4.5 ***Optimization of conditions for 293T/PC12 mixing experiment***

(**A**) *PC12 extract (5 mg total protein, treated with 1 mM DMOG or vehicle control for 4 h before harvesting) was incubated with the indicated amount of 293T extract (transfected with empty vector or PHD3-SPA) for 3 h at 4 °C, followed by FLAG immunoprecipitation. Immunoprecipitates were probed by immunoblotting for FLAG, HIF1α and HIF2α. Fe indicates 250 μg 293T extract was used with the addition of 30 μM Fe^{2+} and 30 μM ascorbate during the mixing step.*

(**B**) *5 mg total PC12 protein was mixed with the indicated amount of 293T extract, immunoprecipitated and analysed as above. DMOG (1 mM) was added to one sample during the mixing step (+D). Immunoprecipitations from mixtures using control-treated PC12 extract; and from mixtures using PC12 extract from cells treated with DMOG for 4 h before harvesting are shown.*

(**C**) *2 mg total protein from 293T cell extract (transfected with empty vector or PHD3-SPA) was incubated with 5 mg extract from PC12 cells treated with DMOG for 4 h before harvesting. In the Mix/IP lanes, 293T extract was mixed with PC12 extract for 3 h at 4 °C followed by FLAG immunoprecipitation. In the IP/Mix lanes, 293T extract was immunoprecipitated using FLAG resin and the resin incubated with PC12 extract for 3 h at 4 °C. Capture of PHD3 and HIF was analysed as above.*

DMOG-treated PC12 extract was used: once again, the amount of co-precipitating HIF titrated with the amount of 293T extract used. Addition of further DMOG (which is predicted to be metabolized to NOG under the mixing conditions) at the mixing stage did not give any additional enhancement in HIF capture.

It was possible that a "cleaner" experiment might have been achieved by immunoprecipitating PHD3 from the 293T extract onto FLAG resin before washing and adding the resin-bound PHD3 to a PC12 lysate. To investigate this possibility I performed two experiments in parallel; in the first, 1.5 mg total protein from 293T extract (PHD3- or control-transfected) was mixed directly with 5 mg total protein from a DMOG-treated PC12 lysate, followed by anti-FLAG immunoprecipitation. In the second, 1.5 mg 293T protein (PHD3- or control-transfected) was precipitated using FLAG resin; following washes, the resin was incubated with 5 mg protein from DMOG-treated PC12 cells. The pulldown of HIF under these two different conditions was analysed by immunoblotting, and showed clearly that immunoprecipitating PHD3 before incubating the resin with PC12 extract resulted in a significant loss of substrate capture (Figure 4.5C), perhaps because PHD3 bound to the affinity resin is in some way "constrained" resulting in suboptimal binding.

These experiments suggested that optimal conditions for substrate capture in this setting involved using an approximate ratio of 293T protein to PC12 protein of 2:5, and mixing these extracts before purifying the PHD3 for analysis. I therefore performed a larger experiment by mixing 100 mg total 293T protein (from PHD3-SPA- or control-transfected cells) with 250 mg total PC12 protein (from cells treated with DMOG or vehicle control). Following mixing, the full SPA purification procedure of

FLAG immunoprecipitation, TEV cleavage and calmodulin sepharose purification was carried out. The aim of this experiment was to capture rat proteins from the PC12 lysate rather than human proteins from the 293T lysate. Therefore, as a control for the protein bands that might be seen immunoprecipitating from the 293T cells alone, 100 mg samples of 293T extract were also purified. Following the SPA purification protein samples were eluted directly into sample buffer and resolved by SDS-PAGE (Figure 4.6). Only one DMOG-inducible band was visible in the immunoprecipitates from the mixing experiment, at around 100 kDa: this was excised, digested with trypsin and analysed by LC-MS/MS. Database searching identified rat HIF2α with a highly significant Mascot ions score of 94 (Table 4.1; four separate peptides assigned), thus fully validating the experimental approach used. However, this experiment did not identify any new potential substrates when the criterion of DMOG inducibility was applied.

4.2.3 *An alternative strategy for capturing DMOG-inducible PHD3 interactors*

The 293T/PC12 mixing experiment was successful at capturing the PHD3/HIF2α interaction, but was not able to identify any novel potential substrates. Clearly it was possible that the mixing strategy was not capturing all possible substrates, given that the two cell lysates were only mixed for a matter of hours at 4 °C. A second proteomic experiment was carried out by Dr Matthew Cockman in order to assess which proteins interact with PHD3 in a DMOG-inducible manner within a single cell type. Here, SPA-tagged constructs of PHD1 – 3 plus FIH and EGFP (as a control) were expressed in 293T cells. Transfected cells were treated with DMOG or vehicle control before harvesting, after which the SPA-tagged enzymes were purified directly from the

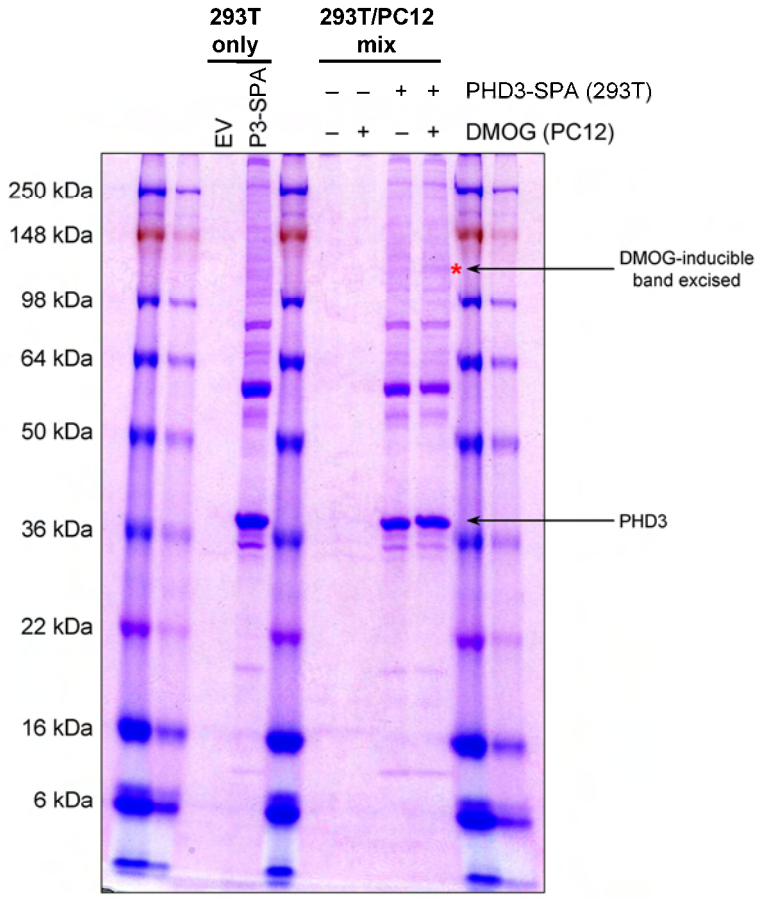


Figure 4.6 ***Proteomic-scale mixing experiment and SPA purification***
PC12 extract (250 mg total protein, treated with 1 mM DMOG or vehicle control for 4 h before harvesting) was incubated with 293T extract (100 mg total protein, transfected with empty vector or PHD3-SPA) for 3 h at 4 °C, followed by SPA purification and SDS-PAGE analysis. Control SPA purifications were carried out on samples of empty vector- and PHD3-SPA-transfected 293T cell extract. The indicated band was excised and analysed by LC-MS/MS.

Protein *Taxonomy*	Accn no (SwissProt)	MW (Da)	MASCOT score	Peptides (residue numbers)	Peptide score
HIF2α *Rattus norvegicus*	Q9JHS1	96656	94	GQVVSGQYR (300 – 308)	18
				YPQQLESR (587 – 594)	28
				SLMGGTCPLMPDK (746 – 758)	27
				HLPPSQPPSTR (783 – 793)	28

Table 4.1
MS/MS assignment of rat HIF2α as a DMOG-inducible protein co-precipitating with PHD3

293T cells with no mixing step: thus enzymes and potential substrates would have the lifetime of the cell under basal conditions in which to interact, rather than the relatively short period of time allowed by the previous mixing strategy. Although this cell line is somewhat derived (and unrelated to the sympathoadrenal lineage) it was used because it does express some endogenous PHD3 and is very amenable to transfection.

Following SPA purification, PHD3 complexes were eluted and resolved by SDS-PAGE: the resulting gel stained with Coomassie blue is shown in Figure 4.7A; the same gel after silver staining is shown in Figure 4.7B. Three candidate proteins were identified from the silver-stained gel as interacting with PHD3 in a DMOG-inducible manner: these bands were excised and digested for LC-MS/MS analysis. Interestingly some interactions that appeared to be suppressed by DMOG were observed, but these were not pursued. The uppermost DMOG-inducible band was not identified. The middle band was assigned as the SV40 large T antigen (two separate peptides, Mascot ions score 107), with the lowest band being assigned as SKIP (one peptide, Mascot ions score 49) (Table 4.2). No HIF band was assigned in this experiment, illustrating that the proteomic strategy based on Coomassie blue- or silver-staining SDS-PAGE gels and excising bands to identify proteins is imperfect and can miss important interacting species. However, it provides a starting point from which to investigate interacting proteins. The remainder of the work described in this chapter involves experiments designed to characterize these interactions in detail.

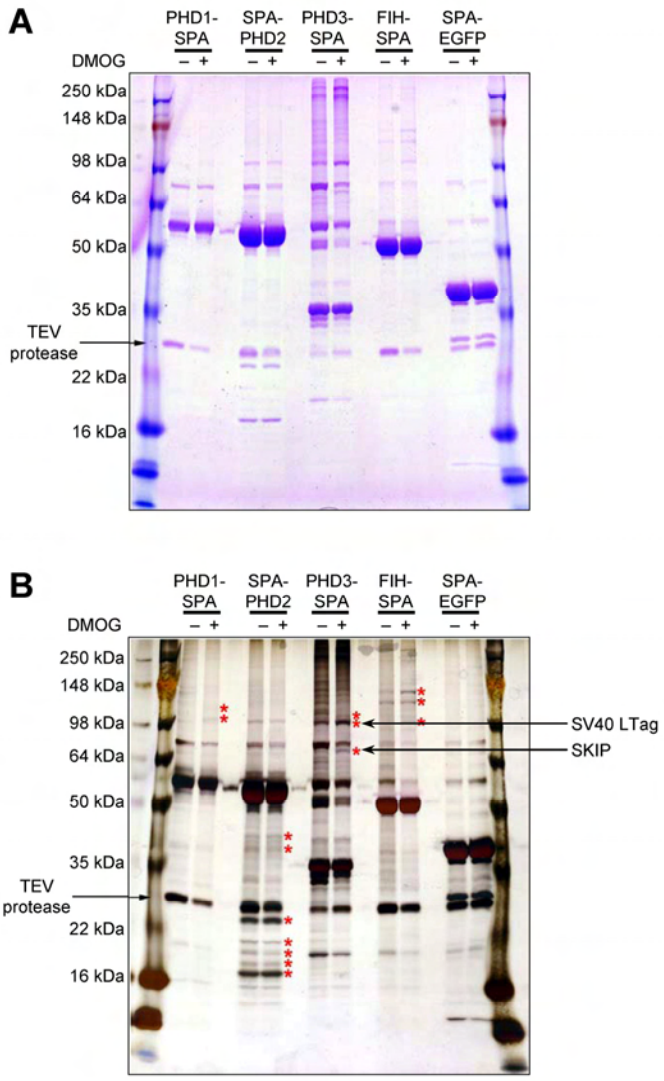


Figure 4.7 *SPA purification of the HIF hydroxylases*
The indicated SPA-tagged constructs were transfected into 293T cells, which were treated with DMOG (1 mM) or vehicle control for 4 h before harvesting and SPA-purification. EGFP-SPA was used as a control to assist in identifying non-specific interacting proteins. Eluates were analysed by SDS-PAGE and DMOG-inducible bands excised and analysed by LC-MS/MS. (**A**) *shows the gel after Coomassie blue staining,* (**B**) *shows the gel after silver staining. This experiment was carried out by Dr Matthew Cockman.*

Protein *Taxonomy*	Accn no (SwissProt)	MW (Da)	MASCOT score	Peptides (residue numbers)	Peptide score
SNW1 (SKIP) *Homo sapiens*	Q13573	61456	49	FVPDKEFSGSDR (472 – 483)	53
Large T antigen *Simian virus 40*	P03070	81530	107	EESLQLMDLLGLER (8 – 21)	30
				DFPSVIEESLPGGLK (239 – 253)	76

Table 4.2
MS/MS identification of SKIP and SV40 large T antigen as DMOG-inducible proteins co-precipitating with PHD3.

4.2.4 *SKIP interacts specifically with PHD3 in a DMOG-inducible manner*

Ski-interacting protein (SKIP, also known as SNW1 or NCoA62) is a 62 kDa component of the spliceosome and transcriptional co-regulator involved in a wide variety of pathways (Folk et al., 2004); it potentiates the activity of a range of transcription factors including vitamin D receptor and CBF1, a member of the Notch signalling pathway.

In order to verify unambiguously that SKIP was interacting with PHD3, I analysed a PHD3 immunoprecipitation by immunoblotting with a SKIP-specific antibody. Cells were treated with DMOG or vehicle control before harvesting, following which the V5-tagged PHD3 was immunoprecipitated. In this experiment, immunodetectable SKIP co-precipitated with PHD3, and the interaction was strongly induced by DMOG treatment (Figure 4.8A). In order to determine whether the interaction was specific to PHD3, I analysed small fractions of the proteomic immunoprecipitation presented in Figure 4.7 by immunoblotting. This experiment showed that although all three PHDs co-precipitated HIF1α, the DMOG-inducible pulldown of SKIP was specific to PHD3 (Figure 4.8B). In order to verify that the interaction between PHD3 and SKIP was not specific to 293T cells, I repeated the PHD3-V5 immunoprecipitations in 293T cells, HeLa cells and HEK293 cells (which are not transformed with SV40 large T antigen). These results showed DMOG-inducible co-precipitation of SKIP with PHD3 in each cell line tested (Figures 4.8C(i) and 4.8C(ii)). Although the interaction in HeLa cells was somewhat weaker than in 293T or HEK293 cells, this is likely due to the much lower levels of SKIP in this cell line (Figure 4.8C(i)); it may also reflect competition between HIF and SKIP for binding to PHD3 as levels of co-immunoprecipitated SKIP were much

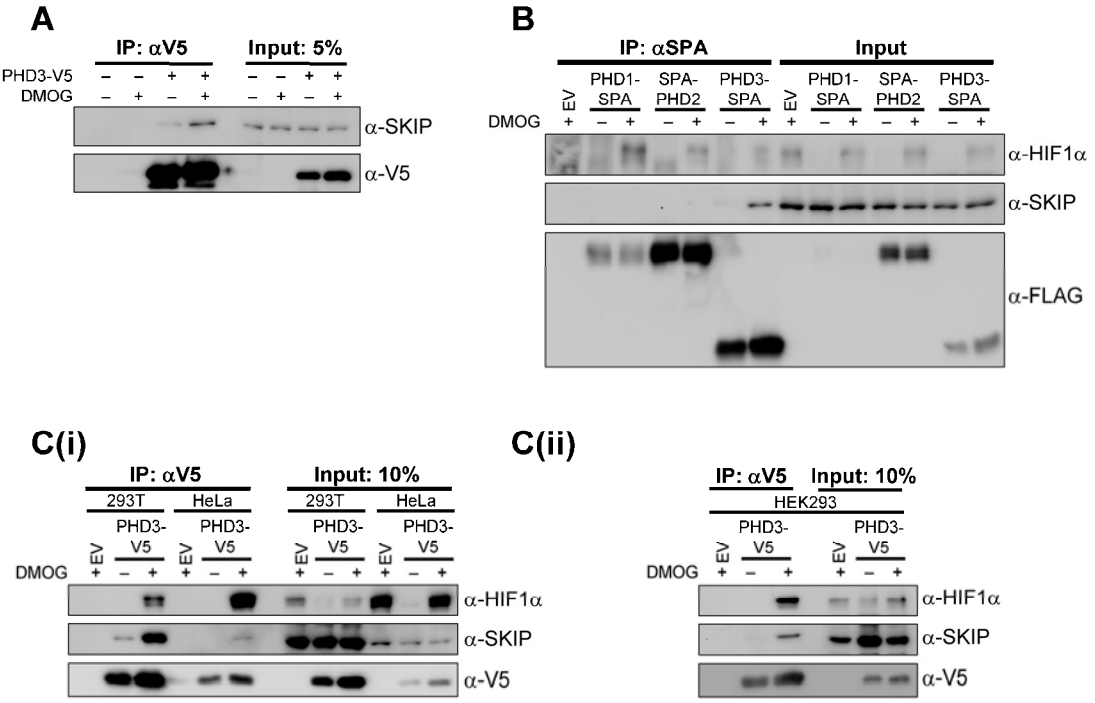


Figure 4.8 ***Validation of the PHD3/SKIP interaction***

(**A**) *293T cells were transfected with PHD3-V5 or empty vector control, and treated with DMOG (1 mM) or vehicle control for 4 h before harvesting. Extracts were immunoprecipitated using V5 resin and immunoprecipitates probed for SKIP and V5.*

(**B**) *Aliquots from the proteomic experiment presented in Figure 4.7 were probed by immunoblotting for FLAG, SKIP and HIF1α.*

(**C**) *293T, HEK293 and HeLa cells were transfected with PHD3-V5 or empty vector (EV), and treated with DMOG (1 mM) or vehicle control for 4 h before harvesting. Extracts were immunoprecipitated using V5 resin and immunoprecipitates probed for SKIP, V5 and HIF1α. Panel* (**i**) *shows IPs and inputs from 293T and HeLa cells; IPs and inputs from HEK293 cells are shown in panel* (**ii**).

lower in HeLa cells where levels of HIF were significantly higher (Figure 4.8C(i)). Thus, the DMOG-dependent interaction of PHD3 and SKIP does not appear to be cell type-specific. The fact that the PHD3/SKIP interaction was observed in HeLa and HEK293 cells demonstrated that it was independent of SV40 large T antigen. SKIP was also detected as a PHD3 interacting protein by a yeast 2-hybrid assay[5] which provides further evidence for a direct PHD3/SKIP interaction.

I decided to attempt an immunoprecipitation using endogenous PHD3 in an effort to demonstrate that the interaction with SKIP was physiological and not an artefact of overexpression. As an initial experiment I overexpressed PHD3-V5 in 293T cells in the presence or absence of DMOG, then immunoprecipitated cell extracts using V5 resin, resin conjugated to a PHD3 monoclonal antibody (188e, (Appelhoff et al., 2004)) or resin conjugated to a commercial PHD3 polyclonal antibody. The immunoprecipitates were probed by immunoblotting for HIF1α and PHD3. Figure 4.9A(i) shows the comparison between V5 immunoprecipitation and PHD3 monoclonal antibody immunoprecipitation; Figure 4.9A(ii) shows the comparison between V5 and PHD3 polyclonal antibody immunoprecipitation. It was only possible to co-precipitate detectable quantities of HIF1α using the V5 antibody: immunoprecipitation with the PHD3 antibodies captured much smaller relative amounts. Therefore I did not pursue attempts to immunoprecipitate endogenous PHD3. An alternative strategy was to immunoprecipitate endogenous SKIP, and probe for co-immunoprecipitating PHD3. In order to determine if immunoprecipiptation of endogenous levels of SKIP was possible, an experiment was performed by Dr Matthew Cockman using 293T cells under

[5] Norma Masson, unpublished data

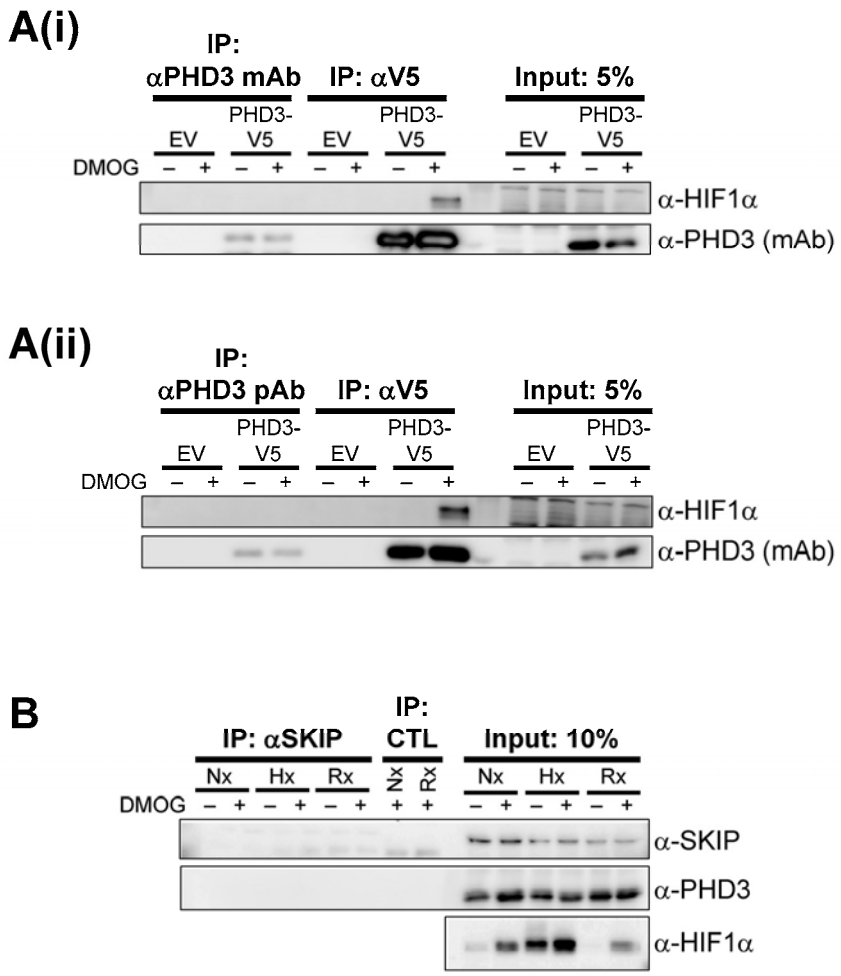


Figure 4.9 ***Attempting to demonstrate an endogenous PHD3/SKIP interaction***
(**A**) *293T cells were transfected with PHD3-V5 or empty vector control (EV). Cell extracts were immunoprecipitated using V5 resin, PHD3 monoclonal antibody-conjugated resin (PHD3 mAb) or PHD3 polyclonal antibody-conjugated resin (PHD3 pAb). Bound proteins were eluted and analysed by immunoblotting for PHD3 (using the PHD3 monoclonal antibody) and HIF1α. Panel* (**i**) *shows the comparison between V5 and PHD3 mAb immunoprecipitation; panel* (**ii**) *shows the comparison between V5 and PHD3 pAb immunoprecipitation.*
(**B**) *293T cells were incubated in normoxia (Nx), hypoxia (Hx, 3% O_2 for 16 h) or reoxygenated (Rx, 16 h Hx followed by 1 h Nx). Following these treatments cells were harvested and extracts subjected to control or anti-SKIP immunoprecipitation. Immunoprecipitates were probed by immunoblotting for SKIP, PHD3 and HIF1α. The experiment in panel* (**B**) *was carried out by Dr Matthew Cockman.*

conditions of normoxia, hypoxia or reoxygenation in the presence or absence of DMOG. This experiment showed that under all the conditions tested, the immunoprecipitation of SKIP was poor. As neither endogenous levels of SKIP nor PHD3 could be effectively immunoprecipitated, it was not possible to demonstrate an interaction between the two proteins with both expressed at their physiological levels.

4.2.5 *Mapping the PHD3-interacting domain of SKIP*

Human SKIP is a 62 kDa protein containing 536 amino acids, of which 36 are proline residues. As one of my aims was to carry out experiments using mass spectrometry to try and identify sites of prolyl hydroxylation, I next conducted an experiment aimed at mapping the PHD3-interacting domain on SKIP in order to determine in which region to focus the mass spectrometric analysis.

The main functional domain of SKIP is termed the SNW domain, because it contains an SNWKN motif that is absolutely conserved from yeast to humans (Folk et al., 1996). The SNW domain lies between residues 176 – 333, and is 90% conserved between species (Prathapam et al., 2002; Prathapam et al., 2001b). Within the SNW domain lies a proline-rich region between residues 218 – 235 (Prathapam et al., 2001a). I also noted by inspection that immediately N-terminal to the SNW domain from residues 171 – 173 there is an 'LAP' motif, with some homology to sites of hydroxylation in HIF. A full-length human SKIP construct (pCGN-HA-SKIP, (Dahl et al., 1998)) was kindly provided by Dr Michael J Hayman (State University of New York, Stony Brook, NY) and used as a template to prepare a series of deletion mutants by PCR (Figure 4.10A); PCR products were cloned into pFLAG-CMV2 with an N-terminal FLAG tag.

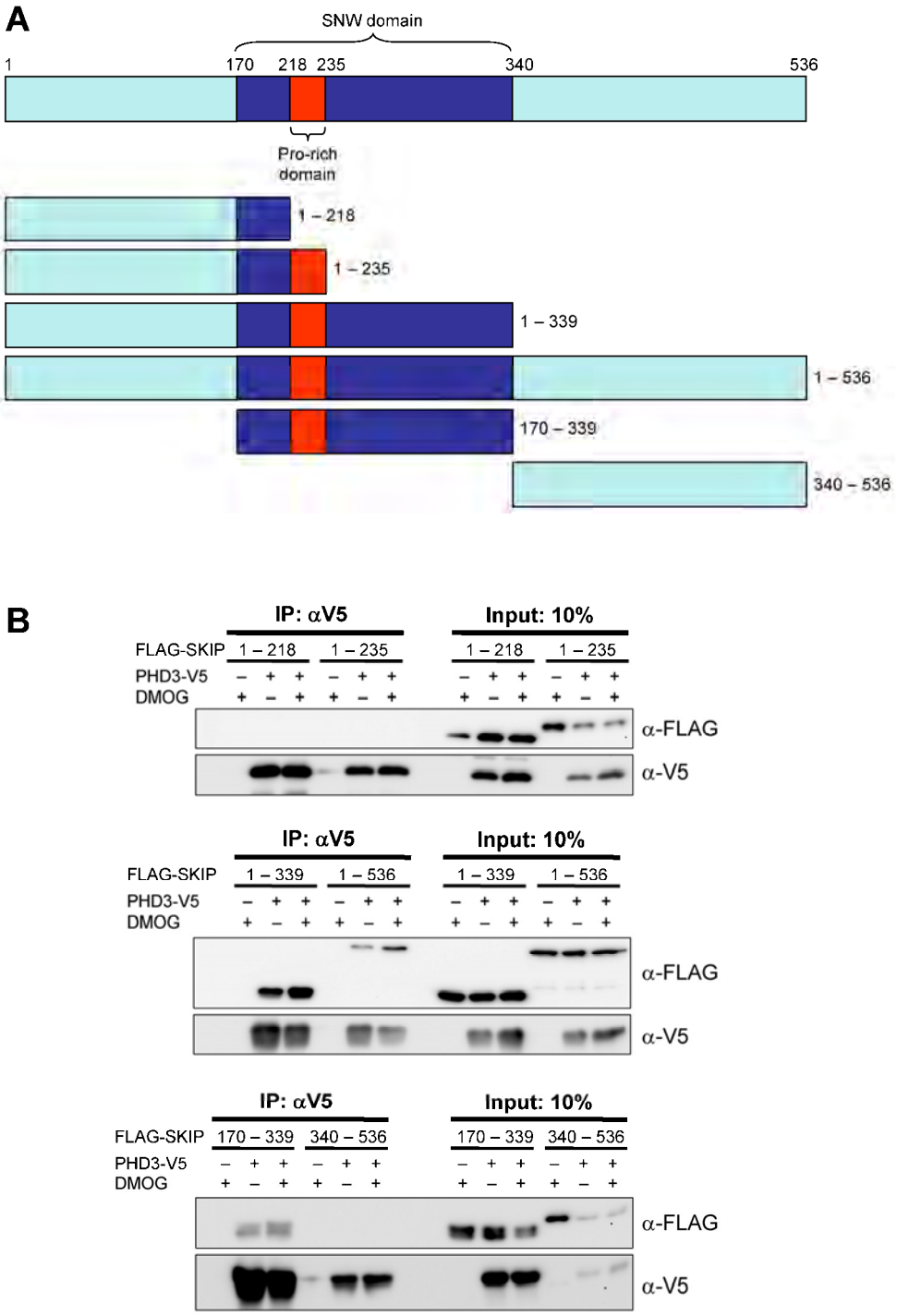


Figure 4.10 ***Mapping the PHD3/SKIP interaction***

(**A**) *Schematic representation of the domain structure of SKIP, showing the deletion mutants prepared.*

(**B**) *The indicated SKIP construct was co-transfected along with PHD3-V5 or empty vector control (EV) into 293T cells. Cells were treated with DMOG (1 mM) or vehicle control for 4 h before harvesting, following which PHD3-V5 was immunoprecipitated. Immunoprecipitates were analysed by immunoblotting for V5 and co-precipitating FLAG-SKIP.*

The sequences cloned were: 1 – 218, an N-terminal construct lacking the proline-rich domain; 1 – 235, an N-terminal construct including the proline-rich domain; 1 – 339, an N-terminal construct including the full SNW domain; 1 – 536, the full length protein; 170 – 339, the SNW domain with a small N-terminal extension to include the LAP motif; and 340 – 536, a C-terminal truncation lacking the SNW domain (Figure 4.10A). These constructs were transfected into 293T cells along with PHD3-V5 (or empty vector as a control) in the presence or absence of DMOG. After cell lysis, anti-V5 immunoprecipitations were carried out to capture transfected PHD3, and immunoprecipitates probed by immunoblotting using anti-FLAG antibody for co-precipitated FLAG-SKIP (Figure 4.10B). This experiment showed no binding of the N-terminus of the molecule to PHD3, even when the proline-rich domain was included (Figure 4.10B, top panel), suggesting that this region of the molecule is not involved in PHD3 binding. The 1 – 339 construct co-precipitated in a DMOG-inducible manner, as did the full-length protein (Figure 4.10B, centre panel). The isolated SNW domain also bound PHD3, although much more weakly than the 1 – 339 construct; no binding of the C-terminus of the molecule to PHD3 was observed (Figure 4.10B, bottom panel). Although the co-transfections were balanced with empty vector where necessary, so that the total amount of DNA transfected was the same in all cases, co-transfection of PHD3 affected the expression levels of some SKIP deletions (either positively or negatively), perhaps reflecting some kind of promoter competition between the two plasmids (Figure 4.10B, inputs). However, the results of the immunoprecipitations suggest that the SNW domain of SKIP is necessary and sufficient for the interaction with PHD3, but that the interaction is significantly enhanced by the addition of a region N-terminal to the SNW domain.

In the absence of antibodies capable of immunoprecipitating endogenous PHD3 or SKIP, as a final control to confirm the veracity of the PHD3/SKIP interaction I conducted an experiment with the aim of co-precipitating endogenous PHD3 using overexpressed SKIP (as all previous pull-down experiments had used overexpressed PHD3). FLAG-SKIP 1 – 339 and 1 – 536 were expressed in 293T cells (along with an empty vector control) in the presence or absence of DMOG; cells were harvested and FLAG-SKIP immunoprecipitated (Figure 4.11). Although the FLAG immunoblot is extremely weak, it demonstrates that both SKIP constructs were successfully captured and that they co-precipitated endogenous PHD3 in a DMOG-inducible fashion.

4.2.6 *Using mass spectrometry to search for prolyl hydroxylation in SKIP*

In an attempt to demonstrate prolyl hydroxylation unambiguously and at a particular residue, I adopted a mass spectrometric strategy for analysing SKIP. An initial experiment used FLAG-SKIP 1 – 536 transfected into 293T cells along with PHD3-V5 or an empty vector control. FLAG-SKIP was immunoprecipitated, resolved by SDS-PAGE and digested in gel with trypsin. Digests were analysed using a Bruker Daltonics HCTplus ion trap instrument: the peptide containing Pro-173 (the prolyl residue embedded in the 'LAP' motif) was not detected, and no prolyl hydroxylations were robustly assigned elsewhere in the molecule. As the tryptic peptide containing Pro-173 did not appear to be amenable to analysis, I conducted a second experiment using full-length SKIP in the absence of PHD3 overexpression to compare digestion with trypsin and endoproteinase LysC. In this experiment a LysC-derived peptide containing Pro-173 was observed.

Having established conditions under which a Pro-173-containing peptide could be detected, I sought to demonstrate PHD3-dependent hydroxylation of SKIP by using stable isotope labelling of amino acids in cell culture (SILAC). In this technique, two populations of cells are grown, one in medium containing normal, unlabelled amino acids ("light" medium), the other in medium containing amino acids labelled with non-radioactive, heavy isotopes ("heavy" medium). After the two sets of cells are treated under different conditions the proteins of interest are immunoprecipitated, pooled and analysed by mass spectrometry: the presence or absence of a mass label enables the origin of a given peptide to be determined, and by pooling samples and analysing them together it is possible to derive quantitative information from the experiment (Ong et al., 2002).

The original SILAC study used deuterated leucine (Ong et al., 2002), but in principle the SILAC experiment allows the use of any amino acid incorporating ^{2}H, ^{13}C or ^{15}N. The most commonly used labelled amino acids are lysine and arginine: trypsin cuts C-terminal to both these residues, and LysC cuts C-terminal to lysine. Thus all tryptic and LysC peptides from the digest of a SILAC experiment using these amino acids should contain at least one mass label (Mann, 2006; Ong and Mann, 2007).

An experimental scheme of the SILAC strategy I adopted is shown in Figure 4.12: 293T cells were seeded at low density and allowed to equilibrate either in normal medium or medium containing $^{13}C_6$, $^{15}N_4$ arginine (for a mass label of +10 Da) and $^{13}C_6$ lysine (for a mass label of +6 Da) for five doublings. After five doublings it is assumed that the label has been fully incorporated into the proteome of the cells (Ong and Mann, 2007).

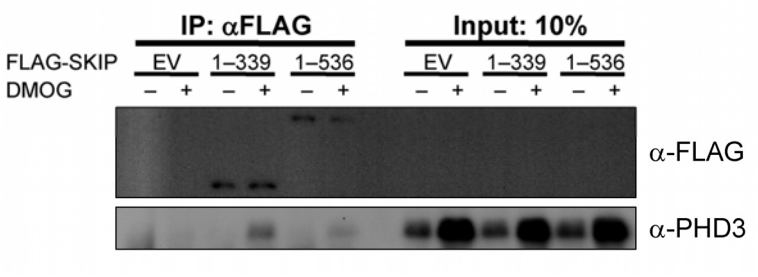


Figure 4.11 ***Co-precipitation of endogenous PHD3 by FLAG-SKIP***
293T cells were immunoprecipitated with the indicated FLAG-SKIP construct or empty vector control, and treated with DMOG (1 mM) or vehicle control for 4 h before harvesting. FLAG-SKIP was immunoprecipitated and immunoprecipitates probed by immunoblotting for FLAG and co-precipitating PHD3.

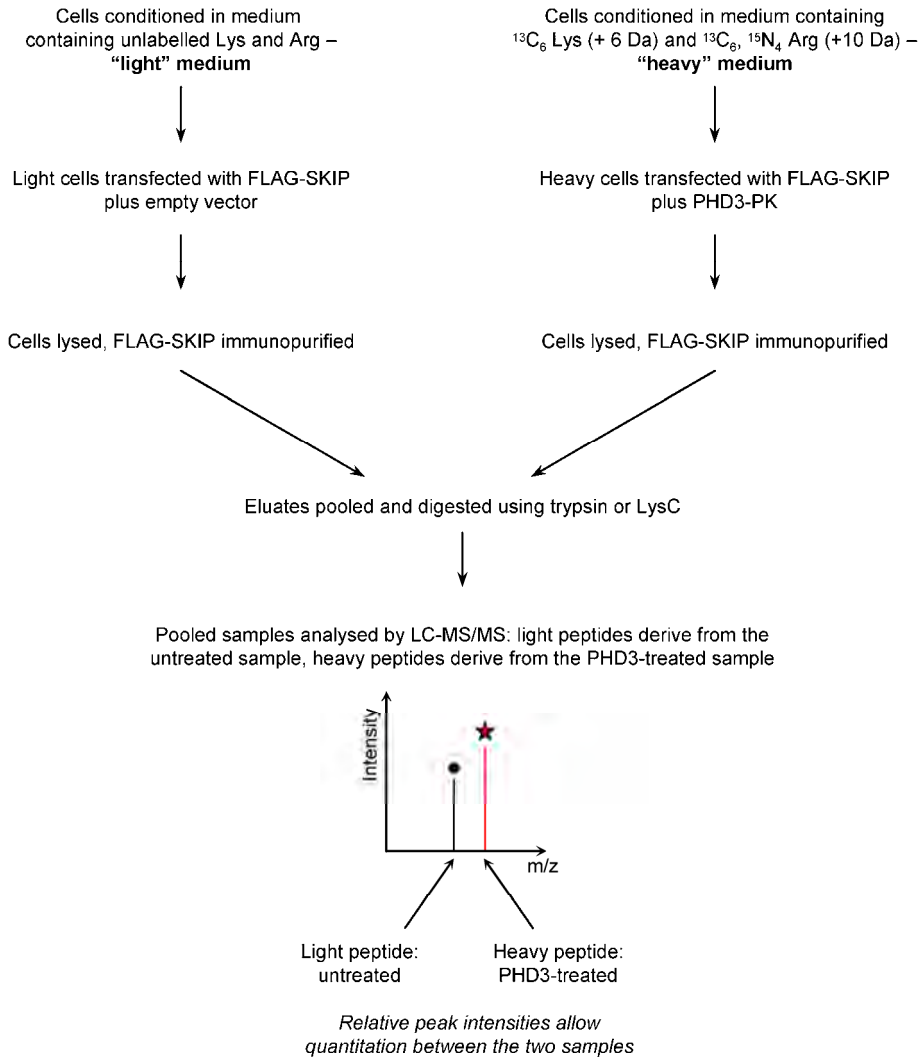


Figure 4.12 ***Schema of SILAC approach***
Schematic of the SILAC approach adopted to identify PHD3-dependent post-translational modifications on SKIP.

"Light" cells were transfected with full-length FLAG-SKIP plus empty vector; "heavy" cells were transfected with full-length FLAG-SKIP plus PHD3-V5. Following the transfection cells were lysed and extracts immunoprecipitated separately. Bound proteins were eluted from the FLAG resin using ammonium hydroxide and eluates pooled, before proteins were digested in solution. As I wanted to avoid biasing this experiment exclusively towards the detection of Pro-173, separate digestions were carried out with trypsin and LysC. Following digestion the pooled samples were analysed using a Micromass QToF instrument with high mass resolution: the LysC digestion covered 59% of the protein sequence with the trypsin digestion covering 49%. Taking into account the overlap between digests, 75% of the protein sequence of SKIP was covered in this experiment. As a control to test the labelling efficiency, an aliquot of the immunoprecipitate from the heavy-labelled cells alone was analysed in parallel by LC-MS/MS and found to contain greater than 90% labelled peptides.

Although several potential prolyl hydroxylations were identified by the database searching software, the majority of these were in peptides that contained methionine (oxidation of which is a common artefact of digestion procedures (Kinter and Sherman, 2000)) and where MS/MS fragmentation data were poor, suggesting a mis-assignment of methionine oxidation by the database search algorithm. The Pro-173-containing peptide was detected in three states: an unoxidized peptide containing no mass label was observed, as was an unoxidized peptide containing both mass labels. Interestingly, a peptide containing a heavy lysine residue had hydroxylation assigned at Pro-173. The MS/MS spectrum of this peptide is shown in Figure 4.13; although it is not possible to assign oxidation with absolute certainty to the prolyl residue, the data indicate an additional mass of +16 Da somewhere in the sequence PAQYIRY.

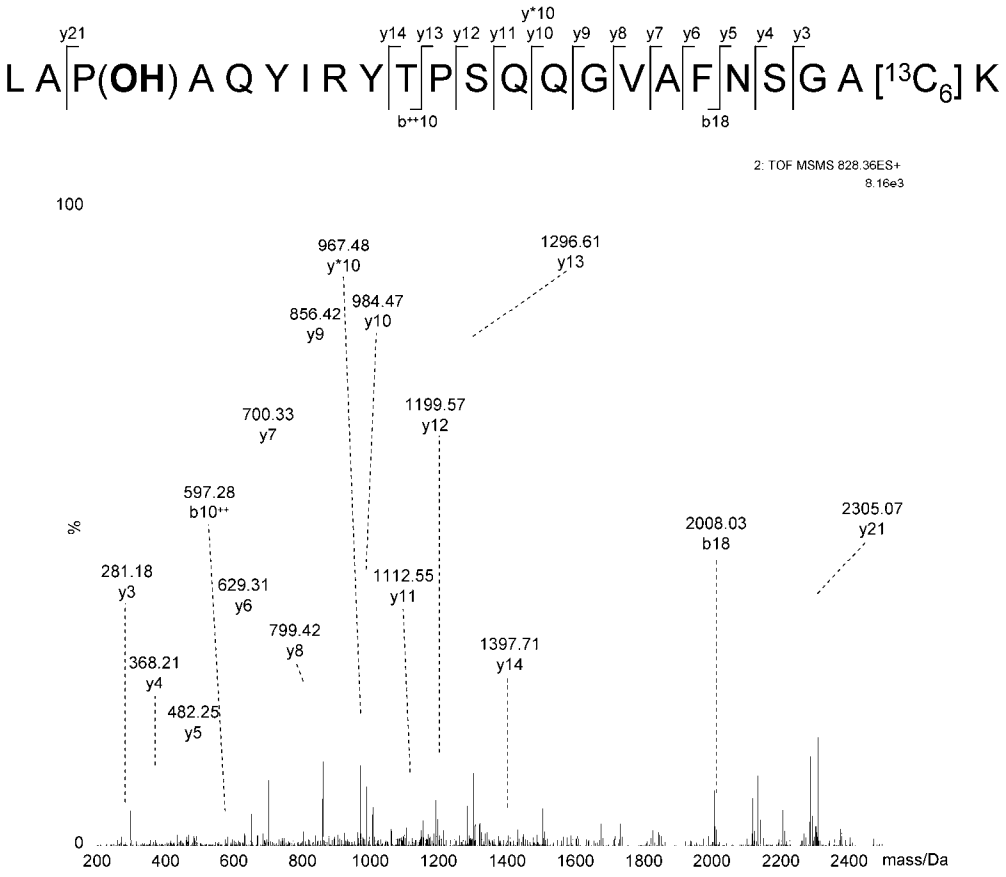


Figure 4.13 ***Evidence for hydroxylation of Pro-173 in SKIP***
MS/MS spectrum showing a LysC-derived peptide from SKIP containing Pro-173, $[M+3H]^{3+}$= m/z *828.36. An additional mass of +16 Da compared to that expected for the unoxidized peptide is observed in the y21 ion, suggesting hydroxylation has occurred in the PAQYIRY region towards the N-terminus of the peptide.*

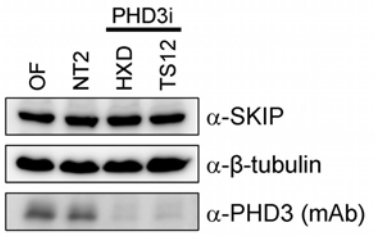


Figure 4.14 ***SKIP levels are not affected by PHD3 knock-down***
293T cells were transfected twice at 24-hour intervals with two independent siRNA duplexes targeting PHD3 (HXD and TS12) and a non-targeting control sequence (NT2). 20 nM doses of duplex were used. As an additional control a mock transfection was carried out using Oligofectamine reagent alone (OF). 48 h after the second siRNA transfection cells were harvested and extracts immunoblotted for PHD3, SKIP and β-tubulin as a loading control.

A further SILAC experiment was carried out in an attempt to make a more robust assignment of prolyl hydroxylation at Pro-173. However this was confounded by the same peptide fragmentation issues as the first experiment, and it did not prove possible to improve upon the data presented in Figure 4.13.

4.2.7 *PHD3 does not affect SKIP levels* in vivo

As it appeared that SKIP did undergo prolyl hydroxylation, I reasoned that this modification could be a signal for degradation as in the case of HIF, and decided to investigate this possibility using PHD3 knock-down. 293T cells were transfected with two independent duplexes targeting PHD3 (Appelhoff et al., 2004). A mock transfection and transfection of a non-targeting sequence were also carried out as controls. Cells were harvested and analysed by immunoblotting. Although it was not possible to control the experiment by immunoblotting for HIF due to the presence of other PHD enzymes in the cells, immunoblotting for PHD3 demonstrated that the siRNA transfections were successful. However, levels of SKIP protein in the cells were not affected (Figure 4.14), suggesting that the variations in the levels of the SKIP deletion proteins in Figure 4.10B were likely to be an artefact of the conditions used for co-transfection in that experiment.

4.2.8 *Attempts to prepare recombinant SKIP in* E. coli

In order to obtain additional evidence that SKIP was hydroxylated by PHD3, I chose to investigate whether a purified recombinant SKIP fragment containing the candidate proline residue might be a substrate for PHD3 *in vitro*. Recombinant proteins can often be expressed in *E. coli* in relatively large quantities, and purified SKIP would enable *in vitro* assays for enzyme turnover and also potentially assist with direct analysis of

hydroxylation by mass spectrometry. A commonly used assay for determining the activity of 2OG dioxygenase enzymes *in vitro* involves monitoring the release of $^{14}CO_2$ from radiolabelled 2OG during the reaction cycle (Figure 4.4). The assay was originally developed for analysis of a rat liver oxygenase (Sabourin and Bieber, 1982) but has more recently been adapted for the analysis of HIF prolyl hydroxylases (reviewed in (Hewitson et al., 2007)). If SKIP was able to support enzyme turnover in this setting, it would be strongly implicated as a substrate for prolyl hydroxylation.

The preparation of a His_6-tagged SKIP construct containing residues 1 – 353 has been described previously (Prathapam et al., 2002). I therefore cloned residues 1 – 353 of human SKIP into the pET-28a(+) vector, which encodes an N-terminal His_6-tag. I then conducted expression trials using *E. coli* strain BL21, using 0.5 mM IPTG to induce expression and incubating at temperatures of 20 °C, 28 °C and 37 °C after induction. Cells were harvested and lysed by sonication before a small-scale batch purification was carried out (Figure 4.15A): whole cell extracts, lysates, wash fractions and eluted fractions were analysed by SDS-PAGE, but did not show any significant expression or purification of a protein with the expected mass. An additional control experiment was carried out to compare the purification products of cells that were left unstimulated or stimulated with IPTG: this showed no significant difference in the two purifications (Figure 4.15B). In order to confirm that the lack of protein expression was not due to a problem either with the bacterial strain or the induction conditions, a pET-28a(+) plasmid containing full-length FIH was transformed into *E. coli* BL21. The FIH-transformed cells were grown and induced in parallel with SKIP-transformed cells: analysis of whole cell extracts by SDS-PAGE showed significant induction of FIH by

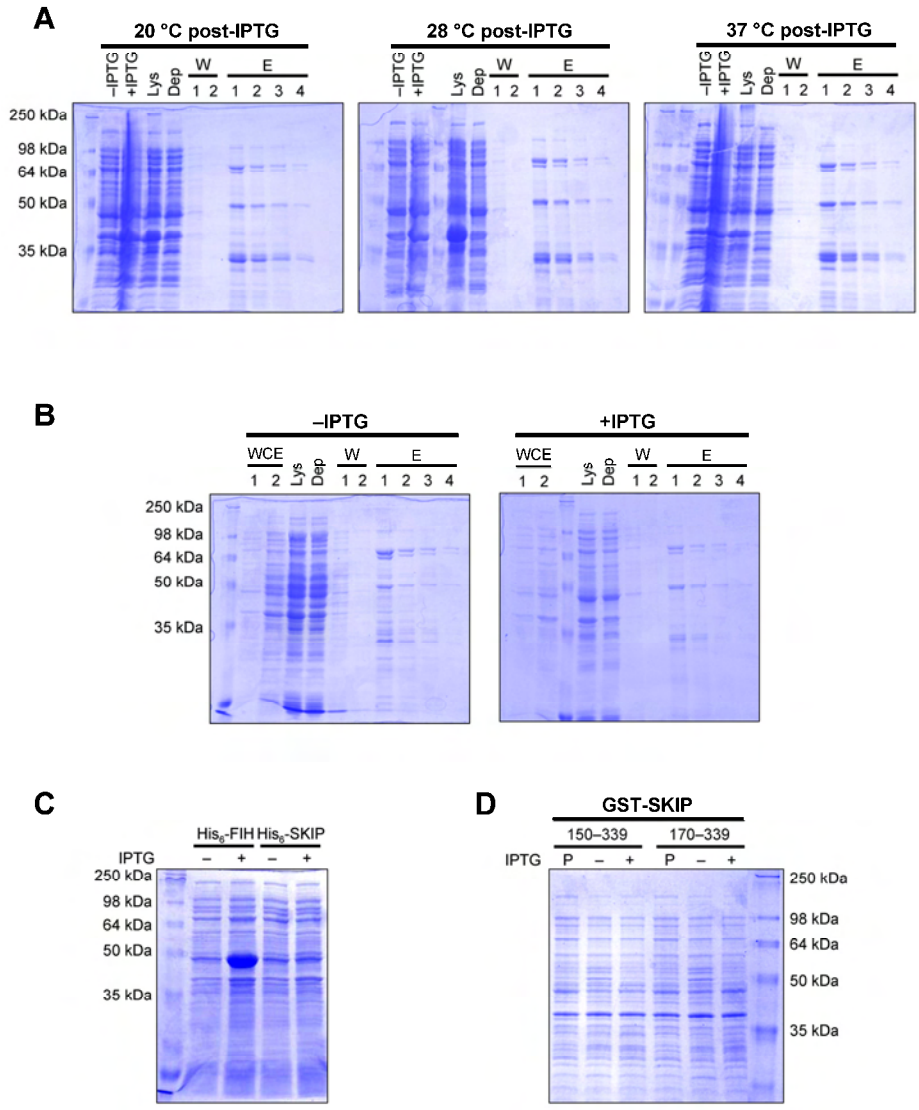


Figure 4.15 *Attempts to prepare recombinant SKIP in* E. coli

(**A**) *BL21 cells were transformed with His_6-SKIP 1 – 353, grown to OD_{600} = 0.6 and then stimulated with 0.5 mM IPTG. Following stimulation cells were incubated at the indicated temperature for a further 4 h. Cells were harvested, sonicated and purified using Ni-NTA resin, with two wash steps using 20 mM imidazole and four elutions using 250 mM imidazole. Whole cell extracts before and after IPTG stimulation (–/+ IPTG), lysates before and after incubation with Ni-NTA resin (Lys/Dep), wash fractions (W1 – 2) and eluted fractions (E1 – 4) were analysed by SDS-PAGE.*

(**B**) *BL21 cells transformed with His_6-SKIP 1 – 353 were grown to OD_{600}= 0.6 and stimulated with 0.5 mM IPTG or left unstimulated. After incubation for a further 4 h at 28 °C, cells were harvested, sonicated and purified as above.*

(**C**) *BL21 cells transformed with His_6-FIH or His_6-SKIP 1 – 353 were grown to OD_{600} = 0.6 and stimulated with 0.5 mM IPTG or left unstimulated. Following stimulation cells were incubated for a further 4 h at 28 °C. Whole cell extracts taken before and after 4 h induction were analysed by SDS-PAGE.*

(**D**) *BL21 cells transformed with GST-SKIP 150 – 339 or 170 – 339 were grown to OD_{600} = 0.6 before stimulation with 0.5 mM IPTG and incubation at 28 °C for a further 4 h. Whole cell extracts from cells pre-IPTG induction (P), after the 4 h incubation with no IPTG induction (–) or after the 4 h incubation with IPTG induction (+) were analysed by SDS-PAGE.*

IPTG but no visible induction of SKIP (Figure 4.15C). In a final attempt to obtain a recombinant SKIP fragment, an alternative expression and purification strategy using GST-tagged protein was devised. GST-SKIP constructs were prepared in pGEX-4T-1, containing residues 150 – 339 and 170 – 339. These were transformed into cells and whole cell extracts analysed by SDS-PAGE both before induction and in stimulated/unstimulated cells after a further 4 hours (Figure 4.15D). Once again, no expression of SKIP was visible by SDS-PAGE. As it did not prove possible to express and purify recombinant SKIP in these experiments, I was unable to carry out a 2OG turnover assay or use purified protein for additional MS/MS analysis.

4.2.9 *SV40 LTag interacts specifically with PHD3 in a DMOG-inducible manner*

Large T antigen is one of the major early gene products encoded by *Simian Virus 40* (SV40): it has a range of biological functions. As well as its involvement in viral DNA replication (Li and Kelly, 1984), LTag has several effects on cell growth: viral infection can produce de-differentiated cells that divide continuously (Endo and Nadal-Ginard, 1998), and expression of LTag alone can induce proliferation in quiescent cells, transform many cell types and cause the formation of tumours in laboratory animals (Fanning and Knippers, 1992). The mechanism by which LTag circumvents cell cycle checkpoints is thought to involve the inhibition or several important cellular tumour suppressor proteins, notably p53 (Jiang et al., 1993; Srinivasan et al., 1997).

One of the DMOG-inducible bands pulled down with PHD3 in Figure 4.7 was identified by MS/MS sequencing as LTag (Table 4.2). Although LTag is clearly not an endogenous human protein, it is used to transform 293T cells where it promotes episomal plasmid replication, enabling this cell line to express proteins at very high

levels, and is of interest because of its role as a transforming oncogene (Fanning and Knippers, 1992). In order to confirm the PHD3/LTag interaction, I transfected 293T cells with PHD3-V5 or empty vector control in the presence or absence of DMOG. Cell extracts were immunoprecipitated using V5 resin then analysed by immunoblotting for V5 and LTag. This experiment confirmed that LTag co-precipitated with PHD3-V5 and that the pull-down was enhanced dramatically by treatment of the cells with DMOG (Figure 4.16A). In order to confirm that the interaction was specific to PHD3 and not a general property of the HIF hydroxylases I analysed small aliquots of the original immunoprecipitations from Figure 4.7 by immunoblotting: this experiment confirmed that DMOG-inducible pull-down of LTag was specific to PHD3 (Figure 4.16B).

Although LTag is not a mammalian protein, I attempted to demonstrate an "endogenous" interaction between PHD3 and LTag in both 293T and COS7 cells (which are also LTag-transformed). As previous experiments shown in Figure 4.9A had demonstrated that the PHD3 antibodies available were not suitable for endogenous immunoprecipitation, I attempted to precipitate endogenous LTag from cells treated with DMOG or vehicle control. Control and anti-LTag IPs confirmed that capture of the protein was very efficient, and also demonstrated co-immunoprecipitation of p53. However, PHD3 co-precipitation was not visible in either case, perhaps because of the low levels of PHD3 detected in the inputs (Figure 4.17A and B).

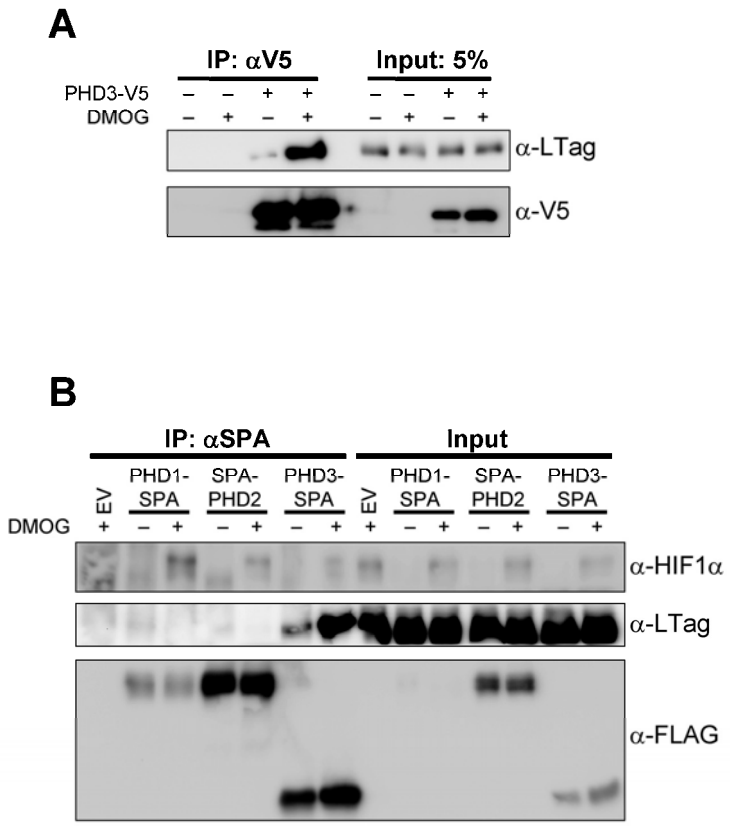


Figure 4.16 ***Validation of the PHD3/LTag interaction***
(**A**) *293T cells were transfected with PHD3-V5 or empty vector control, and treated with DMOG (1 mM) or vehicle control for 4 h before harvesting. Extracts were immunoprecipitated using V5 resin and immunoprecipitates probed for LTag and V5.*
(**B**) *Aliquots of the proteomic experiment presented in Figure 4.7 were probed by immunoblotting for FLAG, LTag and HIF1α.*

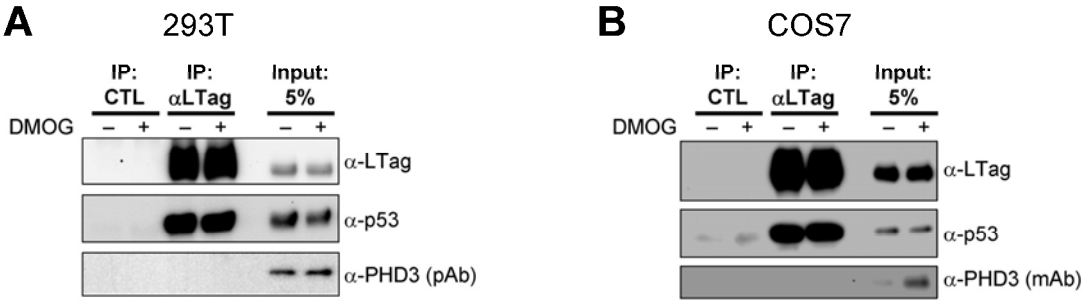


Figure 4.17 ***Attempts to show an endogenous PHD3/LTag interaction***
(**A**) *293T cells were stimulated with 1 mM DMOG or vehicle control for 4 h before harvesting. Extracts were immunoprecipitated using either anti-LTag antibody or an isotype-matched control, following which immunoprecipitates were analysed by immunoblotting for LTag, p53 and PHD3.*
(**B**) *COS7 cells were treated exactly as in* (**A**).

4.2.10 *Attempting to map the PHD3-interacting domain of LTag*

To determine which domain of LTag was interacting with PHD3, I used a plasmid containing full-length LTag (pRSV-Rev LTag) as a template to prepare a range of deletions by PCR, as shown in Table 4.3: this series of deletions included three LTag fragments that had been successfully prepared as recombinant proteins in *E. coli* (Kim et al., 2001a; Lilyestrom et al., 2006; Meinke et al., 2007). As there were potential issues with expressing LTag in a vector that contained an SV40 origin of replication, I ablated the SV40 origin in pcDNA3.1/myc-His A and used this modified vector (pcDNA3.1/myc-His A ΔSV40) as the backbone for the LTag constructs. Expression of this set of LTag deletions was found to be very poor, and so it was not possible to map the PHD3-interacting domain using this approach.

4.2.11 *PHD3 does not affect the interaction of LTag with p53, nor its stability*

Although it was not possible to determine a PHD3-interacting domain of LTag, I noticed by inspection that the protein contains an LxxLLP motif (similar to the HIF hydroxylation sites) at Pro-399. This residue also lies close to the surface through which LTag interacts with p53 (Lilyestrom et al., 2006). It therefore seemed reasonable to ask whether PHD3 might hydroxylate this residue and affect the LTag/p53 interaction. To address this question 293T cells were transfected with PHD3 (or empty vector control), an siRNA sequence targeting PHD3 or a control, non-targeting siRNA sequence (NT2). Anti-LTag or control IPs were carried out, following which cell extracts and immunoprecipitates were analysed by immunoblotting for LTag, p53 and PHD3 (Figure 4.18A). Endogenous levels of PHD3 in 293T cells are modest, but the PHD3 interventions (particularly overexpression) worked satisfactorily. However,

Residues	Comments	Reference
1 – 117*	N-terminus including Retinoblastoma protein binding domain	(Kim et al. 2001a)
131 – 260*	Includes T antigen origin binding domain	(Meinke et al. 2007)
251 – 627*	Includes p53 binding domain and LxxLLP	(Lilyestrom et al. 2006)
118 – 336	Includes T antigen origin binding domain	
337 – 672	Includes p53 binding domain	
370 – 708	C-terminus including LxxLLP	
550 – 708	C-terminus	

* *denotes published recombinant protein*

Table 4.3 ***SV40 LTag expression constructs***
LTag constructs prepared in modified pcDNA3.1/myc-His A ΔSV40 for domain mapping.

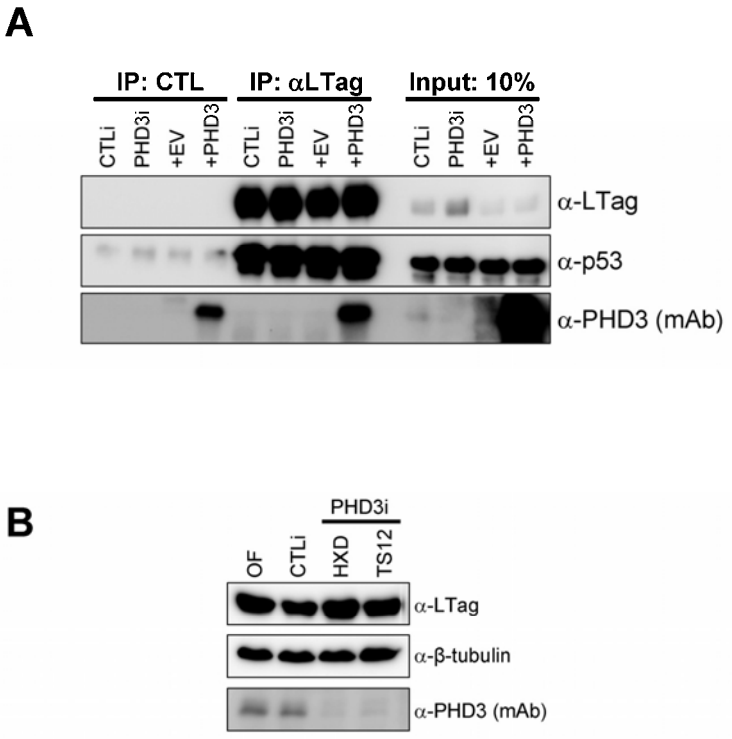


Figure 4.18 ***PHD3 overexpression or knock-down do not affect the LTag/p53 interaction***
(**A**) *293T cells were transfected with control, non-targeting siRNA duplex (CTLi), siRNA targeting PHD3 (PHD3i), empty vector (EV) or PHD3 (PHD3). 48 h after transfection cells were harvested and LTag immunoprecipitates. Immunoprecipitates were analysed by immunoblotting for LTag, p53 and PHD3.*
(**B**) *293T cells were transfected twice at 24-hour intervals two independent siRNA duplexes targeting PHD3 (HXD and TS12) and a non-targeting control sequence (NT2). 20 nM doses of duplex were used. As an additional control a mock transfection was carried out using Oligofectamine reagent alone (OF). 48 h after the second siRNA transfection cells were harvested and extracts immunoblotted for PHD3, SKIP and β-tubulin as a loading control.*

there was no effect on the co-precipitation of p53 with LTag. As it appeared that PHD3 knock-down might be increasing the level of LTag in the input samples, I carried out a further experiment using two independent PHD3 siRNA sequences together with a non-targeting sequence (NT2) and a mock-transfection control (Figure 4.18B). On this occasion the two PHD3 siRNA sequences, although effective at knocking down PHD3 levels, did not influence the total level of LTag in the cell extract, and it appeared that in fact the difference apparent in Figure 4.18A may have been due to a non-specific reduction in LTag levels by the control siRNA sequence NT2: this reduction was also observed to a lesser extent in Figure 4.18B.

4.2.12 *LTag can modestly affect the degradation kinetics of HIF*

PHD3 is strongly hypoxically induced and in certain situations may be the dominant PHD enzyme under hypoxia (Appelhoff et al., 2004). The data in Figure 4.16 suggested that PHD3 may be binding tightly to LTag, since a significant percentage of the total cellular amount of LTag was captured. I therefore reasoned that LTag could be having effects on HIF degradation when cells are reoxygenated after a period of hypoxia. To explore this possibility, five dishes of HEK293 cells were transfected with pRSV-Rev LTag, and a further five with empty vector control. Cells were incubated in hypoxia, following which they were restored to ambient oxygen and the degradation of HIF at the indicated time-points analysed by immunoblotting (Figure 4.19A(i)). A parallel experiment was conducted to compare untransfected HEK293 cells (which contain no LTag) with 293T cells (which are LTag-transformed) directly (Figure 4.19A(ii)). These experiments suggested that LTag may be slowing the degradation of HIF during reoxygenation slightly. As the levels of PHD3 in the HEK293 and 293T cells were

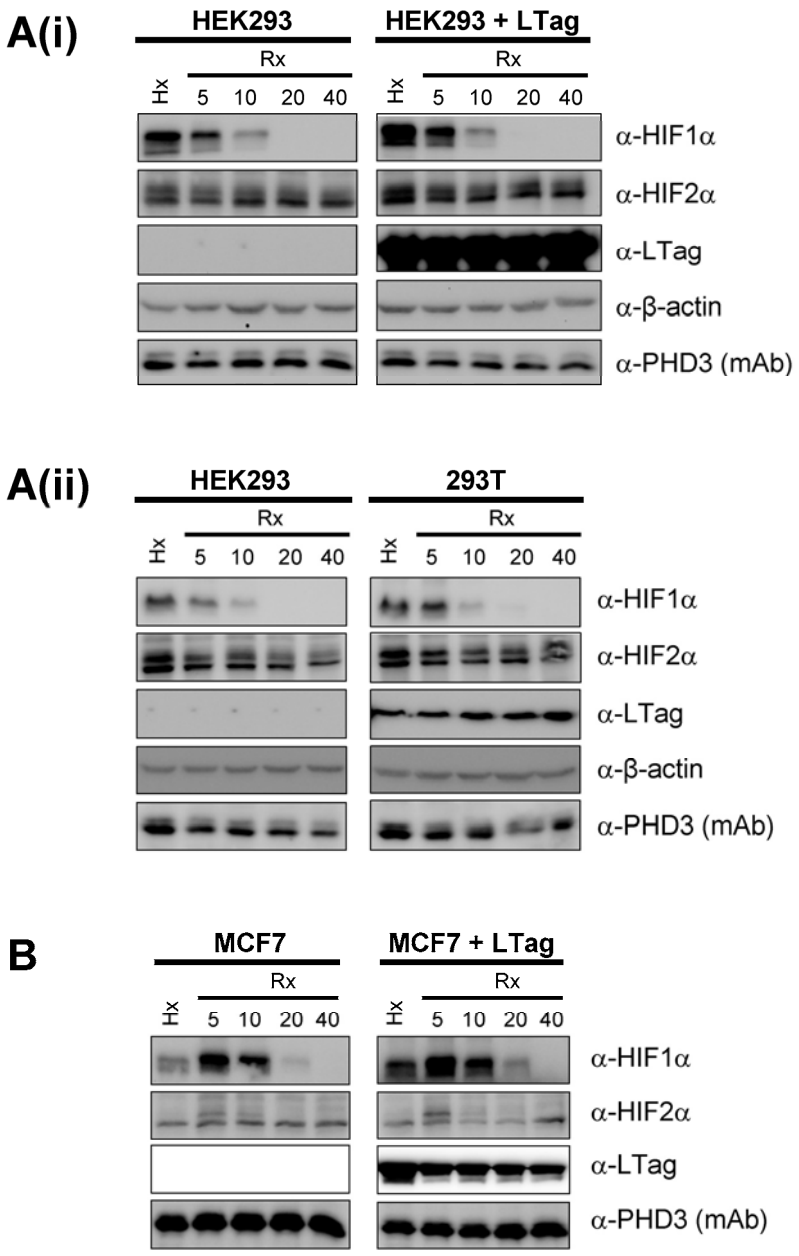


Figure 4.19 ***LTag modestly affects HIF degradation on reoxygenation***

(**A**(**i**)) *HEK293 cells were transfected with LTag or empty vector and incubated in hypoxia (1% O_2) for 16 h. One sample was harvested in hypoxia (Hx). The remainder were reoxygenated (Rx) by transferring back to ambient O_2 and harvested after the indicated number of minutes. Extracts were immunoblotted for HIF1α, HIF2α, LTag, PHD3 and β-actin as a loading control. In (***ii***), untransfected HEK293 and 293T cells were compared directly under exactly the same conditions.*

(**B**) *MCF7 cells were treated exactly as in (***A**(**i**)) *and extracts immunoblotted for HIF1α, HIF2α, LTag and PHD3. Membranes were stained with Coomassie blue to verify equal loading (not shown).*

rather modest, I decided to repeat the experiment using MCF7 cells which have been reported to express PHD3 at a relatively high level (Appelhoff et al., 2004). This experiment showed that overexpression of LTag in the MCF7 cells appeared to result in higher levels of both HIF1α and HIF2α under hypoxia and also slower degradation kinetics upon reoxygenation (Figure 4.19B), possibly by sequestration of cellular PHD3 away from HIF.

4.2.13 *LTag does not affect the cellular localization of PHD3*

Given that LTag appeared to be binding to PHD3 and affecting its activity, I carried out an experiment to determine if expression of LTag was affecting PHD3's cellular localization: whilst PHD3 has been reported to be distributed relatively evenly throughout the cell (Metzen et al., 2003), LTag contains a nuclear localization signal and therefore is predominantly nuclear (Dobbelstein and Roth, 1998). Thus I hypothesized that it was possible that LTag could sequester PHD3 to the nucleus and affect its activity. HEK293 cells were transfected either with pRSV-Rev LTag or an empty vector control. Cells were incubated in normoxia or hypoxia, following which they were harvested and fractionated into nuclear and cytoplasmic components. Extracts were probed by immunoblotting for RNA polymerase II (a protein expected to be located only in the nuclear fraction), p23 (expected only to appear in the cytoplasmic fraction), PHD3, LTag and HIF1α (Figure 4.20). The RNA polymerase II and p23 control immunoblots demonstrated that the cellular fractionation had worked correctly. Unexpectedly, LTag was detected in both the nuclear and the cytoplasmic fractions. No effect of LTag overexpression was therefore observed on the cellular localization of PHD3.

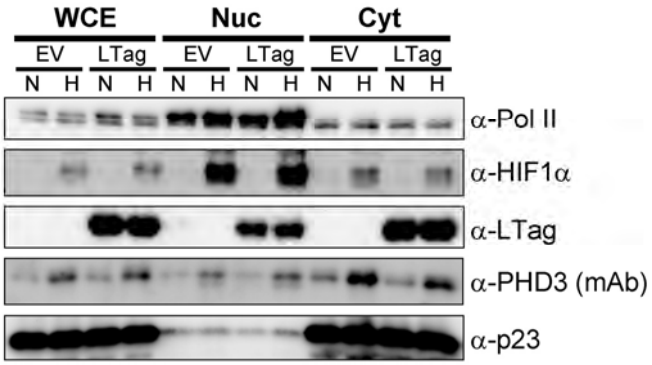


Figure 4.20 ***LTag does not affect the cellular localization of PHD3***
HEK293 cells were transfected with LTag or empty vector control (EV). 24 h after transfection cells were incubated for 16 h in normoxia (N) or hypoxia (1% O_2, H) for 16 h before harvesting and fractionation into nuclear and cytoplasmic components. Whole cell extract (WCE), nuclear (Nuc) and cytoplasmic (Cyt) fractions were analysed by immunoblotting for HIF1α, LTag and PHD3. As controls for the efficiency of the fractionation, extracts were immunoblotted for RNA polymerase II (Pol II) and p23.

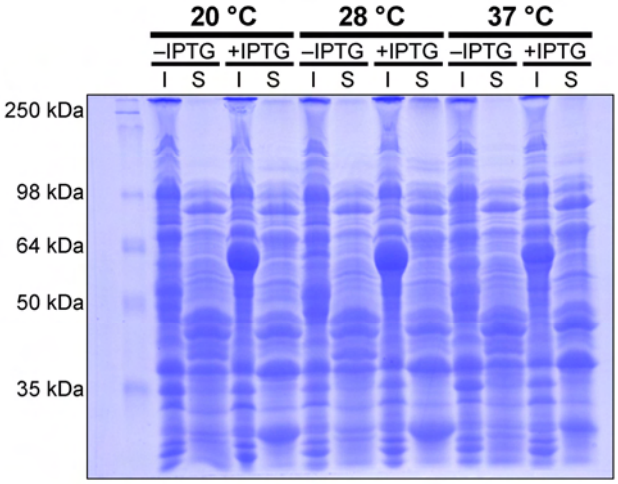


Figure 4.21 ***Attempts to prepare recombinant LTag in*** **E. coli**
BL21 cells were transformed with GST-LTag 251 – 627 and grown to OD_{600} = 0.6 before induction with 0.5 mM IPTG and incubation for a further 4 h at the indicated temperature. Following induction cells were harvested and sonicated; lysates were clarified by centrifugation and samples of the insoluble (I) and soluble (S) fractions analysed by SDS-PAGE.

4.2.14 *Attempts to prepare a recombinant LTag fragment*

The study reporting the structure of LTag complexed to p53 used a GST-tagged fragment containing residues 251 – 627 of LTag (Lilyestrom et al., 2006). Using the pRSV-Tag construct as a PCR template I cloned residues 251 – 627 of LTag into pGEX-4T-1, then tested the expression of this construct in BL21 *E. coli*. Cells were induced with a standard dose of IPTG then incubated at 20 °C, 28 °C or 37 °C after induction. Aliquots of cells were harvested and sonicated, following which soluble and insoluble fractions were analysed by SDS-PAGE (Figure 4.21). This experiment showed that, although a protein of approximately 60 kDa was expressed at a high level at all three post-induction temperatures, expression was almost exclusively insoluble. Different post-induction temperatures did not significantly affect protein solubility.

4.2.15 *Mass spectrometric analysis of LTag*

As it had not been possible to determine a PHD3-interacting domain of LTag, I decided to conduct an unbiased experiment using MS/MS in order to determine whether any residues in LTag (in particular Pro-399) were hydroxylated. Endogenous LTag was immunoprecipitated from cells treated either with DMOG (to inhibit PHDs) or with overexpressed PHD3. In the first experiment, immunoprecipitates were resolved by SDS-PAGE and LTag-containing bands excised and digested using trypsin (Figure 4.22). These digests achieved 32% coverage and 33% coverage of the LTag protein respectively (Table 4.4). Pro-399 was not observed in either case. In order to try and observe this residue, I repeated the experiment but omitted the in-gel digestion step in favour of digestion in solution, which would be expected to reduce sample losses and increase MS/MS coverage. This strategy was successful, and enhanced protein coverage

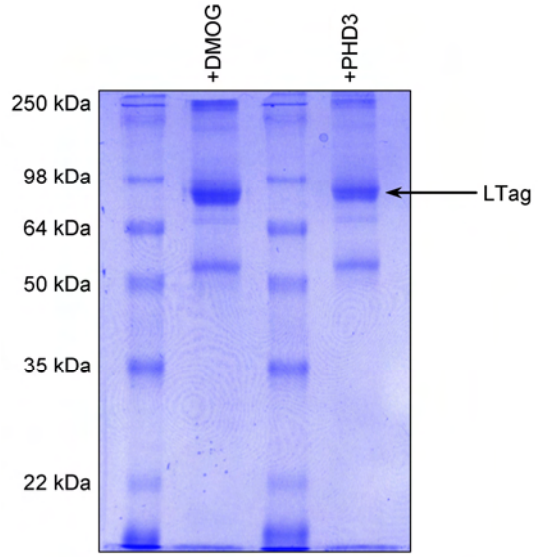


Figure 4.22 ***Immunoprecipitation of LTag for MS analysis***
293T cells were transfected with PHD3 for 24 h or treated with 1 mM DMOG for 4 h before harvesting. After harvesting cell lysates were immunoprecipitated using anti-LTag antibody. After washing, immunoprecipitates were resolved by SDS-PAGE and the indicated bands excised for analysis by LC-MS/MS.

Digest	Cell treatment	LTag score (MASCOT)	Unique peptides	Sequence coverage	LxxLLP detected	LxxLLP hydroxylation	Comments
Gel band	+DMOG	1346	25	32%	No	–	
	+PHD3	1456	25	33%	No	–	
Solution	+DMOG	1898	30	47%	Yes	No	
	+PHD3	2271	30	47%	Yes	No	Hydroxylation assigned at Pro-139. MS/MS data insufficient for robust assignment

Table 4.4
Results of LC-MS/MS analysis of LTag from DMOG- or PHD3-treated cells. Digestions were carried out from gel bands or in solution.

to 47% for both digests. Pro-399 was detected in both cases, but hydroxylation was not observed. Although the search algorithm assigned hydroxylation at an alternative prolyl residue, Pro-139, the MS/MS data were not sufficiently robust to enable an unequivocal assignment.

4.3 Discussion

This chapter has described the successful development of a proteomic strategy for identifying putative novel, non-HIF substrates of the HIF prolyl hydroxylase PHD3. Although it could be argued that the highest chance of capturing important and physiologically relevant interactions between proteins would be in an experiment involving immunoprecipitation of an endogenous protein from its native setting, either in cell culture or from animal tissues, this is frequently not possible. Abundance of the protein of interest may be low (as observed for PHD3 in 293T cells under normoxia in the experiments above), and specific antibodies capable of immunoprecipitating the desired species may not be available. For these reasons proteomic experiments very commonly use overexpressed proteins with an epitope tag in order to identify novel interactions (Gingras et al., 2005).

Based on previous reports on the role of PHD3 in neuronal apoptosis induced by NGF deprivation (Lee et al., 2005; Lipscomb et al., 1999; Lipscomb et al., 2001; Straub et al., 2003), initial efforts focused on the development of a proteomic strategy for identifying potential substrates using the PC12 cell line as a model. It did not prove possible to prepare a stable PC12-derived cell line inducibly expressing PHD3-SPA under the control of a tetracycline-responsive promoter: this may have been because of leaky expression of PHD3 resulting in apoptosis, or simply because of poor transfection efficiency in these cells. In order to counter this difficulty, a mixing strategy was developed using PHD3-SPA from 293T cells as a bait to co-precipitate interacting proteins from PC12 cell extract. Although this method did not succeed in identifying any novel, DMOG-inducible PHD3 binding partners, the pull-down and identification by MS/MS of rat (as opposed to human) HIF2α from the PC12 extract in this system

indicated that the experimental approach was wholly valid. It was possible however that the mixing experiment was only sufficient to capture the strongest PHD3-interacting proteins, and so an alternative approach using 293T extract alone was adopted: this led to the identification of two novel PHD3-interacting proteins, SKIP and LTag.

Having captured interacting species in a proteomic experiment it is important to establish that the interactions are genuine, and not an artefact of protein overexpression. Ideally this would involve the demonstration of an endogenous interaction between the native proteins by an immunoprecipitation from cultured cells or from tissue. However, it was not possible to demonstrate endogenous interactions with PHD3 either for SKIP or LTag. No antibodies were available that would immunoprecipitate PHD3 or SKIP in detectable quantities from cells, and whilst it was possible to immunoprecipitate endogenous levels of LTag efficiently from 293T cells, the levels of PHD3 in this system were barely detectable with the reagents available (Figure 4.9). Although it was not possible to demonstrate endogenous PHD3/SKIP and PHD3/LTag interactions, it would appear that both are robust and specific to PHD3: no binding of either SKIP or LTag was observed to any of the other HIF prolyl or asparaginyl hydroxylase enzymes. It was possible to immunoprecipitate endogenous SKIP using overexpressed PHD3, and *vice versa*. Further, in a separate study the PHD3/SKIP interaction was confirmed independently by yeast 2-hybrid[6].

In the search for novel substrates for an enzyme, after establishing that an interaction is likely to be physiological rather than artefactual, the next step is to confirm that the

[6] Norma Masson, unpublished data

interactor is indeed a substrate. There were multiple pieces of evidence to suggest that both SKIP and LTag may be novel PHD3 substrates: the interaction of PHD3 with both proteins was induced strongly by treating cells with DMOG, which is metabolized *in vivo* to a competitive PHD3 inhibitor. Further, although the issue of whether there is a consensus sequence for HIF prolyl hydroxylation remains an open question (Huang et al., 2002; Li et al., 2004), both proteins contained prolyl residues in a motif with some similarity to the LxxLAP motif reported for HIF (Ivan et al., 2001; Jaakkola et al., 2001; Masson et al., 2001): LAP in the case of SKIP and LxxLLP in the case of LTag. However, these factors alone clearly do not prove an enzyme-substrate relationship, my criterion for which was the unequivocal assignment of a PHD3-dependent prolyl hydroxylation of the putative substrate by tandem mass spectrometry.

To date it has not been possible to assign prolyl hydroxylations with absolute certainty in LTag or SKIP, although there is some evidence to suggest a PHD3-dependent hydroxylation of SKIP at Pro-173. The identification of post-translational hydroxylations can be confounded by a range of other oxidations occurring in proteins (artefactual or otherwise) and so requires high quality MS/MS sequencing data for robust assignment. Although this problem could be partially mitigated by the mutation of methionine residues located within mass spectrometric peptides containing putative sites of prolyl hydroxylation, this strategy may have other unpredicted effects on the conformation or function of a protein and clearly is not appropriate unless a relatively narrow potential site of prolyl hydroxylation has been identified. Further, this tactic would not assist in the assignment of hydroxylation at Pro-173 of SKIP as the tryptic and LysC peptides encompassing Pro-173 do not contain a methionine residue.

Proline is unique among the naturally occurring amino acids due to its cyclic structure, and this can influence MS/MS fragmentation patterns. N-terminal to proline, y-ions (rather than b-ions) tend to form selectively (Unnithan et al., 2007): this has been termed the "proline effect" (Grewal et al., 2004). Although the mechanism underlying this process is not well understood it has been proposed to involve the proton affinity of proline (Ewing et al., 1996) or the conformationally strained structure that the b-ion would be forced to adopt (Vaisar and Urban, 1996). The existence of the proline effect does not however explain the difficulties I have experienced in obtaining a full y-series about prolyl residues for MS/MS sequencing and assignment of hydroxylation: it is possible that this may be due to "kinks" in the conformation of the polypeptide chain introduced by proline, as in my hands asparaginyl hydroxylation has proved far easier to assign with certainty (see Chapters 2 and 3).

Clearly additional MS experiments on both SKIP and LTag will be needed in order to demonstrate prolyl hydroxylation unambiguously: this task has been made easier in the case of SKIP by the identification of an interacting domain in which it seems reasonable to expect any target prolyl residues would be located. However, it has not proved possible to map the domain of LTag which interacts with PHD3, which would make the task of locating a prolyl hydroxylation on this protein significantly more challenging. The failure to prepare and purify SKIP or LTag proteins *in vitro* from *E. coli* has been a significant hindrance to this study. Had purified proteins been available they could have been reacted *in vitro* using co-factors and a source of PHD3 before direct analysis of hydroxylation by mass spectrometry. Alternatively the putative substrates could have been assayed for their ability to support enzyme turnover in a 2OG decarboxylation assay (Hewitson et al., 2007). In view of the importance that purified proteins could

have in assisting with the assignment of SKIP and LTag as PHD3 substrates, it would be worth considering expression systems other than *E. coli* such as the baculoviral infection of insect cells, which has been widely and successfully applied (Kost et al., 2005).

Approaches other than mass spectrometry are available for substrate identification, although they may not give such a full assignment of prolyl hydroxylation. A recent report on RNA polymerase II uses antibodies which are claimed to recognize hydroxylated prolyl residues at specific positions within the protein (Mikhaylova et al., 2008). Alternatively a specific radiochemical assay originally described in 1966 has recently been adapted and used successfully to demonstrate the presence of hydroxyproline in a HIF-based peptide (Juva and Prockop, 1966; Koivunen et al., 2007). Although this approach requires the preparation and purification of putative substrates as peptides or proteins *in vitro*, it enables the existence (or otherwise) of hydroxyproline within the protein to be determined with certainty in advance of launching a mass spectrometric assault to locate the exact site of any hydroxylation.

Following the identification of a novel protein/protein interaction or enzyme/substrate relationship, the final challenge is to determine its function. In the case of a protein such as SKIP, which has pleiotropic functions, this may represent a significant challenge. Mapping of the PHD3-interacting site on SKIP suggested that the two proteins associate *via* the SNW domain: this is the core functional domain of SKIP and 90% conserved between species (Prathapam et al., 2002; Prathapam et al., 2001b). SKIP is involved as a transcriptional coactivator in a huge range of different pathways, reviewed in (Folk et al., 2004). These include steroid receptors such as the vitamin D

receptor (Zhang et al., 2001), the transforming growth factor-β signalling pathway (Dahl et al., 1998), the myogenic transcription factor pathway (Kim et al., 2001b) and the Notch signalling pathway (Zhou et al., 2000b). Further, SKIP can act as a transcriptional repressor, blocking the activity of proteins including the nuclear receptor co-repressor and histone deacetylase 2 (Zhou et al., 2000a). In addition to its roles as a transcriptional coregulator SKIP has also been found to be present in the spliceosome (Neubauer et al., 1998), and since been shown to associate with several partners involved in mRNA processing and splicing (Folk et al., 2004). Cell cycle control is yet another process involving SKIP, with partners such as the retinoblastoma protein and human papilloma virus E7 oncoprotein shown to bind (Prathapam et al., 2001a, 2002). This panoply of SKIP functions means that prolyl hydroxylation in the SNW domain by PHD3 could have some important biological effects, but attempts to analyse these effects may prove a formidable challenge, particularly since hypoxia might impinge on a number of these pathways such as myogenic differentiation and Notch signalling.

LTag, a transforming oncoprotein, influences processes involving cell growth and the cell cycle and binds a range of cellular tumour suppressor proteins (Jiang et al., 1993; Srinivasan et al., 1997). Although a proline residue (Pro-399) contained within an LxxLLP motif is located close to the p53 binding site on the surface of the LTag molecule (Lilyestrom et al., 2006), no hydroxylation was observed at this site, nor was any effect of PHD3 interventions detected on the LTag/p53 interaction. However the experiments in this chapter clearly show that under certain conditions LTag can bind PHD3 very tightly, and may thereby influence HIF degradation by PHD3 sequestration. This result is interesting in view of the oncogenic effect of LTag. Sequestration of

PHD3, for example in a hypoxic tumour, could cause an increase in HIF levels as PHD3 may be the dominant PHD enzyme in these circumstances (Appelhoff et al., 2004). This HIF induction could then assist in tumour growth through mechanisms including the upregulation of glycolysis and induction of angiogenesis. Further, PHD3 may act on HIF2α preferentially (Appelhoff et al., 2004), and a study in renal clear cell carcinoma (RCC) cells has demonstrated that pro-tumorigenic genes appear to respond specifically to HIF2α (Raval et al., 2005). Thus it seems conceivable that by binding and sequestration of PHD3, LTag could result in increased levels of HIF2α and the consequent activation of tumour-promoting genes including cyclin D1, transforming growth factor alpha and vascular endothelial growth factor. However, this interpretation should perhaps be treated with a degree of circumspection: it is not clear whether the levels at which LTag was expressed in the experiments above are physiologically relevant. Further, the stabilizing effect of LTag on HIF appeared to apply both to HIF1α and HIF2α, whilst LTag is not specifically implicated in RCC.

By applying the criterion stated above of unequivocal MS/MS assignment of PHD3-dependent prolyl hydroxylation, the work in this chapter has not rigorously identified any novel PHD3 substrates. However, SKIP and LTag are clearly two promising candidates worthy of further investigation. It is noteworthy that, whilst PHD1 and PHD2 have both been reported to hydroxylate targets other than HIF (Cummins et al., 2006; Mikhaylova et al., 2008), these proposed hydroxylations have also not been definitively assigned using mass spectrometry.

It is of course possible that the results of the experiments reported above reflect a genuine absence of non-HIF substrates for PHD3. A recent genetic study has

investigated the phenotype of *PHD3*$^{-/-}$ mice, in which sympatho-adrenal tissues such as the superior cervical ganglion, adrenal medulla and carotid body are hyperplastic, consistent with a defect in neuronal apoptosis during development in these animals (Bishop et al., 2008). Cultured superior cervical ganglion-derived neurons from *PHD3*$^{-/-}$ animals were also partially protected from apoptosis stimulated by NGF withdrawal when compared to wild type neurons, again consistent with a role for PHD3 in the neuronal apoptosis pathway. However, the protective effect was partially ablated in *PHD3*$^{-/-}$;*HIF2*$\alpha^{+/-}$ (but not *PHD3*$^{-/-}$;*HIF1*$\alpha^{+/-}$) mice, suggesting that HIF2α may also be involved in neuronal apoptosis.

In support of the involvement of a non-HIF pathway in developmental sympathetic neuronal apoptosis, whilst these experiments were under way a follow-up study to Lee *et al.* was published, implicating KIF1Bβ as a downstream target of PHD3 (Schlisio et al., 2008). In this report the authors demonstrate that PHD3-dependent apoptosis occurs in several cell lines derived from the neural crest, and also in a range of non-neural crest lines including U2OS, PC3 and HCT116 carcinoma cells. Using a short hairpin RNA (shRNA) library, the authors demonstrate that knock-down of KIF1Bβ prevents PHD3-induced apoptosis. Consistent with it being a downstream target of PHD3, overexpression of KIF1Bβ alone was sufficient to induce apoptosis in PC12 cells. Interestingly whilst knock-down of PHD3 by shRNA decreased KIF1Bβ levels, knock-down of PHD2, the principal hydroxylase regulating HIF levels under normoxia (Berra et al., 2003), had no effect on KIF1Bβ protein levels thus suggesting once more that neuronal apoptosis may be HIF-independent. Sequencing of the coding *KIF1B*β exons in neuroblastomas, phaeochromocytomas and medulloblastomas (all of which derive from the sympathoadrenal lineage) identified missense *KIF1B*β variants,

supporting a role for KIF1Bβ in the process of neuronal apoptosis. One point to note is that both Lee *et al.* and Schlisio *et al.* used overexpression of PHD3 to induce apoptosis: PHD3 has been reported to aggregate and form multimers (both with itself and other PHDs) in hypoxia, which could raise anxieties about artefactual effects of PHD3 overexpression (Nakayama et al., 2007). However, in the light of the finding that KIF1Bβ is necessary and sufficient for apoptosis, and that its levels can be affected by PHD3 shRNA this seems unlikely.

Taking the findings of Bishop *et al.* and Schlisio *et al.* together it seems that although HIF2α may be involved in PHD3-induced neuronal apoptosis, this does not tell the whole story and there is also a HIF-independent pathway in operation. Thus it still seems reasonable to suggest that PHD3 may indeed have non-HIF substrates. Two recent publications have suggested yet more novel functions of PHD3. Firstly, it has been reported that PHD3 interacts with the activating transcription factor 4 (ATF4) (Köditz et al., 2007). ATF4 is translationally induced under conditions of anoxia, mediates part of the unfolded protein response and is a critical regulator of cell fate decisions. Köditz *et al.* report that ATF4 protein stability is regulated by PHD3 in a pVHL-independent manner: however, whilst DMOG treatment, hypoxia and PHD3 knock-down by siRNA appear to stabilize ATF4 no mass spectrometric analysis has been conducted and therefore it would be premature to infer that ATF4 is indeed a PHD3 substrate. Secondly it has been reported that PHD3 exists in aggregates under hypoxia: these aggregates increase in size significantly on reoxygenation (Rantanen et al., 2008). Further, forced expression of PHD3 in HeLa cells caused protein aggregation and subsequent apoptosis, although this result should be treated with some caution given the findings of Nakayama *et al.* (Nakayama et al., 2007). Taken

together however, these findings provide further evidence that PHD3 is involved in a range of processes other than HIF signalling, which could well involve substrates that are yet to be discovered. Clearly there is much still to learn about the full range of functions and effects of PHD3.

Chapter 5
Final discussion

5.1 Introduction

This thesis has described a range of different studies on novel, "non-HIF" substrates of the HIF hydroxylase enzymes. Chapter 2 concerns a study to characterize the hydroxylation of a recently discovered substrate, Notch1, by FIH. Chapters 3 and 4 describe two alternative approaches for identifying new HIF hydroxylase substrates: a bioinformatic approach to identify sites of FIH-dependent hydroxylation in the ARD-containing protein MYPT1 in Chapter 3, and a proteomic approach to search for novel PHD3 substrates and interactors in Chapter 4. This chapter discusses common themes emerging from these experiments and possible future directions for this work.

5.2 A consensus sequence for ARD hydroxylation by FIH

The experiments described in Chapters 2 and 3 have defined a consensus sequence for the FIH-dependent asparaginyl hydroxylation that is widely present in ARD proteins, and also forms part of published consensus sequences for the ankyrin-repeat motif itself (Barrick et al., 2008; Li et al., 2006; Mosavi et al., 2004). This consensus sequence was validated by a study of the ARD-containing protein MYPT1, where all three of the sites identified *in silico* as conforming fully to the consensus were subsequently shown to be hydroxylation targets. Taking these results together with the observation that around 6% of eukaryotic protein sequences contain an ARD (Barrick et al., 2008), it appears that a wide range of proteins are likely to be substrates for FIH. Thus the work in this thesis has potentially expanded the scope of known protein hydroxylations significantly by defining a large number of putative hydroxylation targets, dispelling the myth that this PTM is rare.

5.3 The function of ARD hydroxylation: structure or signalling?

The analysis of an endogenous sample of purified avian MYPT1 in Chapter 3 has demonstrated beyond doubt that the hydroxylation of ankyrin-repeat proteins by FIH is a true, physiological PTM and not an artefact of the cell culture conditions used in previous reports of ARD hydroxylation (Cockman et al., 2006; Coleman et al., 2007; Ferguson et al., 2007). However, the effect of this modification is not yet fully understood.

The clearest effect of an ankyrin-repeat hydroxylation defined to date has been competitive inhibition of FIH by the ICD of Notch1, resulting in an increase in HIF1α transcriptional activity (Coleman et al., 2007; Zheng et al., 2008). The definition of a K_m for the reaction of a Notch1 ARD protein with FIH in Chapter 2 has provided a kinetic explanation for the effect that is observed, whilst work in Chapter 3 has demonstrated that a range of ARD-containing proteins other than Notch have a similar effect. These results provide support for the argument that a cellular ankyrin "pool" acts as a sink for FIH activity and modulates HIF transcriptional activity under certain conditions (Coleman et al., 2007), and also provide a potential explanation for the observation that FIH appears to be incompletely active towards HIF under normoxic conditions (Stolze et al., 2004). However, the reporter gene assay used to demonstrate this effect *in vivo* is somewhat derived, and it will be of interest to demonstrate an effect of ARD hydroxylation on HIF signalling in a more physiological setting.

There is indirect evidence to suggest that FIH has HIF-independent effects. A phylogenetic analysis in this laboratory has suggested that FIH and ankyrin-repeat proteins evolutionarily pre-date HIF, with an FIH-like gene identified in the unicellular

choanoflagellate organism *Monosiga brevicollis*[7]. In contrast it does not appear that the HIF system is conserved in earlier organisms than the nematode worm *Caenorhabditis elegans* (Taylor, 2001).

The effects of ARD hydroxylation might be structural or related to signalling. No clear effects of FIH-dependent hydroxylation have been demonstrated on the canonical Notch or NF-κB signalling pathways (Cockman et al., 2006; Coleman et al., 2007). Consistent with these reports, no hydroxylation-dependent effects were observed on canonical MYPT1 signalling. Whilst hydroxylation did not affect MYPT1 function under the conditions tested, it is possible that it may have a signalling role in other circumstances (for example in cells under hypoxia or metabolic stress). Alternatively FIH may have an effect on MYPT1 activity in one of the increasing number of non-canonical signalling pathways in which myosin phosphatase appears to be involved, for example the dephosphorylation of histone deacetylase enzymes in transcriptional regulation or the retinoblastoma protein in cell cycle regulation (Matsumura and Hartshorne, 2008). A further possibility is that FIH-dependent hydroxylation may have a critical signalling role in one of the many ARD-containing proteins in the genome that have yet to be assigned as FIH substrates, with the HIF hydroxylase pathway providing clear precedents for hydroxylation as a modification that can be degradative or block key protein/protein interactions.

Biophysical studies on synthetic and natural ankyrin-repeat proteins have indicated that hydroxylation can cause a conformational stabilization of the ARD fold[8]. Whilst it is tempting to speculate that, by analogy with prolyl 4-hydroxylation in collagen, ARD

[7] Mathew Coleman, unpublished data
[8] Leanne Kelly, Ming Yang and Christopher Schofield, personal communication

asparaginyl hydroxylation may be a modification with important structural implications, there are several differences between hydroxylation in collagens and hydroxylation in ARD proteins that imply this may not be the case. A typical collagen triple helix does not form until each α-chain has acquired around 100 4-hydroxyproline (4Hyp) residues (Prockop and Kivirikko, 1995), whilst the numbers of hydroxylations identified in individual ARD proteins to date have been much lower (one in p105 and ASB4, two in IκBα and Notch1 (Cockman et al., 2006; Coleman et al., 2007; Ferguson et al., 2007), three in MYPT1) and there are many β-hairpin loops at which hydroxylation is not observed. The post-translational hydroxylation of collagen is an integral part of the biosynthesis of these proteins, and absolutely required for them to adopt their correct tertiary structure (Prockop and Kivirikko, 1995); by contrast, it does not appear that hydroxylation in an ARD protein is a pre-requisite for correct protein folding as stable ARDs can be expressed in *E. coli*, which lacks an FIH-like gene. Whilst hydroxylations in certain regions of collagen occur to completion at every third residue in repeating Gly-Pro-4Hyp triplets, this thesis and published reports have shown that under physiological conditions ARD hydroxylation appears to be generally incomplete (Cockman et al., 2006; Coleman et al., 2007; Ferguson et al., 2007). Further, whilst the repeating Gly-Xxx-Yyy sequence in collagen is optimized for maximum structural stability, with the presence of a small glycine residue at each third position essential for the adoption of a coiled-coil structure (Myllyharju and Kivirikko, 2004), the sequences of natural ARD proteins do not appear to be optimal with respect to conformational stability (Ferreiro et al., 2007). Indeed, it appears that in some ARD-containing proteins a degree of instability in individual ankyrin repeats or in the overall ARD fold may be required for their biological functions: Notch and IκBα both undergo partial folding transitions upon binding their respective partner proteins (Barrick et al., 2008),

whilst mutations that increase the stability of IκBα result in an attenuation of its interaction with NF-κB and consequently incomplete inhibition of NF-κB activation (Truhlar et al., 2008).

The observation that variations in the stability of an ARD can affect protein/protein interactions raises a third possible role for FIH-mediated asparaginyl hydroxylation in these proteins: modulation of signalling through an indirect effect on binding partners caused by a structural modification. Because of the inherent structural cooperativity in ARD proteins, small perturbations in local structural stability (caused for example by a point mutation or potentially an asparaginyl hydroxylation) can alter the entire "folding energy landscape", re-routeing folding pathways and therefore potentially influencing the folding transitions that the ARD must undergo in order to form an interaction with a partner protein (Barrick et al., 2008). In addition to the reported effect of structural influences in IκBα on NF-κB signalling (Truhlar et al., 2008), a study on a designed ankyrin-repeat protein has shown that alterations in the internal hydrogen-bonding network in an ARD can have structural and conformational effects that may alter interactions with binding partners (Zahnd et al., 2007). Given the number of putative ARD substrates of FIH in the human genome and their range of functions and interacting partners, it seems reasonable to suggest that structural or conformational alterations arising from asparaginyl hydroxylation could potentially have important biological effects.

5.4 Novel substrates of the PHDs

The experiments in Chapters 2 and 3 of this thesis have indicated clearly that FIH has a wide range of protein substrates other than HIF. My work on PHD3 in Chapter 4

suggests that this may also be the case for the HIF prolyl hydroxylases, although further work will be required before it is possible to state definitively whether SKIP and LTag are *bona fide* substrates. For SKIP this task has been facilitated by the definition of a relatively small PHD3-interacting domain between residues 170 – 339, in which to concentrate mass spectrometric or other analyses for prolyl hydroxylation. The definition of a PHD3-interacting domain of LTag was confounded by poor expression of a suite of deletion mutants *in vivo*. However, in the quest to determine whether or not LTag is a true PHD3 substrate, an alternative domain-mapping experiment, perhaps using proteins translated *in vitro* in a cell-free system such as reticulocyte lysate, is a matter of priority as it will enable further analyses for hydroxylation to be targeted rather than attempting to cover the entire 708-residue protein.

The definition of either of these proteins as a PHD3 substrate would provide evidence that the HIF prolyl hydroxylases may have pleiotropic cellular effects. SKIP is of particular interest in this respect as it is a transcriptional coregulator involved in a wide range of signalling pathways (Folk et al., 2004) some of which, such as Notch signalling, have been reported to be influenced by hypoxia (Diez et al., 2007; Gustafsson et al., 2005).

5.5 Closing remarks

This thesis has shown that FIH will catalyse the hydroxylation of a wider range of substrates other than HIF, and provided some evidence to suggest that the same may be true of PHD3. Taking these results together with a recent publication illustrating the collagen prolyl hydroxylase enzyme CP4H1 also hydroxylates Argonaute2, a

protein involved in RNA-induced silencing (Qi et al., 2008), it appears that many of the 2OG dioxygenase enzymes may have multiple substrates with pleiotropic effects. Since there are more than sixty 2OG dioxygenases in the human genome (Loenarz and Schofield, 2008), many of unknown function, it is possible that post-translational protein hydroxylation may be a far more general phenomenon in cell biology than has hitherto been appreciated.

Hypoxia is an important component in both ischaemic and neoplastic illnesses, which between them account for around two thirds of deaths in the Western world. The development of specific inhibitors for the HIF hydroxylases has therefore been of great therapeutic interest. However, the growing body of evidence that HIF hydroxylases (and other 2OG dioxygenases) have a range of other, non-HIF substrates means that hydroxylase inhibition has the potential to impinge on a range of other pathways that are not yet fully understood, with off-target or toxic effects. A complete understanding of the full range of substrates of FIH and the PHDs will therefore be a critical component in the development of targeted and effective therapeutic strategies for manipulating the HIF system.

Chapter 6

Materials and methods

6.1 Reagents

6.1.1 *Chemicals*

Unless indicated otherwise in the text, all chemicals were purchased from Sigma Aldrich. Water was purified using an Elix® 10 system (Millipore), and subsequently further purified through a MilliQ system (Millipore) with a 0.22 µm filter at the outlet. "MilliQ-grade" water was used for all buffers and solutions.

6.1.2 *Buffers*

Phosphate-buffered saline (PBS)

PBS was purchased in tablet form and prepared by dissolving one tablet in 200 ml MilliQ-grade water, for a final concentration of phosphate buffer 0.01 M, KCl 0.0027 M, NaCl 0.137 M, pH 7.4 at 25 °C.

HEPES-buffered saline (HBS)

4-(2-Hydroxyethyl)piperazine-1-ethanesulfonic acid (HEPES) 40 mM, NaCl 200 mM. The pH was adjusted to 7.4 using NaOH 1 M.

Tris acetate-EDTA (TAE)

TAE buffer was purchased as a 10× liquid concentrate and diluted to 1× using MilliQ-grade water for a final concentration of Tris acetate 40 mM, EDTA 1 mM, pH 8.3.

Agarose gel loading buffer (5×)

10× TAE 5 ml, glycerol 5 ml, bromphenol blue 0.05% (w/v).

SDS-PAGE running buffer (10×)

Tris-(hydroxymethyl)aminomethane (Tris) 0.25 M, glycine 1.9 M, SDS 1% (w/v). The 10× concentrate was diluted to 1× using MilliQ-grade water.

Protein transfer buffer (20×)

Tris 0.2 M, glycine 2 M. 1× transfer buffer was prepared using 50 ml 20× concentrate and 100 ml MeOH per litre.

SDS-PAGE resolving (lower) gel buffer (4×)

TrisHCl pH 8.8 1.5 M, sodium dodecylsulfate (SDS) 0.4% (w/v).

SDS-PAGE stacking (upper) gel buffer (4×)

TrisHCl pH 6.8 1.5 M, SDS 0.4% (w/v).

SDS-PAGE sample buffer (6×)

Upper gel buffer (4×) 7 ml, glycerol 30% (v/v), SDS 10% (w/v), DL-dithiothreitol (DTT) 0.6 M, bromphenol blue 0.05% (w/v) in a total volume of 10 ml.

Jie's buffer

NaCl 100 mM (unless indicated otherwise), TrisHCl pH 7.4 20 mM, $MgCl_2$ 5 mM, Nonidet P-40 (NP40) 0.5% (v/v). Complete EDTA-free protease inhibitor cocktail (Roche Applied Science) was added immediately before use if used for cell lysis.

TFBI

KOAc 30 mM, $RbCl_2$ 100 mM, $CaCl_2$ 10 mM, $MnCl_2$ 50 mM, glycerol 15% (v/v). Salts were dissolved in 50 ml MilliQ-grade water before addition of glycerol, following which the pH was adjusted to 5.8 using AcOH, 0.2 M. The solution was made up to 100 ml final volume with MilliQ-grade water, filter-sterilized and stored at 4 °C.

TFBII

3-(*N*-morpholino)propanesulfonic acid 10 mM, $CaCl_2$ 10 mM, $RbCl_2$ 10 mM, glycerol 15% (w/v). Salts were dissolved in 50 ml MilliQ-grade water before addition of glycerol, following which the pH was adjusted to 6.5 using NaOH,

1M. The solution was made up to 100 ml final volume with MilliQ-grade water, filter-sterilized and stored at 4 °C.

CLB

HEPES 10 mM, NaCl 10 mM, KH_2PO_4 1 mM, $NaHCO_3$ 5 mM, EDTA 5 mM, $CaCl_2$ 1 mM, $MgCl_2$ 0.5 mM.

TSE

TrisHCl pH 7.5 10 mM, sucrose 300 mM, EDTA 1 mM, NP40 0.1% (v/v).

Z buffer

Na_2HPO_4 60 mM, NaH_2PO_4 40 mM, KCl 10 mM, $MgSO_4$ 1 mM, pH 7.0 at 25 °C. β-mercaptoethanol was added to 30 mM immediately prior to use.

Tris-buffered saline (TBS)

NaCl 150 mM, TrisHCl pH 6.9 20 mM. DTT was added to 1 mM immediately before use.

EBC

NaCl 150 mM, TrisHCl pH 7.5 20 mM, NP40 0.5% (v/v).

6.1.3 *Cell biology reagents*

Dimethyloxalylglycine (DMOG)	Frontier Biosciences, 100 mM stock in PBS (100x)
Cycloheximide (CHX)	Sigma, 100 mg ml^{-1} stock in DMSO (1000x)

6.2 Bacterial techniques

6.2.1 *Solutions and media*

All bacterial growth media were autoclaved at 121 °C and 100 kPa for 15 minutes before use.

Luria-Bertani medium (LB)

LB was purchased in powder form and made up by dissolving 20 g per litre of MilliQ-grade water before autoclaving. For LB-agar plates 15 g agar (Invitrogen) was also added per litre before autoclaving.

YB

Yeast extract (Invitrogen) 0.5% (w/v), Tryptone (Invitrogen) 2% (w/v), $MgSO_4$ 0.5% (w/v), pH adjusted to 7.6 using KOH before autoclaving.

SOC

SOC medium was purchased from Invitrogen.

Antibiotics

Where necessary for selection, ampicillin was added to solid and liquid culture media for a final concentration of 100 μg ml^{-1}.

6.2.2 *Bacterial strains*

All recombinant manoeuvres and cloning manipulations were carried out in *Escherichia coli* (*E. coli*) strain DH5α except for transformation of plasmids after site-directed mutagenesis which used XL10-Gold® ultracompetent cells (Stratagene). For expression of recombinant proteins, strain BL21 was used.

6.2.3 *Preparation of competent* E. coli *for transformation*

A single bacterial colony was used to inoculate 5 ml of YB and grown overnight. The following morning the primary culture was back-diluted 100-fold into 400 ml pre-warmed YB. Cells were grown to an OD_{550} of 0.5 then cooled on ice and harvested by centrifugation at 3250 *g* and 4 °C for 5 minutes. After discarding the supernatant, cells were resuspended in 160 ml ice-cold TFBI and incubated on ice for 5 minutes. Cells were pelleted as before and supernatant discarded before resuspension in 16 ml ice-cold TFBII and incubation on ice for 15 minutes. The cell suspension was then divided into 100 µl aliquots and stored at –80 °C. A typical transformation efficiency for these cells was approximately 1×10^6 transformants μg^{-1} DNA.

6.2.4 *Transformation*

DH5α (50 µl per transformation) were transformed with either 5 µl of a 10 µl ligation reaction or 50 ng plasmid DNA; BL21 were transformed only with 50 ng plasmid DNA. Cells were thawed on ice, DNA was added, then transformation mixtures incubated on ice for 30 minutes with occasional gentle mixing. Cells were then heat-shocked at 42 °C for 90 s and immediately returned to ice for 2 minutes. After addition of 0.5 ml SOC medium transformation mixes were incubated at 37 °C with shaking at 220 rpm for1 hour. For plasmid transformations 50 µl of the transformation mix was spread onto agar plates containing appropriate antibiotics, then selected overnight at 37 °C; for ligations the bacteria were pelleted by centrifugation at 2000 *g* for 2 minutes before resuspending in 50 µl SOC medium and plating.

6.3 DNA techniques

6.3.1 *Isolation and purification of plasmid DNA*

Small-scale preparations of plasmid DNA for recombinant manipulations and transformation were carried out using a QIAprep spin miniprep kit (Qiagen), based on an alkaline lysis of *E. coli* followed by the adsorption of DNA to silica in high-salt conditions, high-salt washing and low-salt elution. Large-scale plasmid DNA purification for transfection of mammalian cell cultures was carried out using a HiSpeed plasmid maxi kit (Qiagen), based on alkaline lysis, the binding of DNA to an anion-exchange resin under low salt conditions, medium-salt washing and high-salt elution. The eluted DNA was then concentrated and desalted by isopropanol precipitation. The manufacturer's instructions for the use of both kits were followed exactly.

6.3.2 *DNA quantitation*

Double-stranded DNA (dsDNA) was quantitated using a NanoDrop® ND-1000 spectrophotometer with a sample volume of 1.2 µl to measure the absorbance of the solution at 260 nm. Purity was determined by measuring the absorbance at 260 nm and 280 nm: a pure dsDNA solution has an A_{260}/A_{280} ratio of approximately 1.8.

6.3.3 *Amplification of DNA by polymerase chain reaction (PCR)*

Standard 50 µl reactions contained 50 ng plasmid DNA as template, 10 pmol each oligonucleotide primer (see Table 6.4 for primers used), 2.5 U Cloned *Pfu* DNA polymerase (Stratagene), Cloned *Pfu* reaction buffer to 1× and 0.2 mM dNTPs. Thermal cycling was carried out using a PTC-200 Peltier thermal cycler (MJ Research) as follows: 96 °C 45 s, 60 °C 60 s (unless indicated otherwise in Table 6.4), 72 °C 120 s per 1000 base pairs of DNA to be amplified. Following 35 cycles samples were analysed by agarose gel electrophoresis.

6.3.4 *Agarose gel electrophoresis*

Gels for DNA electrophoresis contained agarose 1% (w/v) in TAE buffer plus ethidium bromide to 2 µg ml^{-1}. Samples were loaded in 1× agarose gel loading buffer and electrophoresed at a constant voltage of 120 V. Resolved DNA bands were visualized using a UV transilluminator (UV Products).

6.3.5 *Purification of DNA from agarose gels or from solution*

DNA bands were excised using a UV light source and clean scalpel, and subsequently purified using an illustra GFX™ PCR DNA and gel band purification kit (GE Healthcare) according to the manufacturer's instructions. The same kit was used for purification of PCR products from solution.

6.3.6 *Restriction enzyme digestion*

All restriction endonucleases and reaction buffers were supplied by New England Biolabs. In general, 1 µg plasmid DNA or 15 µl PCR fragment was digested using 10 – 20 U each enzyme and 2 µl appropriate 10× reaction buffer in a total volume of 20 µl. BSA was added to 0.1 mg ml^{-1} where required. Digestion was carried out for 2 hours at the manufacturer's recommended temperature.

6.3.7 *Alkaline phosphatase treatment*

Following restriction enzyme digestion, removal of 5' phosphate groups from digested vector DNA was performed by incubation in the presence of 10 U calf intestinal alkaline phosphatase (New England Biolabs) for 20 minutes at 37 °C.

6.3.8 *Ligation*

Ligation reactions used 20 U T4 DNA ligase (New England Biolabs) and 1× T4 DNA ligase reaction buffer in a total volume of 10 µl. A threefold molar excess of insert

DNA over phosphatased vector was used, with reactions being incubated at room temperature for 2 hours.

6.3.9 *Site-directed mutagenesis (SDM)*

Standard SDM reactions contained 50 ng plasmid DNA as template, 20 pmol each mutagenic oligonucleotide primer (see Table 6.3), 2.5 U Cloned *Pfu* DNA polymerase (Stratagene), Cloned *Pfu* reaction buffer to 1×, 5% (v/v) DMSO and 1 mM dNTPs in a total reaction volume of 50 µl. Reactions were performed in duplicate with two different annealing temperatures: unless indicated otherwise in Table 6.3 standard cycling conditions were 95 °C 30 s, 55 °C or 58 °C 60 s, 68 °C 10 min for 16 cycles. Following cycling, 40 U *Dpn*I (New England Biolabs) was added and template DNA digested for 1 hour at 37 °C. Products were analysed by agarose gel electrophoresis, following which DNA from successful reactions was purified from solution using an illustra GFX™ PCR DNA and gel band purification kit (GE Healthcare) and eluted in 10 µl TrisHCl pH 8.0 10 mM. 5 µl of the purified DNA solution was transformed into XL10-Gold® ultracompetent cells (Stratagene) according to the manufacturer's instructions.

6.3.10 *DNA sequencing*

All plasmid inserts were sequenced using appropriate oligonucleotide primers (see Table 6.4) by Geneservice Ltd, Department of Biochemistry, University of Oxford, in order to verify their integrity.

6.4 Protein techniques

6.4.1 *Protein quantitation*

The protein concentration of cell extracts was quantitated using a detergent-compatible colorimetric assay (DC assay, BioRad). Sample aliquots (5 µl and 1 µl) were prepared in a clear, U-bottomed 96-well plate (Falcon). Working reagent A (an alkaline copper tartrate solution, 20 µl) was added followed by addition of 160 µl reagent B (Folin-Ciocalteu reagent). Samples were incubated at room temperature for 15 minutes before analysis using a Model 550 microplate reader (BioRad) at a wavelength of 655 nm. A lysis buffer blank was prepared in parallel; for absolute quantitation a series of BSA samples of known concentration was used to prepare a standard curve.

Purified recombinant protein solutions were quantitated using a NanoDrop® ND-1000 spectrometer: the absorbance of the solution at 280 nm was measured, and used together with the relative formula mass of the protein and its extinction coefficient (as determined from the protein sequence using the online ProtParam tool, http://www.expasy.org/tools/protparam.html) to calculate the concentration of the solution.

6.4.2 *Sodium dodecylsulfate polyacrylamide gel electrophoresis (SDS-PAGE)*

Discontinuous SDS-PAGE was performed using Mini-Protean III apparatus (BioRad) according to the method of Laemmli (Laemmli, 1970). Resolving gels were prepared containing SDS-PAGE resolving buffer to 1× with the addition of 30% acrylamide:bis-acrylamide mix (37.5:1; BioRad) to the desired specification (ranging from 10% to 15% final concentration). Stacking gels were prepared containing SDS-PAGE stacking buffer to 1× with the addition of 30% acrylamide:bis-acrylamide to a final concentration of

3.9%. All gels contained a final SDS concentration of 0.1% and were polymerized in the presence of ammonium persulfate (APS; 0.1% (w/v) final) and N,N,N',N'-tetramethylethylenediamine (TEMED; 0.1% (v/v) final). Protein samples were boiled in 1× SDS-PAGE sample buffer for 10 minutes before electrophoresis alongside SeeBlue Plus2 pre-stained protein standards (Invitrogen) at a constant current of 20 mA per gel in 1× SDS-PAGE running buffer. Following electrophoresis protein gels were rinsed in MilliQ-grade water and either stained with Imperial Protein Stain (Pierce Biotechnology) and destained in MilliQ-grade water or transferred to membranes for immunoblotting as described below.

6.4.3 *Immunoblotting*

Proteins resolved by SDS-PAGE were electroblotted onto polyvinylidene fluoride (PVDF) membranes (Immobilon-P, Millipore) by tank transfer using Mini-Transblot apparatus (BioRad). Briefly, the transfer cassette containing the pre-equilibrated gel and PVDF membrane, sandwiched between 3MM chromatography paper (Whatman) and fibre pads (BioRad) was assembled under 1× protein transfer buffer to minimize trapping of air bubbles. The cassette was placed in the transfer tank together with an ice block, immersed in 1× transfer buffer and proteins transferred at a constant voltage of 100 V. After 60 minutes membranes were removed from the cassette, rinsed in MilliQ-grade water to remove SDS, and the efficiency of protein transfer assessed by staining using a Ponceau S solution (0.1% (w/v) in AcOH 5% (v/v)) after which membranes were destained using AcOH 5% (v/v).

For immunodetection membranes were transferred to blocking solution (PBS containing TWEEN® 20 0.1% (v/v) and dried non-fat milk 5% (w/v) or BSA 5% (w/v) for phospho-specific antibodies) and incubated for 60 minutes at room temperature

with gentle rocking. Primary antibodies were diluted in blocking solution to the concentration specified in Table 6.1 and applied to the membrane for a minimum of 90 minutes at room temperature, or overnight at 4 °C, with gentle rocking. Following primary antibody incubation, membranes were subjected to a series of washes in PBS containing TWEEN® 20 0.1% (v/v) (PBST): typically membranes were given three brief rinses followed by a 5 minute wash with rocking; this washing step was repeated three times. The appropriate horseradish peroxidase (HRP)-conjugated secondary antibody was diluted to 1:2,000 in blocking solution and added to the membrane for 60 minutes at room temperature with gentle rocking. Where necessary when probing immunoprecipitates, TrueBlot HRP-conjugated secondary antibody (eBioscience) against the appropriate species was used at a 1:1,500 dilution in PBST containing non-fat milk 1%: these secondary antibodies detect the native IgG of the bound primary antibody but not denatured IgG on the membrane from the immunoprecipitation. Following a duplicate series of washing steps to remove non-specifically bound HRP-conjugated antibody, bound HRP activity was visualized by chemiluminescence using SuperSignal West Pico, West Dura or West Femto substrate (Pierce Biotechnology) and a BioSpectrum AC imaging system running LabWorks image acquisition software (UV Products). If chemiluminescence was not sufficiently strong to detect using this imaging system, X-OMAT LS film (Kodak) was used.

6.4.4 *Antibodies*

Primary antibodies were routinely used at a dilution of 1:1,000 for immunoblotting unless specifically stated otherwise. A full list of antibodies used is shown in Table 6.1.

6.4.5 *Preparation of agarose-conjugated antibodies for immunoprecipitation*

Antibodies were conjugated to Protein A Agarose Fast Flow (Upstate Biotechnology): 200 µg antibody was used to each 1 ml bed volume of agarose. For mouse monoclonal antibodies of isotype IgG_1, agarose was equilibrated in 4 bed volumes sodium borate 0.2 M pH 9.0. Antibody was added and tubes incubated for 60 minutes at room temperature with gentle rotation. Beads were washed four times with 10 bv NaCl 3 M, sodium borate 50 mM pH 9.0. Beads were resuspended in 10 bed volumes NaCl 3 M, sodium borate 50 mM pH 9.0 plus dimethylpimelidate 20 mM, and incubated for 30 minutes at room temperature with gentle rotation. The coupling reaction was stopped by rinsing the beads once in ethanolamine 0.2M, pH 8.0 at room temperature for 2 h with gentle mixing, following which beads were washed three times with PBS and once with water. Beads were then washed twice for 3 minutes with glycine 100 mM pH 2.5, and a further three times in PBS, following which beads were resuspended on PBS containing sodium azide 0.02% (w/v) and stored at 4 °C. Rabbit antisera were coupled using an identical procedure except that NaCl 3 M, sodium borate 50 mM, pH 9.0 was replaced throughout with sodium borate 0.2 M, pH 9.0.

Table 6.1 ***Antibodies***

Antigen	Antibody	Dilution	Source/reference
HIF1α (human)	mAb 54; mouse	1:1,000	BD Transduction Labs (610959)
HIF2α (human)	mAb 190b; mouse	1:4	In house (Wiesener et al., 1998)
HIF1α (rat)	pAb; rabbit	1:1,000	Novus Biologicals (100-479)
HIF2α (rat)	pAb PM9; rabbit	1:1,000	In house (Lau et al., 2007)
PHD3	mAb 188e; mouse	1:10	In house (Appelhoff et al., 2004)
PHD3	pAb; rabbit	1:1,000	Novus Biologicals (100-303)
FIH	mAb 162c; mouse	1:1,000	In house (Stolze et al., 2004)
SKIP	pAb; goat	1:500	Santa Cruz (sc-21812)
LTag (SV40)	mAb PAB419; mouse	1:1,000	Cancer Research UK
p53	mAb 19/53BP1; mouse	1:1,000	BD Transduction Labs (612522)
RNA Pol II	mAb A-10; mouse	1:1,000	Santa Cruz (sc-17798)
p23	mAb JJ3; mouse	1:1,000	Abcam (ab2814)
β-tubulin	mAb 2-28-33; mouse	1:15,000	Sigma (T5293)
MYPT1	pAb F38; rabbit	1:20,000	D J Hartshorne (Wu et al., 2003)
MLC	mAb MY-21; mouse	1:10,000	Sigma (M4401)
pMLC (Ser-19)	pAb; rabbit	1:1,000*	Cell Signaling (3671)
pMLC (Ser-19/Thr-18)	pAb; rabbit	1:1,000*	Cell Signaling (3674)
PP1cδ	mAb EP1804Y; rabbit	1:200,000	Abcam (ab53315)
IκBα	mAb 6A920; mouse	1:1,000	Abcam (ab12134)
GFP (*Aequorea victoria)*	pAb; rabbit	1:2,000	Invitrogen (A11122)
HRP-conjugated antibodies			
His_6 tag	mAb H-3; mouse	1:2,000	Santa Cruz (sc-8036)
V5 tag	mAb SV5-Pk1; mouse	1:3,000	AbD Serotec (MCA1360P)
FLAG tag	mAb M2; mouse	1:3,000	Sigma (A8592)
β-actin	mAb AC-15; mouse	1;25,000	Abcam (ab49900)
Agarose affinity conjugates			
V5 tag	mAb V5-10; mouse		Sigma (A7345)
FLAG tag	mAb M2; mouse		Sigma (F2426)

Antigens are human unless indicated otherwise. Antibody: clonality, clone; host species
**BSA 5% in PBST used as blocking solution*

6.5 Mammalian cell culture techniques

6.5.1 *Cell culture*

HEK293, 293T, HeLa, COS7 and MCF7 cells were maintained in Dulbecco's Modified Eagle's Medium (DMEM) supplemented with foetal calf serum (FCS) 10%, L-glutamine 2 mM, penicillin 50 IU ml^{-1} and streptomycin 50 µg ml^{-1}. PC12 cells were maintained in DMEM supplemented with horse serum (Invitrogen; 10%), FCS 5% (heat inactivated by incubation at 55 °C for 30 minutes), L-glutamine 2 mM, penicillin 50 IU ml^{-1} and streptomycin 50 µg ml^{-1}. All cells were grown as monolayers, except PC12 cells which were grown as suspension cultures. Cells were maintained in a humidified atmosphere containing CO_2 5% at 37 °C. Hypoxic incubations were carried out using an Invivo$_2$ 400 hypoxia workstation (Ruskinn Technology) in an atmosphere containing CO_2 5%, the indicated percentage of O_2 and balanced with N_2.

6.5.2 *Plasmid transfection*

Plasmid transfections were performed using FuGENE®6 transfection reagent (Roche Applied Science) according to the manufacturer's instructions. Plasmid doses used were 1 µg per well of a 6-well dish, 4 µg per 10 cm dish or 10 µg per 15 cm dish. Cells were transfected at around 50% confluence. A ratio of 3 µl FuGENE®6 reagent to 1 µg DNA was used: FuGENE®6 reagent was first diluted into serum-free medium (OptiMEM®; Invitrogen), vortex mixed and incubated for 5 minutes at room temperature. Following addition of plasmids, transfection mixtures were vortex mixed and incubated for a further 15 – 45 minutes at room temperature, following which they were added dropwise to the growth medium on the cells. Cells were returned to the incubator and results analysed 24 – 48 h post-transfection. A full list of plasmids used for mammalian transfection is provided in Section 6.8.2.

6.5.3 *siRNA transfection*

siRNA duplexes were transfected at a concentration of 20 nM using Oligofectamine reagent (Invitrogen) according to the manufacturer's instructions. Briefly, for transfection of a 15 cm diameter dish, two tubes were prepared: tube 1 contained 15 µl siRNA duplex (from a 20 µM stock solution) plus 12 ml OptiMEM®, tube 2 contained 30 µl Oligofectamine reagent plus 3 ml OptiMEM®. Tubes 1 and 2 were mixed individually and incubated at room temperature for 5 minutes, following which the contents of the two tubes were combined, mixed and incubated at room temperature for a further 15 minutes. During this second incubation growth medium was aspirated from the cells and they were washed twice with OptiMEM®: after aspiration of the second wash the transfection mixture was added and cells returned to the incubator. After a 4 h incubation, the transfection was concluded by adding 7.5 ml OptiMEM® containing 30% FCS. Two transfections were carried out at 24 h intervals; results were analysed 24 – 48 h after the second transfection. All siRNAs were chemically synthesized and annealed by Ambion, with the exception of control sequence NT2 which was manufactured by Dharmacon. A full list of siRNA duplexes used is shown in Table 6.2.

Table 6.2 *siRNA duplexes*

Targeted transcript	Orientation	Sequence (5'→3')	Reference
NT2	Non-targeting siRNA #2, Dharmacon siCONTROL D-001210-02-05		
dHIF (U43090)	sense	CCU ACA UCC CGA UCG AUG AdTdT	(Berra et al., 2003)
	antisense	UCA UCG AUC GGG AUG UAG GdTdT	
FIH (NM_017902)	sense	GUU GCG CAG UUA UAG CUU CdTdT	(Stolze et al., 2004)
	antisense	GAA GCU AUA ACU GCG CAA CdTdG	
PHD3 (TS12) (NM_022073)	sense	GGA GAG GUC UAA GGC AAU GdTdT	(Appelhoff et al., 2004)
	antisense	CAU UGC CUU AGA CCU CUC CdTdT	
PHD3 (HXD) (NM_022073)	sense	CAG GUU AUG UUC GCC ACG UdTdT	(Appelhoff et al., 2004)
	antisense	ACG UGG CGA ACA UAA CCU GdTdT	

6.5.4 *Mammalian cell lysate preparation*

Before lysis, growth medium was decanted and cells washed twice with ice-cold PBS. For immunoprecipitation and immunoblotting cells were lysed in Jie's buffer containing 1× Complete EDTA-free protease inhibitor cocktail (Roche Applied Science) after aspiration of all remaining traces of PBS: generally 3 ml lysis buffer was used for a 15 cm diameter dish and 1 ml lysis buffer for a 10 cm diameter dish. Cells were scraped into lysis buffer followed by incubation of the mixture for 15 minutes at 4 °C with gentle rotation. Cell detritus was removed by centrifugation in a pre-chilled microcentrifuge for 15 minutes at 14,000 *g* and 4 °C. For phospho-MLC immunoblotting cells were lysed directly into 3× SDS-PAGE sample buffer and sonicated briefly to shear the DNA, after which extracts were boiled for 10 minutes with periodic vortex mixing.

6.5.5 *Immunoprecipitation*

Clarified lysates in Jie's buffer were added to pre-equilibrated antibody-conjugated resin; in general a bed volume of 10 – 15 µl was used per IP together with 1 – 3 ml lysate. Immunoprecipitations were incubated overnight at 4 °C, following which beads were washed 5 – 6 times with 1 ml lysis buffer: sedimentation between washes was carried out by brief centrifugation at 2,000 *g*. After aspiration of the final wash tubes were centrifuged briefly once more to collect all remaining traces of lysis buffer. Beads were then aspirated to dryness using a fine pipette tip. Elution conditions were dependent on the next step of the experiment: for SDS-PAGE and in-gel digestion of proteins for mass spectrometric analysis, elution was directly into 30 µl 2× SDS-PAGE sample buffer followed by boiling and gentle vortex mixing. Some immunoblots also used direct elution into sample buffer. For immunoprecipitations where the presence of antibody used for immunoprecipitation on the membrane had the potential to

interfere with detection, proteins were eluted twice using 3 bed volumes glycine 100 mM, pH 2.5: glycine elutions were carried out for 5 minutes each at room temperature with gentle vortex mixing. Eluates were pooled and neutralized with 0.1 volume TrisHCl 1 M, pH 8 before the addition of SDS-PAGE sample buffer to 1×. For in-solution digestion of proteins for analysis by mass spectrometry, samples were eluted twice into 10 bed volumes NH_4OH 0.5 M, EDTA 0.5 mM. Elutions were carried out at 4 °C for 15 minutes with gentle mixing. For a full list of antibodies and affinity resins used for immunoprecipitation see Table 6.1.

For immunoprecipitation of endogenous MYPT1, 293T cells were lysed in Jie's buffer as described. F38 antibody was added (10 µg per ml cell extract) and immunoprecipitations incubated at 4 °C for 1 h with gentle mixing. Pre-equilibrated Protein A Agarose Fast Flow (Upstate Biotechnology) was added for a final bed volume of 10 – 15 µl, followed by incubation for a further 4 h at 4 °C. Beads were washed as described above and eluted in 30 µl 2× SDS-PAGE sample buffer.

6.5.6 *Cycloheximide chase*

Cycloheximide, an inhibitor of protein synthesis (Siegel and Sisler, 1963), was added to cell growth medium to a final concentration of 100 µg ml^{-1}. At the indicated time-points, cells were harvested using Jie's buffer and extracts analysed by immunoblotting.

6.5.7 *Fractionation of cells into nuclear and cytoplasmic components*

Cellular fractionation was performed essentially as described (Guillemin et al., 2005). Briefly, after washing, the cells from a 15 cm diameter dish were scraped into 1 ml CLB, transferred to a microcentrifuge tube and incubated on ice for 5 minutes. Swollen cells were transferred to a Dounce homogenizer and disrupted on ice by 30

strokes of the pestle, following which 100 µl sucrose 2.5 M was added to restore isotonicity. The extract was centrifuged at 6,300 *g* for 5 minutes at 4 °C to yield pellet 1 and supernatant 1. Supernatant 1 was decanted and centrifuged at 14,000 *g* and 4 °C for 150 minutes to yield pellet 2 and supernatant 2: pellet 2 was the fraction containing membranes and organelles, with supernatant 2 being the cytoplasmic fraction. Pellet 2 was resuspended in 100 µl 1× SDS-PAGE sample buffer, whilst supernatant 2 had SDS-PAGE sample buffer added to 1×. During the 150 minute centrifugation step, pellet 1 was resuspended in 1.5 ml TSE, transferred to a Dounce homogenizer and subjected to 20 further strokes of the pestle. This extract was sedimented by centrifugation at 4,000 *g* and 4 °C for 5 minutes, following which the supernatant was discarded. The resulting pellet was bathed (but not fully resuspended) with 1 ml aliquots of TSE until the washes became clear, following which the supernatant was removed and discarded. The remaining pellet (containing the nuclear fraction) was resuspended in 750 µl 1× SDS-PAGE sample buffer, and DNA sheared with 30 cycles of repeated aspiration and dispensing using a 21-gauge hypodermic needle. Finally, the nuclear fraction was boiled for 10 minutes with occasional vortex mixing. Nuclear, cytoplasmic and whole-cell extracts were analysed by immunoblotting: as controls for the efficiency of the fractionation, samples were probed for RNA Polymerase II (a nuclear protein) and p23 (a cytoplasmic protein).

6.6 Mass spectrometric techniques

All instruments were maintained and operated by Dr Benedikt Kessler, Dr Holger Kramer and Mrs Mariola Edelmann at the Central Proteomics Facility, University of Oxford.

6.6.1 *Digestion of protein from gel bands*

Protein digestion from gel bands used sequencing grade trypsin (Promega), sequencing grade endoproteinase LysC (Sigma) or sequencing grade endoproteinase GluC (Roche Applied Science) and was performed exactly as described (Kinter and Sherman, 2000). Briefly, Coomassie blue-stained gel bands were excised with a clean scalpel and diced into cubes of approximately 1 mm^3. Gel pieces were washed overnight in a solution containing MeOH 50% (v/v) and AcOH 5% (v/v), followed by an additional wash for 2 h the following day. After removal of the wash MeCN was added to dehydrate the gel pieces. After 5 minutes the MeCN was aspirated and gel pieces completely dried in a vacuum centrifuge (Heto). Gel pieces were rehydrated using DTT 10 mM in NH_4HCO_3 100 mM and incubated at room temperature for 30 minutes: this step reduces disulfide bonds completely to assist MS analysis. DTT solution was removed and replaced with iodoacetamide 100 mM in NH_4HCO_3 100 mM to carmabidomethylate cysteine residues and prevent re-formation of any disulfide bonds during the remaining steps of the procedure. Following aspiration of the iodoacetamide solution and an identical dehydration step gel pieces were rehydrated in NH_4HCO_3 100 mM for 10 minutes and dehydrated once more. Proteases were prepared at 20 µg ml^{-1} in NH_4HCO_3 50 mM and used to rehydrate gel pieces for 10 minutes on ice with occasional gentle vortex mixing. After removal of excess protease reagent and addition of NH_4HCO_3 50 mM, digests were incubated overnight at 37 °C. The following day peptides were eluted using a three-step procedure. Firstly NH_4HCO_3 50 mM was added and samples incubated at room temperature for 10 minutes with gentle vortex mixing. Two further elutions were carried out using MeCN 50% (v/v) and HCO_2H 5% (v/v), following which all eluates were pooled and the total volume reduced to approximately 20 µl in a vacuum centrifuge before MS analysis.

6.6.2 *Digestion of proteins in solution*

Proteins eluted from immunoprecipitations using NH_4OH were first precipitated using MeOH and $CHCl_3$. MeOH (400 µl) was added to a sample volume of 100 µl and the mixture vortex mixed vigorously. Following mixing, 100 µl $CHCl_3$ was added and samples vortex mixed once more. After addition of 300 µl MilliQ-grade water and a further vortex mixing step samples were separated by centrifugation at 14,000 *g* for 5 minutes. The top phase was discarded, taking care not to disturb the protein precipitate at the interface, following which 400 µl MeOH was added. Samples were vortex mixed and protein sedimented by centrifugation at 14,000 *g* for 3 minutes. MeOH was removed, leaving a drop to cover the pellet, following which the remaining traces of MeOH were removed using a vacuum centrifuge. Protein pellets were resuspended in 20 µl urea 6 M in TrisHCl pH 7.8 100 mM, followed by addition of 1 µl DTT 200 mM in TrisHCl pH 7.8 100 mM and incubation at room temperature for 60 minutes. Following the addition of 4 µl iodoacetamide 200 mM in TrisHCl pH 7.8 100 mM samples were vortex mixed and incubated at room temperature for a further 60 minutes. After this incubation a further 4 µl DTT 200 mM in TrisHCl pH 7.8 100 mM was added to consume any unreacted iodoacetamide, and samples left to stand at room temperature for 30 – 60 minutes. MilliQ-grade water (155 µl) was added to reduce the urea concentration, followed by the addition of 0.75 µg of the relevant sequencing-grade endoproteinase in 15 µl NH_4HCO_3 50 mM and incubation overnight at 37 °C. The following day reactions were spiked with a further 0.25 µg endoproteinase in 5 µl NH_4HCO_3 50 mM and incubated for a further 4 h at 37 °C. Reactions were stopped by addition of 1 µl neat AcOH and peptides purified using a PepClean C_{18} spin column (Pierce Biotechnology) according to the manufacturer's instructions. Following elution samples were evaporated to dryness in a vacuum

centrifuge then resuspended in 16 µl MeCN 2% (v/v), HCO_2H 0.1% (v/v)for MS analysis.

6.6.3 *LC-MS and LC-MS/MS analysis using Bruker Daltonics HCTplus ion trap instrument*

Digested protein samples were analysed as described (Batycka et al., 2006). Briefly, LC-MS and LC-MS/MS analysis was performed using an Ultimate liquid chromatography system equipped with a Famos autosampler and C_{18} PepMap column (LC Packings). The chromatography system was connected directly to a UV flow cell (Ultimate) and a 3D high-capacity ion trap mass spectrometer (HCTplus, Bruker Daltonics) *via* a pneumatically assisted nano-electrospray source. Silica-coated Picotips (New Objective) were used for electrospray ionization. Instruments were controlled using HyStar 3.0 and EsquireControl 5.2 software (Bruker Daltonics). Raw chromatography data were processed and Mascot-compatible files generated using DataAnalysis 3.2 software (Bruker Daltonics). Searches were performed using Mascot software (Matrix Science, (Perkins et al., 1999)) and the most recent releases of the SwissProt or NCBInr databases, following which MS/MS spectra and extracted ion chromatograms were analysed in detail using DataAnalysis 3.2.

6.6.4 *High-resolution LC-MS analysis using Waters QToF Premier instrument*

Digested protein samples were analysed essentially as described (Cockman et al., 2008). Briefly, nano ultra-performance liquid chromatography was performed on a nanoAcquity UPLC system (Waters) using a 75 µm I.D. x 25 cm C_{18} nanoAcquity UPLC column with 1.7 µm particle size (Waters) coupled to a quadrupole time-of-flight (QToF) Premier tandem mass spectrometer (Waters). Data for quantitation of Notch peptide hydroxylation were acquired in high-definition MS^E mode (low collision energy: 4 eV, high collision energy ramping from 15 eV to 40 eV, switching every

1.5 s). Data for analysis of SKIP and LTag digests were acquired in data-dependent analysis (DDA) mode (MS to MS/MS switching at ion precursor counts greater than 10, MS/MS collision energy dependent on precursor ion mass and charge state). The mass accuracy of the raw data was corrected using glu-fibrinopeptide ($[M + 2H]^{2+}$ = 785.8426 m/z) that was infused into the mass spectrometer as a lock mass during sample analysis. For MS/MS analysis, data were processed using MassLynx 4.1 software (Waters) and searched using Mascot software (Matrix Science (Perkins et al., 1999)) against the most recent release of the SwissProt database. MS/MS spectra were processed for deisotoping and deconvolution using MaxEnt3 (MassLynx 4.1, Waters).

6.6.5 *Stable isotope labelling of amino acids in cell culture (SILAC)*

The SILAC experiment was conducted essentially as described (Cockman et al., 2008). Isotopically-distinct populations of 293T cells were created by serial passage in lysine- and arginine-deficient DMEM (SILAC protein ID and quantitation media kit; Invitrogen) containing dialysed FCS (Invitrogen; 10% (v/v)), L-glutamine 2 mM, penicillin 50 IU ml^{-1} and streptomycin 50 µg ml^{-1} supplemented either with normal isotopic abundance ("light") L-lysine (0.68 µM) and L-arginine (0.54 µM) or with heavy isotopic forms of L-lysine ($^{13}C_6$; Cambridge Isotope Laboratories) and L-arginine ($^{13}C_6{}^{15}N_4$; Cambridge Isotope Laboratories). The "heavy" cell population was transfected with PHD3 after five doublings; the "light" cell population was not transfected but was treated with DMOG (1 mM) for 4 h before harvesting. Following harvesting and immunoprecipitation, eluted IPs were pooled and digested in solution as described in Section 6.6.2, before MS analysis using the QToF Premier instrument as described in Section 6.6.4.

6.6.6 *Quantitation of peptide hydroxylation from extracted ion chromatograms*

Analysis of Notch1 hydroxylation was carried out using the QToF Premier instrument. Chromatographic characteristics and m/z ratios for peptides containing the sites of hydroxylation in Notch1 had been determined previously by Dr Mathew Coleman and Dr Benedikt Kessler. Extracted ion chromatograms (EICs) were prepared using MassLynx 4.1 software (Waters). m/z values used were 859.4 (Asn-1945, unoxidized), 867.4 (Asn-1945, singly oxidized), 875.4 (Asn-1945, doubly oxidized), 884.75 (Asn-2012, unoxidized), 890.08 (Asn-2012, singly oxidized) and 895.40 (Asn-2012, doubly oxidized), with a tolerance of ± 0.05 Da. These masses were used to derive the expected masses of peptides from mutant proteins. For analysis of MYPT1 hydroxylation, samples were initially analysed by MS/MS using the Bruker HCTplus instrument in order to determine the m/z values and chromatographic characteristics of the peptides of interest: samples were then run in LC-MS mode and EICs generated using DataAnalysis 3.2 software (Bruker Daltonics). In both cases relative peak intensities were compared in order to determine the percentage hydroxylation at a given site.

6.7 ***In vitro*** **assays and protein synthesis**

The purified His_6-FIH used in Sections 6.7.3, 6.7.4 and 6.7.5 was a gift from Christopher Schofield's laboratory (Department of Chemistry), and prepared essentially as described except that the His_6-tag was not cleaved (Hewitson et al., 2002).

6.7.1 *Preparation of GST-tagged Notch1 ARD proteins for binding assays*

Overnight cultures of BL21 cells transformed with the indicated Notch1 ARD plasmid were back-diluted 1:25 into 50 ml LB containing ampicillin and were incubated with shaking at 37 °C until the OD_{600} reached 0.8. Cells were induced with IPTG 0.5 mM and incubated at 28 °C with shaking for a further 5 h before harvesting by centrifugation at 3,200 *g* and 4 °C for 15 minutes. Cell pellets were resuspended in 5 ml HBS and hen egg lysozyme added to a concentration of 1 mg ml^{-1} before incubation on ice for 30 minutes. Cells were sonicated on ice with a Vibra-Cell instrument (Sonics) using a microtip, with 6 cycles of 10 s on, 10 s off at an amplitude of 30%, following which cell debris was removed by centrifugation at 3,200 *g* and 4 °C for 15 minutes. Glutathione Sepharose 4 Fast Flow resin (GE Healthcare) was equilibrated in HBS and 100 µl bed volume added to clarified lysates before incubation at 4 °C for 90 minutes with mixing by gentle rotation. GST resin was sedimented by brief centrifugation at 2,000 *g* and washed twice with 1 ml HBS containing NP40 0.5% (v/v), followed by two washes with 1 ml HBS. Proteins were eluted twice with 300 µl HBS containing reduced glutathione 10 mM. Aliquots were analysed by SDS-PAGE following which proteins were dialysed overnight at 4 °C against a large excess of PBS using Slide-A-Lyzer dialysis cassettes (Pierce Biotechnology) with a 2,000 Da molecular weight cut-off. Aliquots were prepared and protein samples stored at –80 °C.

6.7.2 *Preparation of cleaved Notch1 ARD proteins for circular dichroism analysis*

Overnight cultures of BL21 cells transformed with the indicated Notch1 ARD protein were back-diluted 1:25 into 1000 ml LB containing ampicillin and were incubated with shaking at 37 °C until the OD_{600} reached 0.8. Cells were induced with IPTG 0.5 mM and incubated at 28 °C with shaking for a further 5 h before harvesting by centrifugation at 3,200 *g* and 4 °C for 15 minutes. Cell pellets were resuspended in

50 ml HBS and hen egg lysozyme added to a concentration of 1 mg ml^{-1} before incubation on ice for 30 minutes. Cells were sonicated on ice with a Vibra-Cell instrument (Sonics) using a large tip, with 10 cycles of 10 s on, 10 s off at an amplitude of 40%, following which cell debris was removed by centrifugation at 23,000 *g* and 4 °C for 20 minutes. Glutathione Sepharose 4 Fast Flow resin (GE Healthcare) was equilibrated in HBS and 1 ml bed volume added to each clarified lysate, before incubation at 4 °C for 90 minutes. Following incubation, GST resin was sedimented by brief centrifugation at 2,000 *g* followed by three washes with 10 ml PBS containing NP40 0.5% (v/v) and two washes with 10 ml PBS. Following washing beads were resuspended in 10 ml PBS and 30 U thrombin (Sigma) added before overnight digestion at 4 °C. To remove thrombin *p*-aminobenzamidine resin (Sigma) was equilibrated in PBS and 100 µl bed volumes added to each tube before incubation at 4 °C for 60 minutes: this step was repeated using fresh resin. Following *p*-aminobenzamidine clean-up, supernatants were decanted and incubated twice with 250 µl bed volumes of GST resin at 4 °C for 60 minutes to remove contaminating GST and GST-tagged ARD protein. After the final GST purification step supernatants were aspirated, analysed by SDS-PAGE, separated into aliquots and stored at –80 °C.

6.7.3 In vitro *GST pulldown assays*

Binding of Notch1 ARD mutants to FIH was assayed under native conditions using a GST pulldown assay. 1 µg each ARD protein was bound to a 10 µl bed volume of Glutathione Sepharose 4 Fast Flow by mixing in a total volume of 400 µl Jie's buffer at 4 °C for 90 minutes. After this incubation, GST resin was sedimented by brief centrifugation at 2,000 *g* and washed three times with 300 µl Jie's buffer. The beads were resuspended in 400 µl Jie's buffer of the indicated NaCl concentration containing the indicated amount of His_6-FIH, and incubated on a rotator at 4 °C for 60 minutes.

Following this second incubation beads were washed three times with 300 µl Jie's buffer containing the indicated NaCl concentration. After aspiration of all remaining traces of Jie's buffer, bound proteins were eluted in 20 µl 2× sample buffer: 2 µl aliquots of the eluate were analysed by immunoblotting to determine the amount of bound FIH using an anti-His_6-HRP-conjugated antibody (Santa Cruz Biotechnology: see Table 6.1). 10 µl aliquots of the eluate were analysed by SDS-PAGE and Coomassie-blue stained as a control for the amount of Notch ARD protein loaded onto the beads.

6.7.4 *Far-Western blotting*

The binding of Notch1 ARD mutants to FIH was analysed under denaturing conditions using a far-Western blotting assay. 200 ng each Notch1 ARD protein was resolved by SDS-PAGE and electroblotted onto PVDF membranes as described in Section 6.4.3. Instead of a primary antibody, membranes were incubated in blocking solution containing His_6-FIH (1 µg ml^{-1}) or in blocking solution alone as a control. After the usual washing steps (Section 6.4.3) bound His_6-FIH was determined by incubation with His_6-HRP-conjugated antibody and visualized by chemiluminescence using SuperSignal West Pico.

6.7.5 In vitro *kinetic assays*

The K_m and V_{max} values for hydroxylation of the Notch1 ARD by FIH were determined by quantitative mass spectrometry using *in vitro* assay conditions derived from those employed for the determination of 2OG dioxygenase activity by decarboxylation of radioactive 2OG (Hewitson et al., 2007; Sabourin and Bieber, 1982). His_6-FIH (20 nM) was incubated with the indicated concentrations of Notch1 ARD substrate at 37 °C in a reaction mix containing TrisHCl pH 7.5 50 mM, L-ascorbate 4 mM, 2OG 160 µM, iron(II) sulfate 80 µM and DTT 1 mM in a total volume of 20 µl. Reactions were

started by the addition of enzyme, incubated for the indicated length of time and stopped by the addition of 4 µl 6× sample buffer with vortex mixing. Samples were resolved by SDS-PAGE (Section 6.4.2) following which Notch1-ARD containing bands were excised, digested using trypsin and analysed by high-resolution mass spectrometry (Sections 6.6.1, 6.6.4 and 6.6.6).

6.7.6 *Circular dichroism (CD)*

CD experiments were performed using a Chirascan CD spectrometer (Applied Photophysics) equipped with a Peltier temperature controller. The apparatus was equilibrated for 1 hour prior to any commencement of measurement, in accordance with the manufacturer's instructions. Protein samples were buffered in PBS and analysed at a typical concentration of 10 µM using a cuvette with a path length of 1 mm. Protein spectra were recorded from 200 nm to 250 nm in steps of 0.5 nm, with each data point averaged over 1 s. Each spectrum was recorded three times and then averaged. Buffer-only spectra were recorded at the beginning and end of each spectrum acquisition to ensure that the measurements were consistent and no drift in signal was occurring.

Thermal melts were performed at a rate of 2 °C min^{-1} with the signal averaged over 12 s. The temperature inside the cuvette was recorded during the melt and used in subsequent data analysis. Melting experiments were performed in triplicate for each sample. After subtraction of a buffer baseline the data were smoothed and melting temperatures determined by curve-fitting using a two-state model as described (Greenfield, 2004).

6.7.7 *HIF1α CAD reporter gene assays*

For analysis of HIF1α reporter gene activity, HeLa cells were seeded at 5×10^4 per well (400 mm^2) of a 12-well tissue culture dish. The following day each well was transfected with Gal4 DBD-HIF1α CAD (25 ng), UAS.tk.Luciferase (25 ng), β-galactosidase (50 ng) and the indicated ARD plasmid (400 ng), using FuGENE®6 reagent (Section 6.5.2). Cells were transfected in triplicate. After 48 h the growth medium was aspirated and cells washed once with 2 ml ice-cold PBS per well. Following aspiration of all traces of PBS, cells were lysed by the addition of 100 µl Passive Lysis Buffer (PLB, Promega) and freezing at –80 °C for at least 15 minutes. After thawing, cells were scraped into the PLB on ice, extracts aspirated and clarified by centrifugation at 14,000 *g* and 4 °C for 5 minutes. Extracts were then assayed in parallel for luciferase and β-galactosidase activity. For determining luciferase activity, 20 µl cell extract (plus a PLB-only control) was placed in each well of a white, flat-bottomed 96-well plate. Using a Luminoskan Ascent luminometer (Labsystems) 50 µl Luciferase Assay Substrate (Promega) was added and luciferase activity measured. For the determination of β-galactosidase activity, 20 µl cell extract (plus a PLB-only control) was added to 80 µl Z buffer in each well of a clear U-bottomed 96-well plate. Following the addition of 20 µl *o*-nitrophenyl-β-D-galactopyranoside (4 mg ml^{-1}) the plate was incubated at 37 °C with shaking at 200 rpm. Once a faint yellow colour was apparent in all the wells (except the negative control), the reaction was stopped by the addition of 50 µl Na_2CO_3 1 M and the OD measured at 405 nm using a Vmax® kinetic microplate reader (Molecular Devices). Luciferase activity was corrected for transfection efficiency by dividing each luciferase reading by the respective β-galactosidase OD reading, following which the mean and standard error were calculated for each triplicate.

6.7.8 In vitro *transcription/translation of proteins (IVTT)*

Proteins were *in vitro* transcribed/translated using a TNT® T7 quick-coupled rabbit reticulocyte lysate kit (Promega). Reactions were carried out in a total volume of 25 µl containing 20 µl reticulocyte lysate master mix, 1 µl Redivue [^{35}S]-labelled methionine (GE Healthcare) and 1 µg plasmid (which was not linearized). Reactions were incubated at 30 °C for 90 minutes following which translated proteins were either used immediately or stored at –20 °C.

6.7.9 *pVHL capture assays*

Prolyl hydroxylase activity was measured essentially as described (Tuckerman et al., 2004). An N-terminal biotinylated peptide corresponding to residues 556—574 of HIF1α (biotin–DLDLEMLAPYIPMDDDFQL–OH, 'BT19', Peptide Protein Research Ltd) was used as a substrate. Transfected 293T cells were rinsed twice with ice-cold TBS, drained and scraped into the buffer remaining by surface tension. Cells were sonicated on ice (25 pulses of 1 s on, 3 s off at 25% amplitude) using a Sonics VibraCell instrument with microtip. Extracts were clarified by centrifugation at 14,000 *g* for 15 minutes. 5 µl cell extract was incubated at 37 °C with BT19 1 µM in a reaction buffer containing Tris pH 6.9 100 mM, BSA 1 mg ml^{-1}, L-ascorbate 2 mM, DTT 1 mM, catalase 0.24 mg ml^{-1}, 2OG 2 mM and $FeCl_2$ 50 µM in a total volume of 50 µl. The reaction was started by the addition of the cell extract. At the required time points a 20 µl aliquot was removed and quenched by dilution in an equal volume of ice-cold 'stop buffer', EBC buffer containing 300 µM desferrioxamine mesylate (DFO) and 200 µM EDTA. The biotinylated peptide was captured on streptavidin-conjugated magnetic beads (Dynabeads M-280 Streptavidin, Dynal Biotech) by removing a 5 µl aliquot of the stopped reaction and incubating in 'capture buffer' (EBC containing 300 µM DFO) with 2.7 × 10^6 beads on ice for 30 minutes. The reaction mixture was

then removed and the beads washed once with 500 µl capture buffer. The peptide-coated beads were incubated with an excess of [^{35}S]pVHL (produced by IVTT reaction and diluted 4-fold in capture buffer) on ice for 60 minutes. After two further washes with 750 µl capture buffer, the [^{35}S]pVHL was eluted using 10 µl 2× SDS-PAGE sample buffer and quantitated by SDS-PAGE and autoradiography using a Cyclone phosphorimager (Packard BioSystems).

6.8 Plasmids and oligonucleotide primers

6.8.1 *Oligonucleotide primers*

Oligonucleotide primers were custom synthesized by Sigma Aldrich. Full lists of oligonucleotides used for SDM, PCR amplification and DNA sequencing are given in Tables 6.3 and 6.4.

Table 6.3 ***Oligonucleotide primers for SDM***

Template	Mutation	Mutagenic primer* (5' – 3')	Annealing temp/°C
ΔmN1^{ICD}	L1937A	GCAAAGCGCGCGCTGGAGGCC	55
	L1937I	GCAAAGCGCATTCTGGAGGCC	58
	L1937K	GCAAAGCGCAAGCTGGAGGCC	58
	L1937V	GCAAAGCGCGTGCTGGAGGCC	55
	A1942F	GAGGCCAGTTTCGATGCCAAC	55
	D1943A	GCCAGTGCAGCTGCCAACATC	55
	A1944P	AGTGCAGATCCCAACATCCAG	55
	P1954A	GGCCGTACTGCGTTACATGCA	55
	P1954L	GGCCGTACTTTGTTACATGCA	55
	L1955A	GGCCGTACTCCGGCACATGCAGCAGTT	58
	A1958F	CCGTTACATGCATTTGTTTCTGCAGAT	55
	L2004A	CTGGAGGACGCCATCAACTCA	53†
	A2009F	ATCAACTCACATTTTGACGTCAATGCC	55
	D2010A	TCACATGCTGCCGTCAATGCC	58
	L2022A	AAGTCGGCTGCGCATTGGGCG	58
	A2025F	TTGCATTGGTTTGCCGCGGTG	55
	A1926G	CCTTGCACTTGGGTGCCCGATACTC	55
	A1958G	CTCCGTTACATGCAGGAGTTTCTGCAGATGC	55
	A1992G	ACTGATCCTGGGTGCGCGCCTGGCC	55
	A2025G	CTTTGCATTGGGGGGCCGCGGTGAAC	55
	A2058G	CTGTTCCTGGGCGCCCGTGAG	55
	A2091G	CGGGACATCGGACAGGAGCGT	55
	I1989H	ACTCCACTGCACCTGGCTGCG	58
	A2021P	GGCAAGTCGCCTTTGCATTGG	58
	E2051G	AACAACAAGGGGGAGACTCCC	58
MYPT1 ARD	N67A	GCCGACATCGCTTACGCCAAT	55
	N100A	GCAAATATTGCTCAACCTGAT	55
	N226A	GGCTATGATGTTGCTATTAAAGACTAT	53†

Thermal cycling conditions were as stated in Section 6.3.9.
** sense primer shown; antisense primers are the exact reverse complement in all cases*
† 100 ng template used

Table 6.4 ***Oligonucleotide primers for cloning and sequencing***

Name	Primer (5' – 3')	Restriction site	Application	Annealing temp/°C
mN1_ARD_F	CGGGATCCGTCATCTCTGACTTATCTAC	*Bam*HI	Subcloning Notch1 ARD	55
mN1_ARD_R	GGAATTCTTAGTACTCATCCAAAAGCCG	*Eco*RI	Subcloning Notch1 ARD	55
MYPT1_ARD_F	GCTAGGATCCATGAAGATGGCGGAC	*Bam*HI	Subcloning MYPT1 ARD	60
MYPT1_ARD_R	ATCGTCTAGAGTCCCGTTTTTCACT	*Xba*I	Subcloning MYPT1 ARD	60
SKIP_1F_A	TTCCGGAATTCAATGGCGCTCACCAGCTTTTTACC	*Eco*RI	Cloning (SKIP)	58
SKIP_170F_A	AACCGGAATTCAAAATTGGCTCCTGCTCAG	*Eco*RI	Cloning (SKIP)	58
SKIP_340F	AAGGGGAATTCAACTCATGTGGAAAAAGAGG	*Eco*RI	Cloning (SKIP)	58
SKIP_218R	CGGGCTCTAGACTAAATTTTCTTATTAATC	*Xba*I	Cloning (SKIP)	58
SKIP_235R	CTCTCTCTAGACTATCGGCTAGGAGAATGC	*Xba*I	Cloning (SKIP)	58
SKIP_339R_A	CTCAATCTAGACTATTTGATCCCAGCTCTTC	*Xba*I	Cloning (SKIP)	58
SKIP_ENDR	CTCTCTCTAGACTATTCCTTCCTCCTCTTC	*Xba*I	Cloning (SKIP)	58
SKIP_1F_B	TTACTACATATGGCGCTCACCAGCTTTTTACC	*Nde*I	Cloning (SKIP)	60
SKIP_353R	TTACTAGGATCCCTAATCCCTCTCACGTGCCTCC	*Bam*HI	Cloning (SKIP)	60
SKIP_150F	TTCCGGGATCCGCCTTAGAAAAATCTGTATC	*Bam*HI	Cloning (SKIP)	60
SKIP_170F_B	TTCCGGGATCCAAATTGGCTCCTGCTCAG	*Bam*HI	Cloning (SKIP)	60
SKIP_339R_B	CTCAAGTCGACCTATTTGATCCCAGCTCTTC	*Sal*I	Cloning (SKIP)	60
LTag_1F	AATGCGAATTCATGGATAAAGTTTTAAAC	*Eco*RI	Cloning (LTag)	60
LTag_118F	AATGCGAATTCATGGCTGACTCTCAACATTCT	*Eco*RI	Cloning (LTag)	60
LTag_131F	AATGCGAATTCATGAAGGTAGAAGACCCCAAG	*Eco*RI	Cloning (LTag)	60
LTag_251F	AATGCGAATTCATGGGGTTAAAGGAGCATGAT	*Eco*RI	Cloning (LTag)	60
LTag_337F	AATGCGAATTCATGTGCCAACAGGCTGTTGAT	*Eco*RI	Cloning (LTag)	60
LTag_370F	AATGCGAATTCATGGATAGGATGGATATAATG	*Eco*RI	Cloning (LTag)	60
LTag_550F	AATGCGAATTCATGAAAGATTATTTAAAGCAT	*Eco*RI	Cloning (LTag)	60
LTag_117R	AATGCCTCGAGAGTAGCCTCATCATCACT	*Xho*I	Cloning (LTag)	60
LTag_260R	AATGCCTCGAGTTCTGGATTAAAATCATG	*Xho*I	Cloning (LTag)	60
LTag_336R	AATGCCTCGAGTATGGTTTTTTGGTTTTT	*Xho*I	Cloning (LTag)	60
LTag_627R	AATGCCTCGAGATCTAAAACTCCAATTCC	*Xho*I	Cloning (LTag)	60
LTag_672R	AATGCCTCGAGCTGAAATGAGCCTTGGGA	*Xho*I	Cloning (LTag)	60
LTag_ENDR	AATGCCTCGAGTGTTTCAGGTTCAGGGGG	*Xho*I	Cloning (LTag)	60
T7F	TAATACGACTCACTATAGGG	n/a	Sequencing	50
T7R	GCTAGTTATTGCTCAGCGG	n/a	Sequencing	50
SP6	ATTTAGGTGACACTATAG	n/a	Sequencing	50
bGHR	TAGAAGGCACAGTCGAGG	n/a	Sequencing	50
pGEX5	GGGCTGGCAAGCCACGTTTGGTG	n/a	Sequencing	50
pGEX3	CCGGGAGCTGCATGTGTCAGAGG	n/a	Sequencing	50

6.8.2 *Plasmids for protein expression in mammalian cells*

pEF mN1^{ICD}

DNA sequence encoding residues 1751 – 2531 of mouse Notch1 in pEF6 with C-terminal V5 tag. From Mathew Coleman (Coleman et al., 2007).

pcDNA3 ΔmN1^{ICD}

DNA sequence encoding residues 1751 – 2191 of mouse Notch1 in pcDNA3 with C-terminal V5 tag. From Mathew Coleman (Coleman et al., 2007).

pcDNA3 ΔmN1^{ICD} point mutants

All point mutants were prepared from pcDNA3 ΔmN1^{ICD} by SDM (Section 6.3.9) using the mutagenic oligonucleotide primers and conditions shown in Table 6.3.

pEF6 FIH

Full-length human FIH in pEF6. From Mathew Coleman (Coleman et al., 2007).

pEF6 FIH D201A

Full-length human FIH with D201A point mutation in pEF6. From Mathew Coleman (Coleman et al., 2007).

pGal4DBD-HIF1α-CAD

DNA sequence encoding residues 652 – 826 of human HIF1α with an N-terminal Gal4 DNA binding domain in pGal. From Christopher Pugh (Pugh et al., 1997).

pUAS-tk-luc

Two copies of a 17-base pair Gal4 upstream activating site and the tk promoter inserted into pA3LUC. From Christopher Pugh (Pugh et al., 1997).

pEF-β-gal

Full length β-galactosidase gene cloned into pEF6. From Mathew Coleman.

pCMV6 MYPT1

Full-length human MYPT1 in pCMV6 with N-terminal myc tag. Gift from Michael Olson, University of Glasgow, UK.

pEF1/V5-His A MYPT1 ARD

The DNA sequence encoding residues 1 – 296 of human MYPT1 with a C-terminal V5-His_6 tag in pEF1/V5-His A. Amplified by PCR using MYPT1_ARD_F and MYPT1_ARD_R primers, cloned between *Bam*HI and *Xba*I restriction sites.

pEF1/V5-His A MYPT1 ARD mutants

Point mutants were prepared from pEF1/V5-His A MYPT1 ARD using the mutagenic oligonucleotide primers shown in Table 6.3.

pEF1/V5-His A AnkyrinR

This plasmid encoded residues 402 – 827 of human AnkyrinR with C-terminal V5-His_6 tag in pEF1/V5-His A. From Mathew Coleman.

pEYFP/Rabankyrin

Full-length human Rabankyrin5 with N-terminal EYFP tag in pEYFP. Gift from Marino Zerial, Max Plack Institute of Molecular Cell Biology and Genetics, Dresden, Germany (Schnatwinkel et al., 2004).

pcDNA3/RNaseL-GFP

Full-length human RNaseL with C-terminal GFP tag in pcDNA3. Gift from Catherine Bisbal, Institute of Human Genetics, Montpelier, France (Le Roy et al., 2000).

pCR3 IκBα-HA

Full-length human IκBα cloned into pCR3 with a C-terminal HA epitope tag. From Matthew Cockman (Cockman et al., 2006).

pcDNA3 HA-pVHL

Full-length human pVHL cloned into pcDNA3 with an N-terminal HA tag. From Matthew Cockman (Cockman et al., 2000).

pcDNA3 PHD3

Full-length human PHD3 in pcDNA3. From David Mole (Epstein et al., 2001).

pcDNA3 PHD3 V5

Full-length human PHD3 in pcDNA3 with a C-terminal V5 epitope. From Rebecca Appelhoff.

pcDNA3 PHD3 TAP

Full-length human PHD3 in pcDNA3 with a C-terminal TAP tag (Rigaut et al., 1999). From Matthew Cockman.

pcDNA3 PHD3 SPA

Full-length human PHD3 in pcDNA3 with a C-terminal SPA tag (Zeghouf et al., 2004). From Matthew Cockman.

pcDNA3 PHD1 SPA

Full-length human PHD1 in pcDNA3 with a C-terminal SPA tag (Zeghouf et al., 2004). From Matthew Cockman.

pcDNA3 SPA PHD2

Full-length human PHD2 in pcDNA3 with an N-terminal SPA tag (Zeghouf et al., 2004). From Matthew Cockman.

pCGN HA SKIP

Full-length human SKIP with an N-terminal HA tag in pCGN. Gift from Michael Hayman, State University of New York, Stony Brook, NY USA (Dahl et al., 1998).

pFLAG-CMV2 SKIP deletion constructs

The indicated fragments of human SKIP were amplified by PCR from pCGN HA SKIP using the appropriate oligonucleotide primers (Table 6.4; number in primer name indicates the residue at which the primer initiates/terminates, F denotes forward primer, R denotes reverse primer). PCR products were ligated into pFLAG-CMV2 (which encodes an N-terminal FLAG tag) between the *Eco*RI and *Xba*I restriction sites.

pRSV-Rev LTag

Full-length SV40 large T antigen in pRSV-Rev. From Aleksandra Watson.

pcDNA3.1(+)/myc-His A ΔSV40

*Not*I enzyme was used to digest pcDNA3.1(+)/myc-His A vector and remove the SV40 origin of replication: fragments were resolved by agarose gel electrophoresis and the large fragment re-ligated to give pcDNA3.1(+)/myc-His A ΔSV40.

pcDNA3.1(+)/myc-His A ΔSV40 LTag deletions

The indicated fragments of SV40 LTag were amplified by PCR from pRSV-Rev LTag using the appropriate oligonucleotide primers (Table 6.4; number in primer name indicates the residue at which the primer initiates/terminates, F denotes forward primer, R denotes reverse primer). PCR products were ligated into pcDNA3.1(+)/myc-His A ΔSV40 (which encodes a C-terminal myc/His_6 tag) between the *Eco*RI and *Xho*I restriction sites.

6.8.3 *Plasmids for protein expression in bacteria*

pGEX-4T-1 mN1 ARD constructs

These plasmids encoded residues 1898 – 2105 of mouse Notch1. The wild-type plasmid was from Mathew Coleman (Coleman et al., 2007). The mutant ARD constructs were amplified from the respective pcDNA3 ΔmN1^{ICD} plasmids using mN1_ARD_F and mN1_ARD_R oligonucleotide primers (Table 6.4) by PCR and ligated into pGEX-4T-1 (which encodes an N-terminal GST tag) between the *Bam*HI and *Eco*RI restriction sites.

pET28a(+) FIH

Full-length human FIH, cloned into pET28a(+) (which encodes an N-terminal His_6-tag) between the *Nde*I and *Bam*HI restriction sites. Gift from Kirsty Hewitson (Hewitson et al., 2002).

pET28a(+) SKIP 1 – 353

The DNA sequence encoding residues 1 – 353 of human SKIP was amplified by PCR from pCGN HA SKIP using primers SKIP_1F_B and SKIP_353R (Table 6.4), and ligated between the *Nde*I and *Bam*HI restriction sites in pET28a(+).

pGEX-4T-1 SKIP 150 – 339

The DNA sequence encoding residues 150 – 339 of human SKIP was amplified by PCR from pCGN HA SKIP using primers SKIP_150F and SKIP_339R_B (Table 6.4), and ligated between the *Bam*HI and *Sal*I restriction sites in pGEX-4T-1.

pGEX-4T-1 SKIP 170 – 339

The DNA sequence encoding residues 170 – 330 of human SKIP was amplified by PCR from pCGN HA SKIP using primers SKIP_170F and SKIP_339R_B (Table 6.4), and ligated between the *Bam*HI and *Sal*I restriction sites in pGEX-4T-1.

pGEX-4T-1 LTag 251 – 627

The DNA fragment encoding residues 251 – 627 of LTag was subcloned directly from pcDNA3.1/myc-His A ΔSV40 LTag 251 – 627 into pGEX-4T-1 using a *Eco*RI/*Xho*I restriction digest.

Chapter 7
Bibliography

Alberts, B., Johnson, A., Lewis, J., Raff, M., Roberts, K., and Walter, P. (2002). Molecular Biology of the Cell, 4th edn (New York, Garland Science).

Alessi, D., MacDougall, L.K., Sola, M.M., Ikebe, M., and Cohen, P. (1992). The control of protein phosphatase-1 by targetting subunits. Eur J Biochem *210*, 1023-1035.

Annunen, P., Autio-Harmainen, H., and Kivirikko, K.I. (1998). The Novel Type II Prolyl 4-Hydroxylase Is the Main Enzyme Form in Chondrocytes and Capillary Endothelial Cells, whereas the Type I Enzyme Predominates in Most Cells. J Biol Chem *273*, 5989-5992.

Annunen, P., Helaakoski, T., Myllyharju, J., Veijola, J., Pihlajaniemi, T., and Kivirikko, K.I. (1997). Cloning of the Human Prolyl 4-Hydroxylase α Subunit Isoform α(II) and Characterization of the Type II Enzyme Tetramer. The α(I) and α(II) subunits do not form a mixed α(I)α(II)β_2 tetramer. J Biol Chem *272*, 17342-17348.

Appelhoff, R.J., Tian, Y.M., Raval, R.R., Turley, H., Harris, A.L., Pugh, C.W., Ratcliffe, P.J., and Gleadle, J.M. (2004). Differential function of the prolyl hydroxylases PHD1, PHD2, and PHD3 in the regulation of hypoxia-inducible factor. J Biol Chem *279*, 38458-38465.

Arimura, T., Suematsu, N., Zhou, Y.-B., Nishimura, J., Satoh, S., Takeshita, A., Kanaide, H., and Kimura, A. (2001). Identification, Characterization, and Functional Analysis of Heart-specific Myosin Light Chain Phosphatase Small Subunit. J Biol Chem *276*, 6073-6082.

Arnesen, T., Kong, X., Evjenth, R., Gromyko, D., Varhaug, J.E., Lin, Z., Sang, N., Caro, J., and Lillehaug, J.R. (2005). Interaction between HIF-1α (ODD) and hARD1 does not induce acetylation and destabilization of HIF-1α. FEBS Lett *579*, 6428-6432.

Artavanis-Tsakonas, S., Rand, M.D., and Lake, R.J. (1999). Notch Signaling: Cell Fate Control and Signal Integration in Development. Science *284*, 770-776.

Bae, S.H., Jeong, J.W., Park, J.A., Kim, S.H., Bae, M.K., Choi, S.J., and Kim, K.W. (2004). Sumoylation increases HIF-1α stability and its transcriptional activity. Biochem Biophys Res Commun *324*, 394-400.

Baek, J.H., Mahon, P.C., Oh, J., Kelly, B., Krishnamachary, B., Pearson, M., Chan, D.A., Giaccia, A.J., and Semenza, G.L. (2005). OS-9 interacts with hypoxia-inducible factor 1α and prolyl hydroxylases to promote oxygen-dependent degradation of HIF-1α. Mol Cell *17*, 503-512.

Bannister, A.J., and Kouzarides, T. (1996). The CBP co-activator is a histone acetyltransferase. Nature *384*, 641-643.

Barnes, A.M., Chang, W., Morello, R., Cabral, W.A., Weis, M., Eyre, D.R., Leikin, S., Makareeva, E., Kuznetsova, N., Uveges, T.E., *et al.* (2006). Deficiency of Cartilage-Associated Protein in Recessive Lethal Osteogenesis Imperfecta. N Engl J Med *355*, 2757-2764.

Barrick, D., Ferreiro, D.U., and Komives, E.A. (2008). Folding landscapes of ankyrin repeat proteins: experiments meet theory. Curr Opin Struct Biol *18*, 27-34.

Barth, S., Nesper, J., Hasgall, P.A., Wirthner, R., Nytko, K.J., Edlich, F., Katschinski, D.M., Stiehl, D.P., Wenger, R.H., and Camenisch, G. (2007). The Peptidyl Prolyl *cis/trans* Isomerase FKBP38 Determines Hypoxia-Inducible Transcription Factor Prolyl-4-Hydroxylase PHD2 Protein Stability. Mol Cell Biol *27*, 3758-3768.

Batycka, M., Inglis, N.F., Cook, K., Adam, A., Fraser-Pitt, D., Smith, D.G.E., Main, L., Lubben, A., and Kessler, B.M. (2006). Ultra-fast tandem mass spectrometry scanning combined with monolithic column liquid chromatography increases throughput in proteomic analysis. Rapid Commun Mass Spectrom *20*, 2074-2080.

Berra, E., Benizri, E., Ginouvès, A., Volmat, V., Roux, D., and Pouysségur, J. (2003). HIF prolyl-hydroxylase 2 is the key oxygen sensor setting low steady-state levels of HIF-1α in normoxia. EMBO J *22*, 4082-4090.

Berta, M.A., Mazure, N., Hattab, M., Pouysségur, J., and Brahimi-Horn, M.C. (2007). SUMOylation of hypoxia-inducible factor-1α reduces its transcriptional activity. Biochem Biophys Res Commun *360*, 646-652.

Bilton, R., Mazure, N., Trottier, E., Hattab, M., Déry, M.-A., Richard, D.E., Pouysségur, J., and Brahimi-Horn, M.C. (2005). Arrest-defective-1 Protein, an Acetyltransferase, Does Not Alter Stability of Hypoxia-inducible Factor (HIF)-1α and Is Not Induced by Hypoxia or HIF. J Biol Chem *280*, 31132-31140.

Bishop, T., Gallagher, D., Pascual, A., Lygate, C.A., de Bono, J.P., Nicholls, L.G., Ortega-Saenz, P., Oster, H., Wijeyekoon, B., Sutherland, A.I., *et al.* (2008). Abnormal Sympathoadrenal Development and Systemic Hypotension in *PHD3*$^{-/-}$ Mice. Mol Cell Biol *28*, 3386-3400.

Bishop, T., Lau, K.W., Epstein, A.C.R., Kim, S.K., Jiang, M., Rourke, D., Pugh, C.W., Gleadle, J.M., Taylor, M.S., Hodgkin, J., *et al.* (2004). Genetic Analysis of Pathways Regulated by the von Hippel-Lindau Tumor Suppressor in *Caenorhabditis elegans*. PLoS Biol *2*, e289.

Bracken, C.P., Fedele, A.O., Linke, S., Balrak, W., Lisy, K., Whitelaw, M.L., and Peet, D.J. (2006). Cell-specific regulation of hypoxia-inducible factor (HIF)-1α and HIF-2α stabilization and transactivation in a graded oxygen environment. J Biol Chem *281*, 22575-22585.

Bracken, C.P., Whitelaw, M.L., and Peet, D.J. (2003). The hypoxia-inducible factors: key transcriptional regulators of hypoxic responses. Cell Mol Life Sci *60*, 1376-1393.

Bradley, C.M., and Barrick, D. (2002). Limits of cooperativity in a structurally modular protein: response of the Notch ankyrin domain to analagous alanine substitutions in each repeat. J Mol Biol *324*, 373-386.

Bray, S.J. (2006). Notch signalling: a simple pathway becomes complex. Nat Rev Mol Cell Biol *7*, 678-689.

Brou, C., Logeat, F., Gupta, N., Bessia, C., LeBail, O., Doedens, J.R., Cumano, A., Roux, P., Black, R.A., and Israël, A. (2000). A novel proteolytic cleavage involved in Notch signaling: the role of the disintegrin-metalloprotease TACE. Mol Cell *5*, 207-216.

Bruick, R.K., and McKnight, S.L. (2001). A conserved family of prolyl-4-hydroxylases that modify HIF. Science *294*, 1337-1340.

Cabral, W.A., Chang, W., Barnes, A.M., Weis, M., Scott, M.A., Leikin, S., Makareeva, E., Kuznetsova, N.V., Rosenbaum, K.N., Tifft, C.J., *et al.* (2007). Prolyl 3-hydroxylase 1 deficiency causes a recessive metabolic bone disorder resembling lethal/severe osteogenesis imperfecta. Nat Genet *39*, 359-365.

Cantarini, M.C., de la Monte, S.M., Pang, M., Tong, M., D'Errico, A., Trevisani, F., and Wands, J.R. (2006). Aspartyl-asparagyl β hydroxylase over-expression in human hepatoma is linked to activation of insulin-like growth factor and notch signaling mechanisms. Hepatology *44*, 446-457.

Cao, W., Mattagajasingh, S.N., Xu, H., Kim, K., Fierlbeck, W., Deng, J., Lowenstein, C.J., and Ballermann, B.J. (2002). TIMAP, a novel CAAX box protein regulated by TGF-β 1 and expressed in endothelial cells. Am J Physiol Cell Physiol *283*, C327-337.

Carbia-Nagashima, A., Gerez, J., Perez-Castro, C., Paez-Pereda, M., Silberstein, S., Stalla, G.K., Holsboer, F., and Arzt, E. (2007). RSUME, a small RWD-containing protein, enhances SUMO conjugation and stabilizes HIF-1α during hypoxia. Cell *131*, 309-323.

Cash, T.P., Pan, Y., and Simon, M.C. (2007). Reactive oxygen species and cellular oxygen sensing. Free Radic Biol Med *43*, 1219-1225.

Chang, B., Chen, Y., Zhao, Y., and Bruick, R.K. (2007). JMJD6 Is a Histone Arginine Demethylase. Science *318*, 444-447.

Cheng, J., Kang, X., Zhang, S., and Yeh, E.T. (2007). SUMO-specific protease 1 is essential for stabilization of HIF1α during hypoxia. Cell *131*, 584-595.

Clifton, I.J., McDonough, M.A., Ehrismann, D., Kershaw, N.J., Granatino, N., and Schofield, C.J. (2006). Structural studies on 2-oxoglutarate oxygenases and related double-stranded β-helix fold proteins. J Inorg Biochem *100*, 644-669.

Cockman, M.E., Lancaster, D.E., Stolze, I.P., Hewitson, K.S., McDonough, M.A., Coleman, M.L., Coles, C.H., Yu, X., Hay, R.T., Ley, S.C., *et al.* (2006). Posttranslational hydroxylation of ankyrin repeats in IκB proteins by the hypoxia-inducible factor (HIF) asparaginyl hydroxylase, factor inhibiting HIF (FIH). Proc Natl Acad Sci U S A *103*, 14767-14772.

Cockman, M.E., Masson, N., Mole, D.R., Jaakkola, P., Chang, G.W., Clifford, S.C., Maher, E.R., Pugh, C.W., Ratcliffe, P.J., and Maxwell, P.H. (2000). Hypoxia inducible factor-α binding and ubiquitylation by the von Hippel-Lindau tumor suppressor protein. J Biol Chem *275*, 25733-25741.

Cockman, M.E., Webb, J.D., Kramer, H.B., Ratcliffe, P.J., and Kessler, B.M. (2008). Proteomic-based identification of novel Factor Inhibiting HIF (FIH) substrates indicates widespread asparaginyl hydroxylation of ankyrin repeat domain-containing proteins. Mol Cell Proteomics *In review*.

Coleman, M.L., McDonough, M.A., Hewitson, K.S., Coles, C., Mecinovic, J., Edelmann, M., Cook, K.M., Cockman, M.E., Lancaster, D.E., Kessler, B.M., *et al.* (2007). Asparaginyl Hydroxylation of the Notch Ankyrin Repeat Domain by Factor Inhibiting Hypoxia-inducible Factor. J Biol Chem *282*, 24027-24038.

Coleman, M.L., and Ratcliffe, P.J. (2007). Oxygen sensing and hypoxia-induced responses. Essays Biochem *043*, 1-16.

Compernolle, V., Brusselmans, K., Acker, T., Hoet, P., Tjwa, M., Beck, H., Plaisance, S., Dor, Y., Keshet, E., Lupu, F., *et al.* (2002). Loss of HIF-2α and inhibition of VEGF impair fetal lung maturation, whereas treatment with VEGF prevents fatal respiratory distress in premature mice. Nat Med *8*, 702-710.

Costas, M., Mehn, M.P., Jensen, M.P., and Que, L. (2004). Dioxygen activation at mononuclear nonheme iron active sites: Enzymes, models, and intermediates. Chem Rev *104*, 939-986.

Cummins, E.P., Berra, E., Comerford, K.M., Ginouvès, A., Fitzgerald, K.T., Seeballuck, F., Godson, C., Nielsen, J.E., Moynagh, P., Pouysségur, J., *et al.* (2006). Prolyl hydroxylase-1 negatively regulates IκB kinase-β, giving insight into hypoxia-induced NFκB activity. Proc Natl Acad Sci U S A *103*, 18154-18159.

Dahl, R., Wani, B., and Hayman, M.J. (1998). The ski oncoprotein interacts with Skip, the human homolog of Drosophila Bx42. Oncogene *16*, 1579-1586.

Dames, S.A., Martinez-Yamout, M., De Guzman, R.N., Dyson, H.J., and Wright, P.E. (2002). Structural basis for HIF-1α/CBP recognition in the cellular hypoxic response. Proc Natl Acad Sci U S A *99*, 5271-5276.

Dayan, F., Roux, D., Brahimi-Horn, M.C., Pouysségur, J., and Mazure, N.M. (2006). The oxygen sensor factor-inhibiting hypoxia-inducible factor-1 controls expression of distinct genes through the bifunctional transcriptional character of hypoxia-inducible factor-1α. Cancer Res *66*, 3688-3698.

Diez, H., Fischer, A., Winkler, A., Hu, C.-J., Hatzopoulos, A.K., Breier, G., and Gessler, M. (2007). Hypoxia-mediated activation of Dll4-Notch-Hey2 signaling in endothelial progenitor cells and adoption of arterial cell fate. Exp Cell Res *313*, 1-9.

Dinchuk, J.E., Focht, R.J., Kelley, J.A., Henderson, N.L., Zolotarjova, N.I., Wynn, R., Neff, N.T., Link, J., Huber, R.M., Burn, T.C., *et al.* (2002). Absence of Post-translational Aspartyl β-Hydroxylation of Epidermal Growth Factor Domains in Mice Leads to Developmental Defects and an Increased Incidence of Intestinal Neoplasia. J Biol Chem *277*, 12970-12977.

Dobbelstein, M., and Roth, J. (1998). The large T antigen of *simian virus 40* binds and inactivates p53 but not p73. J Gen Virol *79*, 3079-3083.

Duncan, T., Trewick, S.C., Koivisto, P., Bates, P.A., Lindahl, T., and Sedgwick, B. (2002). Reversal of DNA alkylation damage by two human dioxygenases. Proc Natl Acad Sci U S A *99*, 16660-16665.

Dupuy, D., Aubert, I., Dupérat, V.G., Petit, J., Taine, L., Stef, M., Bloch, B., and Arveiler, B. (2000). Mapping, characterization, and expression analysis of the SM-20 human homologue, C1orf12, and identification of a novel related gene, SCAND2. Genomics *69*, 348-354.

Ebert, P.S., and Prockop, D.J. (1962). The hydroxylation of proline to hydroxyproline during the synthesis of collagen in chick embryos. Biochem Biophys Res Commun *8*, 305-309.

Ehrismann, D., Flashman, E., Genn, D.N., Mathioudakis, N., Hewitson, K.S., Ratcliffe, P.J., and Schofield, C.J. (2007). Studies on the activity of the hypoxia-inducible-factor hydroxylases using an oxygen consumption assay. Biochem J *401*, 227-234.

Elkins, J.M., Hewitson, K.S., McNeill, L.A., Seibel, J.F., Schlemminger, I., Pugh, C.W., Ratcliffe, P.J., and Schofield, C.J. (2003). Structure of Factor-inhibiting Hypoxia-inducible Factor (HIF) Reveals Mechanism of Oxidative Modification of HIF-1α. J Biol Chem *278*, 1802-1806.

Elvidge, G.P., Glenny, L., Appelhoff, R.J., Ratcliffe, P.J., Ragoussis, J., and Gleadle, J.M. (2006). Concordant regulation of gene expression by hypoxia and 2-oxoglutarate-dependent dioxygenase inhibition: the role of HIF-1α, HIF-2α, and other pathways. J Biol Chem *281*, 15215-15226.

Ema, M., Taya, S., Yokotani, N., Sogawa, K., Matsuda, Y., and Fujii-Kuriyama, Y. (1997). A novel bHLH-PAS factor with close sequence similarity to hypoxia-inducible factor 1α regulates the VEGF expression and is potentially involved in lung and vascular development. Proc Natl Acad Sci U S A *94*, 4273-4278.

Endo, T., and Nadal-Ginard, B. (1998). Reversal of myogenic terminal differentiation by SV40 large T antigen results in mitosis and apoptosis. J Cell Sci *111*, 1081-1093.

Epstein, A.C., Gleadle, J.M., McNeill, L.A., Hewitson, K.S., O'Rourke, J., Mole, D.R., Mukherji, M., Metzen, E., Wilson, M.I., Dhanda, A.*, et al.* (2001). *C. elegans* EGL-9 and mammalian homologs define a family of dioxygenases that regulate HIF by prolyl hydroxylation. Cell *107*, 43-54.

Erslev, A. (1953). Humoral regulation of red cell production. Blood *8*, 349-357.

Ewing, N.P., Zhang, X., and Cassady, C.J. (1996). Determination of the Gas-Phase Basicities of Proline and its Di- and Tripeptides with Glycine: The Enhanced Basicity of Prolylproline. J Mass Spectrom *31*, 1345-1350.

Falnes, P.Ø., Johansen, R.F., and Seeberg, E. (2002). AlkB-mediated oxidative demethylation reverses DNA damage in *Escherichia coli*. Nature *419*, 178-182.

Fanning, E., and Knippers, R. (1992). Structure and Function of *Simian Virus 40* Large Tumor Antigen. Annu Rev Biochem *61*, 55-85.

Feng, J., Ito, M., Ichikawa, K., Isaka, N., Nishikawa, M., Hartshorne, D.J., and Nakano, T. (1999). Inhibitory Phosphorylation Site for Rho-associated Kinase on Smooth Muscle Myosin Phosphatase. J Biol Chem *274*, 37385-37390.

Ferguson, J.E., III, Wu, Y., Smith, K., Charles, P., Powers, K., Wang, H., and Patterson, C. (2007). ASB4 Is a Hydroxylation Substrate of FIH and Promotes Vascular Differentiation via an Oxygen-Dependent Mechanism. Mol Cell Biol *27*, 6407-6419.

Ferreiro, D.U., Cervantes, C.F., Truhlar, S.M.E., Cho, S.S., Wolynes, P.G., and Komives, E.A. (2007). Stabilizing IκBα by "Consensus" Design. J Mol Biol *365*, 1201-1216.

Folk, P., Půta, F., Krpejsová, L., Blahusková, A., Markos, A., Rabino, M., and Dottin, R.P. (1996). The homolog of chromatin binding protein Bx42 identified in *Dictyostelium*. Gene *181*, 229-231.

Folk, P., Půta, F., and Skružný, M. (2004). Transcriptional coregulator SNW/SKIP: the concealed tie of dissimilar pathways. Cell Mol Life Sci *61*, 629-640.

Frei, C., and Edgar, B.A. (2004). *Drosophila* Cyclin D/Cdk4 Requires HIF-1 Prolyl Hydroxylase to Drive Cell Growth. Dev Cell *6*, 241-251.

Fujioka, M., Takahashi, N., Odai, H., Araki, S., Ichikawa, K., Feng, J., Nakamura, M., Kaibuchi, K., Hartshorne, D.J., Nakano, T.*, et al.* (1998). A New Isoform of Human Myosin Phosphatase Targeting/Regulatory Subunit (MYPT2): cDNA Cloning, Tissue Expression, and Chromosomal Mapping. Genomics *49*, 59-68.

Fukuba, H., Takahashi, T., Jin, H.G., Kohriyama, T., and Matsumoto, M. (2008). Abundance of aspargynyl-hydroxylase FIH is regulated by Siah-1 under normoxic conditions. Neurosci Lett *433*, 209-214.

Fukuba, H., Yamashita, H., Nagano, Y., Jin, H.G., Hiji, M., Ohtsuki, T., Takahashi, T., Kohriyama, T., and Matsumoto, M. (2007). Siah-1 facilitates ubiquitination and degradation of factor inhibiting HIF-1α (FIH). Biochem Biophys Res Commun *353*, 324-329.

Gavin, A.-C., Bosche, M., Krause, R., Grandi, P., Marzioch, M., Bauer, A., Schultz, J., Rick, J.M., Michon, A.-M., Cruciat, C.-M.*, et al.* (2002). Functional organization of the yeast proteome by systematic analysis of protein complexes. Nature *415*, 141-147.

Gerken, T., Girard, C.A., Tung, Y.-C.L., Webby, C.J., Saudek, V., Hewitson, K.S., Yeo, G.S.H., McDonough, M.A., Cunliffe, S., McNeill, L.A.*, et al.* (2007). The Obesity-Associated *FTO* Gene Encodes a 2-Oxoglutarate-Dependent Nucleic Acid Demethylase. Science *318*, 1469-1472.

Gingras, A.-C., Aebersold, R., and Raught, B. (2005). Advances in protein complex analysis using mass spectrometry. J Physiol *563*, 11-21.

Gingras, A.-C., Gstaiger, M., Raught, B., and Aebersold, R. (2007). Analysis of protein complexes using mass spectrometry. Nat Rev Mol Cell Biol *8*, 645-654.

Glorieux, F.H. (2008). Osteogenesis imperfecta. Best Pract Res Clin Rheumatol *22*, 85-100.

Goldberg, M.A., Dunning, S.P., and Bunn, H.F. (1988). Regulation of the erythropoietin gene: evidence that the oxygen sensor is a heme protein. Science *242*, 1412-1415.

Goldberg, M.A., Glass, G.A., Cunningham, J.M., and Bunn, H.F. (1987). The regulated expression of erythropoietin by two human hepatoma cell lines. Proc Natl Acad Sci U S A *84*, 7972-7976.

Gordan, J.D., Bertout, J.A., Hu, C.-J., Diehl, J.A., and Simon, M.C. (2007a). HIF-2α Promotes Hypoxic Cell Proliferation by Enhancing c-Myc Transcriptional Activity. Cancer Cell *11*, 335-347.

Gordan, J.D., Thompson, C.B., and Simon, M.C. (2007b). HIF and c-Myc: Sibling Rivals for Control of Cancer Cell Metabolism and Proliferation. Cancer Cell *12*, 108-113.

Gradin, K., Takasaki, C., Fujii-Kuriyama, Y., and Sogawa, K. (2002). The transcriptional activation function of the HIF-like factor requires phosphorylation at a conserved threonine. J Biol Chem *277*, 23508-23514.

Greenfield, N.J. (2004). Analysis of Circular Dichroism Data. Methods Enzymol *383*, 282-317.

Grewal, R.N., El Aribi, H., Harrison, A.G., Siu, K.W.M., and Hopkinson, A.C. (2004). Fragmentation of Protonated Tripeptides: The Proline Effect Revisited. J Phys Chem B *108*, 4899-4908.

Gronke, R.S., VanDusen, W.J., Garsky, V.M., Jacobs, J.W., Sardana, M.K., Stern, A.M., and Friedman, P.A. (1989). Aspartyl β-hydroxylase: *in vitro* hydroxylation of a synthetic peptide based on the structure of the first growth factor-like domain of human factor IX. Proc Natl Acad Sci U S A *86*, 3609-3613.

Gronke, R.S., Welsch, D.J., VanDusen, W.J., Garsky, V.M., Sardana, M.K., Stern, A.M., and Friedman, P.A. (1990). Partial purification and characterization of bovine liver aspartyl β-hydroxylase. J Biol Chem *265*, 8558-8565.

Gu, Y.Z., Moran, S.M., Hogenesch, J.B., Wartman, L., and Bradfield, C.A. (1998). Molecular characterization and chromosomal localization of a third α-class hypoxia inducible factor subunit, HIF3α. Gene Expr *7*, 205-213.

Guillemin, I., Becker, M., Ociepka, K., Friauf, E., and Nothwang, H.G. (2005). A subcellular prefractionation protocol for minute amounts of mammalian cell cultures and tissue. Protemics *5*, 35-45.

Gundogan, F., Elwood, G., Greco, D., Rubin, L.P., Pinar, H., Carlson, R.I., Wands, J.R., and de la Monte, S.M. (2007). Role of aspartyl-(asparaginyl) β-hydroxylase in placental implantation: relevance to early pregnancy loss. Hum Pathol *38*, 50-59.

Gustafsson, M.V., Zheng, X., Pereira, T., Gradin, K., Jin, S., Lundkvist, J., Ruas, J.L., Poellinger, L., Lendahl, U., and Bondesson, M. (2005). Hypoxia Requires Notch Signaling to Maintain the Undifferentiated Cell State. Dev Cell *9*, 617-628.

Hautala, T., Byers, M.G., Eddy, R.L., Shows, T.B., Kivirikko, K.I., and Myllylä, R. (1992). Cloning of human lysyl hydroxylase: Complete cDNA-derived amino acid sequence and assignment of the gene (PLOD) to chromosome 1p36.3→p36.2. Genomics *13*, 62-69.

Heidbreder, M., Frohlich, F., Johren, O., Dendorfer, A., Qadri, F., and Dominiak, P. (2003). Hypoxia rapidly activates HIF-3α mRNA expression. FASEB J *17*, 1541-1543.

Heikkinen, J., Risteli, M., Wang, C., Latvala, J., Rossi, M., Valtavaara, M., and Myllylä, R. (2000). Lysyl Hydroxylase 3 Is a Multifunctional Protein Possessing Collagen Glucosyltransferase Activity. J Biol Chem *275*, 36158-36163.

Helaakoski, T., Vuori, K., Myllylä, R., Kivirikko, K.I., and Pihlajaniemi, T. (1989). Molecular cloning of the α-subunit of human prolyl 4-hydroxylase: the complete cDNA-derived amino acid sequence and evidence for alternative splicing of RNA transcripts. Proc Natl Acad Sci U S A *86*, 4392-4396.

Hernan, R., Heuermann, K., and Brizzard, B. (2000). Multiple Epitope Tagging of Expressed Proteins for Enhanced Detection. BioTechniques *20*, 789-793.

Hershko, A., and Ciechanover, A. (1998). The ubiquitin system. Annu Rev Biochem *67*, 425-479.

Hewitson, K.S., McNeill, L.A., Riordan, M.V., Tian, Y.-M., Bullock, A.N., Welford, R.W., Elkins, J.M., Oldham, N.J., Bhattacharya, S., Gleadle, J.M.*, et al.* (2002). Hypoxia-inducible Factor (HIF) Asparagine Hydroxylase Is Identical to Factor Inhibiting HIF (FIH) and Is Related to the Cupin Structural Family. J Biol Chem *277*, 26351-26355.

Hewitson, K.S., Schofield, C.J., and Ratcliffe, P.J. (2007). Hypoxia-Inducible Factor Prolyl-Hydroxylase: Purification and Assays of PHD2. Methods Enzymol *435*, 25-42.

Hirano, K., Phan, B.C., and Hartshorne, D.J. (1997). Interactions of the Subunits of Smooth Muscle Myosin Phosphatase. J Biol Chem *272*, 3683-3688.

Hirose, K., Morita, M., Ema, M., Mimura, J., Hamada, H., Fujii, H., Saijo, Y., Gotoh, O., Sogawa, K., and Fujii-Kuriyama, Y. (1996). cDNA cloning and tissue-specific expression of a novel basic helix-loop-helix/PAS factor (Arnt2) with close sequence similarity to the aryl hydrocarbon receptor nuclear translocator (Arnt). Mol Cell Biol *16*, 1706-1713.

Hirsilä, M., Koivunen, P., Günzler, V., Kivirikko, K.I., and Myllyharju, J. (2003). Characterization of the human prolyl 4-hydroxylases that modify the hypoxia-inducible factor. J Biol Chem *278*, 30772-30780.

Hoffman, E.C., Reyes, H., Chu, F.F., Sander, F., Conley, L.H., Brooks, B.A., and Hankinson, O. (1991). Cloning of a factor required for activity of the Ah (dioxin) receptor. Science *252*, 954-958.

Hogenesch, J.B., Gu, Y.Z., Jain, S., and Bradfield, C.A. (1998). The basic-helix-loop-helix-PAS orphan MOP3 forms transcriptionally active complexes with circadian and hypoxia factors. Proc Natl Acad Sci U S A *95*, 5474-5479.

Hogenesch, J.B., Gu, Y.Z., Moran, S.M., Shimomura, K., Radcliffe, L.A., Takahashi, J.S., and Bradfield, C.A. (2000). The basic helix-loop-helix-PAS protein MOP9 is a brain-specific heterodimeric partner of circadian and hypoxia factors. J Neurosci *20*, RC83.

Holster, T., Pakkanen, O., Soininen, R., Sormunen, R., Nokelainen, M., Kivirikko, K.I., and Myllyharju, J. (2007). Loss of Assembly of the Main Basement Membrane Collagen, Type IV, but Not Fibril-forming Collagens and Embryonic Death in Collagen Prolyl 4-Hydroxylase I Null Mice. J Biol Chem *282*, 2512-2519.

Hu, C.-J., Sataur, A., Wang, L., Chen, H., and Simon, M.C. (2007). The N-Terminal Transactivation Domain Confers Target Gene Specificity of Hypoxia-inducible Factors HIF-1α and HIF-2α. Mol Biol Cell *18*, 4528-4542.

Hu, C.J., Wang, L.Y., Chodosh, L.A., Keith, B., and Simon, M.C. (2003). Differential roles of hypoxia-inducible factor 1α (HIF-1α) and HIF-2α in hypoxic gene regulation. Mol Cell Biol *23*, 9361-9374.

Huang, J., Zhao, Q., Mooney, S.M., and Lee, F.S. (2002). Sequence Determinants in Hypoxia-inducible Factor-1α for Hydroxylation by the Prolyl Hydroxylases PHD1, PHD2, and PHD3. J Biol Chem *277*, 39792-39800.

Hulse, J.D., Ellis, S.R., and Henderson, L.M. (1978). Carnitine biosynthesis. β-Hydroxylation of trimethyllysine by an α-ketoglutarate-dependent mitochondrial dioxygenase. J Biol Chem *253*, 1654-1659.

Hutton, J.J., Kaplan, A., and Udenfriend, S. (1967a). Conversion of the amino acid sequence Gly-Pro-Pro in protein to Gly-Pro-Hyp by collagen proline hydroxylase. Arch Biochem Biophys *121*, 384-391.

Hutton, J.J., Tappel, A.L., and Udenfriend, S. (1967b). Cofactor and substrate requirements of collagen proline hydroxylase. Arch Biochem Biophys *118*, 231-240.

Ikeda, M., and Nomura, M. (1997). cDNA cloning and tissue-specific expression of a novel basic helix-loop-helix/PAS protein (BMAL1) and identification of alternatively spliced variants with alternative translation initiation site usage. Biochem Biophys Res Commun *233*, 258-264.

Isaacs, J.S., Jung, Y.J., Mole, D.R., Lee, S., Torres-Cabala, C., Chung, Y.-L., Merino, M., Trepel, J., Zbar, B., Toro, J.*, et al.* (2005). HIF overexpression correlates with biallelic loss of fumarate hydratase in renal cancer: Novel role of fumarate in regulation of HIF stability. Cancer Cell *8*, 143-153.

Ito, M., Nakano, T., Erdődi, F., and Hartshorne, D.J. (2004). Myosin phosphatase: structure, regulation and function. Mol Cell Biochem *259*, 197-209.

Ivan, M., Kondo, K., Yang, H., Kim, W., Valiando, J., Ohh, M., Salic, A., Asara, J.M., Lane, W.S., and Kaelin, W.G., Jr. (2001). HIFα targeted for VHL-mediated destruction by proline hydroxylation: implications for O_2 sensing. Science *292*, 464-468.

Iwai, K., Yamanaka, K., Kamura, T., Minato, N., Conaway, R.C., Conaway, J.W., Klausner, R.D., and Pause, A. (1999). Identification of the von Hippel-Lindau tumor-suppressor protein as part of an active E3 ubiquitin ligase complex. Proc Natl Acad Sci U S A *96*, 12436-12441.

Iyer, N.V., Kotch, L.E., Agani, F., Leung, S.W., Laughner, E., Wenger, R.H., Gassmann, M., Gearhart, J.D., Lawler, A.M., Yu, A.Y.*, et al.* (1998). Cellular and developmental control of O_2 homeostasis by hypoxia-inducible factor1α. Genes Dev *12*, 149-162.

Jaakkola, P., Mole, D.R., Tian, Y.M., Wilson, M.I., Gielbert, J., Gaskell, S.J., Kriegsheim, A., Hebestreit, H.F., Mukherji, M., Schofield, C.J.*, et al.* (2001). Targeting of HIF-α to the von Hippel-Lindau ubiquitylation complex by O_2-regulated prolyl hydroxylation. Science *292*, 468-472.

Jenkins, C.L., Bretscher, L.E., Guzei, I.A., and Raines, R.T. (2003). Effect of 3-Hydroxyproline Residues on Collagen Stability. J Am Chem Soc *125*, 6422-6427.

Jeong, J.W., Bae, M.K., Ahn, M.Y., Kim, S.H., Sohn, T.K., Bae, M.H., Yoo, M.A., Song, E.J., Lee, K.J., and Kim, K.W. (2002). Regulation and destabilization of HIF-1α by ARD1-mediated acetylation. Cell *111*, 709-720.

Jiang, B.H., Zheng, J.Z., Leung, S.W., Roe, R., and Semenza, G.L. (1997). Transactivation and inhibitory domains of hypoxia-inducible factor 1α. Modulation of transcriptional activity by oxygen tension. J Biol Chem *272*, 19253-19260.

Jiang, D., Srinivasan, A., Lozano, G., and Robbins, P.D. (1993). SV40 T antigen abrogates p53-mediated transcriptional activity. Oncogene *8*, 2805-2812.

Juva, K., and Prockop, D.J. (1966). Modified procedure for the assay of H^3 or C^{14}-labelled hydroxyproline. Anal Biochem *15*, 77-83.

Kaluz, S., Kaluzová, M., and Stanbridge, E.J. (2008). Does inhibition of degradation of hypoxia-inducible factor (HIF) α always lead to activation of HIF? Lessons learnt from the effect of proteasomal inhibition on HIF activity. J Cell Biochem *104*, 536-544.

Kaye, G.W.C., and Laby, T.H. (1973). Tables of Physical and Chemical Constants, 14th edn (London, Longman).

Kelly, S.M., Jess, T.J., and Price, N.C. (2005). How to study proteins by circular dichroism. Biochim Biophys Acta *1751*, 119-139.

Kim, H.-Y., Ahn, B.-Y., and Cho, Y. (2001a). Structural basis for the inactivation of retinoblastoma tumor suppressor by SV40 large T antigen. EMBO J *20*, 205-304.

Kim, Y.-J., Noguchi, S., Hayashi, Y.K., Tsukahara, T., Shimizu, T., and Arahata, K. (2001b). The product of an oculopharyngeal muscular dystrophy gene, poly(A)-binding protein 2, interacts with SKIP and stimulates muscle-specific gene expression. Hum Mol Genet *10*, 1129-1139.

Kimura, K., Ito, M., Amano, M., Chihara, K., Fukata, Y., Nakafuku, M., Yamamori, B., Feng, J., Nakano, T., Okawa, K.*, et al.* (1996). Regulation of myosin phosphatase by Rho and Rho-Associated kinase (Rho-kinase). Science *273*, 245-248.

Kinter, M., and Sherman, N.E. (2000). Protein sequencing and identification using tandem mass spectrometry (New York, John Wiley & Sons Inc.).

Klose, R.J., and Zhang, Y. (2007). Regulation of histone methylation by demethylimination and demethylation. Nat Rev Mol Cell Biol *8*, 307-318.

Köditz, J., Nesper, J., Wottawa, M., Stiehl, D.P., Camenisch, G., Franke, C., Myllyharju, J., Wenger, R.H., and Katschinski, D.M. (2007). Oxygen-dependent ATF-4 stability is mediated by the PHD3 oxygen sensor. Blood *110*, 3610-3617.

Koivunen, P., Hirsilä, M., Gunzler, V., Kivirikko, K.I., and Myllyharju, J. (2004). Catalytic properties of the asparaginyl hydroxylase (FIH) in the oxygen sensing pathway are distinct from those of its prolyl 4-hydroxylases. J Biol Chem *279*, 9899-9904.

Koivunen, P., Hirsilä, M., Kivirikko, K.I., and Myllyharju, J. (2006). The Length of Peptide Substrates Has a Marked Effect on Hydroxylation by the Hypoxia-inducible Factor Prolyl 4-Hydroxylases. J Biol Chem *281*, 28712-28720.

Koivunen, P., Tiainen, P., Hyvärinen, J., Williams, K.E., Sormunen, R., Klaus, S.J., Kivirikko, K.I., and Myllyharju, J. (2007). An Endoplasmic Reticulum Transmembrane Prolyl 4-Hydroxylase Is Induced by Hypoxia and Acts on Hypoxia-inducible Factor α. J Biol Chem *282*, 30544-30552.

Kolondra, A., Grzybek, M., Chorzalska, A., and Sikorski, A.F. (2008). The 22.5 kDa spectrin-binding domain of ankyrinR binds spectrin with high affinity and changes the spectrin distribution in cells *in vivo*. Protein Expr Purif *60*, 157-164.

Kondo, K., and Kaelin, W.G., Jr. (2001). The von Hippel-Lindau tumor suppressor gene. Exp Cell Res *264*, 117-125.

Kost, T.A., Condreay, J.P., and Jarvis, D.L. (2005). Baculovirus as versatile vectors for protein expression in insect and mammalian cells. Nat Biotechnol *23*, 567-575.

Kouzarides, T. (2007). Chromatin Modifications and Their Function. Cell *128*, 693-705.

Kukkola, L., Hieta, R., Kivirikko, K.I., and Myllyharju, J. (2003). Identification and Characterization of a Third Human, Rat, and Mouse Collagen Prolyl 4-Hydroxylase Isoenzyme. J Biol Chem *278*, 47685-47693.

Kuznetsova, A.V., Meller, J., Schnell, P.O., Nash, J.A., Ignacak, M.L., Sanchez, Y., Conaway, J.W., Conaway, R.C., and Czyzyk-Krzeska, M.F. (2003). von Hippel-Lindau protein binds hyperphosphorylated large subunit of RNA polymerase II through a proline hydroxylation motif and targets it for ubiquitination. Proc Natl Acad Sci U S A *100*, 2706-2711.

Laemmli, U.K. (1970). Cleavage of structural proteins during the assembly of the head of bacteriophage T4. Nature *227*, 680-685.

Lan, F., Nottke, A.C., and Shi, Y. (2008). Mechanisms involved in the regulation of histone lysine demethylases. Curr Opin Cell Biol *20*, 316-325.

Lancaster, D.E., McDonough, M.A., and Schofield, C.J. (2004a). Factor inhibiting hypoxia-inducible factor (FIH) and other asparaginyl hydroxylases. Biochem Soc Trans *32*, 943-945.

Lancaster, D.E., McNeill, L.A., McDonough, M.A., Aplin, R.T., Hewitson, K.S., Pugh, C.W., Ratcliffe, P.J., and Schofield, C.J. (2004b). Disruption of dimerization and substrate phosphorylation inhibit factor inhibiting hypoxia-inducible factor (FIH) activity. Biochem J *383*, 429-437.

Lando, D., Peet, D.J., Gorman, J.J., Whelan, D.A., Whitelaw, M.L., and Bruick, R.K. (2002a). FIH-1 is an asparaginyl hydroxylase enzyme that regulates the transcriptional activity of hypoxia-inducible factor. Genes Dev *16*, 1466-1471.

Lando, D., Peet, D.J., Whelan, D.A., Gorman, J.J., and Whitelaw, M.L. (2002b). Asparagine hydroxylation of the HIF transactivation domain: a hypoxic switch. Science *295*, 858-861.

Larsen, M.R., Trelle, M.B., Thingholm, T.E., and Jensen, O.N. (2006). Analysis of posttranslational modifications of proteins by tandem mass spectrometry. BioTechniques *40*, 790-798.

Lau, K.W., Tian, Y.M., Raval, R.R., Ratcliffe, P.J., and Pugh, C.W. (2007). Target gene selectivity of hypoxia-inducible factor-α in renal cancer cells is conveyed by post-DNA-binding mechanisms. Br J Cancer *96*, 1284-1292.

Le Roy, F., Laskowska, A., Silhol, M., Salehzada, T., and Bisbal, C. (2000). Characterization of RNABP, an RNA binding protein that associates with RNase L. J Interferon Cytokine Res *20*, 635-644.

Leahy, D.J., Dann, C.E., Longo, P., Perman, B., and Ramyar, K.X. (2000). A Mammalian Expression Vector for Expression and Purification of Secreted Proteins for Structural Studies. Protein Expr Purif *20*, 500-506.

Lee, S., Nakamura, E., Yang, H., Wei, W., Linggi, M.S., Sajan, M.P., Farese, R.V., Freeman, R.S., Carter, B.D., Kaelin, W.G.*, et al.* (2005). Neuronal apoptosis linked to EglN3 prolyl hydroxylase and familial pheochromocytoma genes: Developmental culling and cancer. Cancer Cell *8*, 155-167.

Li, D., Hirsilä, M., Koivunen, P., Brenner, M.C., Xu, L., Yang, C., Kivirikko, K.I., and Myllyharju, J. (2004). Many Amino Acid Substitutions in a Hypoxia-inducible Transcription Factor (HIF)-1α-like Peptide Cause Only Minor Changes in Its Hydroxylation by the HIF Prolyl 4-Hydroxylases: substitution of 3,4-dehydroproline or azetidine-2-carboxylic acid for the proline leads to a high rate of uncoupled 2-oxoglutarate decarboxylation. J Biol Chem *279*, 55051-55059.

Li, J., Mahajan, A., and Tsai, M.-D. (2006). Ankyrin Repeat: A Unique Motif Mediating Protein-Protein Interactions. Biochemistry *45*, 15168-15178.

Li, J.J., and Kelly, T.J. (1984). *Simian virus 40* DNA replication *in vitro*. Proc Natl Acad Sci U S A *81*, 6973-6977.

Lilyestrom, W., Klein, M.G., Zhang, R., Joachimiak, A., and Chen, X.S. (2006). Crystal structure of SV40 large T-antigen bound to p53: interplay between a viral oncoprotein and a cellular tumor suppressor. Genes Dev *20*, 2373-2382.

Lindblad, B., Lindstedt, G., Tofft, M., and Lindstedt, S. (1969). The mechanism of α-ketoglutarate oxidation in coupled enzymatic reactions. J Am Chem Soc *91*, 4604-4606.

Lindstedt, G., and Lindstedt, S. (1970). Cofactor requirements of γ-butyrobetaine hydroxylase from rat liver. J Biol Chem *245*, 4178-4186.

Linke, S., Stojkoski, C., Kewley, R.J., Booker, G.W., Whitelaw, M.L., and Peet, D.J. (2004). Substrate Requirements of the Oxygen-sensing Asparaginyl Hydroxylase Factor-inhibiting Hypoxia-inducible Factor. J Biol Chem *279*, 14391-14397.

Lipscomb, E.A., Sarmiere, P.D., Crowder, R.J., and Freeman, R.S. (1999). Expression of the SM-20 Gene Promotes Death in Nerve Growth Factor-Dependent Sympathetic Neurons. J Neurochem *73*, 429-432.

Lipscomb, E.A., Sarmiere, P.D., and Freeman, R.S. (2001). SM-20 Is a Novel Mitochondrial Protein That Causes Caspase-dependent Cell Death in Nerve Growth Factor-dependent Neurons. J Biol Chem *276*, 5085-5092.

Lisy, K., and Peet, D.J. (2008). Turn me on: regulating HIF transcriptional activity. Cell Death Differ *15*, 642-649.

Loenarz, C., and Schofield, C.J. (2008). Expanding chemical biology of 2-oxoglutarate oxygenases. Nat Chem Biol *4*, 152-156.

Lubman, O.Y., Korolev, S.V., and Kopan, R. (2004). Anchoring Notch genetics and biochemistry; structural analysis of the ankyrin domain sheds light on existing data. Mol Cell *13*, 619-626.

MacDonald, J.A., Borman, M.A., Murányi, A., Somlyo, A.V., Hartshorne, D.J., and Haystead, T.A.J. (2001). Identification of the endogenous smooth muscle myosin phosphatase-associated kinase. Proc Natl Acad Sci U S A *98*, 2419-2424.

Mahon, P.C., Hirota, K., and Semenza, G.L. (2001). FIH-1: a novel protein that interacts with HIF-1α and VHL to mediate repression of HIF-1 transcriptional activity. Genes Dev *15*, 2675-2686.

Makino, Y., Cao, R., Svensson, K., Bertilsson, G., Asman, M., Tanaka, H., Cao, Y., Berkenstam, A., and Poellinger, L. (2001). Inhibitory PAS domain protein is a negative regulator of hypoxia-inducible gene expression. Nature *414*, 550-554.

Makino, Y., Kanopka, A., Wilson, W.J., Tanaka, H., and Poellinger, L. (2002). Inhibitory PAS domain protein (IPAS) is a hypoxia-inducible splicing variant of the hypoxia-inducible factor-3α locus. J Biol Chem *277*, 32405-32408.

Mann, M. (2006). Functional and quantitative proteomics using SILAC. Nat Rev Mol Cell Biol *7*, 952-958.

Masson, N., Willam, C., Maxwell, P.H., Pugh, C.W., and Ratcliffe, P.J. (2001). Independent function of two destruction domains in hypoxia-inducible factor-α chains activated by prolyl hydroxylation. EMBO J *20*, 5197-5206.

Matsumura, F., and Hartshorne, D.J. (2008). Myosin phosphatase target subunit: Many roles in cell function. Biochem Biophys Res Commun *369*, 149-156.

Maxwell, P.H., Wiesener, M.S., Chang, G.W., Clifford, S.C., Vaux, E.C., Cockman, M.E., Wykoff, C.C., Pugh, C.W., Maher, E.R., and Ratcliffe, P.J. (1999). The tumour suppressor protein VHL targets hypoxia-inducible factors for oxygen-dependent proteolysis. Nature *399*, 271-275.

McDonough, M.A., Li, V., Flashman, E., Chowdhury, R., Mohr, C., Lienard, B.M., Zondlo, J., Oldham, N.J., Clifton, I.J., Lewis, J., *et al.* (2006). Cellular oxygen sensing: Crystal structure of hypoxia-inducible factor prolyl hydroxylase (PHD2). Proc Natl Acad Sci U S A *103*, 9814-9819.

McGinnis, K., Ku, G.M., VanDusen, W.J., Fu, J., Garsky, V., Stern, A.M., and Friedman, P.A. (1996). Site-Directed Mutagenesis of Residues in a Conserved Region of Bovine Aspartyl (Asparaginyl) β-Hydroxylase: Evidence That Histidine 675 Has a Role in Binding Fe^{2+}. Biochemistry *35*, 3957-3962.

McMullen, B.A., Fujikawa, K., Kisiel, W., Sasagawa, T., Howald, W.N., Kwa, E.Y., and Weinstein, B. (1983). Complete amino acid sequence of the light chain of human blood coagulation factor X: evidence for identification of residue 63 as β-hydroxyaspartic acid. Biochemistry *22*, 2875-2884.

McNeill, L.A., Bethge, L., Hewitson, K.S., and Schofield, C.J. (2005). A fluorescence-based assay for 2-oxoglutarate-dependent oxygenases. Anal Biochem *336*, 125-131.

Meinke, G., Phelan, P., Moine, S., Bochkareva, E., Bochkarev, A., Bullock, P.A., and Bohm, A. (2007). The Crystal Structure of the SV40 T-Antigen Origin Binding Domain in Complex with DNA. PLoS Biol *5*, e23.

Metzen, E., Berchner-Pfannschmidt, U., Stengel, P., Marxsen, J.H., Stolze, I., Klinger, M., Huang, W.Q., Wotzlaw, C., Hellwig-Bürgel, T., Jelkmann, W.*, et al.* (2003). Intracellular localisation of human HIF-1α hydroxylases: implications for oxygen sensing. J Cell Sci *116*, 1319-1326.

Michaely, P., Tomchick, D.R., Machius, M., and Anderson, R.G.W. (2002). Crystal structure of a 12 ANK repeat stack from human ankyrinR. EMBO J *21*, 6387-6396.

Mikhaylova, O., Ignacak, M.L., Barankiewicz, T.J., Harbaugh, S.V., Yi, Y., Maxwell, P.H., Schneider, M., Van Geyte, K., Carmeliet, P., Revelo, M.P.*, et al.* (2008). The von Hippel-Lindau Tumor Suppressor Protein and Egl-9-Type Proline Hydroxylases Regulate the Large Subunit of RNA Polymerase II in Response to Oxidative Stress. Mol Cell Biol *28*, 2701-2717.

Mitsui, T., Inagaki, M., and Ikebe, M. (1992). Purification and characterization of smooth muscle myosin-associated phosphatase from chicken gizzards. J Biol Chem *267*, 16727-16735.

Mizuno, K., Hayashi, T., Peyton, D.H., and Bachinger, H.P. (2004). The Peptides Acetyl-(Gly-3(*S*)Hyp-4(*R*)Hyp)$_{10}$-NH_2 and Acetyl-(Gly-Pro-3(*S*)Hyp)$_{10}$-NH_2 Do Not Form a Collagen Triple Helix. J Biol Chem *279*, 282-287.

Mohr, O.L. (1919). Character changes caused by mutation of an entire region of a chromosome in *Drosophila*. Genetics *4*, 275-282.

Moorhead, G., Johnson, D., Morrice, N., and Cohen, P. (1998). The major myosin phosphatase in skeletal muscle is a complex between the β-isoform of protein phosphatase 1 and the MYPT2 gene product. FEBS Lett *438*, 141-144.

Morello, R., Bertin, T.K., Chen, Y., Hicks, J., Tonachini, L., Monticone, M., Castagnola, P., Rauch, F., Glorieux, F.H., Vranka, J.*, et al.* (2006). CRTAP Is Required for Prolyl 3-Hydroxylation and Mutations Cause Recessive Osteogenesis Imperfecta. Cell *127*, 291-304.

Mosavi, L.K., Cammett, T.J., Desrosiers, D.C., and Peng, Z.-y. (2004). The ankyrin repeat as molecular architecture for protein recognition. Protein Sci *13*, 1435-1448.

Mukherji, M., Chien, W., Kershaw, N.J., Clifton, I.J., Schofield, C.J., Wierzbicki, A.S., and Lloyd, M.D. (2001). Structure-function analysis of phytanoyl-CoA 2-hydroxylase mutations causing Refsum's disease. Hum Mol Genet *10*, 1971-1982.

Mumm, J.S., Schroeter, E.H., Saxena, M.T., Griesemer, A., Tian, X., Pan, D.J., Ray, W.J., and Kopan, R. (2000). A ligand-induced extracellular cleavage regulates γ-secretase-like proteolytic activation of Notch1. Mol Cell *5*, 197-206.

Murányi, A., MacDonald, J.A., Deng, J.T., Wilson, D.P., Haystead, T.A.J., Walsh, M.P., Erdődi, F., Kiss, E., Wu, Y., and Hartshorne, D.J. (2002). Phosphorylation of the myosin phosphatase target subunit by integrin-linked kinase. Biochem J *366*, 211-216.

Murray-Rust, T.A., Oldham, N.J., Hewitson, K.S., and Schofield, C.J. (2006). Purified recombinant hARD1 does not catalyse acetylation of Lys532 of HIF-1α fragments *in vitro*. FEBS Lett *580*, 1911-1918.

Myllyharju, J. (2003). Prolyl 4-hydroxylases, the key enzymes of collagen biosynthesis. Matrix Biol *22*, 15-24.

Myllyharju, J., and Kivirikko, K.I. (2004). Collagens, modifying enzymes and their mutations in humans, flies and worms. Trends Genet *20*, 33-43.

Myllylä, R., Tuderman, L., and Kivirikko, K.I. (1977). Mechanism of the Prolyl Hydroxylase Reaction. Eur J Biochem *80*, 349-357.

Myllylä, R., Wang, C., Heikkinen, J., Juffer, A., Lampela, O., Risteli, M., Ruotsalainen, H., Salo, A., and Sipilä, L. (2007). Expanding the lysyl hydroxylase toolbox: New insights into the localization and activities of lysyl hydroxylase 3 (LH3). J Cell Physiol *212*, 323-329.

Mylonis, I., Chachami, G., Samiotaki, M., Panayotou, G., Paraskeva, E., Kalousi, A., Georgatsou, E., Bonanou, S., and Simos, G. (2006). Identification of MAPK phosphorylation sites and their role in the localization and activity of hypoxia-inducible factor-1α. J Biol Chem *281*, 33095-33106.

Nakayama, K., Frew, I.J., Hagensen, M., Skals, M., Habelhah, H., Bhoumik, A., Kadoya, T., Erdjument-Bromage, H., Tempst, P., Frappell, P.B.*, et al.* (2004). Siah2 Regulates Stability of Prolyl-Hydroxylases, Controls HIF1α Abundance, and Modulates Physiological Responses to Hypoxia. Cell *117*, 941-952.

Nakayama, K., Gazdoiu, S., Abraham, R., Pan, Z.-Q., and Ronai, Z. (2007). Hypoxia-induced assembly of prolyl hydroxylase PHD3 into complexes: implications for its activity and susceptibility for degradation by the E3 ligase Siah2. Biochem J *401*, 217-226.

Nečas, E., and Thorling, E.B. (1972). Unresponsiveness of erythropoietin-producing cells to cyanide. Am J Physiol *222*, 1187-1190.

Neubauer, G., King, A., Rappsilber, J., Calvio, C., Watson, M., Ajuh, P., Sleeman, J., Lamond, A., and Mann, M. (1998). Mass spectrometry and EST-database searching allows characterization of the multi-protein spliceosome complex. Nat Genet *20*, 46-50.

Nissi, R., Autio-Harmainen, H., Marttila, P., Sormunen, R., and Kivirikko, K.I. (2001). Prolyl 4-hydroxylase Isoenzymes I and II Have Different Expression Patterns in Several Human Tissues. J Histochem Cytochem *49*, 1143-1154.

O'Rourke, J.F., Tian, Y.M., Ratcliffe, P.J., and Pugh, C.W. (1999). Oxygen-regulated and transactivating domains in endothelial PAS protein 1: Comparison with hypoxia-inducible factor-1α. J Biol Chem *274*, 2060-2071.

Oehme, F., Ellinghaus, P., Kolkhof, P., Smith, T.J., Ramakrishnan, S., Hutter, J., Schramm, M., and Flamme, I. (2002). Overexpression of PH-4, a novel putative proline 4-hydroxylase, modulates activity of hypoxia-inducible transcription factors. Biochem Biophys Res Commun *296*, 343-349.

Ogryzko, V.V., Kotani, T., Zhang, X., Schiltz, R.L., Howard, T., Yang, X.-J., Howard, B.H., Qin, J., and Nakatani, Y. (1998). Histone-like TAFs within the PCAF Histone Acetylase Complex. Cell *94*, 35-44.

Ohh, M., Park, C.W., Ivan, M., Hoffman, M.A., Kim, T.Y., Huang, L.E., Pavletich, N., Chau, V., and Kaelin, W.G. (2000). Ubiquitination of hypoxia-inducible factor requires direct binding to the β-domain of the von Hippel-Lindau protein. Nat Cell Biol *2*, 423-427.

Okochi, M., Steiner, H., Fukumori, A., Tanii, H., Tomita, T., Tanaka, T., Iwatsubo, T., Kudo, T., Takeda, M., and Haass, C. (2002). Presenilins mediate a dual intramembranous γ-secretase cleavage of Notch-1. EMBO J *21*, 5408-5416.

Okubo, S., Ito, M., Takashiba, Y., Ichikawa, K., Miyahara, M., Shimizu, H., Konishi, T., Shima, H., Nagao, M., Hartshorne, D.J.*, et al.* (1994). A Regulatory Subunit of Smooth Muscle Myosin Bound Phosphatase. Biochem Biophys Res Commun *200*, 429-434.

Ong, S.-E., Blagoev, B., Kratchmarova, I., Kristensen, D.B., Steen, H., Pandey, A., and Mann, M. (2002). Stable Isotope Labeling by Amino Acids in Cell Culture, SILAC, as a Simple and Accurate Approach to Expression Proteomics. Mol Cell Proteomics *1*, 376-386.

Ong, S.-E., and Mann, M. (2007). A practical recipe for stable isotope labeling by amino acids in cell culture (SILAC). Nat Protocols *1*, 2650-2660.

Ozer, A., and Bruick, R.K. (2007). Non-heme dioxygenases: cellular sensors and regulators jelly rolled into one? Nat Chem Biol *3*, 144-153.

Påhlman, S., Stockhausen, M.T., Fredlund, E., and Axelson, H. (2004). Notch signaling in neuroblastoma. Semin Cancer Biol *14*, 365-373.

Paltoglou, S., and Roberts, B.J. (2007). HIF-1α and EPAS ubiquitination mediated by the VHL tumour suppressor involves flexibility in the ubiquitination mechanism, similar to other RING E3 ligases. Oncogene *26*, 604-609.

Parra, M., Mahmoudi, T., and Verdin, E. (2007). Myosin phosphatase dephosphorylates HDAC7, controls its nucleocytoplasmic shuttling, and inhibits apoptosis in thymocytes. Genes Dev *21*, 638-643.

Peng, J., Zhang, L., Drysdale, L., and Fong, G.H. (2000). The transcription factor EPAS-1/hypoxia-inducible factor 2α plays an important role in vascular remodeling. Proc Natl Acad Sci U S A *97*, 8386-8391.

Percy, M.J., Zhao, Q., Flores, A., Harrison, C., Lappin, T.R., Maxwell, P.H., McMullin, M.F., and Lee, F.S. (2006). A family with erythrocytosis establishes a role for prolyl hydroxylase domain protein 2 in oxygen homeostasis. Proc Natl Acad Sci U S A *103*, 654-659.

Perkins, D.N., Pappin, D.J.C., Creasy, D.M., and Cottrell, J.S. (1999). Probability-based protein identification by searching sequence databases using mass spectrometry data. Electrophoresis *20*, 3551-3567.

Peterkofsky, B., and Udenfriend, S. (1963). Conversion of Proline to Collagen Hydroxyproline in a Cell-free System from Chick Embryo. J Biol Chem *238*, 3966-3977.

Pollard, P.J., Brière, J.J., Alam, N.A., Barwell, J., Barclay, E., Wortham, N.C., Hunt, T., Mitchell, M., Olpin, S., Moat, S.J., *et al.* (2005). Accumulation of Krebs cycle intermediates and over-expression of HIF1α in tumours which result from germline FH and SDH mutations. Hum Mol Genet *14*, 2231-2239.

Prathapam, T., Kühne, C., and Banks, L. (2001a). The HPV-16 E7 oncoprotein binds Skip and suppresses its transcriptional activity. Oncogene *20*, 7677-7685.

Prathapam, T., Kühne, C., and Banks, L. (2002). Skip interacts with the retinoblastoma tumor suppressor and inhibits its transcriptional repression activity. Nucl Acids Res *30*, 5261-5268.

Prathapam, T., Kühne, C., Hayman, M., and Banks, L. (2001b). Ski interacts with the evolutionarily conserved SNW domain of Skip. Nucl Acids Res *29*, 3469-3476.

Price, J.C., Barr, E.W., Tirupati, B., Bollinger, J.M.J., and Krebs, C. (2003). The First Direct Characterization of a High-Valent Iron Intermediate in the Reaction of an α-Ketoglutarate-Dependent Dioxygenase: A High-Spin Fe(IV) Complex in Taurine/α-Ketoglutarate Dioxygenase (TauD) from *Escherichia coli*. Biochemistry *42*, 7497-7508.

Price, N.C., and Dwek, R.A. (1979). Principles and Problems in Physical Chemistry for Biochemists, 2nd edn (Oxford, Oxford University Press).

Prockop, D.J., and Juva, K. (1965). Synthesis of hydroxyproline *in vitro* by the hydroxylation of proline in a precursor of collagen. Proc Natl Acad Sci U S A *53*, 661-668.

Prockop, D.J., and Kivirikko, K.I. (1995). Collagens: Molecular Biology, Diseases, and Potentials for Therapy. Annu Rev Biochem *64*, 403-434.

Pugh, C.W., O'Rourke, J.F., Nagao, M., Gleadle, J.M., and Ratcliffe, P.J. (1997). Activation of hypoxia-inducible factor-1; definition of regulatory domains within the α subunit. J Biol Chem *272*, 11205-11214.

Pugh, C.W., Tan, C.C., Jones, R.W., and Ratcliffe, P.J. (1991). Functional analysis of an oxygen-regulated transcriptional enhancer lying 3' to the mouse erythropoietin gene. Proc Natl Acad Sci U S A *88*, 10553-10557.

Qi, H.H., Ongusaha, P.P., Myllyharju, J., Cheng, D., Pakkanen, O., Shi, Y., Lee, S.W., Peng, J., and Shi, Y. (2008). Prolyl 4-hydroxylation regulates Argonaute 2 stability. Nature *455*, 421-424.

Rantanen, K., Pursiheimo, J., Hogel, H., Himanen, V., Metzen, E., and Jaakkola, P.M. (2008). Prolyl Hydroxylase PHD3 Activates Oxygen-dependent Protein Aggregation. Mol Biol Cell *19*, 2231-2240.

Rautavuoma, K., Takaluoma, K., Sormunen, R., Myllyharju, J., Kivirikko, K.I., and Soininen, R. (2004). Premature aggregation of type IV collagen and early lethality in lysyl hydroxylase 3 null mice. Proc Natl Acad Sci U S A *101*, 14120-14125.

Raval, R.R., Lau, K.W., Tran, M.G., Sowter, H.M., Mandriota, S.J., Li, J.L., Pugh, C.W., Maxwell, P.H., Harris, A.L., and Ratcliffe, P.J. (2005). Contrasting properties of hypoxia-inducible factor 1 (HIF-1) and HIF-2 in von Hippel-Lindau-associated renal cell carcinoma. Mol Cell Biol *25*, 5675-5686.

Rigaut, G., Shevchenko, A., Rutz, B., Wilm, M., Mann, M., and Séraphin, B. (1999). A generic protein purification method for protein complex characterization and proteome exploration. Nat Biotech *17*, 1030-1032.

Ruotsalainen, H., Sipilä, L., Vapola, M., Sormunen, R., Salo, A.M., Uitto, L., Mercer, D.K., Robins, S.P., Risteli, M., Aszodi, A.*, et al.* (2006). Glycosylation catalyzed by lysyl hydroxylase 3 is essential for basement membranes. J Cell Sci *119*, 625-635.

Ryan, H.E., Lo, J., and Johnson, R.S. (1998). HIF-1α is required for solid tumor formation and embryonic vascularization. EMBO J *17*, 3005-3015.

Ryle, M.J., Padmakumar, R., and Hausinger, R.P. (1999). Stopped-Flow Kinetic Analysis of *Escherichia coli* Taurine/α-Ketoglutarate Dioxygenase: Interactions with α-Ketoglutarate, Taurine, and Oxygen. Biochemistry *38*, 15278-15286.

Sabourin, P., and Bieber, L. (1982). Purification and characterization of an α-ketoisocaproate oxygenase of rat liver. J Biol Chem *257*, 7460-7467.

Sainson, R.C.A., and Harris, A.L. (2006). Hypoxia-regulated differentiation: let's step it up a Notch. Trends Mol Med *12*, 141-143.

Sang, N., Stiehl, D.P., Bohensky, J., Leshchinsky, I., Srinivas, V., and Caro, J. (2003). MAPK signaling up-regulates the activity of hypoxia-inducible factors by its effects on p300. J Biol Chem *278*, 14013-14019.

Schlisio, S., Kenchappa, R.S., Vredeveld, L.C.W., George, R.E., Stewart, R., Greulich, H., Shahriari, K., Nguyen, N.V., Pigny, P., Dahia, P.L.*, et al.* (2008). The kinesin KIF1Bβ acts downstream from EglN3 to induce apoptosis and is a potential 1p36 tumor suppressor. Genes Dev *22*, 884-893.

Schnatwinkel, C., Christoforidis, S., Lindsay, M.R., Uttenweiler-Joseph, S., Wilm, M., Parton, R.G., and Zerial, M. (2004). The Rab5 Effector Rabankyrin-5 Regulates and Coordinates Different Endocytic Mechanisms. PLoS Biol *2*, e261.

Schofield, C.J., and Ratcliffe, P.J. (2004). Oxygen sensing by HIF hydroxylases. Nat Rev Mol Cell Biol *5*, 343-354.

Schultz, J., Milpetz, F., Bork, P., and Ponting, C.P. (1998). SMART, a simple modular architecture research tool: Identification of signaling domains. Proc Natl Acad Sci U S A *95*, 5857-5864.

Schweisguth, F. (2004). Regulation of Notch Signaling Activity. Curr Biol *14*, R129-R138.

Scortegagna, M., Ding, K., Oktay, Y., Gaur, A., Thurmond, F., Yan, L.J., Marck, B.T., Matsumoto, A.M., Shelton, J.M., Richardson, J.A.*, et al.* (2003). Multiple organ pathology, metabolic abnormalities and impaired homeostasis of reactive oxygen species in *Epas1*$^{-/-}$ mice. Nat Genet *35*, 331-340.

Semenza, G.L., Nejfelt, M.K., Chi, S.M., and Antonarakis, S.E. (1991). Hypoxia-inducible nuclear factors bind to an enhancer element located 3' to the human erythropoietin gene. Proc Natl Acad Sci U S A *88*, 5680-5684.

Semenza, G.L., and Wang, G.L. (1992). A nuclear factor induced by hypoxia via de novo protein synthesis binds to the human erythropoietin gene enhancer at a site required for transcriptional activation. Mol Cell Biol *12*, 5447-5454.

Seth, P., Krop, I., Porter, D., and Polyak, K. (2002). Novel estrogen and tamoxifen induced genes identified by SAGE (Serial Analysis of Gene Expression). Oncogene *21*, 836-843.

Shi, Y., Lan, F., Matson, C., Mulligan, P., Whetstine, J.R., Cole, P.A., Casero, R.A., and Shi, Y. (2004). Histone demethylation mediated by the nuclear amine oxidase homolog LSD1. Cell *119*, 941-953.

Shimizu, H., Ito, M., Miyahara, M., Ichikawa, K., Okubo, S., Konishi, T., Naka, M., Tanaka, T., Hirano, K., and Hartshorne, D.J. (1994). Characterization of the myosin-binding subunit of smooth muscle myosin phosphatase. J Biol Chem *269*, 30407-30411.

Siegel, M.R., and Sisler, H.D. (1963). Inhibition of Protein Synthesis in vitro by Cycloheximide. Nature *200*, 675.

Simone, C., Stiegler, P., Forcales, S.-V., Bagella, L., De Luca, A., Sartorelli, V., Giordano, A., and Puri, P.L. (2004). Deacetylase recruitment by the C/H3 domain of the acetyltransferase p300. Oncogene *23*, 2177-2187.

Skinner, J.A., and Saltiel, A.R. (2001). Cloning and identification of MYPT3: a prenylatable myosin targetting subunit of protein phosphatase 1. Biochem J *356*, 257-267.

Srinivasan, A., McClellan, A.J., Vartikar, J., Marks, I., Cantalupo, P., Li, Y., Whyte, P., Rundell, K., Brodsky, J.L., and Pipas, J.M. (1997). The amino-terminal transforming region of *simian virus 40* large T and small t antigens functions as a J domain. Mol Cell Biol *17*, 4761-4773.

Stenflo, J. (1991). Structure-function relationships of epidermal growth factor modules in vitamin K-dependent clotting factors. Blood *78*, 1637-1651.

Stenflo, J., Holme, E., Lindstedt, S., Chandramouli, N., Tsai Huang, L.H., Tam, J.P., and Merrifield, R.B. (1989). Hydroxylation of aspartic acid in domains homologous to the epidermal growth factor precursor is catalyzed by a 2-oxoglutarate-dependent dioxygenase. Proc Natl Acad Sci U S A *86*, 444-447.

Stenflo, J., Lundwall, Å., and Dahlbäck, B. (1987). β-Hydroxyasparagine in domains homologous to the epidermal growth factor precursor in vitamin K-dependent protein S. Proc Natl Acad Sci U S A *84*, 368-372.

Stetten, M.R. (1949). Some aspects of the metabolism of hydroxyproline studied with the aid of isotopic nitrogen. J Biol Chem *181*, 31-37.

Stolze, I.P., Tian, Y.M., Appelhoff, R.J., Turley, H., Wykoff, C.C., Gleadle, J.M., and Ratcliffe, P.J. (2004). Genetic analysis of the role of the asparaginyl hydroxylase factor inhibiting hypoxia-inducible factor (HIF) in regulating HIF transcriptional target genes. J Biol Chem *279*, 42719-42725.

Straub, J.A., Lipscomb, E.A., Yoshida, E.S., and Freeman, R.S. (2003). Induction of SM-20 in PC12 cells leads to increased cytochrome *c* levels, accumulation of cytochrome *c* in the cytosol, and caspase-dependent cell death. J Neurochem *85*, 318-328.

Takeda, K., Ho, V.C., Takeda, H., Duan, L.-J., Nagy, A., and Fong, G.-H. (2006). Placental but Not Heart Defects Are Associated with Elevated Hypoxia-Inducible Factor α Levels in Mice Lacking Prolyl Hydroxylase Domain Protein 2. Mol Cell Biol *26*, 8336-8346.

Takeuchi, T., Watanabe, Y., Takano-Shimizu, T., and Kondo, S. (2006). Roles of *jumonji* and *jumonji* family genes in chromatin regulation and development. Dev Dyn *235*, 2449-2459.

Tan, I., Ng, C.H., Lim, L., and Leung, T. (2001). Phosphorylation of a Novel Myosin Binding Subunit of Protein Phosphatase 1 Reveals a Conserved Mechanism in the Regulation of Actin Cytoskeleton. J Biol Chem *276*, 21209-21216.

Tanaka, J., Ito, M., Feng, J., Ichikawa, K., Hamaguchi, T., Nakamura, M., Hartshorne, D.J., and Nakano, T. (1998). Interaction of Myosin Phosphatase Target Subunit 1 with the Catalytic Subunit of Type 1 Protein Phosphatase. Biochemistry *37*, 16697-16703.

Tanaka, N., Nakanishi, M., Kusakabe, Y., Goto, Y., Kitade, Y., and Nakamura, K.T. (2004). Structural basis for recognition of 2',5'-linked oligoadenylates by human ribonuclease L. EMBO J *23*, 3929-3938.

Tanimoto, K., Makino, Y., Pereira, T., and Poellinger, L. (2000). Mechanism of regulation of the hypoxia-inducible factor-1α by the von Hippel-Lindau tumor suppressor protein. EMBO J *19*, 4298-4309.

Taylor, M.S. (2001). Characterization and comparative analysis of the EGLN gene family. Gene *275*, 125-132.

Terrak, M., Kerff, F., Langsetmo, K., Tao, T., and Dominguez, R. (2004). Structural basis of protein phosphatase 1 regulation. Nature *429*, 780-784.

Thrash-Bingham, C.A., and Tartof, K.D. (1999). aHIF: a Natural Antisense Transcript Overexpressed in Human Renal Cancer and During Hypoxia. J Natl Cancer Inst *91*, 143-151.

Tiainen, P., Pasanen, A., Sormunen, R., and Myllyharju, J. (2008). Characterization of Recombinant Human Prolyl 3-Hydroxylase Isoenzyme 2, an Enzyme Modifying the Basement Membrane Collagen IV. J Biol Chem *283*, 19432-19439.

Tian, H., Hammer, R.E., Matsumoto, A.M., Russell, D.W., and McKnight, S.L. (1998). The hypoxia-responsive transcription factor EPAS1 is essential for catecholamine homeostasis and protection against heart failure during embryonic development. Genes Dev *12*, 3320-3324.

Tian, H., McKnight, S.L., and Russell, D.W. (1997). Endothelial PAS domain protein 1 (EPAS1), a transcription factor selectively expressed in endothelial cells. Genes Dev *11*, 72-82.

Tóth, A., Kiss, E., Gergely, P., Walsh, M.P., Hartshorne, D.J., and Erdődi, F. (2000a). Phosphorylation of MYPT1 by protein kinase C attenuates interaction with PP1 catalytic subunit and the 20 kDa light chain of myosin. FEBS Lett *484*, 113-117.

Tóth, A., Kiss, E., Herberg, F.W., Gergely, P., Hartshorne, D.J., and Erdődi, F. (2000b). Study of the subunit interactions in myosin phosphatase by surface plasmon resonance. Eur J Biochem *267*, 1687-1697.

Truhlar, S.M.E., Mathes, E., Cervantes, C.F., Ghosh, G., and Komives, E.A. (2008). Pre-folding IκBα Alters Control of NF-κB Signaling. J Mol Biol *380*, 67-82.

Tryggvason, K., Majamaa, K., Risteli, J., and Kivirikko, K.I. (1979). Partial purification and characterization of chick-embryo prolyl 3-hydroxylase. Biochem J *183*, 303-307.

Tsukada, Y.-i., Fang, J., Erdjument-Bromage, H., Warren, M.E., Borchers, C.H., Tempst, P., and Zhang, Y. (2006). Histone demethylation by a family of JmjC domain-containing proteins. Nature *439*, 811-816.

Tuckerman, J.R., Zhao, Y., Hewitson, K.S., Tian, Y.-M., Pugh, C.W., Ratcliffe, P.J., and Mole, D.R. (2004). Determination and comparison of specific activity of the HIF-prolyl hydroxylases. FEBS Lett *576*, 145.

Tuderman, L., Myllylä, R., and Kivirikko, K.I. (1977). Mechanism of the Prolyl Hydroxylase Reaction. Eur J Biochem *80*, 341-348.

Uchida, T., Rossignol, F., Matthay, M.A., Mounier, R., Couette, S., Clottes, E., and Clerici, C. (2004). Prolonged Hypoxia Differentially Regulates Hypoxia-inducible Factor HIF-1α and HIF-2α Expression in Lung Epithelial Cells: Implication of Natural Antisense HIF-1α. J Biol Chem *279*, 14871-14878.

Unnithan, A.G., Myer, M.J., Veale, C.J., and Danell, A.S. (2007). MS/MS of Protonated Polyproline Peptides: The Influence of N-terminal Protonation on Dissociation. J Am Soc Mass Spectrom *18*, 2198-2203.

Urlinger, S., Baron, U., Thellmann, M., Hasan, M.T., Bujard, H., and Hillen, W. (2000). Exploring the sequence space for tetracycline-dependent transcriptional activators: Novel mutations yield expanded range and sensitivity. Proc Natl Acad Sci U S A *97*, 7963-7968.

Vaisar, T., and Urban, J. (1996). Probing Proline Effect in CID of Protonated Peptides. J Mass Spectrom *31*, 1185-1187.

Valtavaara, M., Papponen, H., Pirttilä, A.-M., Hiltunen, K., Helander, H., and Myllylä, R. (1997). Cloning and Characterization of a Novel Human Lysyl Hydroxylase Isoform Highly Expressed in Pancreas and Muscle. J Biol Chem *272*, 6831-6834.

Valtavaara, M., Szpirer, C., Szpirer, J., and Myllylä, R. (1998). Primary Structure, Tissue Distribution, and Chromosomal Localization of a Novel Isoform of Lysyl Hydroxylase (Lysyl Hydroxylase 3). J Biol Chem *273*, 12881-12886.

van der Rest, M., and Garrone, R. (1991). Collagen family of proteins. FASEB J *5*, 2814-2823.

Van Slyke, D.D., and Hiller, A. (1921). An Unidentified Base among the Hydrolytic Products of Gelatin. Proc Natl Acad Sci U S A *7*, 185-186.

Vaz, F.M., and Wanders, R.J. (2002). Carnitine biosynthesis in mammals. Biochem J *361*, 417-429.

Veit, G., Kobbe, B., Keene, D.R., Paulsson, M., Koch, M., and Wagener, R. (2006). Collagen XXVIII, a Novel von Willebrand Factor A Domain-containing Protein with Many Imperfections in the Collagenous Domain. J Biol Chem *281*, 3494-3504.

Vranka, J.A., Sakai, L.Y., and Bächinger, H.P. (2004). Prolyl 3-Hydroxylase 1, Enzyme Characterization and Identification of a Novel Family of Enzymes. J Biol Chem *279*, 23615-23621.

Walsh, C.T. (2006). Posttranslational modification of proteins: expanding nature's inventory (Englewood, CO, Roberts and Company Publishers).

Wang, C., Luosujärvi, H., Heikkinen, J., Risteli, M., Uitto, L., and Myllylä, R. (2002). The third activity for lysyl hydroxylase 3: galactosylation of hydroxylysyl residues in collagens *in vitro*. Matrix Biol *21*, 559-566.

Wang, G.L., Jiang, B.H., Rue, E.A., and Semenza, G.L. (1995a). Hypoxia-inducible factor 1 is a basic-helix-loop-helix-PAS heterodimer regulated by cellular O_2 tension. Proc Natl Acad Sci U S A *92*, 5510-5514.

Wang, G.L., Jiang, B.H., and Semenza, G.L. (1995b). Effect of Protein Kinase and Phosphatase Inhibitors on Expression of Hypoxia Inducible Factor 1. Biochem Biophys Res Commun *216*, 669-675.

Wang, G.L., and Semenza, G.L. (1993a). Characterization of hypoxia-inducible factor 1 and regulation of DNA binding activity by hypoxia. J Biol Chem *268*, 21513-21518.

Wang, G.L., and Semenza, G.L. (1993b). Desferrioxamine induces erythropoietin gene expression and hypoxia-inducible factor 1 DNA-binding activity: implications for models of hypoxia signal transduction. Blood *82*, 3610-3615.

Wang, G.L., and Semenza, G.L. (1995). Purification and characterization of hypoxia-inducible factor 1. J Biol Chem *270*, 1230-1237.

Wang, V., Davis, D.A., Haque, M., Huang, L.E., and Yarchoan, R. (2005). Differential gene up-regulation by hypoxia-inducible factor-1α and hypoxia-inducible factor-2α in HEK293T cells. Cancer Res *65*, 3299-3306.

Welford, R.W.D., Schlemminger, I., McNeill, L.A., Hewitson, K.S., and Schofield, C.J. (2003). The Selectivity and Inhibition of AlkB. J Biol Chem *278*, 10157-10161.

Wierzbicki, A.S., Mitchell, J., Lambert-Hammill, M., Hancock, M., Greenwood, J., Sidey, M.C., de Belleroche, J., and Gibberd, F.B. (2000). Identification of genetic heterogeneity in Refsum's disease. Eur J Hum Genet *8*, 649-651.

Wiesener, M.S., Turley, H., Allen, W.E., Willam, C., Eckardt, K.U., Talks, K.L., Wood, S.M., Gatter, K.C., Harris, A.L., Pugh, C.W., *et al.* (1998). Induction of Endothelial PAS Domain Protein-1 by Hypoxia: Characterization and Comparison With Hypoxia-Inducible Factor-1α. Blood *92*, 2260-2268.

Wu, Y., Erdődi, F., Murányi, A., Nullmeyer, K.D., Lynch, R.M., and Hartshorne, D.J. (2003). Myosin phosphatase and myosin phosphorylation in differentiating C2C12 cells. J Muscle Res Cell Motil *24*, 499-511.

Wu, Y., Murányi, A., Erdődi, F., and Hartshorne, D.J. (2005). Localization of Myosin Phosphatase Target Subunit and its Mutants. J Muscle Res Cell Motil *26*, 123-134.

Xian, Z.-H., Zhang, S.-H., Cong, W.-M., Yan, H.-X., Wang, K., and Wu, M.-C. (2006). Expression of aspartyl beta-hydroxylase and its clinicopathological significance in hepatocellular carcinoma. Mod Pathol *19*, 280-286.

Zahnd, C., Wyler, E., Schwenk, J.M., Steiner, D., Lawrence, M.C., McKern, N.M., Pecorari, F., Ward, C.W., Joos, T.O., and Plückthun, A. (2007). A designed ankyrin repeat protein evolved to picomolar affinity to Her2. J Mol Biol *369*, 1015-1028.

Zampetaki, A., Mitsialis, S.A., Pfeilschifter, J., and Kourembanas, S. (2004). Hypoxia induces macrophage inflammatory protein-2 (MIP-2) gene expression in murine macrophages via NF-κB: the prominent role of p42/p44 and PI3 kinase pathways. FASEB J *18*, 1090-1092.

Zeghouf, M., Li, J., Butland, G., Borkowska, A., Canadien, V., Richards, D., Beattie, B., Emili, A., and Greenblatt, J.F. (2004). Sequential Peptide Affinity (SPA) System for the Identification of Mammalian and Bacterial Protein Complexes. J Proteome Res *3*, 463-468.

Zhang, C., Baudino, T.A., Dowd, D.R., Tokumaru, H., Wang, W., and MacDonald, P.N. (2001). Ternary Complexes and Cooperative Interplay between NCoA-62/Ski-interacting Protein and Steroid Receptor Coactivators in Vitamin D Receptor-mediated Transcription. J Biol Chem *276*, 40614-40620.

Zhang, Y., and Reinberg, D. (2001). Transcription regulation by histone methylation: interplay between different covalent modifications of the core histone tails. Genes Dev *15*, 2343-2360.

Zheng, X., Linke, S., Dias, J.M., Zheng, X., Gradin, K., Wallis, T.P., Hamilton, B.R., Gustafsson, M., Ruas, J.L., Wilkins, S.*, et al.* (2008). Interaction with factor inhibiting HIF-1 defines an additional mode of cross-coupling between the Notch and hypoxia signaling pathways. Proc Natl Acad Sci U S A *105*, 3368-3373.

Zhou, J., Kelly, W.L., Bachmann, B.O., Gunsior, M., Townsend, C.A., and Solomon, E.I. (2001). Spectroscopic Studies of Substrate Interactions with Clavaminate Synthase 2, a Multifunctional α-KG-Dependent Non-Heme Iron Enzyme: Correlation with Mechanisms and Reactivities. J Am Chem Soc *123*, 7388-7398.

Zhou, S., Fujimuro, M., Hsieh, J.J.D., Chen, L., and Hayward, S.D. (2000a). A Role for SKIP in EBNA2 Activation of CBF1-Repressed Promoters. J Virol *74*, 1939-1947.

Zhou, S., Fujimuro, M., Hsieh, J.J.D., Chen, L., Miyamoto, A., Weinmaster, G., and Hayward, S.D. (2000b). SKIP, a CBF1-Associated Protein, Interacts with the Ankyrin Repeat Domain of NotchIC To Facilitate NotchIC Function. Mol Cell Biol *20*, 2400-2410.

Acknowledgments

Firstly, thanks to Chris Pugh for giving me the opportunity to study for a DPhil in the Ratcliffe lab, and for giving your help, advice and expertise so freely over the last few years. Thanks also to Peter Ratcliffe for supervisory input.

Thanks to Benedikt, Holger and Mariola for your endless patience and invaluable assistance with mass spectrometry – we got there in the end.

To the members of the Ratcliffe group, past and present, thanks for making the lab such a great place to work. Thanks to David for knowing everything about Excel and always taking an interest; to Tammie for being a statistical guru and finding me a place to live for the last few months; to Norma for your time-saving tips, PHD3-based ideas and wicked sense of humour; to Ya-Min for your encyclopaedic knowledge of antibodies and ready smile; to Alex for all the laughs and the French lessons (pomme de terre!); to Dr Rebecca J Appelhoff – your sage emails from the other side of the world have kept me going on more than one occasion; to Julie for proofreading and helping me stay sane over the last few weeks; to Paddy for a bottomless supply of flatus and *Daily Mails*, without which writing up wouldn't have been quite the same; to Lynn for always making the time to listen and always knowing the right thing to say – I hope I was able to do the same when it mattered.

Special thanks to the two postdocs who had the dubious honour of supervising me in the lab. Matt, thanks for your unfailing friendship, good humour, wise advice and technical wizardry (except for the sodium azide/HRP trick, which sucks). Mat, thanks for your top "Notch" sarcasm, support, encouragement and everything else, but most of all thanks for believing in me all the times when I didn't.

Finally, for twenty-six years of love, support and the occasional nappy change, very special thanks to my family. This thesis is dedicated to you.